Cognitive approach for representing the haptic physical human-humanoid interaction

Antoine Bussy

▶ **To cite this version:**

Antoine Bussy. Cognitive approach for representing the haptic physical human-humanoid interaction. Automatic. Université Montpellier II - Sciences et Techniques du Languedoc, 2013. English. NNT : 2013MON20090 . tel-01017162v2

HAL Id: tel-01017162

https://theses.hal.science/tel-01017162v2

Submitted on 25 Jun 2014

HAL is a multi-disciplinary open access archive for the deposit and dissemination of scientific research documents, whether they are published or not. The documents may come from teaching and research institutions in France or abroad, or from public or private research centers.

L'archive ouverte pluridisciplinaire **HAL**, est destinée au dépôt et à la diffusion de documents scientifiques de niveau recherche, publiés ou non, émanant des établissements d'enseignement et de recherche français ou étrangers, des laboratoires publics ou privés.

UNIVERSITÉ MONTPELLIER 2
SCIENCES ET TECHNIQUES DU LANGUEDOC

THÈSE

pour obtenir le grade de

DOCTEUR DE L'UNIVERSITÉ MONTPELLIER 2
Discipline : SYAM – Systèmes Automatiques et Microélectroniques
École Doctorale : I2S – Information, Structures, Systèmes

présentée par

Antoine BUSSY

Équipes d'accueil : LABORATOIRE D'INFORMATIQUE, DE ROBOTIQUE ET DE MICROÉLECTRONIQUE DE MONTPELLIER
CNRS-AIST JRL, UMI3218/CRT (TSUKUBA, JAPON)

Titre :

Approche cognitive pour la représentation de l'interaction proximale haptique entre un homme et un humanoïde

Présentée et soutenue publiquement le 10 octobre 2013

JURY

Florent	LAMIRAUX	Rapporteurs
Étienne	BURDET	
Ganesh	GOWRISHANKAR	Examinateurs
Ken'ichi	YANO	
André	CROSNIER	Directeurs de thèse
Abderrahmane	KHEDDAR	

Remerciements

Avant tout, je souhaiterais remercier Abderrahmane Kheddar et André Crosnier pour leur encadrement tout au long de la thèse. Leur aide, leur soutien, mais aussi leurs recadrements, ont été extrêmement précieux.

En second lieu, je tiens à remercier les membres du jury pour avoir accepter d'examiner ce travail. Merci à Étienne Burdet, Florent Lamiraux, Ganesh Gowrishankar et Ken'ichi Yano pour leurs retours et corrections qui ont contribué à améliorer ce manuscrit.

Je voudrais remercier François tout particulièrement pour son amitié et son aide tout au long de ma thèse. C'est simple, je crois qu'il n'a jamais refusé malgré mes nombreuses sollicitations! Un grand merci également à Sébastien Druon qui m'a soutenu et remotivé dans une période pas évidente.

Merci à Pierre et Damien pour les franches rigolades qui m'ont permis de décompresser. Pour cela, je peux aussi remercier Benjamin, Stan et Adrien au JRL, mais également Divine, Alejandro, Camilla, Alessandra, Joris et Joven pour Montpellier. Merci à eux pour leur amitié.

Merci à Eiichi Yoshida pour son accueil au JRL et à Tokiko Uga pour son aide avec la vie quotidienne japonaise. Je voudrais aussi remercier Kenji Kaneko pour son aide précieuse lorsqu'il y avait un problème avec HRP-2. Merci d'ailleurs à HRP-2 d'avoir résisté à (presque) tout ce que je lui ai fait subir.

J'aimerais remercier tous les membres, actuels et anciens, du JRL que j'ai pu croiser, Paul Evrard tout particulièrement. Mais également Sébastien L., Toréa, Martin, Karim, Julie, Thomas, Hervé, Maxime, Grégoire et Gerardo.

Je voudrais également remercier tous ceux que j'ai croisé au LIRMM: Philippe Fraisse, Andrea, Florent, Arnaud, David, Nicolas, les deux Guillaume, Johann et tous ceux que j'aurais oublié.

Merci à Airi, Yi-Ching, Rafael, Samson, Hur, Lorraine et Camille d'avoir accepté de participer à mes expérimentations sur le robot HRP-2.

Je tiens à remercier Claudia, Morgane, Loic, Liam, Arnaud, Timothée, Dionysios, Dipanjan, Gaurav, Aurore, Vincent, Jérôme, Matthieu, François, Michael, Colas et Cécile d'avoir accepté de jouer les cobayes pour mes expérimentations à Marseille. Merci tout particulièrement à Jean-Louis Vercher, Marie-Laure Mille et Thelma Coyle pour leur accueil et leur aide à l'ISM.

Enfin, un grand merci à toute a famille pour leur soutien inconditionnel, notamment à ma grand-mère Claude et à Mimie.

Contents

List of Figures

List of Tables

Introduction

PHYSICAL Human Robot Interaction is a field of high interest and challenge in modern robotic science and technology. Ingredients for autonomous robots are still cramped within research laboratories in academia and industries whereas it is very likely time for them to be invited into homes and offices to become a part of our everyday life. And to make that final leap, robots will need to master physical interaction with humans.

For this purpose, security matters as a first priority by Asimov's First Law of Robotics:

"A robot may not injure a human being or, through inaction, allow a human being to come to harm."

Robots are machines that are capable of producing significant mechanical power and thus can harm humans. The death of Robert Williams, reported to be the first man killed by a robot in 1979, is a sad example of this evidence. Service robots for home services (e.g. elderly or frail persons assistance) need the ability to interact physically gently and safely with humans. To deal with the safety issue, the first solution is to build robot with limited power, and size, such as the Aibo from Sony and Nao from Aldebaran. The limited power of their actuators makes them inherently safe for humans. But they cannot assist with everyday tasks such as gardening, carrying groceries or helping a human to transport a cumbersome piece of furniture. Their capacities are often limited to social interaction without contact such as through sound (language) or gestures. And these capacities have to be remarkable if they do not want to be relegated to the level of an expensive toy. The second solution is to implement safe behaviors for robots when they interact with humans, while in the same time, being able to produce high power to assist them when necessary. For instance, when carrying a cumbersome piece of furniture with a human, a robot should be able to handle a

significant part of the object's mass without endangering the human. Researching on safety behaviors of human-humanoid pHRI is certainly very important and challenging; it is also likely that it should be tackled closely with the planning and the control strategies, but it is out of scope of this thesis. We consider it as an entire investigation of its own.

Physical contact, i.e. touch, plays an important in exploring our surrounding but also in our social communication with others. Because it can harm, physical contact brings confidence in the touched person or object. Physical interaction is closely linked to proxemics. It is also a matter of togetherness. Physical contact is important in human relationships because every day, we shake hands, we hug, we pat, etc. The more a person trusts someone, the closer to her/him s/he will be comfortable to be. Understanding and efficiently reproducing physical interaction as part of service robotics capabilities allow bringing robots within the personal and intimate spaces[1] of humans; we say co-shared space and close contact interactions. With such capabilities, we believe that service robots are better accepted by their human users and thus be able to better assist them.

But safe interaction is not the only issue of physical human-robot interaction (pHRI). When two persons interact physically, they perceive intentions from each other. Getting back to the example of transporting a piece of furniture: human dyads are able to guess each other's intentions to move the object in a certain direction and at a certain velocity. They are able to negotiate the direction and velocity, without being a burden to each other and even without much of voice communication: they are *proactive* to each other. Guessing each other's intention and proactivity are key features in human-human interaction. Therefore, robots for human partnership must be endowed with the capability to guess/understand human's intentions instantly for a variety of tasks that requires physical interaction, such as carrying an object together, walking hand in hand or handshaking.

Aside from the necessity to master physical interaction, for daily life tasks in homes and offices, robots must be adapted to such places. For instance, wheels can quickly become unpractical in a human environment with stairs. And to assist humans in everyday tasks, it may need arms and hands, as well as eyes to see objects of interest. This is why biped humanoid robots are envisaged also as service robots in domotics and offices. Their anthropomorphic shape makes them well-adapted to our environment. We therefore do not need to adapt the infrastructure of such environments to the robots. The same argument stands for assisting us in tasks. To do so, robots need not act as humans would. But behaving like a human, in addition to the humanoid shape, would create expectations of the human. Indeed, the human partner would expect the robot to behave no differently than a human or more generally from what it expects from the robot as motion for a given task.

In this thesis, we focus on the task of transporting an object together, which is a typical case scenario in the literature of pHRI. Our approach is to learn from human dyads observations in performing this task, and then to program the appropriate control strategy in the humanoid HRP-2 to perform that task with a human partner.

In the first chapter, we briefly review the state-of-the-art of pHRI. The chapter does not

[1] The personal space lies between 50 and 120cm from a person, while the intimate space lies within 50cm. The intimate space is for embracing, touching and whispering. The personal space is for interactions among good friends or family members.

pretend to be exhaustive in details but important principles are reported. Most implementations rely on impedance control [32] to endow robots with safe dynamic behaviors. Several teams proposed to control humanoid robots performing the transportation task with a human [43] [62] [46], but only with wheeled robots. To our best knowledge, only two teams proposed implementations for biped human-sized humanoid robots [74] at AIST and our team [19].

In the second chapter, we set-up a human motion/force capture system to monitor human dyads performing the transportation task. From collected and analyzed data, we make the following important observations:

1. the task is impacted by the oscillatory nature of the human gait,
2. no particular gait synchronization between the two partners is necessary to complete the task,
3. the trajectory of the transported object in the world frame can be described by Constant Velocity Phases (CVPs).

The last observation is the keystone of the implementation of the transportation task on the HRP-2, which is described in the third chapter. To assure safe interaction, we enforce an impedance constraint on the robot's grippers. The main contribution of this chapter lies in the reference trajectory that is used in the impedance constraint. The robot generates this trajectory by guessing the human's intentions. It tries to guess these intentions by selecting *motion primitives* –elementary bricks of motion –based on information from haptic cues. The set of motion primitives we used is defined from the observation of CVPs.

In the fourth chapter, we study the performances of our implementation by comparing our approach to Evrard's [19] in a user study. The main result of this chapter is that, although our implementation improves the energy performance the human has to spend because of the robot, participants still prefer the other. We try to find an explanation for this by performing a second user study to see if training the human partner to our control scheme impacts its performances. We also compare the results with the human dyads data from the second chapter.

In the last chapter, we expose several potential extensions to our work. We first investigate, with a user study, whether a reduction of the noise made by the robot may improve how humans feel about our control scheme. A second lead is to improve the robot's stability, and thus its walking capacities, by using the physical interaction with the human. We present preliminary results where the robot is able to stabilize itself through physical interaction. We also present generalizations to our control framework to two other haptic tasks: walking hand in hand with the robot and handshaking. Finally, we briefly report the possibility to couple pHRI with visual servoing.

In the chapter to come, we review the state-of-the-art in the field of physical Human-Robot Interaction.

1 Physical Human Robot Interaction: State of the art

Contents

ROBOTIC technology has considerably evolved in terms of hardware, software and applications. Nowadays, progress in robotics is noticeably fast, so that parallel is often made with the history of computers to sketch in our imagination what the robotic revolution is expected to outcome. At the very beginning, robot played a major role in the economic

Figure 1.1: Example of telerobotics in hazardous environments. Employees at the Dounreay's Prototype Fast Reactor site in Caithness, Scotland, are forced to use robotic arms because of the high levels of radiation on the glass.

growth era. They were rather automation machines, confined in a safety-restricted space in industrial factories. Their space of operation and that of the human workers were strictly exclusive. Robots were assigned repetitive tasks and substituted humans in most of their physical interaction tasks at production lines.

First physical interaction between humans and robots appeared undeniably with telerobotics technology. In telerobotics, robots were used in order to extend human gesture and physical interaction in environments that are hostile to humans. Its principle is to have a robotic arm, called the "slave", that operates at a distance under full control of another robotic arm, called the "master", that is fully operated by a human through direct interaction. The master role is twofold: in one hand, the user uses it like a joystick that provides the desired motion to the slave robot; in the other hand, being actuated, it can freeze its configuration to render force feedback when the slave robot is in contact with the environment. This dual role is made through a bilateral coupling, where the slave robot tracks the motion of the master arm; in return the master arm tracks the motion of the slave arm. Such a bilateral coupling constrains the motion of the master arm when the slave arm encounters a contact, that is then felt through an implicit force feedback reacting to the one applied by the user. As we can see, in bilateral coupling or force reflecting telerobotics, the human interacts directly with a robotic arm to control another robot. Telerobotics is generally applied in hazardous environments where automation is not possible and where, very often, the presence of the human is dangerous or costly, as pictured in Fig. 1.1.

Telerobotics technology also allowed the emerging of the field of wearable exoskeletons called human extenders. Human extenders are robotic devices that are worn by a human to provide her/him extra capabilities in motion and force strength [38]. Exoskeletons are human motion and/or force capabilities amplifiers, and are used in movies (Alien), construction, and military applications. Recently, exoskeletons became very popular in medical applications [1]. As they work tidily in physical contact with humans, they raise critical issues of safety and robustness.

Robots have evolved in shapes and services. From industry and hazardous applications, they were found new social applications. For example, telerobotics technology, that was

Figure 1.2: Cobot A7-15 is a collaborative robot that allows reducing the arduousness and the risks for operators in difficult manual tasks.

devised for the highly radiated environments of nuclear plants, finds applications in minimally invasive telesurgery, telesurveillance, or more generally, the telecontrol of wide purpose robots. Even exoskeletons, and robots in general, are now being applied as wider purpose assistance devices, for human workers or elderly or impaired persons, such as assisting persons to take their meal [53]. Now robots are considered as companions and, with upcoming applications, they are bound to share their operational space with humans. Cobots is an example of a new generation of robots that, alike haptic devices, will be used as direct touch sophisticated tools in different industrial applications, as in Fig. 1.2.

Recent service mobile robots, including humanoid robots, are also considered as human partners. That is, a working agent to assist a human worker in various joint actions, among which physical joint actions. Humanoid robots are interesting since they are shaped like humans and hence can effectively use the human working and living space without additional or specific fitting-outs or arrangements. But humanoid robots are also more challenging to control relatively to wheeled mobile robots. In standalone mode, it is already hard to plan and control a humanoid robot to walk, to manipulate, or to do both [7, 11]. Our thesis is to challenge this problem in human-humanoid physical interaction via a conjoint manipulated object. Examples of such tasks are illustrated in Fig 1.3.

1.1 Human-Robot Haptic Joint Action

Our work challenges Human-Humanoid Robot Haptic Joint Actions. Such actions are illustrated by the Fig 1.4. They are actions that a human and a robot do *together* with a sustained contact, such as dancing [65], handshaking [5, 70], object manipulation [74], walking hand-in-hand, hugging [12, 64], arm wrestling, surgery [66], or exoskeletons enhancing a human's

Figure 1.3: Two humans collaborating to cross-cut a tree (left) and to carry a table (right).

physical capacities [59].

The important characteristic of Human-Robot Haptic Joint Actions is that the human and the robot interact physically, hence it is more often termed physical Human-Robot Interaction or pHRI. During pHRI, the human and the robot exchange mechanical power and heat, exert forces on one another (Newton's third law) by means of a common contact surface. They also share common velocities and temperatures[1]. Some researches focus on thermal interaction and heat transfer [6,25]. Others focus on tactile interaction [4], where importance is given to the repartition of forces over the contact surface as for hugging. On the contrary, our work focuses on haptic joint actions where the interaction can be described by the net force and torque exchanged through the surface and the mean velocity of the points of the surface[2]. For instance, during an object manipulation, we are mostly interested in the object trajectory; therefore, only the net force exerted on the manipulator's end effector is of interest. In contrast, during a hug, the net force applied by each hugger is zero and yields no information; thus the repartition of the forces over the contact surface is important. Handshaking is a good mixed example. Although all the implementations reviewed in [5] focus on the net force, the pressure exerted on the hand and the temperature are also important: no-one likes to shake a cold hand or when the handshake's grip is too strong (used to show or communicate dominance) [61].

Therefore it is primordial when studying pHRI to well define in what form energy is exchanged and what are the physic quantities that are exchanged and shared. In this work, we focus only on transfers of mechanical power, the mean velocity of the points of the surface of contact and the net force applied on it. We do not consider the tactile aspect nor the thermal transfers.

1.1.1 Purpose of pHRI

Studying pHRI has three main purposes:

[1]Note that they exchange extensive properties and share intensive properties. In the following, we might loosely use the term "exchange of forces".

[2]This supposes a non-sliding contact.

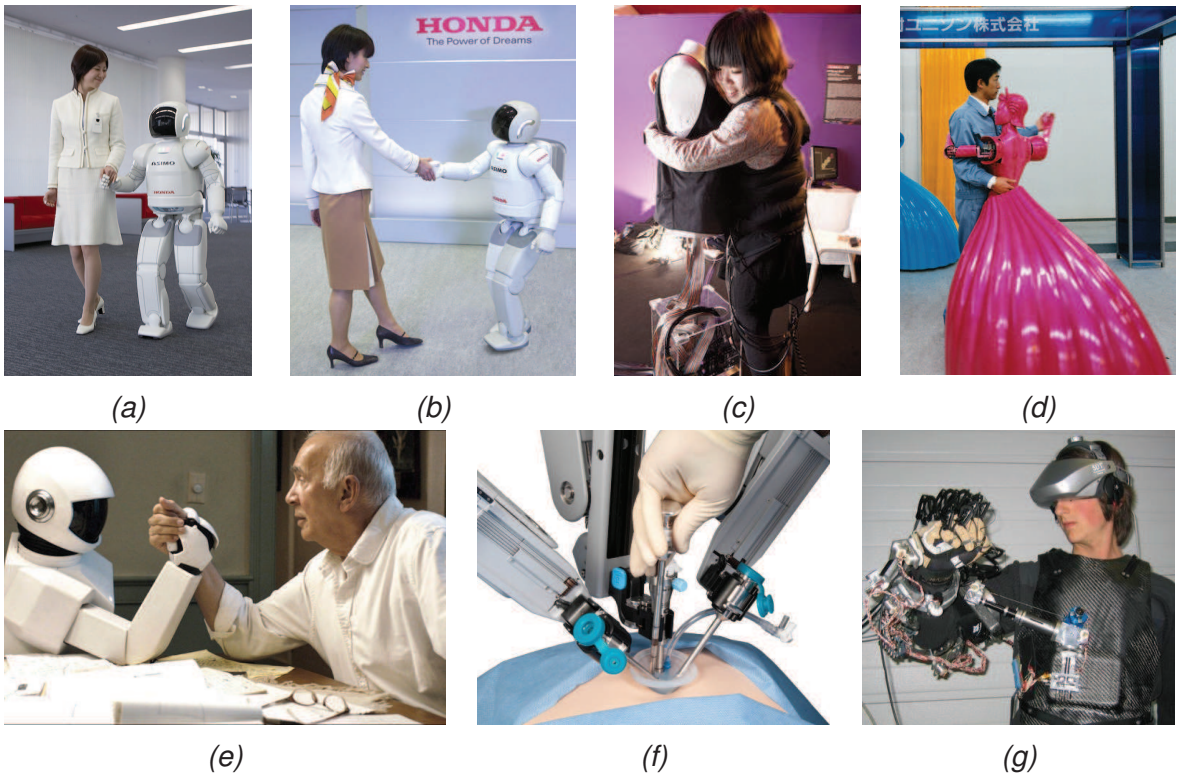

Figure 1.4: Examples of pHRI. From left to right, top to bottom: (a) Honda's Asimo Humanoid robot walking while holding a hand, then (b) handshaking, (c) Sense-Roid Tactile jacket used in a hug, (d) a dancing robot partner (Tohoku University), (e) robot and Human arm-wrestling ("Robot and Frank" movie, 2012), (f) Robot-assisted surgery, (g) a robot operator strapped into telepresence devices (a stereo video helmet, the ESA exoskeleton and a human hand exoskeleton, European Space Agency).

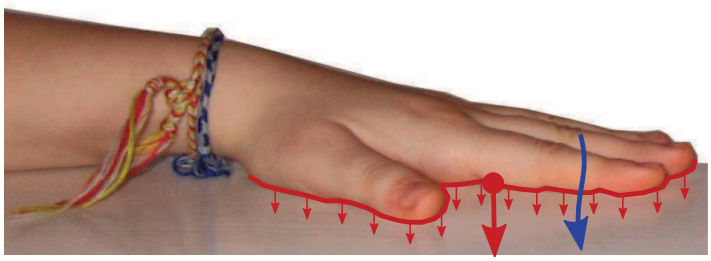

Figure 1.5: Example of contact between a human hand and a table. The red line represents the surface of contact. The small red arrows represent the elementary forces applied by the hand on the table, while the big red one represents the net force. The blue arrow represents a heat transfer.

- to study physical Human-Human Interaction (pHHI),
- to design robots that can live among/with humans,
- to design robots that can work with humans.

Studying pHHI

pHHI and pHRI are strongly linked. It is certainly possible to design pHRI without inspiration and/or study from pHHI. The most widespread example is the car. However, it requires learning and it does not allow piloting a plane. Deriving interaction models from pHHI and implementing them into pHRI endows the robot with a behavior the human can understand/identify to. Thus the human is able to interact more *intuitively* with the robot, with few or no learning. For instance, it is easy for two humans to carry an object together on a predefined trajectory. Each partner assumes the other to have similar capacities and behavior as himself, giving a knowledge of the other partner's limits and an ability to guess his intentions [60]. A partner might answer the question "What would I do in his place?" (empathy) to predict the partner's intentions [37, 51]. However, Jarassé *et al.* [33] propose a more a global framework for pHRI where the robot not necessarily acts as an helper. Inspired from game theory, the robot could endow various behaviors, such as co-activity, competition, collaboration, assistance and education.

Furthermore, pHRI is a powerful tool to validate pHHI models. Because identifying the parameters of a complex pHHI model can be difficult, it may be easier to implement the model on a robot to check that similar measures are obtained, and if similar behaviors can be reproduced. In [57], Reed studies how two humans collaborate to move a crank; he then implements a control law for a robotized motor to perform the task with a human. Reed conducts a Turing-like test where a human subject performs the task with the robotized motor but is told he is collaborating with a human. Most subjects believed that they are indeed collaborating with a human, and not with a robot. However, Reed is not able to reproduce with the human-robot pair all the behaviors observed during the collaboration between two humans. Reed's work example also shows that pHRI might help to correct/complete the pHHI model, which in turn will help to implement better pHRI.

The benefits of pHRI are not limited to the study of collaboration between humans. Robots are also used to study how humans physically interact with the environment, where they are used to simulate the environment [34]. The same robot can then be used to validate algorithms that implement human-like behaviors in the same environment [72, 73].

Robots living among/with Humans, Acceptability

Besides, robots are more and more present in humans' daily life, as Aibo from Sony and Nao from Aldebaran (Figure 1.6), and thus they gain a social dimension. As people like to pet a dog, they would like to interact physically with robots. Humanoid robots able of efficient pHRI would enable many new applications in domotics or service robotics. Because physical interaction requires close contact, it involves risk [41] and might cause more apprehension

Figure 1.6: Examples of social robots: Aldebaran's Nao (left) and Sony's Aibo (right).

Figure 1.7: RIBA nurse robot carrying a patient.

or fear. One cause may be that physical interaction is more intimate than verbal or visual interaction, but also more dangerous. For instance, when a human tries to pet a cat he does not know, he first does it carefully to not scare the animal and not being clawed. In a second time, once the apprehension is overcome, the human might pet the cat more generously. In a similar way, a successful pHRI would be very reassuring and helps forging a bond of confidence, a closeness, between the human and the robot. Therefore, the robot would be less perceived as a machine tool, or a mere object, but as a permanently present supporting partner or companion. Strong pHRI skills would increase robots' acceptability in the society.

One must not forget that a main characteristic of robots is that they are machines. Machines that can hurt people, such as cars, planes or chainsaws. Industrial and domestic accidents with machines are common. Robert Williams was the first man killed by a robot in 1979. But robot are also machines that can be broken if wrongly used. Therefore, it is necessary to build robots that can safely live among humans.

Besides, a robot could be useful in situations that require interaction, such as putting a person in bed or help him/her to walk, such as the RIBA robot portrayed in Fig. 1.7.

Robots working with Humans

The major advantage of pHRI is to take advantage of the synergy between humans and robots. Humans have great cognitive capacities while the robots have great physical capacities. The typical task is to transport a heavy and/or bulky object –typically a beam or a

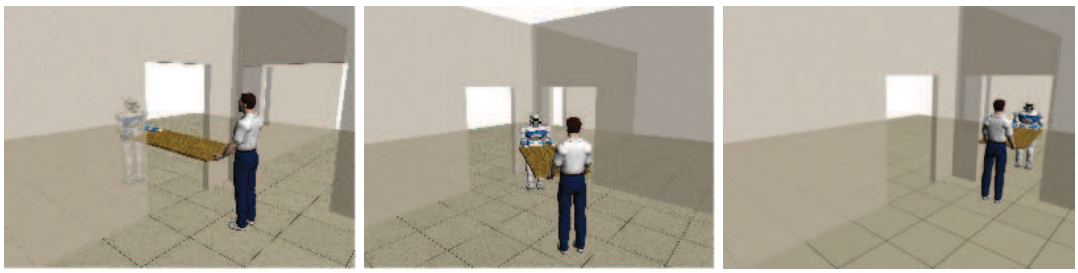

Figure 1.8: Example of pHRI task. The human-robot dyad has to carry the beam through two doors that form a 90° angle. The dimensions of the beam are too big to perform the task with a single bend, so that the human has to pass backward through the first door and forward through the second one.

table– from one point to another in an unmodelled environment [42], (see Figure 1.8). In this example, the robot is in charge to carry the gravitational load of the object, while the human directs the horizontal trajectory of the object. We speak of *Collaborative Tasks*. In this example, a major problematic in pHRI arises: a robot needs the antagonistic capacities to perform tasks that require great strength while maintaining safety for humans. This concern is again more critical when the robot is in direct interaction and/or contact with the human. The best example of this problematic is the exoskeleton [59]. The exoskeleton must enhance the human's physical capacities without hurting him.

The robot must be able to input a lot of power into the external environment while limiting the power exchanged with the human. This limited power exchange between the human and the robot cannot be fully eliminated because it is the mean of communication between them.

Physical Human Robot Interaction poses great challenges and new opportunities. Mastering physical interaction is crucial if one wants to extend the field of operation of robots, to homes and offices particularly. To that end, studying how humans interact physically may prove to be useful, and endow robots with the ability to live and work with and among humans.

1.1.2 Humanoid Robots

In this work, we are interested in humanoid robots, which look like humans. Strictly speaking, humanoid robots are biped robots, with two legs, two arms, a torso and a head. However, since biped walking planning and control is still a challenging research issue, this definition is often extended to wheeled robots with a human-like upper body.

Using humanoid robots has several advantages. The human shape, as Aldebaran Romeo robot's (Fig. 1.9), can be reassuring for the human, because it allows the human to identify himself to the robot, to accept the robot as a companion, which increases the robot's acceptability.

More importantly, the human is expecting the robot to have a human-like behavior (*embodiment*). For our collaborative transportation task for instance, the human may not ask

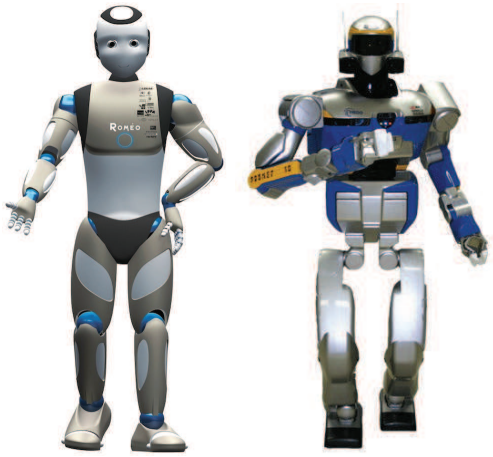

Figure 1.9: Aldebaran Romeo (left) and Kawada HRP-2 (right) Humanoid Robots.

himself how he can transport the table with the robot, he will simply assume that the robot will behave just like another human. Which stresses the necessity to implement a human-like behavior for such tasks and robots. Similarly, communication with a humanoid robot about body parts or motions is straightforward since movement types as "give me your hand" or "walk with me" also makes sense for the robot.

Finally, biped humanoid robots are adapted to our environment, they are *adaptable* for most situations. The human has designed his environment – buildings, houses, every object of daily life – given the characteristics of his own body, his physical capacities and movement patterns. Therefore, having the same anatomy allows the robot to interact more easily with our human environment. It is not necessary to adapt our environment, as home furniture, to allow robots to be used within it.

However, there are drawbacks to the use of biped humanoid robots, especially concerning their balance during gait. Balance is a crucial issue for bipeds. The first strategy is to avoid falling at all cost. Algorithms based on the Zero-Moment-Point algorithm allow the robot to correct its actions to keep balance. However, situations happen where the robot starts to fall; a strategy would be to quickly plan a new step to recover. When this not possible, the robot must be endowed with the ability to protect itself and not hurting the persons around it while falling. In this case, the robot should also be able to stand back up after falling. This is a very complex and challenging problem that is being addressed in current research [36] and is considered as out of the scope of this thesis.

1.2 Impedance Control for pHRI

Thirty years ago, Neville Hogan introduced impedance control in robotics as a solution for manipulation tasks [32]. The approach consists in regulating the robot's dynamic behavior at its *interaction ports* with the external environment. An interaction port is a place at which power may be exchanged with the environment. The interaction port is defined by a set of motion and force variables such that $P = F^T v$, where v i a vector of velocities (or angu-

lar velocities) along different degrees of freedom at the contact point, F is a corresponding vector of forces (or torques), and P is the power that flows between the robot and the environment through the contact point. The robot's dynamic behavior is regulated by enforcing a force-velocity equality constraint at the interaction port

$$\begin{cases} G(F, v) = 0 \\ P = F^T v \end{cases} \tag{1.1}$$

where G is a dynamic operator, i.e. it can include differentiation and integration. The basic impedance elements are depicted in Table 1.1

Table 1.1: Basic Mechanical Elements and their Laplace-Transformed Impedance.

Element	Diagram	$\frac{F}{v}$
Mass	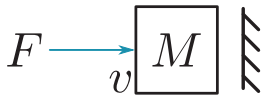	Ms
Damper	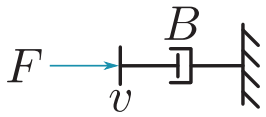	B
Spring	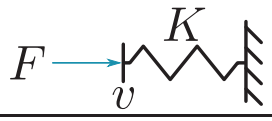	$\frac{K}{s}$

The following less general formula is used in practice (Fig. 1.10)

$$\begin{cases} F = M(\ddot{x} - \ddot{x}_d) + B(\dot{x} - \dot{x}_d) + K(x - x_d) \\ P = F^T v \end{cases} \tag{1.2}$$

where x is an integral of v, x_d is the impedance nodic reference, M, B and K are positive symmetric matrices (not necessarily constants). The equation $P = F^T v$ is often omitted. Impedance is defined relatively to a nonstationary reference frame, a *node*. The ground pictured in Table 1.1 schematics may be moving, even accelerating. This motion of the reference is modelled by the nodic reference x_d. Note that F and v may be a force and velocity in a Cartesian frame or a torque and articular velocity, as long as the constraint $P = F^T v$ holds.

From this point, we will consider the case where v is the velocity of a given end-effector of the robot – typically the hand of the robot – in a Cartesian fixed world frame and F is the force exerted on this end-effector by the environment in the same frame. The impedance nodic reference x_d is also expressed in the world frame.

There are two major ways to implement constraint (1.2):

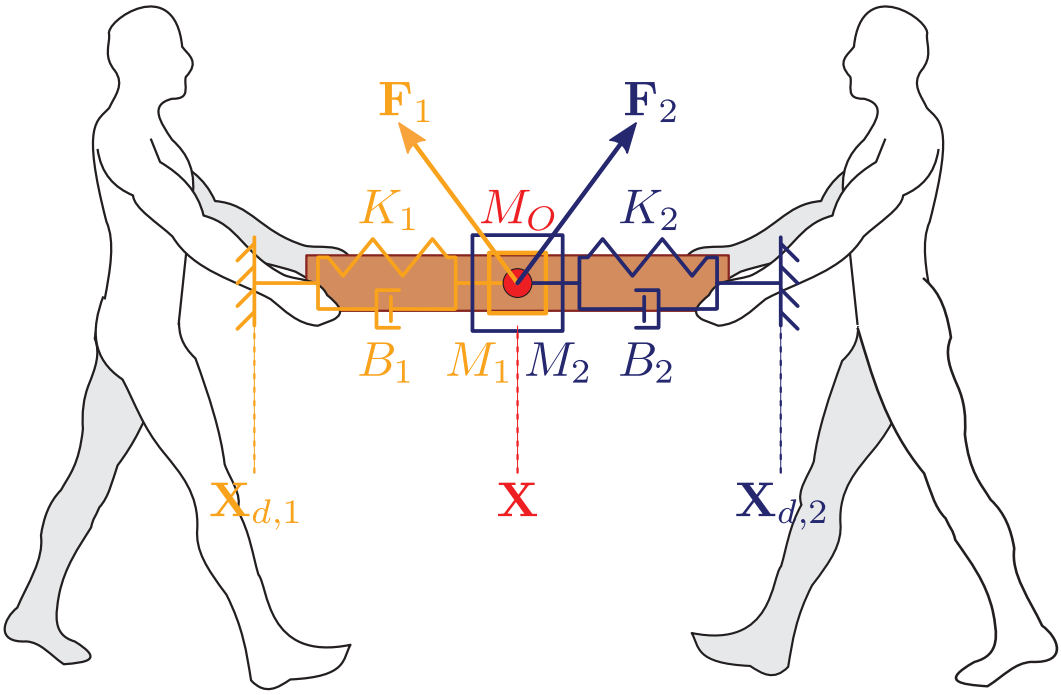

Figure 1.10: Impedance constraint example for collaborative object manipulation.

- as an admittance $v = Y(F)$, e.g. force-input/velocity-output, with a position controller with force feedback;

- as an impedance $F = Z(v)$, e.g. velocity-input/force-output, with a force controller with position feedback.

Strictly speaking, only the latter one is called impedance control, whereas the former is called admittance control. However, since they are equivalent when Y and Z are invertible, we may loosely use impedance control for both.

The purpose of impedance control is to regulate the mechanical power a robot can input in interaction, with a human or the environment. With position control, the goal is to reach a given position and rejecting any disturbance or error, regardless of power considerations. Therefore, if the robot meets an unexpected obstacle, it would use more power to try and reach its desired position, which is likely to damage both the robot and the obstacle. This is a higher concern if the obstacle is a human being.

By contrast, impedance control would make the robot more compliant. The alternative to position control would be to implement a spring behavior. On contact with the obstacle, the robot's trajectory would deviate from the intended one and absorb the shock. Of course, the power exchanged between the robot and the obstacle might increase if the robot tries to pursue its intended trajectory. However, the compliance gives more time to the robot to adapt its intended trajectory [28], or to the obstacle to move if it is a human. Therefore, impedance control is a keystone for safety in pHRI, which explains its popularity [3, 42, 55, 56]. It is so

successful that compliant actuators have been designed [29]. Such actuators, named variable stiffness actuators or VSA, allow to regulate compliance at the hardware level.

1.2.1 Stability during pHRI

When impedance controlled, a robot can theoretically adopt any dynamic behavior. However, stability –having a bounded output in response to bounded inputs– may not be guaranteed while interacting with a human, or more generally with an unknown environment, because a system that is stable in isolation may become unstable when coupled to an environment that is also stable. To address this problem, the generic solution is to enforce passivity [52]. Another solution, specific to pHRI, is to take into account the range of the human own impedance to improve the performance and the stability of impedance control [8, 14, 69].

1.3 Collaborative Transportation Task

In our work, we focus on a collaborative transportation task as pictured in Figure 1.8. In this example, the human and the robot move a table-like object from a room to another; thus the task requires locomotion. Although mobile robots and freeflyer robots have been developed, the precise localization of the robot in the world frame remains a challenging issue, which explains why much research is devoted to fixed-base robots. Therefore, many of the state-of-the-art approaches involve either object manipulation in a restricted workspace, or point-to-point object transportation over a distance below one meter. However, all of these research works, as well as our work, only consider the net force each partner –the human and the robot– exert on the object, and the velocity of the object, or possibly the mechanical power exchanges [21]. Because we consider that both partners are firmly holding the carried object, the system constituted by the object and both partners' hands is modelled as a rigid body.

One specificity of such a task is the indirect physical interaction through the transported object. It shares many similarities with tasks that require direct contact. For instance, in a handshaking task, both partners' hands can be considered to be the object to move. However, direct contact with a robot generates more apprehension than with an object between the human and the robot.

Twenty years ago, Kosuge implemented one of the first Human-Robot Haptic Joint Action [42]. The goal was to allow several robotic arms to carry an object with a human. Each robotic arm was impedance controlled to exhibit a mass-damper behavior. This is more or less the same dynamic behavior as a supermarket's trolley. Thus the robot has a reactive behavior, but it is passive. As we said, transporting an object with the robot is similar to moving a trolley full of goods. The main advantage is that no knowledge or model of how humans perform the task is necessary. Besides, the robot's behavior is very predictable and thus any human can perform the task without training. Concerning the interaction, the drawback of using a mass-damper dynamic behavior is the proportional relationship between the force applied by the human and the velocity of the robot's end-effector. To maintain a constant high velocity, the human needs to exert a high force on the object. This is even more

problematic when the robot is a legged humanoid robot, whom a high force will unbalance and eventually topple. Thus the velocity of transportation is limited by the interaction.

1.3.1 Proactivity

A solution to solve this drawback is to give a *proactive* behavior to the robot. Proactivity is the capacity for the robot partner to anticipates locally the human motion or more generally human expectations and act appropriately, to *take initiative*. In other words, it means the capability for the robot to guess the human partner's intentions and use them in the motion planning and control strategy. Ideally, the motion of the robot theoretically matches that of the human partner with no lag (and vice-versa). As an example, consider a motorized trolley with a force sensor on the handle. When a force is detected on the handle, it can be interpreted as an intention to push the trolley; so the motors turn on to assist the human in pushing the trolley. This would lead to rebalance the distribution of roles (cognitive vs. physical) in the execution of the task, tending to equal human-robot responsibility sharing [40].

The problem is that it requires guessing the human's intentions, which in fact is rooted in the brain. Besides, we do not want a proactive behavior of the robot that requires training for the human operator; the robot's behavior should meet the human partner's expectations. Therefore, there are benefits in studying how two humans collaborate to perform a transportation task, in order to extract interaction models that can be used to implement a proactive behavior on the robot. This would endow the robot with haptics skills mimicking the intuitive, smooth, and inherently safe way in which humans perform haptic joint actions, and add a cognitive dimension to the robot's behavior.

1.3.2 Enhancement considering the object's geometry

Arai *et al.* [3] noticed that Kosuge's scheme performed poorly when the object was long (and thus the distance between the robot and the human was great), especially when moving backwards and turning at the same time. Consider again the example of the trolley. When it is pulled backwards straightly, it is easy to maneuver. However, try to turn after having reached a certain velocity and the trolley will be brought along by its inertia: the trolley slide-slips. The problem with Kosuge's scheme was similar: it was difficult for the human to control the trajectory of the robot's end-effector that is at the other side of the object, because it requires a great amount of torque from the human. Therefore Arai *et al.* proposed an anisotropic impedance control[3] to prevent this slide-slip effect by enforcing a higher damping on the axis that is normal to the line that links the robot's and human's grip on the object.

This example highlights an important problematic on how to choose the impedance parameters. To decrease the mechanical power the human has to input to guide the robot, impedance should be chosen as low as possible, while ensuring coupled stability. However, Arai's observation shows that low impedance parameters could impede the manipulability of the object. Therefore, a high impedance in a given direction could ease the human's task,

[3]The impedance parameters were constant and isotropic in the horizontal plane in Kosuge's implementation.

or *guide* her/him. This approach has been generalized and formalized by Dumora *et al.* [15] using motion guides or virtual mechanisms theory. In this approach, the robot has the capacity to impose one constraint among a predefined set on the object motion, each constraint being described by a Jacobian matrix. For instance, the robot has the ability to constraint the object so that it can only translate along one axis or rotate around one axis. Finding the right guide/constraint that matches the human's intentions would be helpful for the human partner.

1.3.3 Obstacle Avoidance

Hirata *et al.* [31] proposed a scheme where two robots help a human to transport an object and to avoid obstacles that are on the path. The authors' system consists in two wheeled robots placed under the object to carry it at each extremity. The human pushes the object from above, like a trolley. Both robots are impedance controlled as in [42]. When one of them detects a close obstacle with a Laser optical system, it increases its damping. From the human's point-of-view, this causes one side of the object to be suddenly harder to push than the other, thus inducing a rotation of the object to avoid the obstacle.

The two previous cases are good examples of the advantages of tuning impedance parameters, but are restrictive to very particular cases, e.g. very constrained by the task context. Another strategy consists in mimicking the human's dynamic behavior.

1.3.3.1 From pHHI and/or learning

The method proposed by Rahman *et al.* [55,56] consists in extracting and recording the temporal evolution of the impedance parameters from two humans doing the same task before replaying these during the pHRI task. Rahman *et al.* monitored the forces applied by each partner on the object as well as its position. From these data, they estimated the impedance parameters at each time step with an Auto Regressive eXogenous (ARX) Model, using the impedance model

$$F(t) = M(t)\ddot{x}(t) + B(t)\dot{x}(t) + K(t)x(t) \tag{1.3}$$

The implementation on the robot consists in detecting the beginning of the task with a velocity threshold and replaying the evolution of the impedance parameters. The main problem of the control scheme is that it is only valid if the pHRI task is repeated identically to the pHHI task the impedance parameters are extracted from. This approach is no longer valid if the human decides to move the object more slowly or farther. Besides, if an unintended event occurs –such as an unseen obstacle coming through– that requires to go back for instance, the robot is not able to adapt.

This simple approach can be made more robust with learning techniques, for example Robot Learning from Demonstration [9](RLfD). Firstly, the task between two humans is not studied directly; a human teacher teleoperates the robot with a PHANToM device with force feedback, as shown in Fig. 1.11, while it performs the task with a human partner. This teaching phase was repeating several time with various lengths of motion. The curve

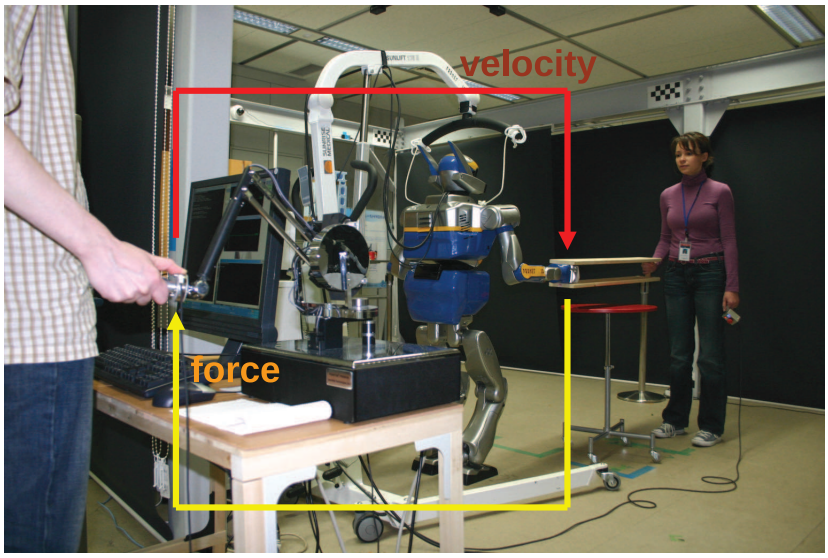

Figure 1.11: Teacher teaching the robot to perform a collaborative lifting task with a human operator. The teacher uses a Phantom device with force feedback.

$(F(t), v(t))$, parametrized by time t, at the robot's end-effector, therefore the robot's end-effector impedance Z, is encoded in a Gaussian Mixture Model (GMM). Then the robot could reproduce the task with the human partner using Gaussian Mixture Regression (GMR). In other words, RLfD consists in automatically decomposing the $(F(t), v(t))$ curve in phases during the teaching phase, then using a Hidden Markov Model to determine the transitions from one phase to another during the reproduction of the task. Thus the robot is more able of adaptation. However, the object is passive and no external perturbations are considered.

1.3.3.2 According to task phases

With RLfD, a decomposition in phases in done algorithmically. For an object transportation task, Tsumugiwa *et al.* [68] proposed the simple following decomposition in sections:

1. the beginning section
2. the working section
3. the positioning section
4. the normal section

At start-up, the robot's damping is medium. When the robot detects an increase of mechanical work applied on its end effector, it considers it as an intention to start the task and thus enter the beginning section. During this phase, the robot's damping is lowered not to impede the acceleration of the object. When the damping has reached its minimal value, the robot enters the working section, where the human partner transport the object. A force

threshold detects the human partner's intention to brake, and thus the robot enters the positioning. Its damping is highly increased to prevent overshoots and to allow the human to position the object with more precision. When the mean mechanical work applied on the robot's end-effector goes too low, the robot detects the end of the task and enters the normal section where the damping is restored to the medium value.

A similar approach is developed by Dutta and Obinata [16], where damping is kept low during the acceleration phase and increased during deceleration. The damping is changed according to the range the velocity of the robot's end effector is in.

With the same observation that the robot's damping should be decreased (resp. increased) when the human wishes to accelerate (resp. decelerate), Duchaine and Gosselin related the damping factor to the force derivative [13]. Indeed the authors interpret an increasing (resp. decreasing) force as an intention to accelerate (resp. decelerate). Hence the formula for the robot's end-effector damping:

$$B(t) = B_0 - \alpha \dot{F} \tag{1.4}$$

where F is a force signal from sensors. Thus the impedance constraint is as follows

$$F = M\ddot{x} + (B_0 - \alpha \dot{F})\dot{x} \tag{1.5}$$

More than just decreasing the damping, this control law allows negative damping; the robot is therefore actively assisting the human. However, it requires to differentiate online the force signal from sensors, which is not a trivial issue since force signals are very noisy, although efficient algorithms exist [63].

1.3.3.3 Trajectory-referenced Impedance

Another way to be proactive is to estimate the trajectory intended by the human partner and then use this estimation as the impedance nodic reference. This is the approach proposed by Maeda *et al.* [48] and Corteville *et al.* [10]. Both used the minimum-jerk model for the human intended trajectory. This model necessitates to define the starting time and position (t_0, x_0) as well as the final time and position (t_f, x_f), where we suppose initial and final zero velocities and accelerations. Thus the trajectory $x(t)$ is

$$\begin{cases} x(t) = (x_f - x_0)(6\tau^5 - 15\tau^4 + 10\tau^3) \\ \tau = \dfrac{t - t_0}{t_f - t_0} \end{cases} \tag{1.6}$$

This model was proposed by Flash and Hogan [24] for point-to-point motions. The challenge to use this model is that the final time and position (t_f, x_f) intended by the human are not known and must thus be estimated. Maeda *et al.* used a weighted least-squares method, and used the estimated trajectory $\hat{x}_d$ as the nodic reference of the stiffness part, i.e.

$$F = M\ddot{x} + B\dot{x} + K(x - \hat{x}_d) \tag{1.7}$$

The authors show that the unnecessary energy transfer between the human and the robot is lesser with this estimation than without.

On the other hand, Corteville *et al.* consider the final position x_f known. The duration of the motion, therefore the final time t_f, is evaluated in a first trial. Then this estimation is updated in real-time with an extended Kalman filter during the following trials. The estimated trajectory $\hat{x}_d$ is used as the nodic reference of the damping part of the impedance, and the stiffness part is zero:

$$F = M\ddot{x} + B(\dot{x} - \alpha\hat{\dot{x}}_d) \tag{1.8}$$

where $\alpha \in [0, 1]$ is an assistance coefficient. In the experiments, it took a couple of trials for the human-robot pair to adapt to each-other. A major issue is that such an approach is very restrictive to point-to-point motions, and do not apply to general case motions. Even for short distances, Miossec and Kheddar showed that the minimum jerk model was not the best fit [50].

Thobbi *et al.* [67] also use a Kalman Filter to predict the human's intended trajectory, using a constant acceleration model. Besides they also use the error of prediction as a homotopy factor [18]; when the prediction is bad, the robot falls back to a reactive behavior, rather than proactive.

Except Hirata *et al.* 's, all these implementations concerned point-to-point transportation of an object over small distances and small durations –less than one meter and no more than a few seconds. More specifically, they do not require the locomotion of the robot.

1.4 Collaborative Manipulation and Locomotion

1.4.1 Passive Approaches

The first example of a collaborative manipulation between a robot and a human that required locomotion was demonstrated by Kosuge in 2000 [43] with the Mobile Robot Helper.

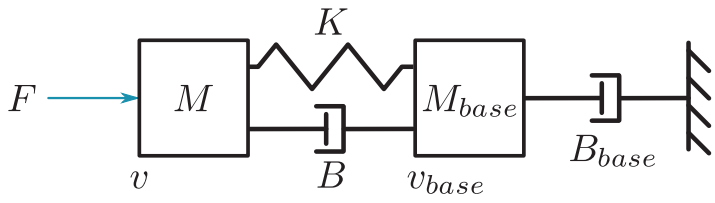

Figure 1.12: Mobile Robot Helper dynamic behavior.

The Mobile Robot helper is a wheeled humanoid robot. The dynamic behavior implemented links the external force F exerted on the robot's end-effector to its velocity v and the locomotion velocity v_{base} (Fig. 1.12). The impedance equations are

$$\begin{cases} F = M\ddot{x} + B(\dot{x} - \dot{x}_{base}) - K(x - x_{base}) & \text{(1.9a)} \\ F = M\ddot{x} + M_{base}\ddot{x}_{base} + B_{base}\dot{x}_{base} & \text{(1.9b)} \end{cases}$$

These equations are solved in x and x_{base} as an admittance with a force F input. The first equation expresses the compliance of the robot's arms, while the second expresses the global dynamic behavior of the robot (arms + base). This global dynamic behavior is similar to the one proposed by Kosuge for a fixed-based robot [42] (Section 1.3).

An interesting point in this approach is the "transparency" of the arms, e.g. the stiffness and damping of the arms is not perceived by the human partner. Indeed, according to (1.9b), from the human partner's point a view, the robot reacts as an inertia-damped system –the base– and a second inertia system –the arms. We classify this approach as a "Body guides Hands" strategy. The haptic cues are used to induce locomotion of the robot's base as described in (1.9b). Then, the robot's grippers are controlled to be compliant around the base's trajectory, which is (1.9a).

Yokoyama *et al.* [74] proposed a similar approach for the legged humanoid robot HRP-2. The arms are compliant around a fixed posture, similarly to (1.9a). When the human partner pulls the objects, the force exerted on the robot's grippers causes a displacement Δx of these grippers from the fixed posture. This Δx is then used to compute a reference velocity v_{CoM} for the robot's CoM

$$v_{CoM} = G\Delta x \tag{1.10}$$

Steps are generated to track this reference velocity v_{CoM}. This approach was also replicated on the Cosero robot by Stückler and Behnke on the Cosero wheeled robot [62].

We also classify these two approaches as "Body guides Hands" strategies. It might seem contradictory with (1.10) that expresses that the velocity of the body is computed from the grippers' displacement, which would include them in the "Hands guide Body" strategies. However, the grippers are compliant around a fixed posture, i.e. they are compliant relatively to the robot's body. In that sense, we can consider these strategies as "Body guides Hands" ones.

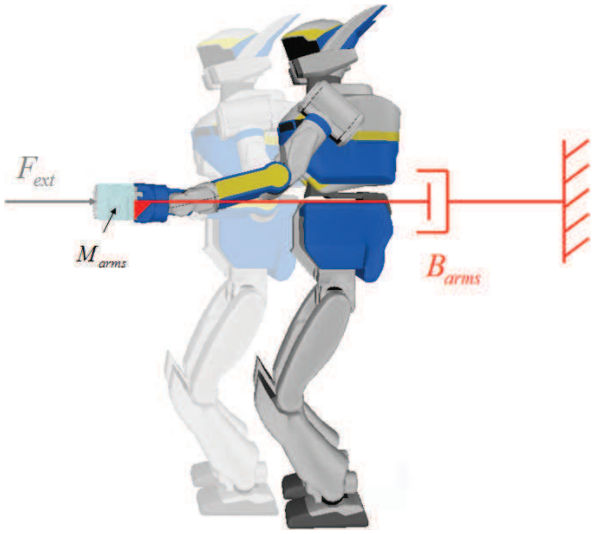

Figure 1.13: Evrard's implementation for a collaborative transportation task.

In [19], Evrard used an engineering approach inspired from Kosuge's [43], where the

robot's grippers behave as a mass-damper system attached to the object on the horizontal plane as illustrated in Fig. 1.13. On the vertical axis, the robot carries half of the object weight. This is more or less the same dynamic behavior as a supermarket's trolley. Regarding the robot's locomotion, when the difference between the arm and the supporting feet goes beyond a predefined threshold, a step is planned to recover the offset at the next step. Thus the gait generation is decoupled from the upper-body motion of the robot.

This is an example of "Hands guide Body", since the mass-damper behavior is implemented in the world frame, independently from the CoM's motion.

1.4.2 Proactive Approach

All these approaches implement a pure passive behavior of the robot and lack proactivity. Lawitzky *et al.* [46] proposes to mix learning and planning approaches to implement a more proactive behavior. Learning methods allow the robot to predict the human partner's intentions but only after several trials. Besides the robot loses proactivity as uncertainty increases. In contrast, planning provides the robot with an active behavior. In [46] the robot has the knowledge of both the environment and the goal position. Therefore, the robot is able, at every time, to plan a trajectory to reach the goal position. However, using only planning would let no choice to the human partner but to follow the robot. This is why mixing both planning and learning is interesting. Two successful blends are proposed: one based on uncertainty, the other on a cost to go. With the first strategy, the robot realize a linear homotopy blending of both learned and planning controllers, where the homotopy parameter is the certainty of the learning algorithms: if the certainty is high, the learned controller dominates, while the robot falls back towards the planning controller when uncertainty decreases. In the second strategy, the planning controller modifies, if necessary, the output of the learned controller output to maximize its scalar product with the planning output. In other words, if the output of the learned controller output is roughly in the same direction as the planning output (positive scalar product), it is not modified. However, if the scalar product is negative, the learning controller output is rotated to form a right angle with the planning output. Both methods endow the robot with proactivity due to planning, while allowing an adaptation to the human through learning.

The main drawback of this approach is that it is specific to goal-directed tasks, i.e. tasks where the final goal is known and shared by the robot and the human. It is also necessary that the robot has a full knowledge of the environment –the obstacles mainly– in order to plan the task.

1.5 Conclusion

Physical Human-Robot Interaction aims at endowing robots with the capacity to interact physically with humans so that they can share our everyday environment, that is our homes and offices, and also assist humans in everyday life.

The first concern that arises is safety. Robots must not harm humans, nor themselves,

during interaction. Impedance control is a major advance in this regard, as it allows giving safe dynamic behaviors to robots: impedance control is helpful for limiting the mechanical power exchanged between the robot and its environment. Because of its efficiency and simplicity, it has become very widespread in the literature. Using passive impedance constraints, robots were quickly able to perform transportation tasks with humans. The advantage of this approach is twofold: it is easy to implement, and it requires no knowledge of the human's intentions. In this regard, it can be considered as the reference to which any other implementation of pHRI should be compared.

This success was followed by many leads of improvements. Indeed, with a passive dynamic behavior, the robot is adding a load on the human partner. Notably, robots were not as efficient as humans in performing collaborative tasks. Many strategies were proposed to alleviate this load. And in order to endow robots with human-like capacities to collaborate with humans, as proactivity, researchers turned to neuroscience. However, human-human joint actions are only starting being studied [60] and no model exists. Human motion models for specific tasks, such as the minimum jerk model, exist and successful applications were derived from it in pHRI. However, such approaches remain restricted to specific motions.

This problem of the specificity of approaches is global to the pHRI field. Most approaches are very task specific, i.e. they cannot be reused or generalized to other tasks. Learning methods can also be considered task specific. They can certainly be employed to learn various tasks, but robots are not yet able to use the learning of one given task to be proactive another one. Other approaches rely on particular cases, where the robot has some knowledge about the task, such as the final goal of the task and/or the environment. Each contribution consists in a little piece of intelligence gained by robots, a global strategy to endow robots with the ability to interact with humans in various situations remains to be found. Much remains to do in the pHRI field. And with such promising benefits for society –the widespread of robots in society– it is easy to understand why it is and will be an attractive and promising research field.

In the next chapter, we present a study about how human dyads perform a one degree-of-freedom task and which observations we can apply to improve human-robot interaction.

2 Monitoring human haptic joint action: 3 cases study

Contents

In the previous chapter, we presented the various approaches to implement pHRI. We highlighted that an engineering approach could let the human operator move the beam with the robot, but had several drawbacks. The major problem was a lack of pro-activity.

In this chapter we study several tasks performed by a human-human dyad in order to enhance the behavior of a humanoid robot performing the same tasks with a human partner. We use a motion capture system along with force-torque sensors to monitor three different tasks performed by eight dyads. The three tasks concern jointly moving a table-like object; one of the tasks involves locomotion. We narrow our observations to the sole locomotion task.

Our observations focus on the coupling between the gait and the motion of the subjects' hands, as well as on the synchronization between the two partners' gaits. We also identified a model of the task during locomotion; it consists in a decomposition of the object motion into subtasks: acceleration, deceleration and constant velocity phases.

2.1 Ground Reaction Force Measurement Systems

Measuring the force applied by a foot on the ground is not always simple. Firstly, the terminology "force applied by a foot on the ground" is inaccurate as it can be understood as the complete distribution of the contact forces between the foot and the ground or as the net reaction force between them. To our best knowledge, no system to measure the former exists. However, floor or in-shoe systems to measure the distribution of foot pressure on the ground exists. A result of such measures is shown in Figure 2.1. Such measurements lack the horizontal components and therefore do not allow calculating the net ground reaction force.

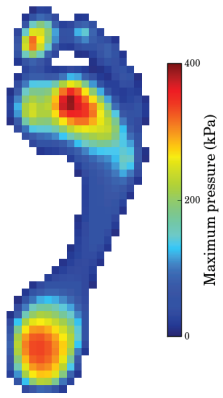

Figure 2.1: Example foot pressure distribution.

The most widespread system to measure the net contact force between the foot and the ground are force plates (Figure 2.2). Force plates allow monitoring the net ground reaction force, the position of the center of pressure and the vertical moment of force, which can be used to compute the full net ground reaction torsor. Similarly to optical motion capture with markers, this technique is the reference for net ground reaction force measurement in biomechanics research. The drawbacks of this technique is that the force plates are fixed to the ground. Several of them are needed to fully monitor large scale motions, and the subject must step on it.

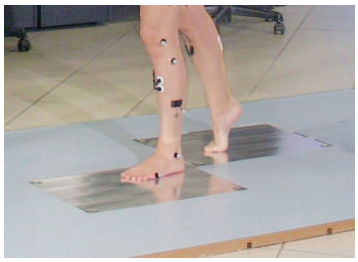

Figure 2.2: Subject walking on force plates.

2.1.1 Design of Foot-located Force Measurement System

To address the drawbacks of force plates, we need a foot-located force measurement system. Its requirements are to measure the net ground reaction torsor of the foot while impairing the subject's walking as less as possible. An in vivo technique allows measuring the Achille tendon load with an optic fiber [22], as the load is related to the fiber's deformation. However, we do not consider it in our study because it requires a medical procedure.

As no commercial portable system was available to measure the force under the feet, we designed our own. The basic idea is to fix a force-torque sensor on each foot of each subject. We have ATI Mini45 FT sensors at our disposition. They are compact enough to be placed under the foot (height: 16mm, diameter: 45mm, weight: 92g). Their vertical force range $F_{z,max}$ of 1160N is enough to measure the net ground reaction force during walking, as the maximal force intensity during gait is approximatively 130% of the body weight. The subject maximal mass m_{max} is therefore around 91kg (Eq. (2.1)).

$$m_{max} = \frac{F_{z,max}}{1.3g} = \frac{1160}{1.3 \times 9.81} \approx 91kg \tag{2.1}$$

where g is the gravitational acceleration intensity.

The force sensor is mounted between two thin foot-shaped plates of aluminum, and a sole is glued to the lower aluminum plate. Unfortunately, the force sensor is quickly saturated on its torque components. The torque range τ_{max} is 20Nm. Thus, the distance d to the center of the sensor one needs to apply the force $F_{z,max}$ to saturate the sensor in torque is about 17mm (Eq. (2.2)).

$$d = \frac{\tau_{max}}{F_{z,max}} = \frac{20}{1160} \approx 0.017m \tag{2.2}$$

Moreover the system is too rigid, which impairs the subject's gait. Liedtke et al. developed a functional similar system [47], the ForceShoe™system, with two sensors on each foot, which is shown in Figure 2.3. This system has only recently been commercialized by Xsens[1].

[1] `http://www.xsens.com/en/general/forceshoe`

Figure 2.3: ForceShoe™system. Each shoe is composed of two force sensors and two motion sensors.

2.1.2 Choice for the study

Because of the non-availability of a robust and portable ground force measurement system, we did not monitor the net ground reaction force during the transportation task experiment.

2.2 Experimental Setup

Figure 2.4: Experimental setup. The operational volume is a rectangular parallelepiped (4m long, 3m large and 2m high). The operational volume is separated in two zones: one with force plates in the foreground, one for the locomotion task in the background.

2.2.1 Tasks and Scenarios

Our purpose is to study the transportation of a table-like object by two human partners. For simplicity, we restrict the transportation to one direction. Even so, the task is complex in the sense that it involves both manipulation and locomotion, and it might be difficult to find an invariant. Therefore, we also monitor two more elementary tasks where the subjects move the object together without walking, in which an invariant might be found more easily. In total, three tasks are monitored.

For the first task (1D task), the two subjects are asked to move the object horizontally while standing on forces plates shown in Figure 2.4. They have to move it to one side of the dyad (always the same for all dyads, imposed by the experimenter), then, without marking any pause, move it back to the other side, and finally back to the start position, as shown on Figure 2.5 (left).

The second task (2D task) is similar to the 1D task, except that the subjects are to move the object both horizontally and vertically. The imposed trajectory of the object is square-shaped : to one side, up, to the other side, down, and back to the start position (Figure 2.5, middle).

The last task is a locomotion task in which the subjects move the object over a few meters – one subject walks backwards, the other forwards – and turn back to come back to the initial position (Figure 2.5, right).

In all scenarios, the subjects are asked to maintain the object's orientation as constant as they can.

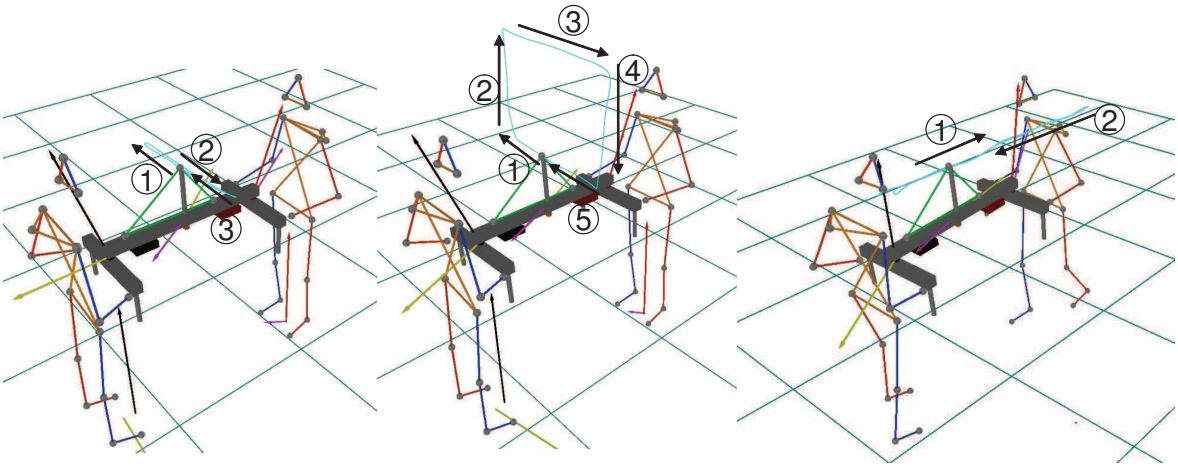

Figure 2.5: Tasks Description. From left to right : the 1D task, the 2D task and the locomotion task.

For each task, we define three scenarios with different role assignments :

- No role assignment (Free)
- Subject 1 is leader, subject 2 is follower (1L2F)
- Subject 1 is follower, subject 2 is leader (1F2L)

The different assignments are always acquired in this order so that the subjects are not spoken of role assignment for the no-role-assignment scenario. The start signal of the task is given by the experimenter in the first scenario, and is left to the appreciation of the leader in the two last.

2.2.2 With or without Visual Perception

Although our HRP-2 robot has video cameras, we do not intend to use visual perception to perform a collaborative task with a human partner. Apart from its cameras, the robot has sensory feedback from

- its encoders, to measure its joints position
- an accelerometer and a gyroscope, to measure the translational and rotational acceleration of its chest in the world Cartesian frame (position and orientation are estimated from these measures with a Kalman filter)
- four 6-axis force sensors in its feet and at its wrists.

The question arises whether the subjects should be blindfolded or not. For instance, consider how a following partner detects when the leader starts the task. Here is a case that is observed in some of our data. The leader starts backwards and the follower forwards. At start-up, the leader initiates a step backwards. To do so, he slightly bends forwards for equilibrium, thus pushing slightly the object, applying a force in the opposite direction he intends to go. Once the step is initiated, the leader pulls on the object. Note that in our experimental setup, if the follower does not know in advance when the leader starts the task, he does know the starting direction. Therefore, the push on the object cannot be misinterpreted. Our point is rather that, in this example, the follower detects the start of the task thanks to visual perception of the leader starting a step rather than haptic cues.

Blindfolding the subjects ensures that the subjects do not rely on visual perception to collaborate and thus rely mostly on haptic cues. However, it may greatly disturb them; they are likely to be more cautious and not to perform the task as they would with visual feedback. In other words, they would perform the task poorly, not because they do not have enough sensory feedback to do it, but rather because they do not have as much sensory feedback as they are used to. And we want our robot to perform the task as a non-blindfolded human being would.

For these reasons, we do not blindfold the subjects.

2.2.3 Data Acquisition System

The forces and moments applied by the subjects on the object are measured by two ATI Mini45 FT sensors mounted on each side of the object. The forces and moments applied by the subjects on the ground during 1D and 2D tasks are measured by two force plates : an AMTI OR6-6-2000 and a Kistler 9281CA. All forces data are sampled at 500 Hz.

The subjects' postures are acquired using a Vicon WorkStation 624 system with five MCam2 cameras. An overall of 40 passive markers of 8 millimeters of diameter – 18 and 19 for the two subjects and 3 for the object – are used. The positioning of the markers is described in Figure 2.6. The trajectories of the markers are sampled at 100Hz.

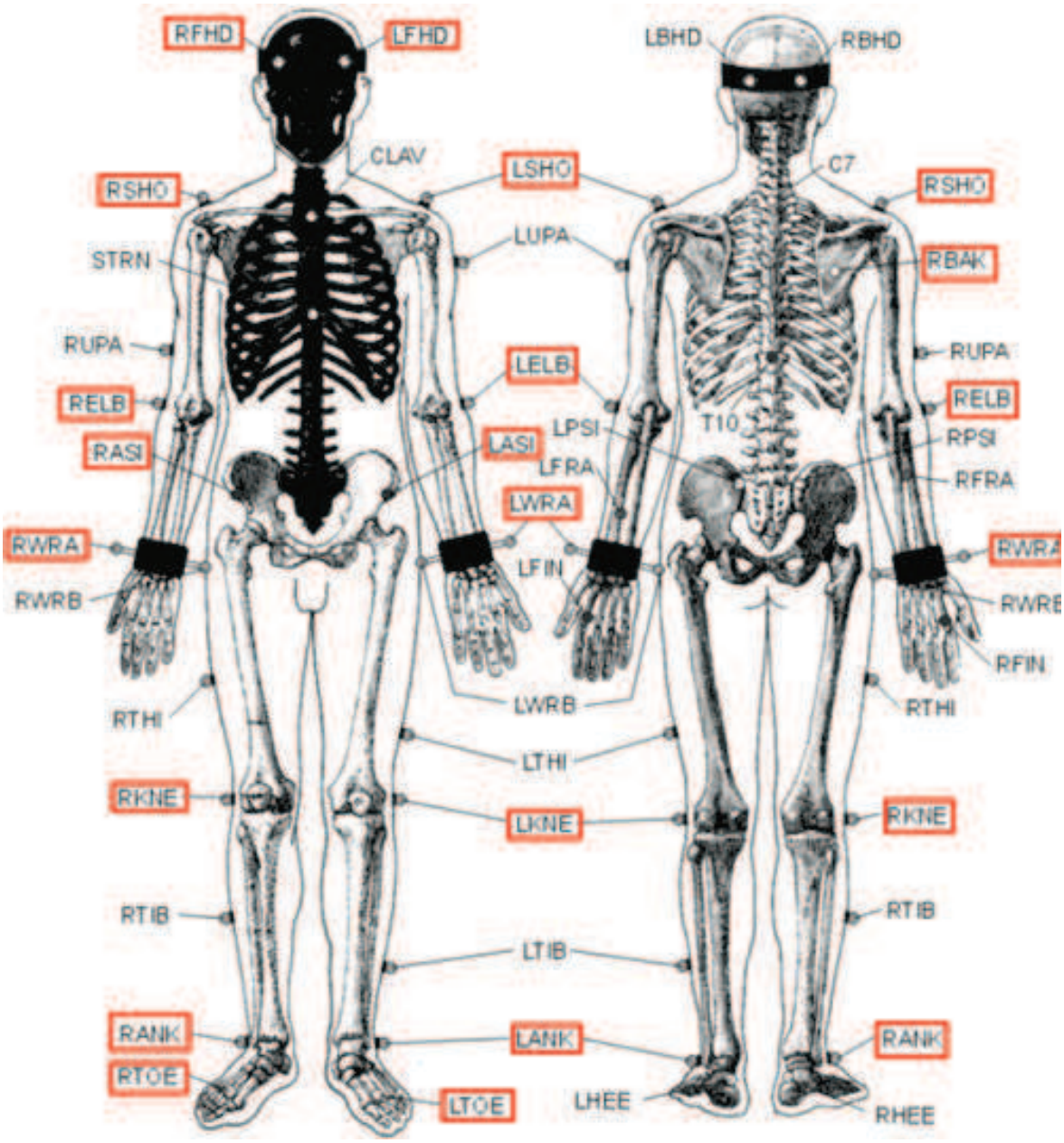

Figure 2.6: Plug-In-Gait Model: the default Vicon markers positioning for whole body motion capture. We use a subset of it (red boxes) to limit the number of markers and thus data processing.

The Vicon system is also composed of a Giganet which is an acquisition unit. It samples the data from the cameras as well as any plugged analog signal. Therefore we directly plug

the force sensors and the force plates on the Giganet, and external synchronization between the different signals is not required.

The table-like object is specifically designed for the experiment, as we need the force-torque sensors to be mounted on it. Moreover, it has to be as non-obstructive as possible in order to avoid markers' occlusion: the table plate is replaced by a simple beam. Besides, a cylindric rod is added on the middle of this beam, so that we can add more load if necessary. The object weights 10kg. The object can be divided into three parts:

- the handles for subject 1,
- the handles for subject 2,
- the middle part.

This division is important because the force sensors are mounted between the handles and the middle part and therefore measure the forces and torques applied on the middle part.

2.2.4 Subjects

We acquire data with sixteen healthy subjects (eight dyads), aged 14-32 (mean 25), four female, twelve male, fifteen right-handed, one mixed-handed. For every dyad, we acquire each couple task-scenario five times, which gives a total of forty-five acquisitions by dyad.

2.3 Observations

Our purpose is to program a humanoid robot so that it can perform the transportation task with a human partner. Thus we focus on the study of the locomotion task.

The locomotion task involves both object manipulation and walking, each of which has been extensively studied separately. It has been demonstrated that human beings perform point-to-point movements with roughly straight hand trajectories [23] and a bell-shaped velocity profile [24]. However, the curvature of the hand trajectory increases when subjects are asked to move the hand very quickly [23]: the subjects trade straightness of trajectory for higher velocity.

Adding locomotion requires whole body coordination. For instance, consider the task of carrying a bottle. To prevent the bottle from falling from the hand, one compresses the bottle to produce a vertical friction force. The heavier the bottle is, the tighter the grasp must be. It is also the case if an additional vertical force is applied on the bottle. During the gait, the heel periodically strikes the floor and produces an impact force on the body, which slightly accelerates the bottle vertically. Thus, walking with the bottle requires a tighter grasp. One strategy might be to apply a constant tight grasp on the bottle. Gysin et al. demonstrate that the human adapts the grasping force s/he applies on the object to absorb the additional inertial forces during the gait [26] [27]. Furthermore, the authors show that the human anticipates these inertial forces rather than sense them and react.

This example shows that walking while performing a task can be more complex that just walking and performing the task, as new problematics arise from the coupling. Therefore, one major problematic in our study is: how does walking impact the object transportation?

2.3.1 Data Visualization with AMELIF

Since the visualizer provided with the Vicon software does not allow vizualizing data from floating position force sensors, we use our dynamic simulation framework AMELIF [39] to visualize the data as in Figure 2.7. The Vicon software only allows visualizing forces measured by immobile force plates.

As a dynamic simulator, AMELIF provides functionalities to visualize kinematics and also forces applied on any point of an object. Each marker is represented by a gray ball. Markers are linked by colored segments to visualize whole body motion. Note that the segments' motion does not correspond exactly to the motion of the subjects' skeleton, because the markers are not positioned at the center of the articulations. We also design a dynamic model of the table-like object carried by the subjects. Forces and moments are displayed at the center of the force sensor that measured them. The moments are also displayed at the Center of Mass (CoM) of the object's middle part.

A Graphical User Interface (GUI) was added to AMELIF, using the wxWidgets[2] library, so that the data could be played at various speeds (from 1/8x to 8x) or frame by frame. The GUI also featured a playlist to load different trials and plot data of interest with MATLAB.

Moreover AMELIF already integrates dynamic models to simulate the dynamics of poly-articular bodies. It is possible to replay a motion captured scene dynamically with a more complete experimental set-up that would allow us to identify the dynamics of the subjects during the tasks. It can even be used to recalculate the dynamics.

2.3.2 Hip Swing Compensation

While walking, human beings swing their hip laterally to the direction of walking in order to keep balance. This lateral swing affects the trajectory of the subject's wrists and therefore the object's: it is a coupling between the gait and the manipulation. An example is shown in Figure 2.8. The temporal curve of Figure 2.8 (right) supports the hypothesis of a coupling between the hips' and wrists' lateral swinging motions as extrema are synchronized. In the present experiment, we investigate how the lateral swinging motion of the hips impacts the lateral swinging motion of the wrists in amplitude. In the following, we use the denomination *lateral swing* for the lateral swinging motion.

We consider the motion of the subjects hips and wrists projected on the horizontal floor. In other words, we do not consider the vertical component of these trajectories in the global frame.

The example shown in Figure 2.8 gives the intuition of what lateral swing is. It is an oscillatory motion around the general direction of walking. The subjects are asked to walk

[2]http://www.wxwidgets.org/

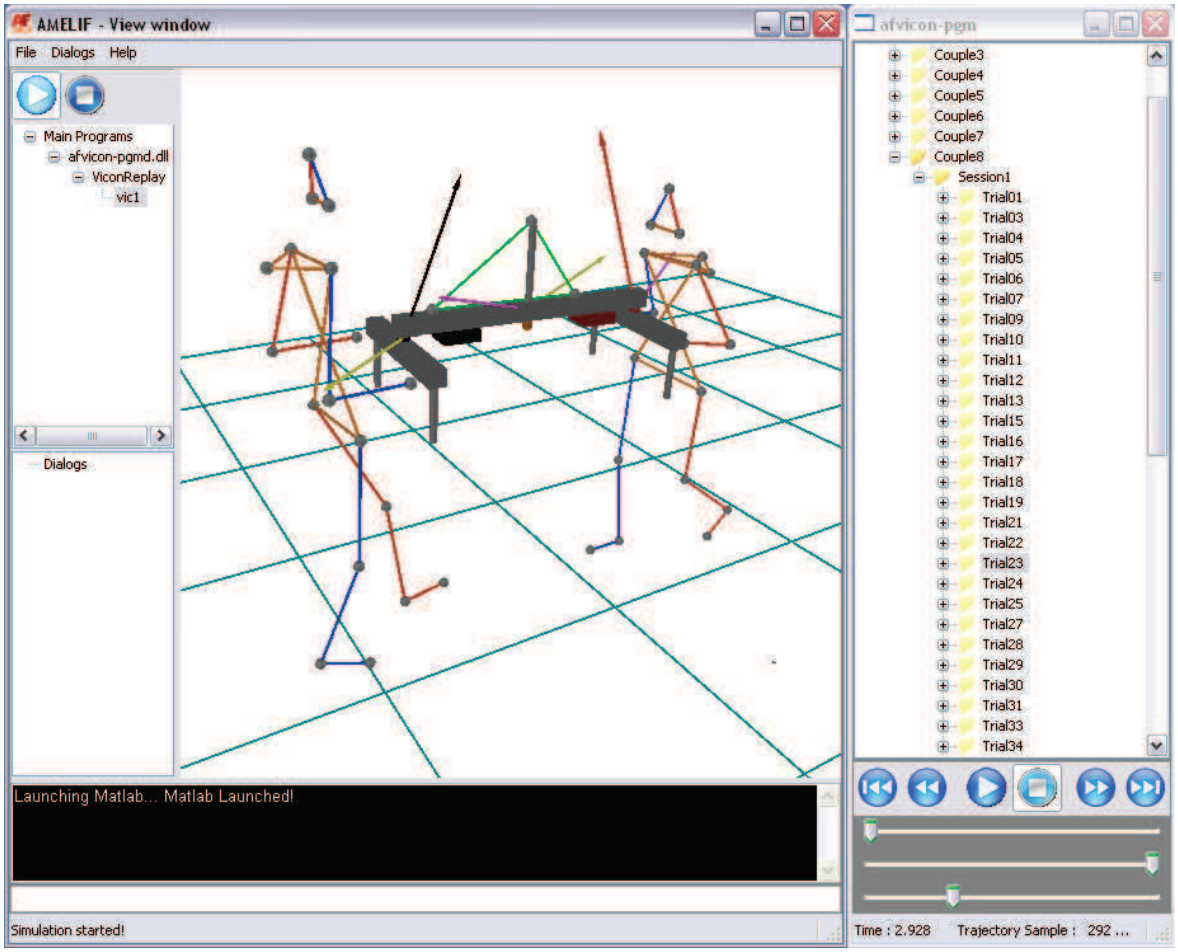

Figure 2.7: Visualization on AMELIF

along the x-axis. However, the trajectory of the hips indicates that in this case the subject slightly deviates from the x-axis. This deviation is less evident if we consider the trajectory of the wrists. To eliminate this deviation, we perform a Principal Component Analysis (PCA) to obtain a detrended parametrized trajectory $(x_{detrend}, y_{detrend})$, where the general direction of motion is the x-axis. Finally, we compute the global lateral swing amplitude a within

$$a = \max_t y_{detrend}(t) - \min_t y_{detrend}(t) \tag{2.3}$$

Because the amplitude of the lateral swing is not constant over a trial, because the general direction of motion may be slightly curved, this *global* amplitude is bigger than the *local* amplitude of each swinging motion and therefore than their mean. It must be seen as the maximum margin of the lateral swing for the considered trial. The histograms of the global amplitude of the lateral swings of the wrists and hips are shown in Figure 2.9. The hip lateral swing amplitude mean is 0.1424m (std 0.0406m) and the wrist lateral swing amplitude mean is 0.1099m (std 0.0343m). The statistics of their ratio show that most of the time the wrists lateral swing is dampened compared to the hips lateral swing.

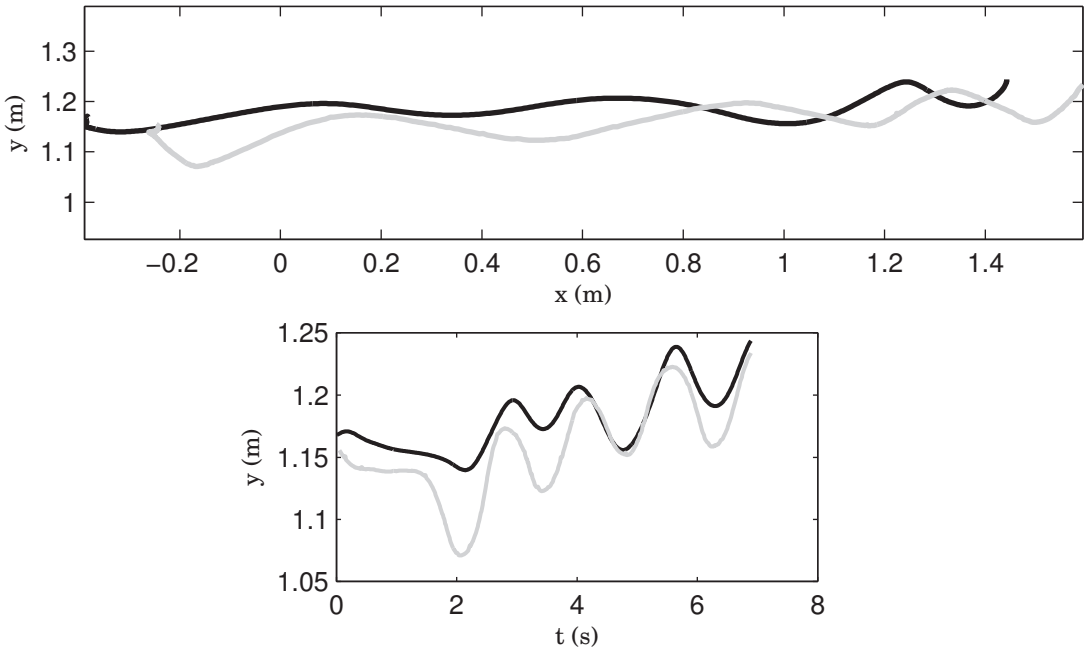

Figure 2.8: Example of swinging motion of the wrists (black) and hips (gray) in the XY-plane (top) and over time (bottom). The black and gray curves are the mean trajectories of markers RWRA and LWRA, and RASI and LASI respectively (See Figure 2.6. The subject walks from the negative x towards the positive x. The direction of swinging is y.

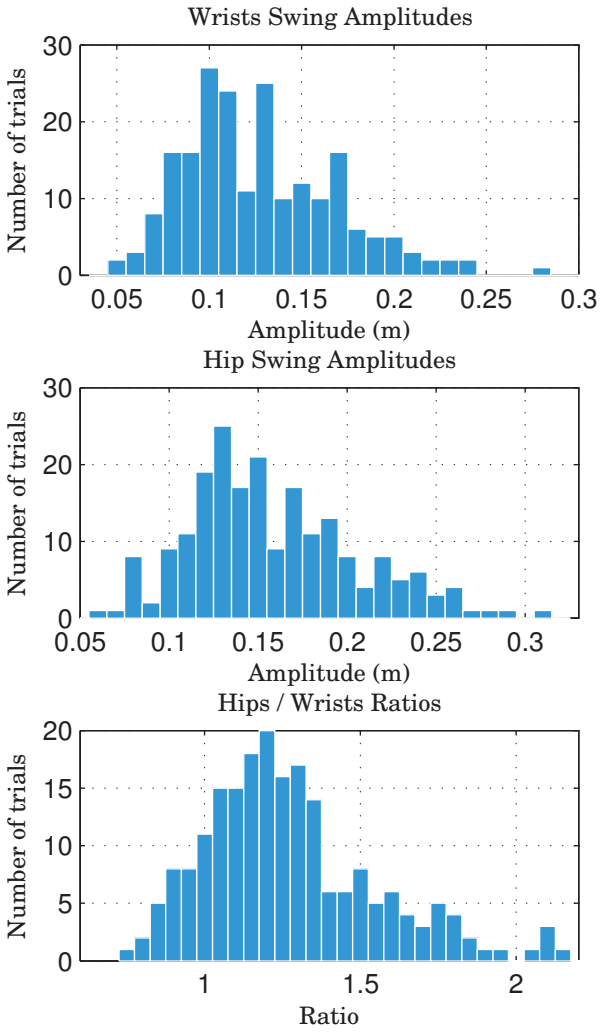

Figure 2.9: Swing amplitude margins of the wrists (top) and hip (middle) and their ratio (bottom).

This study of the lateral swing brings precious information. Firstly, it gives an indicator of the wrists lateral swing we should aim for when controlling our robot. The key length is 10 to 15 centimeters. Secondly, there is a coupling between the lateral motion of the wrists and the lateral motion of the hip; they are synchronized. Therefore the lateral motion of the hands is synchronized with the subject's gait. As both subjects are holding the object, they have to synchronize the lateral swing of their hands to keep the object's orientation constant. Consequently, by transitivity, we can make the assumption that the subjects have to synchronize their gait, which is studied is the next subsection.

2.3.3 Gait Synchronization

As we have seen in previous section, during the locomotion task, the motion of the subjects' hands is coupled to their own gait. And as both subjects are holding the same object, it is reasonable to assume that the subjects' gaits might be synchronized. Besides, if there is a synchronization, what is the synchronization pattern?

Firstly, their gaits *must* be coupled. Both subjects are holding the object and therefore they both have the same hands' velocity constraint. They must regulate their gait velocity to prevent the object from colliding with their torso or their arms to extend too much. In that way, they must at least synchronize their gait velocities. In the previous part, we have hinted that the gait might be perfectly synchronized, e.g. that both subjects might set the foot on and off the floor synchronously. Given the geometry of the task, there are two possible different synchronization patterns (Fig. 2.10), or *gait patterns*:

- the *lateral* synchronization. The feet on the same side are synchronized; as the subjects are facing each other, one subject's right foot and the other's left foot are synchronized (Fig. 2.11 bottom).
- the *diagonal* synchronization. The feet on the opposite side are synchronized; as the subjects are facing each other, the subjects' right feet are synchronized (Fig. 2.11 top).

We watch each trial with our visualizer (Section 2.3.1) to determine when gaits are synchronized or not. The statistics are reported in Table 2.1. It shows that synchronization is preferred (65.8% of trials) but in a large part of the trials (34.2%) a desynchronization occurs. It also shows that no specific gait pattern (lateral or diagonal) is preferred over the other.

However, synchronization does occur in two thirds of the trials, and these results do not show *why* it occurs. One possible explanation may be energy efficiency. Consider the analog example of rowing. If the rowers do not row synchronously, the boat moves more slowly and in a less straight direction than it would in the case of a synchronous rowing. Our task is similar, although the desynchronization has less drastic effects. For example, it causes strain on the upper body of the subject. Let's explain. Synchronization can also be observed at the hip of the subjects as in Figure 2.12. The subjects' hips are mechanically connected through each subjects' torso and arms and the object. The system torso and arm of each subject can be considered as a deformable body. For simplicity, we only consider the deformation in the direction of the motion. Because of the gait, the trajectory of both subjects' hips oscillates. If

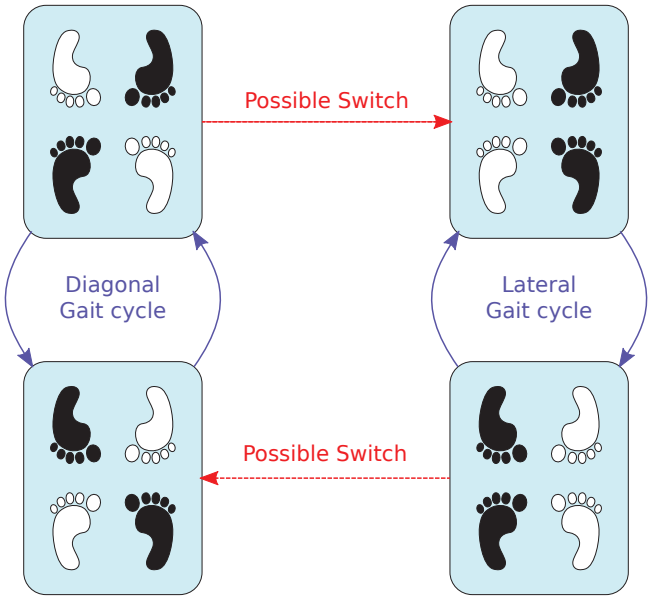

Figure 2.10: Gait Patterns of a synchronized walking dyad. Black feet represent the support feet, white feet represent the swing feet.

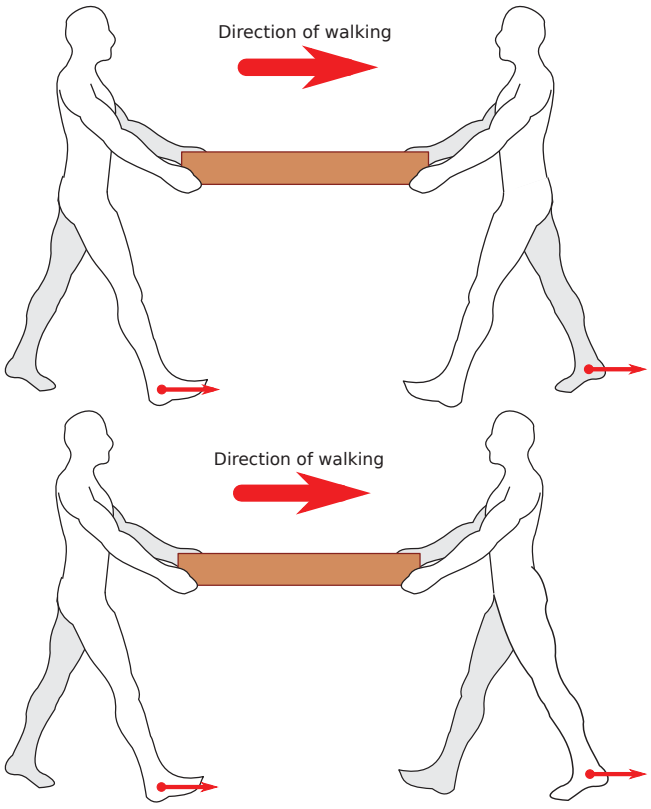

Figure 2.11: Diagonal (top) and Lateral (bottom) Gait Patterns. Small red arrows indicate the swinging legs.

Table 2.1: Steps synchronization patterns repartition in trials. Most of the time, dyads synchronize their steps in a two-beat gait, e.g. with synchronized footfalls. The synchronization can be either diagonal or lateral and a switch (→) may occur in the middle of the task. Desync denotes a non-synchronized gait. Other regroups more infrequent patterns, but they all contain a part with a non-synchronized gait (desync), as Lateral → desync → Diagonal for instance.

Step Pattern	Free	1L2F	1F2L	Total	Total (%)
Diagonal	7	5	10	22	18.3
Lateral	3	5	8	16	13.3
Diagonal → Lateral	10	9	7	26	21.7
Lateral → Diagonal	6	6	3	15	12.5
Diagonal → desync	7	5	2	14	11.7
Lateral → desync	1	2	5	8	6.7
Other	6	8	5	19	15.8
Total	40	40	40	120	100

these oscillations are not in phase, the subjects' torso and arms are compressed or stretched. The subjects might synchronize their gait by minimizing this strain.

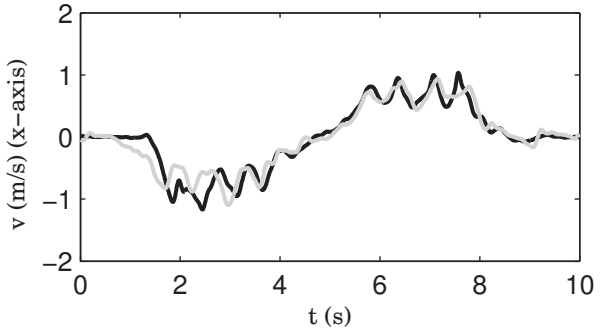

Figure 2.12: Velocities of hip markers in the motion direction (x-axis) for subject 1 (black, RASI) and subject 2 (gray, LASI). The oscillations in the velocities are caused by the gait. The oscillations in both subjects' hip velocities synchronize after a few steps.

However, in a non-negligible part of the trials, desynchronization occurs and no gait pattern was preferred, which shows that it does not impede the execution of the task. The consequence of this result is of prime importance for controlling our robot: *it is not necessary for a humanoid robot to identify the human partner's gait timings, nor the gait pattern, to plan a step: the knowledge of these timings and of the gait patterns is not necessary to control the locomotion of the robot during a joint transportation task.*

2.3.4 Phases Decomposition of the Motion

So far we have focused on how the subjects' gait impacts the lateral swing of their wrists and therefore the object's, and how both subjects' gaits are coupled. However, we have yet to study an essential part of the task: the object's motion. The goal of the task is to transport the table-like object along the x-axis, forwards and backwards. When visualizing the trajectory of the object's center of mass along the x-axis, in the global world frame, we notice three important properties:

- the object trajectory's shape is the same for all trials,
- the object trajectories are smooth in comparison to the subjects' hips trajectories,
- the object velocity is constant for a couple of seconds during the transportation.

These properties are confirmed when we plot the object velocity along the x-axis, as shown in Figure 2.13: *the object velocity shows a double-trapezoidal shape*. The object's motion can be decomposed this way:

- the object is not moving (initial state),
- the object accelerates forwards,
- the object moves forwards at constant velocity,
- the object brakes,
- the object is not moving (in some trials, this phase is not present),
- the object accelerates backwards,
- the object moves backwards at constant velocity,
- the object brakes,
- the object is not moving (final phase).

The object's motion is decomposed in a sequence of Constant Velocity Phases (CVPs) and Acceleration/Braking Phases (ABPs). In this study, as the operational volume is limited, the ABPs are almost as long as CVPs. However, with larger scale tasks, they become negligible and during these phases, velocity can be roughly approximated by an affine function of time. These phases – CVPs and ABPs – can be considered as subtasks. The decomposition of a task in subtasks is recurrent in the literature. When Flash studied point-to-point movements of the hand [23], the trajectory of the hand was described as a roughly straight line. However, Flash noticed that all trajectories ended with a hook. In this case, the task can be decomposed in two subtasks: a transportation task to get to the neighborhood of the target position and a positioning task to get to the target position with more accuracy. Reed [57] showed

that during a collaborative task, the subjects specialize: one subject takes the acceleration in charge while the other do the braking. This suggests that both partners decomposed the task into an acceleration subtask and a deceleration subtask; then each subtask was realized by one partner.

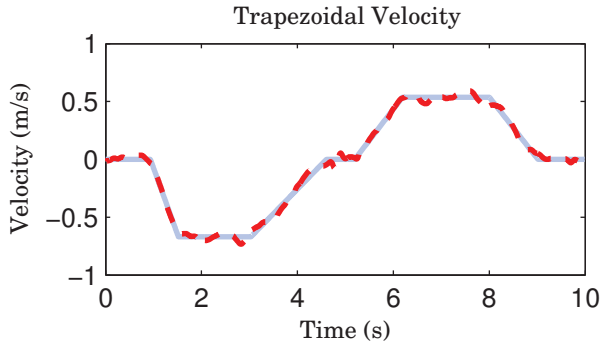

Figure 2.13: Trapezoidal Approximation (in light blue) of the object's velocity (in dashed red).

To support our observation, we fit all the object's velocities from our data with a five CVP decomposition. In other words, we fit each profile with a trapezoidal approximation as in Figure 2.13: for each trial, we seek to identify the forwards and backwards velocities (2 parameters) and the phases switch moments (8 parameters). Therefore we obtain a different trapezoidal approximation for each trial. However, any trapezoidal approximation can be transformed into another by scaling the time and amplitude *for each line segment*, thus defining a normalization transformation for each trial. Finally, we use this same transformation to normalize the measured velocities. All velocity profiles are successfully fitted with a trapezoidal approximation with a mean correlation coefficient of 0.997 (standard deviation: 0.0019). Normalized results are shown in Fig. 2.14. Contrariwise, the forces applied by each partner on the x-axis in the global world frame show no such similarities as pictured in Fig. 2.15.

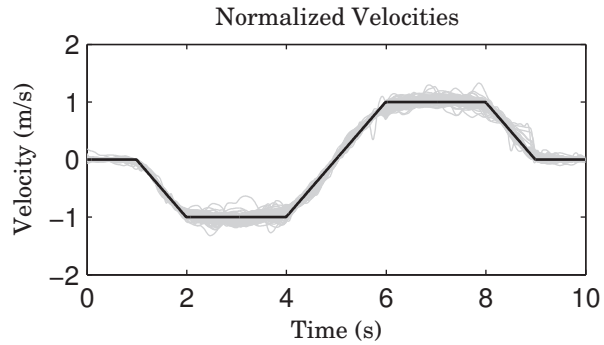

Figure 2.14: Normalized velocity (in gray) and the trapezoidal approximation (in black). Velocity profiles were normalized so that they have the same trapezoidal approximation. To cope with four and five CVP decomposition, we cut the middle-motion zero-velocity phase when it exists.

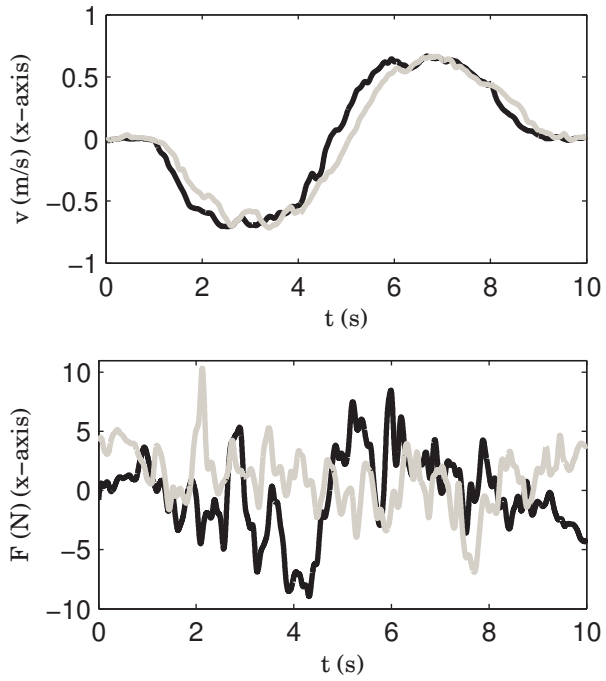

Figure 2.15: The top figure shows the velocity of the object on the x-axis in two consecutive trials with the same dyad (black, then gray curve). The curves are almost identical. The bottom figure shows the force applied on the object on the x-axis by the same subject in the same two consecutive trials. No evident force pattern can be identified.

During the CVPs, the object velocity is only roughly constant. The velocity slightly oscillates at the gait frequency, if not as much as the hip marker velocity as in Figure 2.12. This indicates that the upper body (torso and arms) plays an important role in damping the oscillatory disturbance the gait is, and thus partly decouples the transportation of the object from the gait.

To sum up, the locomotion task can be naturally described in the global world frame by a decomposition in subtasks that are identified (CVPs and ABPs). Besides, the motion of the object along the x-axis is mostly decoupled from the gait.

2.4 Conclusion

In this chapter, we have demonstrated that during a table-like object transportation, the gait can be considered as a disturbance on the object motion, that is more or less damped. The gait induces oscillatory disturbances – especially laterally – on the object motion. As we have demonstrated that synchronization between the two subjects' gait – in timing and gait pattern – is not necessary to complete the task, we can assume a minimal coupling between the transportation and the gait, that is that the object's and the gait mean velocities must be identical. This motivates our choice to use Herdt's Walking Pattern Generator [30] as a black box that reactively generates footsteps for our robot from the input of a desired center

of mass' velocity.

We have also shown that the transportation can be naturally described in the global world frame, with a good approximation, as a sequence of subtasks (Constant Velocity Phases and Acceleration/Braking Phases). This simple model of task has the advantage to be independent from the gait, as well as using the global world reference frame. In the next chapter, we will use this decomposition into CVPs and ABPs, that we name *motion primitives*, to implement a pro-active behavior on the HRP-2 Humanoid Robot.

3

Programming human-humanoid haptic joint actions from human dyad models

Contents

In the previous chapter, a psychophysical experiment with dyads transporting a beam revealed that they favour phases of constant velocity during motion. Our study also suggests that no gait pattern nor synchronization between the partners emerges during the task, therefore walking pattern generation can be decoupled from the arm coordination strategy.

From these observations, we propose in this chapter an impedance-based model for human-humanoid haptic joint action to perform a similar transportation task. We validate the approach on the HRP-2 humanoid robot. First, the formalization of the control strategy for a transportation task along one direction is presented. Then, we propose an extension of our approach in 3D, including turns.

3.1 Introduction

When two humans collaborate to perform the transportation of an object, such as a beam or a table, they are able to establish an intuitive coordination, guess the other partner's intentions and act accordingly. Mutual understanding of each other's intention translates into *proactive* behaviors and good cooperation and synchronization of the dyad during the task. Moreover, both partners may alternatively share the leadership of the task during its execution and take decisions such as turning or stopping, relying on the information they share and the context. In the course of the task, because one might know and/or perceive something the other does not, a share of the leadership is desirable [40]. Proactive cooperation that permits leadership switching and intuitive role distribution are two characteristics we want to reproduce with a humanoid robot performing such a task with a human partner (see illustration on Fig. 3.1): *proactivity* and *intuitive role switching*.

Early works on physical Human-Robot Interaction (pHRI) gave the robot a restricted role [42]. Its role was to carry a part of the object's vertical load at the cost of an increase of the horizontal 'load'. Such an approach forces the human operator to apply more forces than necessary in order to move the object due to the causality of the robot's control law. Proactivity aims at solving this problem: guessing the human partner's intentions in order to decrease this horizontal load. A possible approach is to regulate the robot's impedance according to the perceived intentions [13] [70] as outlined is Chapter 1. An alternative way to be proactive is to guess the human partner's intended trajectory. This is the approach chosen in [48] [10] and also the one we choose in this work. Note that both approaches are not exclusive.

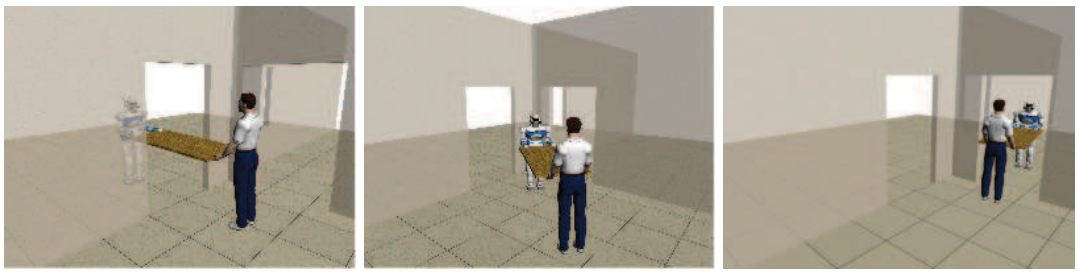

Figure 3.1: Example of scenario. The human-robot dyad has to carry the table through two doors that form a 90° angle. The dimensions of the table are too big to perform the task with a single bend, so that the human has to pass backward through the first door and forward through the second one. The human assumes the leadership of the task as he is walking backward through the first door, and then is guided by the robot through the second door.

Relatively to existing work, our approach distinguishes in its capability to guess the human partner's intentions for a wide variety of motions, while [48] and [10] only consider point-to-point movements. Furthermore, we distinguish the recognition of the partner's intended trajectory from the action undertaken to help him/her. Our proactive follower acts similarly to a leader. The difference is that it chooses to follow a trajectory determined from a guess of its partner's intentions rather than from its own volition. Thus the robot's dynamic behavior is independent from the role distribution; the role distribution only affects how the impedance nodic reference is planned.

In Section 3.2, we propose an impedance-based model for leader and follower modes and how it can be used for role switching. We describe how a motion decomposition allows to recognize intended trajectories in Section 3.3, and test our approach on the HRP-2 robot. Then we extend this approach to the 3D case in Section 3.4. Interactive planning and context perception are required for the robot to behave as a leader, which is beyond the scope of this thesis. Therefore we design the leadership for the robot as a human operator remotely controlling the humanoid robot with a joystick in Section 3.5. We test the global 3D scheme in Section 3.6 by making the HRP-2 humanoid robot perform the transportation scenario of Fig. 3.1 with a human partner.

3.2 Impedance based model for haptic joint action

3.2.1 Context

In this chapter, we are interested in the transportation of a rigid beam-shaped object from one place to another over several meters. Thus it requires locomotion. This task is performed by two partners: a human and a humanoid. Such a task does not require a complex manipulation of the object, so that both partners always grip the object at the same positions. We also assume they use both their hands.

3.2.2 Requirements and desired behavior

We choose an impedance model for the low level dynamic behavior of the robot during a collaborative task, since it has been extensively used in the pHRI field for decades. As seen in Chapter 2, human dyads favor constant velocities (in the Cartesian world frame), which motivates our choice of an impedance model in such a frame.

The purpose of this section is to design an impedance model for human-humanoid physical interaction that can be used for both leader and follower modes. In [17], Evrard proposed the following homotopy impedance model

$$\mathbf{F} = (1-\alpha)\Big[-M_F\ddot{\mathbf{X}} - B_F\dot{\mathbf{X}}\Big] + \alpha\Big[B_L(\dot{\mathbf{X}}_d - \dot{\mathbf{X}}) + K_L(\mathbf{X}_d - \mathbf{X})\Big] \tag{3.1}$$

where $\mathbf{X}$ is the end-effector trajectory in the world frame, $\mathbf{X}_d$ is the impedance nodic reference in leader mode, $\mathbf{F}$ the force applied on this end-effector, M_F and B_F (resp. B_L and K_L) are impedance parameters in a pure follower mode (resp. pure leader mode). Here the homotopy parameter α might vary in $[0, 1]$ over time, and thus allows a smooth switching between a leader ($\alpha = 1$) and a follower ($\alpha = 0$) impedance model.

A drawback in this approach is the necessity to design and tune two models, e.g. the impedance parameters M_F, B_F, B_L and K_L in this case. But more importantly, the global stability of the homotopy controller is not guarantee when α vary in $[0, 1]$, as pointed out in [40]. In the following, we thus fix constant impedance parameters – inertia, damping and stiffness – and focus on how to determine the impedance nodic reference $\mathbf{X}_d$ depending on the mode.

3.2.3 Notations and Hypotheses

In this work, we only study translations, as well as rotations around the vertical axis (of the flat and horizontal ground, i.e. the axis aligned with the gravity field). Therefore we adopt a 4-dimension Cartesian notation in the world frame for the vector of forces $\mathbf{F}$ and the vectors of positions $\mathbf{X}$.

$$\mathbf{X} = \begin{bmatrix} x \\ y \\ z \\ \theta \end{bmatrix} \qquad \mathbf{F} = \begin{bmatrix} f_x \\ f_y \\ f_z \\ \tau_z \end{bmatrix} \tag{3.2}$$

In the following, we consider constant impedance parameters M, B and K so that we only deal with second order differential equations with constant coefficients. Besides, we choose the impedance parameters matrices to be symmetric positive definite. Thus every solution converges asymptotically to a particular one. To remain independent from the initial conditions, we adopt a *class representation* of the solution of such differential equations. We note $\bar{\mathbf{Y}}$ the set of solution where $\mathbf{Y}$ is a particular solution, and keeping in mind that every solution in $\bar{\mathbf{Y}}$ asymptotically converges to $\mathbf{Y}$.

Unless specified otherwise, all variables are time-dependent.

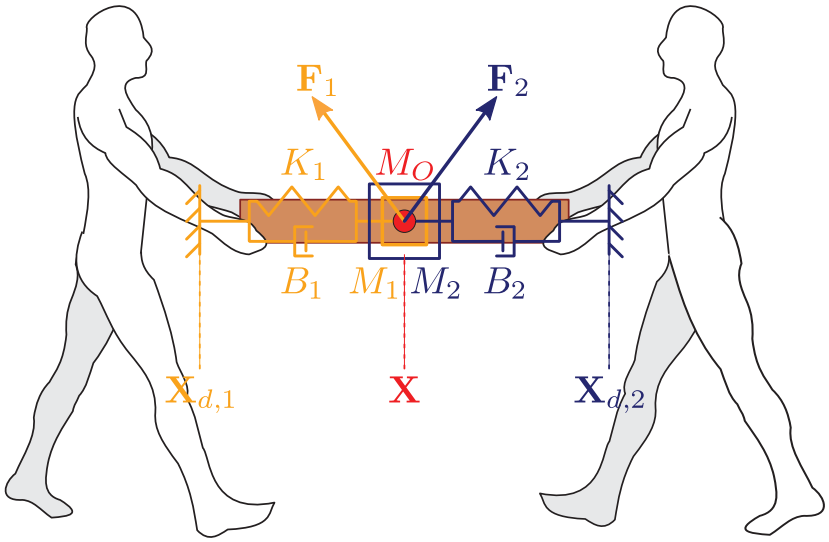

Figure 3.2: Impedance Model.

3.2.4 Proposed Impedance Model

In this section, we study a model of haptic joint action where two partners jointly transport a rigid object. We model the interaction between each partner and the object with a linear impedance constraint in the world frame

$$\mathbf{F}_i = M_i(\ddot{\mathbf{X}}_{d,i} - \ddot{\mathbf{X}}) + B_i(\dot{\mathbf{X}}_{d,i} - \dot{\mathbf{X}}) + K_i(\mathbf{X}_{d,i} - \mathbf{X}) \tag{3.3}$$

for $i \in \{1, 2\}$, where $\mathbf{X}$ is the object's Center of Mass (CoM) trajectory in the world frame, $\mathbf{X}_{d,i}$ is the intended trajectory for the object's CoM by partner i, and $\mathbf{F}_i$ is the force applied at the object's CoM by partner i. M_i, B_i and K_i are the inertia, damping and stiffness matrices, and are constant symmetric positive definite. These impedance parameters are the projection of the i-th partner's arms dynamic behavior in the operational space. This model implies that both partners are interacting at the object's CoM, as in Figure 3.2, which is not true in practice since they are holding the object at different points and with both hands. Moreover, we might wish to express a partner's impedance at a point that is neither the object's CoM, nor the grasping point, but any point that is rigidly linked to the object, as we do in Section 3.4.4. These problems are partially addressed in Appendix A.

The object's inertia at CoM is

$$M_O = \begin{bmatrix} mI_3 & 0 \\ 0 & I_\theta \end{bmatrix} \tag{3.4}$$

The only forces exerted on the object are the forces from each partner $\mathbf{F}_1$ and $\mathbf{F}_2$ and the gravity $M_O\mathbf{G}$ where $\mathbf{G} = \begin{bmatrix} 0 \\ 0 \\ -g \\ 0 \end{bmatrix}$. Thus its motion is governed by the simple following

dynamic equation

$$M_O(\ddot{\mathbf{X}} - \mathbf{G}) = \mathbf{F}_1 + \mathbf{F}_2 \tag{3.5}$$

At first, we suppose that both partners have the same intended trajectory $\mathbf{X}_d$ for the object in the impedance constraint (3.3). Substituting $\mathbf{F}_1$ and $\mathbf{F}_2$ in equation (3.5) using (3.3) yields

$$M_O(\ddot{\mathbf{X}}-\mathbf{G})+(M_1+M_2)(\ddot{\mathbf{X}}-\ddot{\mathbf{X}}_d)+(B_1+B_2)(\dot{\mathbf{X}}-\dot{\mathbf{X}}_d)+(K_1+K_2)(\mathbf{X}-\mathbf{X}_d)=0 \tag{3.6}$$

whose solution is not $\bar{\mathbf{X}}_d$ in general. The dynamics of the object bias the trajectory that deviates from $\mathbf{X}_d$, so that it is not accurately realized. To solve this, we add a prediction of the object dynamics, as a feed-forward, to equation (3.3) which becomes

$$\mathbf{F}_i = \alpha_i M_O(\ddot{\mathbf{X}}_d - \mathbf{G}) + M_i(\ddot{\mathbf{X}}_d - \ddot{\mathbf{X}}) + B_i(\dot{\mathbf{X}}_d - \dot{\mathbf{X}}) + K_i(\mathbf{X}_d - \mathbf{X}) \tag{3.7}$$

with $\alpha_1 + \alpha_2 = 1$, so that (3.6) yields

$$(M_O + M_1 + M_2)(\ddot{\mathbf{X}} - \ddot{\mathbf{X}}_d) + (B_1 + B_2)(\dot{\mathbf{X}} - \dot{\mathbf{X}}_d) + (K_1 + K_2)(\mathbf{X} - \mathbf{X}_d) = 0 \tag{3.8}$$

whose solution is $\bar{\mathbf{X}}_d$.

Equation (3.8) shows that if one can correctly predict the dynamics of the object for the intended trajectory $\mathbf{X}_d$, i.e. its inertia and all the forces exerted on it, it is possible to use this prediction as a feed-forward and adapt the impedance constraint so that the desired trajectory $\mathbf{X}_d$ is reached. In our case, it means estimating the object inertia matrix M_O. This is the case for the object mass, which can easily be evaluated at the experiment start-up by measuring the force vertical component. In our implementation we neglect the rotational inertia I_θ and estimate it as zero.

3.2.5 Behavior in Collaborative Mode

In previous section, we supposed that both partners shared the same intended trajectory $\mathbf{X}_d$. Here we study what happens when they do not. More importantly, we want to determine what information one partner can deduce about the other partner's intended trajectory from haptic cues, when considering the model of Fig. 3.2.

3.2.5.1 Hypotheses

We make the following hypotheses

- **Perfect Self-Knowledge:** Each partner has a perfect knowledge of its own impedance parameters M_i, B_i and K_i, and its own intended trajectory $\mathbf{X}_{d,i}(t)$.
- **Model Symmetry Projection:** Each partner projects its own model on the other, e.g. each partner assumes the other functions with the same model as him. In this case, it results in the perfect knowledge of the whole system structure of Fig. 3.2.
- **Other's Parameters Ignorance:** Each partner has no a-priori knowledge of the other partner's impedance parameters M_j, B_j and K_j, nor its intended trajectory $\mathbf{X}_{d,j}(t)$.

The haptic cues each partner has access to are the force $\mathbf{F}_i$ he/she applies on the object and the trajectory of the object $\mathbf{X}$. Our findings in Chapter 2 suggest that human dyads tend to prefer constant velocity phases. Therefore, we will suppose constant velocity intended trajectories for each partner, that is

$$\mathbf{X}_{d,i}(t) = \mathbf{V}_{d,i}t + \mathbf{X}^0_{d,i} \tag{3.9}$$

for $i \in \{1, 2\}$, where $\mathbf{V}_{d,i}$ and $\mathbf{X}^0_{d,i}$ are constant. Note that this assumption is not valid in transition phases. However, during transition phases, our model strongly depends on initial conditions we do not know, which is why we rather focus on the asymptotic behavior of the model.

As in equation (3.7), we assume both partners are sharing the gravity load so that the term $M_O\mathbf{G}$ cancels out from the object dynamics. Thus, for simplicity, we do not write this term anymore, and the object dynamics when manipulated by two partners can be simply written as

$$M_O\ddot{\mathbf{X}} = \mathbf{F}_1 + \mathbf{F}_2 \tag{3.10}$$

where the only external forces applied on the object are the forces $\mathbf{F}_1$ and $\mathbf{F}_2$ applied by the partners 1 and 2 respectively.

3.2.5.2 Results

Given the previous hypotheses, we demonstrate the following three results:

1. **Average Object Velocity:** The resulting object velocity converges to the mean of the partners' intended velocities, weighted by their stiffness, which corroborates the findings in [50],
2. **Increasing Internal Forces:** A difference of constant intended velocities between the partners leads to increasing internal forces over time,
3. **Partner-wise Velocities Formula:** A difference of constant intended velocities between the partners is linearly linked to a difference between the intended velocity of each partner and the object velocity.

The main result is Result 1. We obtain it by solving the object dynamics given our model. Results 2 and 3 are corollaries of Result 1 obtained by using it to compute forces (Result 2) and the other partner's velocity (Result 3). One important consequence of these results is that it is not possible for one partner to estimate the other's intended velocity without some knowledge about his/her stiffness parameters.

3.2.5.3 Demonstration

Using the hypothesis of a constant velocity intended trajectory, we write the impedance constraints (3.7) for each partner, without gravity compensation

$$\mathbf{F}_i = -M_i\ddot{\mathbf{X}} + B_i(\mathbf{V}_{d,i} - \dot{\mathbf{X}}) + K_i(\mathbf{V}_{d,i}t + \mathbf{X}^0_{d,i} - \mathbf{X}) \tag{3.11}$$

Substituting F_1 and F_2 in the object dynamics (3.10) yields

$$M_O\ddot{\mathbf{X}} = \sum_{i=1,2} -M_i\ddot{\mathbf{X}} + B_i(\mathbf{V}_{d,i} - \dot{\mathbf{X}}) + K_i(\mathbf{V}_{d,i}t + \mathbf{X}^0_{d,i} - \mathbf{X}) \tag{3.12}$$

Our goal is to find a particular solution toward which any other solution converges over time. To that end, we regroup all terms in $\mathbf{X}$ on the left-hand side

$$(M_O + M_1 + M_2)\ddot{\mathbf{X}} + (B_1 + B_2)\dot{\mathbf{X}} + (K_1 + K_2)\mathbf{X} = \sum_{i=1,2} B_i\mathbf{V}_{d,i} + K_i(\mathbf{V}_{d,i}t + \mathbf{X}^0_{d,i}) \tag{3.13}$$

We have a linear differential equation in $\mathbf{X}$ with a first order polynomial as a second member. In this case, a conventional method to find a particular solution $\mathbf{X}_p$ is to look for it as a first order polynomial, e.g.

$$\mathbf{X}_p(t) = \mathbf{V}_0 t + \mathbf{X}_0 \tag{3.14}$$

where $\mathbf{V}_0$ and $\mathbf{X}_0$ are coefficients to determine. Replacing $\mathbf{X}$ by $\mathbf{X}_p$ in (3.13) gives

$$\begin{aligned}(B_1 + B_2)\mathbf{V}_0 + (K_1 + K_2)(\mathbf{V}_0 t + \mathbf{X}_0) =& (K_1\mathbf{V}_{d,1} + K_2\mathbf{V}_{d,2})t \\ &+ B_1\mathbf{V}_{d,1} + B_2\mathbf{V}_{d,2} + K_1\mathbf{X}_{d,1} + K_2\mathbf{X}_{d,2}\end{aligned} \tag{3.15}$$

Polynomial coefficients identification yields

$$\begin{cases} \mathbf{V}_0 = (K_1 + K_2)^{-1}(K_1\mathbf{V}_{d,1} + K_2\mathbf{V}_{d,2}) \\ \mathbf{X}_0 = (K_1 + K_2)^{-1}\Big[B_1(\mathbf{V}_{d,1} - \mathbf{V}_0) + B_2(\mathbf{V}_{d,2} - \mathbf{V}_0) + K_1\mathbf{X}^0_{d,1} + K_2\mathbf{X}^0_{d,2}\Big] \end{cases} \tag{3.16}$$

The solution of the object dynamic equation (3.12) is $\bar{\mathbf{X}}_p = \mathbf{V}_0 t + \mathbf{X}_0$, which demonstrates Result 1: *the resulting object velocity is – converges to – the mean of the partners' intended velocities, weighted by their stiffness*. Besides, the partner with the greater stiffness will impose its/his/her intended velocity to the object.

To demonstrate Result 2, we focus on the forces $\mathbf{F}_1$ and $\mathbf{F}_2$ applied by each partner, or rather their asymptotic convergence $\bar{\mathbf{F}}_1$ and $\bar{\mathbf{F}}_2$. When re-introducing this solution in (3.11), we obtain

$$\bar{\mathbf{F}}_i = B_i(\mathbf{V}_{d,i} - \mathbf{V}_0) + K_i\Big[(\mathbf{V}_{d,i} - \mathbf{V}_0)t + (\mathbf{X}^0_{d,i} - \mathbf{X}_0)\Big] \tag{3.17}$$

Using (3.16), we finally get

$$\begin{cases} \bar{\mathbf{F}}_1 = (\kappa_{12}t + \beta_{12})(\mathbf{V}_{d,1} - \mathbf{V}_{d,2}) + \kappa_{12}(\mathbf{X}^0_{d,1} - \mathbf{X}^0_{d,2}) \\ \bar{\mathbf{F}}_2 = (\kappa_{21}t + \beta_{21})(\mathbf{V}_{d,2} - \mathbf{V}_{d,1}) + \kappa_{21}(\mathbf{X}^0_{d,2} - \mathbf{X}^0_{d,1}) \end{cases} \tag{3.18}$$

where

$$\begin{cases} \kappa_{ij} = K_i K^{-1}_{1+2} K_j \\ \beta_{ij} = B_i K^{-1}_{1+2} K_j - K_i K^{-1}_{1+2} B_i K^{-1}_{1+2} K_j + K_i K^{-1}_{1+2} B_j K^{-1}_{1+2} K_i \\ K_{1+2} = K_1 + K_2 \end{cases} \tag{3.19}$$

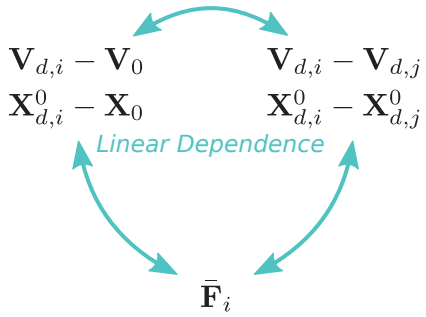

Figure 3.3: Linear Dependencies between forces and velocity/position differences.

Equation (3.18) shows that $\mathbf{V}_{d,1} \neq \mathbf{V}_{d,2}$ *is not a sustainable situation, since the forces applied by each partner increase linearly with the difference*. Besides, *a partner cannot estimate the intended velocity of the other partner from haptic cues – force and velocity – from the object without also knowing his/her/its impedance parameters*. The dyad has thus interest in realizing $\mathbf{V}_{d,1} = \mathbf{V}_{d,2}$. In this case, (3.16) becomes

$$\begin{cases} \mathbf{V}_0 = \mathbf{V}_{d,1} = \mathbf{V}_{d,2} \\ \mathbf{X}_0 = (K_1 + K_2)^{-1}(K_1\mathbf{X}^0_{d,1} + K_2\mathbf{X}^0_{d,2}) \end{cases} \tag{3.20}$$

and (3.18)

$$\begin{cases} \bar{\mathbf{F}}_1 = \kappa_{12}(\mathbf{X}^0_{d,1} - \mathbf{X}^0_{d,2}) \\ \bar{\mathbf{F}}_2 = \kappa_{21}(\mathbf{X}^0_{d,2} - \mathbf{X}^0_{d,1}) \end{cases} \tag{3.21}$$

The trajectory $\mathbf{X}_p$ is an average trajectory of the two intended trajectories, weighted by the stiffness parameters of each partner. The force felt by each partner depends linearly on the distance difference $\mathbf{X}^0_{d,1} - \mathbf{X}^0_{d,2}$. Similarly, both partners have interest in realizing the state $\mathbf{X}^0_{d,1} = \mathbf{X}^0_{d,2}$ to lower internal forces.

Result 1 expresses the object velocity as a function of both partners' intended velocity. Result 3 aims at inverting Result 1 to express the other partner's intended velocity as a function of the object velocity and its own intended velocity. It is easily done for the velocity part by subtracting $\mathbf{V}_{d,i}$ in (3.16). For brevity, we give the formula for the positions without demonstration:

$$\begin{cases} \mathbf{V}_{d,i} - \mathbf{V}_{d,j} = K_j^{-1}K_{1+2}(\mathbf{V}_{d,i} - \mathbf{V}_0) \\ \mathbf{X}^0_{d,i} - \mathbf{X}^0_{d,j} = K_j^{-1}K_{1+2}(\mathbf{X}^0_{d,i} - \mathbf{X}_0) \\ \qquad\qquad + (K_j^{-1}B_i - K_j^{-1}B_jK_{1+2}^{-1}K_iK_j^{-1}K_{1+2})(\mathbf{V}_{d,i} - \mathbf{V}_0) \end{cases} \tag{3.22}$$

which is Result 3. It shows that an asymptotic difference between the intended velocity of a partner and the object velocity indicates a difference of intended velocity between the partners.

3.2.6 Summary and Discussion

To summarize, we have demonstrated three important results:

1. **Average Object Velocity:** The resulting object velocity converges to the mean of the partners' intended velocities, weighted by their stiffness,

$$\begin{cases} \mathbf{V}_0 = (K_1 + K_2)^{-1}(K_1\mathbf{V}_{d,1} + K_2\mathbf{V}_{d,2}) \\ \mathbf{X}_0 = (K_1 + K_2)^{-1}\Big[B_1(\mathbf{V}_{d,1} - \mathbf{V}_0) + B_2(\mathbf{V}_{d,2} - \mathbf{V}_0) + K_1\mathbf{X}^0_{d,1} + K_2\mathbf{X}^0_{d,2}\Big] \end{cases} \tag{3.16}$$

2. **Increasing Internal Forces:** A difference of constant intended velocities between the partners leads to increasing internal forces over time,

$$\begin{cases} \bar{\mathbf{F}}_1 = (\kappa_{12}t + \beta_{12})(\mathbf{V}_{d,1} - \mathbf{V}_{d,2}) + \kappa_{12}(\mathbf{X}^0_{d,1} - \mathbf{X}^0_{d,2}) \\ \bar{\mathbf{F}}_2 = (\kappa_{21}t + \beta_{21})(\mathbf{V}_{d,2} - \mathbf{V}_{d,1}) + \kappa_{21}(\mathbf{X}^0_{d,2} - \mathbf{X}^0_{d,1}) \end{cases} \tag{3.18}$$

3. **Partner-wise Velocities Formula:** A difference of constant intended velocities between the partners is linearly linked to a difference between the intended velocity of each partner and the object velocity,

$$\begin{cases} \mathbf{V}_{d,i} - \mathbf{V}_{d,j} = K_j^{-1}K_{1+2}(\mathbf{V}_{d,i} - \mathbf{V}_0) \\ \mathbf{X}^0_{d,i} - \mathbf{X}^0_{d,j} = K_j^{-1}K_{1+2}(\mathbf{X}^0_{d,i} - \mathbf{X}_0) \\ \qquad\qquad + (K_j^{-1}B_i - K_j^{-1}B_jK_{1+2}^{-1}K_iK_j^{-1}K_{1+2})(\mathbf{V}_{d,i} - \mathbf{V}_0) \end{cases} \tag{3.22}$$

These results demonstrate that having two different intended velocities is not a sustainable situation since it results in internal forces increasing linearly over time and difference in intended velocities (Result 2). Therefore, ideally, both partners should have the same desired trajectory [40]. These statements are already well known and predicting a human partner's desired trajectory is one of the main challenges in the pHRI field. However Result 3 shows that it is not possible for one partner to estimate the other partner's intended velocity from haptic cues without the knowledge of his stiffness parameters. This leads to question the hypothesis of the ignorance of the other partner's impedance parameters. We could complete the Model Symmetry Projection hypothesis by adding that a partner also projects its own impedance parameters on the other, e.g. supposing that both partners have the same impedance parameters. However, Results 2 and 3 also introduce interesting linear relationships between forces and velocity differences that are pictured in Fig. 3.3. These relationships show that *asymptotically* reducing the forces, or the difference between its own intended velocity (and position) and the object's, to zero is equivalent to matching the other partner's intended velocity (and position). These findings will be used in Section 3.3.2.

Furthermore, *how $\mathbf{X}_d$ is determined is completely independent of our control law, so that it can be used independently from the level of leadership/followship within the partners*. The difference between these modes lies in the trajectory planning of $\mathbf{X}_d$. For a humanoid robot

to have a proactive follower behavior, $\mathbf{X}_d$ must be planned to match the human partner's intentions at best.

Besides, assuming we have trajectory planners for each of the three modes (standalone, leader, follower), it is now possible to switch the robot behavior as theorized in [40] [18] by switching the planners, without changing the control law that regulates the physical interaction.

3.2.7 Limits of this model

In reality, both partners are interacting with the object at different points, not at the CoM. This makes the problem of the asymptotic convergence of the object trajectory more complex. This problem is partially addressed in Appendix A. Moreover the human impedance, when projected in the Cartesian world frame, is not likely to be linear. Thus, we assume that the results enunciated in the Section 3.2.6 still hold in the task of our interest.

3.3 1D Follower Trajectory Planner

In this section, we propose a basic trajectory planner for the follower mode dedicated to a one-degree-of-freedom transportation task to allow the robot to replicate the task monitored with human dyads presented in Chapter 2.

3.3.1 Object motion decomposition into primitives

To be proactive as a follower, the robot first needs to correctly guess the human partner's intentions (in terms of next motion), and thus to locally anticipate his/her intended actions or trajectories. Motion prediction of the human partner has been addressed throughout the literature in pHRI. The strategy generally aims at reducing the problem to the estimation of handful parameters that allows generating a complete motion. The most known example is the minimum jerk model used in [48] [10]. However this model is always rather applied to point-to-point motions and does not fit for motions going beyond the reach of the arm or even to motion for which the target point is not well defined. When two humans perform a transportation task of an object, they might talk to give each other indications, such as "turn left", "go forward" or "stop".

Based on this observation, we suggest to decompose the motion into constant velocity phases, as it was addressed for handshaking [70] and dancing [65]. Each i-th phase is characterized by the velocity amplitude $\mathcal{V}_i$ and eventually its start t_i and end time t_{i+1}. We separate the case where $\mathcal{V}_i = 0$ from the others to obtain two template sub-motions, or *motion primitives*:

- **Stop:** no motion;
- **Walk:** walk forward or backward.

Consider the example of the task performed by the human dyads studied in Chapter 2. From a still initial position (**Stop**), the dyads start walking forward (**Walk**) before stopping (**Stop**) and walking backwards (**Walk**). They stop at a still position to finish the task (**Stop**). Thus, the task can be decomposed into **Stop**, **Walk**, **Stop**, **Walk** and **Stop**.

This may seem simplistic, but the approach will be extended in Section 3.4. This method is not specific to the follower mode. A sequence of primitives can also be used to describe a desired trajectory for the standalone and leader modes. However this approach greatly simplifies the estimation of the leader intentions in the follower mode. A parallel can be established with speech recognition where primitives would be words and the complete motion would be a sentence.

The problem that arises in this model is the transition from one phase to the other. In Chapter 2, we used an affine function for fitting purposes. However, as we need the impedance nodic reference $\mathbf{X}_d$ to be twice-differentiable, this solution is not an option. The sequence of the velocity amplitudes $\mathcal{V}_i$ and the start and end timings t_i and t_{i+1} allow us to build a piecewise-constant velocity function over time $\mathcal{V}$. Therefore it does not represent a feasible trajectory; it should rather be considered as a simplified velocity plan, i.e. a template. Then we filter this velocity plan $\mathcal{V}$ with the second-order critically-damped filter, whose transfer function in the Laplace domain is

$$\frac{\dot{\mathbf{X}}_d}{\mathcal{V}}(s) = \frac{\omega_0^2}{(s+\omega_0)^2} \tag{3.23}$$

and thus we obtain the impedance nodic reference $\mathbf{X}_d$ and its derivatives. ω_0 characterizes how quickly the plan switches from one velocity $\mathcal{V}_i$ to the other. We chose $\omega_0 = 5$ rad.s^{-1} so that the rising time is around one second.

3.3.2 Reactive Generation of Primitives Sequences

In a first time, we focus on the motion primitive **Walk** and on how its velocity parameter $\mathcal{V}_i$ is determined. As seen in Section 3.2.5, even when assuming that the human partner's behavior fits our model, determining her/his intended velocity from haptic cues is impossible without the knowledge of the impedance parameters. In this part, we show how adapting the robot's intended velocity to the object's can lead to a matching between the robot's and the human's intended velocities.

In Section 3.2.5, we demonstrated an important relationship:

$$\begin{cases} \mathbf{V}_{d,r} - \mathbf{V}_{d,h} = K_h^{-1} K_{r+h} (\mathbf{V}_{d,r} - \mathbf{V}_0) \\ \mathbf{X}^0_{d,r} - \mathbf{X}^0_{d,h} = K_h^{-1} K_{r+h} (\mathbf{X}^0_{d,r} - \mathbf{X}_0) \\ \qquad\qquad + (K_h^{-1} B_r - K_h^{-1} B_h K_{r+h}^{-1} K_r K_h^{-1} K_{r+h})(\mathbf{V}_{d,r} - \mathbf{V}_0) \end{cases} \tag{3.24}$$

where the indexes r and h indicates robot and human related variables respectively. In our case, we suppose we are in the hypothetical state where

- filter (3.23) has converged so that the robot intended constant velocity is $\mathbf{V}_{d,r} = \mathcal{V}_i$,

- the human partner has a constant intended velocity $\mathbf{V}_{d,h}$,
- the object velocity has converged to $\mathbf{V}_0$.

Our goal is to adapt the velocity plan $\mathcal{V}$ so that $\mathcal{V} = \mathbf{V}_{d,h}$. As stated above, it is difficult to estimate $\mathbf{V}_{d,h}$ without the knowledge of the human partner's stiffness parameter K_h. An example of our adaptation strategy is pictured in Fig. 3.4. Equation (3.24) shows that $\mathbf{V}_{d,r} = \mathbf{V}_0$ implies $\mathbf{V}_{d,r} = \mathbf{V}_{d,h}$ asymptotically. Thus, at step $i+1$ we adapt the robot's velocity plan $\mathcal{V}$ with the current object velocity at step i

$$\mathcal{V}_{i+1} = \mathbf{V}_{0,i} \tag{3.25}$$

where the index i means the i-th step of the primitive sequence. This adaptation triggers a transition phase; after convergence, the new object's resulting velocity $\mathbf{V}_{0,i+1}$ has changed. According to Result 1, it is a weighted average of $\mathbf{V}_{d,h}$ and $\mathbf{V}_{d,r}$. Thus, by adapting repeatedly the robot's velocity plan with the object's velocity, the robot's intended velocity $\mathbf{V}_{d,r}$ will converge towards the human's $\mathbf{V}_{d,h}$ as pictured in Fig. 3.4.

To prove it, we use Result 3 at the $i-1$-th step

$$\mathbf{V}_{d,h} - \mathbf{V}_{d,r} = K_r^{-1} K_{r+h} (\mathbf{V}_{d,h} - \mathbf{V}_{0,i-1}) \tag{3.26}$$

After convergence, i.e. $\mathbf{V}_{d,r} = \mathcal{V}_{i-1}$, and replacing $\mathbf{V}_{0,i-1}$ by $\mathcal{V}_i$ from (3.25), we obtain

$$\mathbf{V}_{d,h} - \mathcal{V}_{i-1} = K_r^{-1} K_{r+h} (\mathbf{V}_{d,h} - \mathcal{V}_i) \tag{3.27}$$

Rearranging terms gives

$$\begin{cases} \mathcal{V}_i - \mathbf{V}_{d,h} = K_{r+h}^{-1} K_r (\mathcal{V}_{i-1} - \mathbf{V}_{d,h}) \\ \qquad\qquad = (K_{r+h}^{-1} K_r)^i (\mathcal{V}_0 - \mathbf{V}_{d,h}) \end{cases} \tag{3.28}$$

we obtain a geometric progression of $\mathcal{V}_i$ towards $\mathbf{V}_{d,h}$. Since we are considering the one direction walking (i.e. 1D) case, the stiffness parameters are strictly positive scalars k_r and k_h so that

$$\mathcal{V}_i - \mathbf{V}_{d,h} = \left(\frac{k_r}{k_r + k_h} \right)^i (\mathcal{V}_0 - \mathbf{V}_{d,h}) \tag{3.29}$$

Since $\frac{k_r}{k_r+k_h} < 1$, $\mathcal{V}_i$ converges towards $\mathbf{V}_{d,h}$ at each iteration i. The speed of convergence is determined by the factor $\frac{k_r}{k_r+k_h}$, so that k_r must not be much greater than k_h. Note that it is in the worst-case scenario where the human partner does not change his/her intended velocity. In the best-case scenario, the human partner would also adapt his/her velocity, so that the convergence of intended velocities is quicker.

We need to choose a frequency of adaptation. On the one hand, it should be low enough so that the object velocity converges before a new adaptation. On the other hand, the velocity plan has to be frequently adapted so that it converges quickly towards the human intended

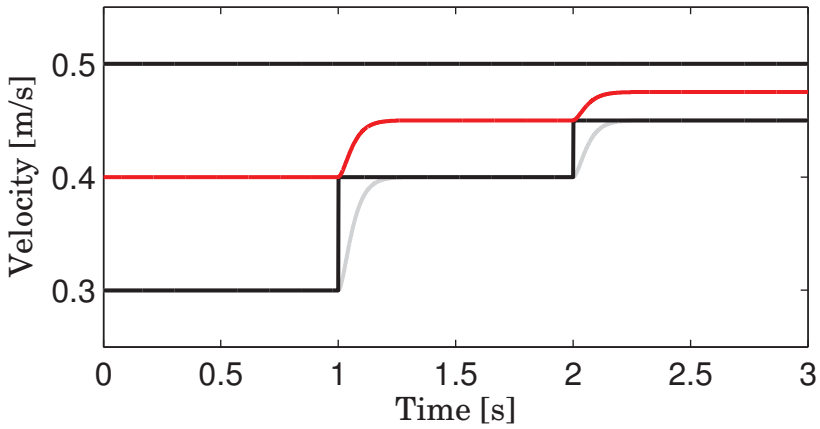

Figure 3.4: Example of Velocity Adaptation. The human has a constant intended velocity at 0.5 m/s (upper black line). Each second, the robot adapts its velocity plan $\mathcal{V}$ (lower black line) to the object's velocity (red line). After a transition phase, the object velocity converges and the robot can adapt its velocity plan again. Repeating this process brings the robot's velocity plan closer and closer to the human's. The grey line pictures the robot's intended trajectory, which is a filtered of the velocity plan $\mathcal{V}$.

velocity. Thus we adapt the velocity plan $\mathcal{V}$ every τ seconds (with τ around one second) with the following formula:

$$\mathcal{V}(t) = \frac{1}{\tau}\int_{t-\tau}^{t} \dot{\mathbf{X}}(u)\mathrm{d}u \tag{3.30}$$

We use a mean value of the object velocity $\dot{\mathbf{X}}$ instead of an instantaneous value because it is perturbed by oscillations from the robot's gait. The choice of τ as the period of gait (0.8 seconds) also reduces the effects of these oscillations.

This algorithm allows the robot to adapt its intended velocity to the human's, but it does not allow trajectory matching. Indeed, with $\mathbf{V}_{d,r} = \mathbf{V}_{d,h}$, the position part equation in system (3.24) becomes

$$\mathbf{X}^0_{d,r} - \mathbf{X}^0_{d,h} = K_h^{-1} K_{r+h}(\mathbf{X}^0_{d,r} - \mathbf{X}_0) \tag{3.31}$$

Our strategy consists in adding an offset velocity to the velocity plan so that the distance $\mathbf{X}_0 - \mathbf{X}^0_{d,r}$ is filled in τ_{pos} seconds, which gives the complete velocity plan update algorithm

$$\text{every } \tau \text{ seconds, } \mathcal{V} = \frac{1}{\tau}\int_{t-\tau}^{t} \dot{\mathbf{X}}(u)\mathrm{d}u + \frac{\mathbf{X}(t) - \mathbf{X}_{d,r}(t)}{\tau_{pos}} \tag{3.32}$$

Now we focus on the **Stop** primitive. The velocity plan amplitude is trivial; it is $\mathcal{V} = 0$. The question is when to transit from and to this primitive. Considering the velocity equation in (3.24) in the particular case where $\mathbf{V}_{d,r} = 0$ yields

$$\mathbf{V}_0 = K_{r+h}^{-1} K_h \mathbf{V}_{d,h} \tag{3.33}$$

The object velocity is an average of the velocity intended by the human. Therefore we use a velocity threshold to detect the human's intention to start the motion: if the velocity of the object goes beyond that threshold, the robot switches to the primitive **Walk**. We couple it to a force threshold. Force thresholds, however, are less reliable. When holding an object together, two humans might be comfortable with a non-negligible level of internal forces, that Reed referred to as "Haptic Presence" [57]. Moreover, this level of internal forces depends on the subjects.

The question of the first value of the velocity plan $\mathcal{V}$ after the switch to **Walk** arises. Obviously, we cannot use the update algorithm from (3.32) since it will return a small velocity that is clearly far from the human's intention. The best solution would be to estimate this intended velocity somehow, which is far from being trivial. Besides, we are interested in transportation over large distances, so this transition phase's duration is negligible compared to the constant velocity phases. Therefore, we fix this velocity to a default velocity for τ seconds; after this time lapse we update the velocity plan using a formula similar to (3.32)

$$\mathcal{V} = \dot{\mathbf{X}}(t) + \frac{\mathbf{X}(t) - \mathbf{X}_{d,r}(t)}{\tau_{pos}} \tag{3.34}$$

Finally, we will explain the transition from the primitive **Walk** to **Stop**. Again, the main switching mechanism uses two velocity thresholds. The first one detects great velocity amplitude decreases, e.g. whether the difference between the current velocity plan and the object trajectory is above a threshold

$$|\mathcal{V}| - \left|\dot{\mathbf{X}}\right| > \mathbf{V}_{thresh,1} \tag{3.35}$$

The second switching mechanism detects whether the velocity plan is too low, e.g.

$$|\mathcal{V}| < \mathbf{V}_{thresh,2} \tag{3.36}$$

As for detecting the human's intention to start the motion, we added a force threshold. If one of these conditions is fulfilled, the robot detects an intention to stop the motion.

The start and stop detection mechanisms prevent the robot from having a low intended velocity. This makes sense for a transportation task, where the goal is to move the object over large distances. However, this makes precise positioning of the object harder.

This primitive sequencing is implemented with a Finite State Machine (FSM), which reactively generates motion primitives for a follower mode. Though it roughly estimates the leader's intentions, it allows us to test the proposed control scheme on the HRP-2 humanoid robot.

3.3.3 Implementation on the HRP-2 Humanoid Robot

The proposed control scheme with its different modules is described in Fig. 3.5. We detail the different components in the following parts.

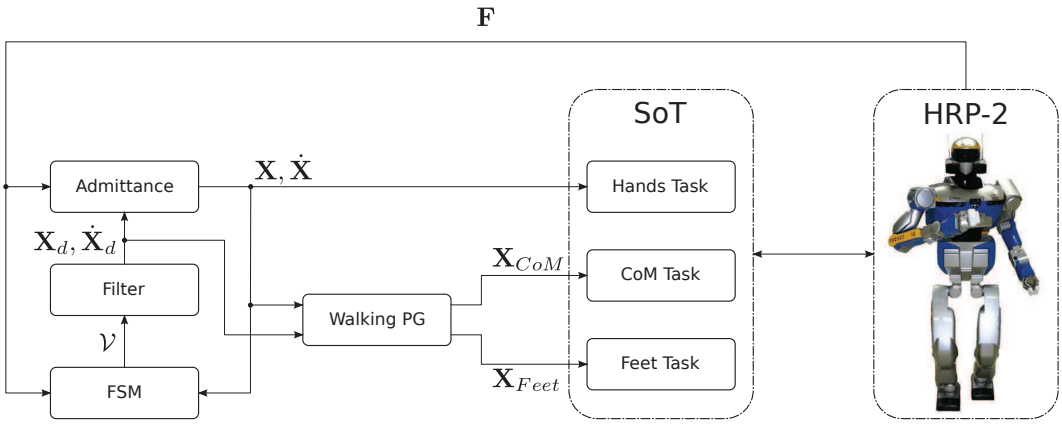

Figure 3.5: The Complete Control scheme.

3.3.3.1 Admittance Control

The core part of the implementation is to enforce the impedance constraint (3.7) at the robot's grippers, in the world frame, that we recall hereafter

$$\mathbf{F} = -\alpha M_O(\ddot{\mathbf{X}}_d - \mathbf{G}) + M(\ddot{\mathbf{X}} - \ddot{\mathbf{X}}_d) + B(\dot{\mathbf{X}} - \dot{\mathbf{X}}_d) + K(\mathbf{X} - \mathbf{X}_d) \tag{3.37}$$

In this version, the signs are the opposite from (3.7) since $\mathbf{F}$ is the force felt by the robot from the object instead of the force applied by the robot on the object. The robot's grippers are position-controlled through the Stack-of-Tasks (SoT) developed in [49], which uses generalized inverted kinematics to resolve a set prioritized operational space tasks. The SoT allows defining various tasks –positioning the grippers in the world frame in our case– and uses the robot redundancy to realize them simultaneously. Therefore we choose to implement an admittance controller.

The HRP-2 humanoid robot is equipped with two force-torque sensors mounted on each wrist that measure two 4D screw vectors $\mathbf{F}_{left}$ and $\mathbf{F}_{right}$, which are computed in the world frame. Since the robot is holding the object rigidly, without changing grasping points, our strategy is to control both grippers as a unique end-effector. To that end, we transpose both forces from sensors at the same point $\mathbf{X}$ and sum them to obtain $\mathbf{F}$, e.g.

$$\mathbf{F} = P_{left}^T(\theta)\mathbf{F}_{left} + P_{right}^T(\theta)\mathbf{F}_{right} \tag{3.38}$$

where

$$\begin{aligned} P_{left}(\theta) &= \begin{bmatrix} 1 & 0 & 0 & -l_{l,x}\sin\theta - l_{l,y}\cos\theta \\ 0 & 1 & 0 & l_{l,x}\cos\theta - l_{l,y}\sin\theta \\ 0 & 0 & 1 & 0 \\ 0 & 0 & 0 & 1 \end{bmatrix} \\ P_{right}(\theta) &= \begin{bmatrix} 1 & 0 & 0 & -l_{r,x}\sin\theta - l_{r,y}\cos\theta \\ 0 & 1 & 0 & l_{r,x}\cos\theta - l_{r,y}\sin\theta \\ 0 & 0 & 1 & 0 \\ 0 & 0 & 0 & 1 \end{bmatrix} \end{aligned} \tag{3.39}$$

$\mathbf{L}_l = \begin{bmatrix} l_{l,x} & l_{l,y} & 0 & 0 \end{bmatrix}^T$ and $\mathbf{L}_r = \begin{bmatrix} l_{r,x} & l_{r,y} & 0 & 0 \end{bmatrix}^T$ are the positions of the left and right grippers relatively to point $\mathbf{X}$ in the object frame. θ is the orientation of the object in the world frame – and therefore the robot's grippers' too, as well as the fourth component of $\mathbf{X}$. Both $\mathbf{L}_l$ and $\mathbf{L}_r$ are constant vectors. In our implementation we choose

$$\begin{cases} l_{l,x} = l_{r,x} = 0 \\ l_{l,y} = -l_{r,y} = \dfrac{l}{2} \end{cases} \tag{3.40}$$

where l is the distance between the object's handles the robot is gripping. In that case, the point $\mathbf{X}$ we control is the geometric middle of the force sensors' centers. Unlike in Section 3.2, the point $\mathbf{X}$ is not the object CoM, nor a common point of interaction with the human partner. Therefore, the impedance-based model we developed is only an approximation.

Concerning the choice of parameters in the impedance constraint (3.37), we choose $\alpha = 1/2$, which supposes an equal sharing of the task. However, since the force sensors are mounted at the robot's wrists, the "object" the robot is transporting with the human is the system composed of the real object and its own grippers. Therefore, the term $\alpha M_O(\ddot{\mathbf{X}}_d - \mathbf{G})$ that compensates the object's dynamics should include the robot's grippers inertia. Therefore, we rewrite the impedance constraint

$$\mathbf{F} = -\tilde{M}_O(\ddot{\mathbf{X}}_d - \mathbf{G}) + M(\ddot{\mathbf{X}} - \ddot{\mathbf{X}}_d) + B(\dot{\mathbf{X}} - \dot{\mathbf{X}}_d) + K(\mathbf{X} - \mathbf{X}_d) \tag{3.41}$$

with

$$\tilde{M}_O = \begin{bmatrix} (\alpha m + 2m_{gripper})I_3 & 0 \\ 0 & 0 \end{bmatrix} \tag{3.42}$$

Note that we chose $\tilde{M}_O$ to be diagonal although point $\mathbf{X}$ is not the object's CoM. Besides, we neglect the angular inertia.

The impedance parameters M, B and K are diagonal matrices that are tuned experimentally (Table 3.1) in a non-walking mode.

Table 3.1: Stiffness, Damping and Inertia coefficients, tuned heuristically

Stiffness	Damping	Inertia
$K_{xy} = 50$N/m	$B_{xy} = 90$N.s/m	$M_{xy} = 8$kg
$K_z = 250$N/m	$B_z = 100$N.s/m	$M_z = 8$kg
$K_\theta = 30$N/rad	$B_\theta = 70$N.s/rad	$M_\theta = 8$kg.m^2

To compute $\mathbf{X}$ from (3.41), we first perform the substitution $\Delta\mathbf{X} = \mathbf{X} - \mathbf{X}_d$ to get

$$M\Delta\ddot{\mathbf{X}} + B\Delta\dot{\mathbf{X}} + K\Delta\mathbf{X} = \mathbf{F} + \tilde{M}_O(\ddot{\mathbf{X}}_d - \mathbf{G}) \tag{3.43}$$

Since M, B and K are diagonal matrices, equation (3.43) is a set of six independent differential equations if we consider the right member to be constant over the time interval that

interests us. The robot control loop runs at 200Hz, e.g. with a time step $\mathrm{d}t$ of 5ms. Our goal is to compute $\Delta\mathbf{X}_k = \Delta\mathbf{X}(t = k\mathrm{d}t)$ and $\Delta\dot{\mathbf{X}}_k = \Delta\dot{\mathbf{X}}(t = k\mathrm{d}t)$ for every $k \in \mathbb{N}$. To that end, at each time step, we analytically solve the following Cauchy problem

$$\begin{cases} M\Delta\ddot{\mathbf{X}} + B\Delta\dot{\mathbf{X}} + K\Delta\mathbf{X} = \left[\mathbf{F} + \tilde{M}_O(\ddot{\mathbf{X}}_d - \mathbf{G})\right]_{t=(k+1)\mathrm{d}t} \\ \Delta\mathbf{X}(t = k\mathrm{d}t) = \Delta\mathbf{X}_k \\ \Delta\dot{\mathbf{X}}(t = k\mathrm{d}t) = \Delta\dot{\mathbf{X}}_k \end{cases} \tag{3.44}$$

where the second member is assumed constant over the interval $[t + k\mathrm{d}t, t + (k + 1)\mathrm{d}t]$. The values of the solution at time $t + (k + 1)\mathrm{d}t$ are the values $\Delta\mathbf{X}_{k+1}$ and $\Delta\dot{\mathbf{X}}_{k+1}$. The solution on one degree of freedom (we use small letters instead) is

$$\begin{cases} \Delta x_{k+1} = \dfrac{1}{\omega_1 - \omega_2}\left[\dfrac{1}{m_x}(f_x + \tilde{m}_O\ddot{x}_d)_{t=(k+1)\mathrm{d}t}\left(\dfrac{1 - \exp(-\omega_2\mathrm{d}t)}{\omega_2} - \dfrac{1 - \exp(-\omega_1\mathrm{d}t)}{\omega_1}\right)\right. \\ \qquad \left. + \exp(-\omega_2\mathrm{d}t)\,(\omega_1\Delta x_k + \Delta\dot{x}_k) - \exp(-\omega_1\mathrm{d}t)\,(\omega_2\Delta x_k + \Delta\dot{x}_k)\right] \\ \Delta\dot{x}_{k+1} = \dfrac{1}{\omega_1 - \omega_2}\left[\dfrac{1}{m_x}(f_x + \tilde{m}_O\ddot{x}_d)_{t=(k+1)\mathrm{d}t}\Big(\exp(-\omega_2\mathrm{d}t) - \exp(-\omega_1\mathrm{d}t)\Big)\right. \\ \qquad \left. - \omega_2\exp(-\omega_2\mathrm{d}t)\,(\omega_1\Delta x_k + \Delta\dot{x}_k) + \omega_1\exp(-\omega_1\mathrm{d}t)\,(\omega_2\Delta x_k + \Delta\dot{x}_k)\right] \end{cases} \tag{3.45}$$

where

$$\begin{cases} \omega_1 = \dfrac{b_x + \sqrt{b_x^2 - 4k_xm_x}}{2m_x} \\ \omega_2 = \dfrac{b_x - \sqrt{b_x^2 - 4k_xm_x}}{2m_x} \end{cases} \tag{3.46}$$

and we suppose $b_x^2 - 4k_xm_x > 0$. The advantage of formulation (3.45) is that it can easily be defined when ω_2 is very small by using the Taylor expansion

$$\frac{1 - \exp(-\omega_2\mathrm{d}t)}{\omega_2} = \mathrm{d}t - \omega_2\frac{\mathrm{d}t^2}{2} + o(\omega_2^2\mathrm{d}t^2) \tag{3.47}$$

which is defined by continuity for $\omega_2 = 0$. This occurs when k_x is chosen to be zero ($m_x > 0$), and thus allows choosing a zero stiffness without changing the integration scheme.

Finally, from $\Delta\mathbf{X}$ and $\Delta\dot{\mathbf{X}}$ we compute $\mathbf{X}$ and $\dot{\mathbf{X}}$ with

$$\begin{cases} \mathbf{X} = \mathbf{X}_d + \Delta\mathbf{X} \\ \dot{\mathbf{X}} = \dot{\mathbf{X}}_d + \Delta\dot{\mathbf{X}} \end{cases} \tag{3.48}$$

which are the outputs of the admittance controller in Fig. 3.5. Since $\mathbf{X}$ is not the trajectory of the grippers, but of their geometric middle, the grippers' trajectories that are effectively given to the SoT needs to be geometrically computed using $\mathbf{L}_l$ and $\mathbf{L}_r$.

3.3.3.2 Walking

An important aspect of the transportation task is to move the object over large distances, thus requiring walking from the robot. We choose a strategy where the gait and the motion of the grippers are minimally coupled. More precisely, we command the velocity of the robot's gait so that the motion of the robot's body keeps up with the motion of the grippers.

To that end, we used a modified version of the walking Pattern-Generator (PG) developed in [30] for the locomotion (biped walking task). The PG generates on-line a trajectory for the Center of Mass (CoM) of the robot as well as trajectories for the feet, that are also executed using the SoT controller. These trajectories are computed by means of a quadratic optimization with linear constraints, which is made possible by the use of a linearized simplified model of the robot and a state-of-the-art quadratic problem solver. The PG minimizes, among others, the error between the CoM velocity and an input velocity, and the CoM jerk, with constraints on the robot's Zero Moment Point (ZMP) to ensure its balance while walking.

The PG takes a 3D desired CoM velocity as an input: two translation and one angular velocities. The PG plans a gait so that the robot's CoM reaches and maintains a velocity as close as possible from this velocity input, while respecting the robot's constraints. This planning is made over one gait cycle, i.e. 1.6s, and is recomputed every 0.1s. Thus, 1.5s of the plan generated by the PG is not directly used to control the robot's gait. However, it is important to generate a stable and fluid gait. The prevision of the immediate future is important to obtain a good gait.

Therefore we can take advantage of our detection of the human's intentions. For instance, the FSM detects that the human wishes to move the object forwards from a velocity threshold and selects the **Walk** primitive. Even if the FSM detects the wrong intention, a velocity plan $\mathcal{V}$ is generated for the next 0.8s. And although the actual velocity might be low, the short term goal of the robot is to reach a high velocity within the next second. In other words, when an intention is detected, an intended velocity $\dot{\mathbf{X}}_d$ of the grippers is generated for the second to come. Thus we have an idea of the motion to come and can use this knowledge to help the PG to perform better.

Assuming a constant velocity plan $\mathcal{V}$, it is easy to compute the intended velocity $\dot{\mathbf{X}}_d$ of the grippers for any time t using (3.23). At time t, we use the grippers' intended velocity at horizon τ, i.e. $\dot{\mathbf{X}}_d(t+\tau)$, as the desired CoM velocity input of the PG. In practice, we use $\tau = 0.8$s.

Besides, we regulate this velocity input with a proportional controller so that the relative position of the robot's CoM and grippers remains constant, as well as the relative orientation of its feet and grippers. However, walking produces oscillatory motions by nature, especially on the lateral component, so we add dead-zones so that the proportional controller does not compensate these oscillations. In the case of lateral motion, the dead-zone produces an undesired static error: the robot's grippers and body are visibly not aligned. We add an integrative term to align them; the integration is performed over a walk cycle.

To summarize, the robot's gait velocity is reactively adapted to the grippers' velocity, but the knowledge of the human partner's intentions is also used to improve the quality of the

robot's gait.

3.3.3.3 Results

Figure 3.6: HRP-2 realizing the 1D transportation task as a proactive follower with a human partner, walking forwards (first line) and then backwards (last line).

As pictured in Fig. 3.6, our robot successfully performed the task with a human leading the task, though at limited velocity. Trajectories $\mathbf{X}$ and $\mathbf{X}_d$ are shown in Fig. 3.7. Their corresponding velocities are shown in Fig. 3.8. The trapezoidal velocity profile of Fig. 2.14 was reproduced and the robot correctly detected the start, move-back and stop of the motion.

If we look at the forces in Fig. 3.9, most of the time, our control law results in forces that counteract the motion, i.e. the robot inputs negative power on the object, whereas it is always the case for the passive control law. However, when the motion starts, our control law quickly produces less forces, especially when the object effective and desired velocities are the same, where the force comes back to the dyadic-contraction initial value. During constant velocity phases, for any velocity, the human partner can exert the force s/he feels comfortable with, without affecting the task execution. The more important force variations occur during the transition phases, which only represent a small part of the overall motion.

Oscillations can be observed in the velocity profile (see Fig. 3.8, top); we did not precisely investigate their origin. We suspect they might be caused by the robot's stepping. Nonetheless they do not destabilize our pHRI controller.

3.4 Proactive 3D-Trajectory Planner

In this Section, we extend the 1D Trajectory Planner of Section 3.3 to allow the robot to perform a 3D transportation task with the human. We first assume that the concept of motion primitives extends to walking in any direction with turns, which finally proved to be the case.

3.4.1 Motion Primitives

We complete the list of motion primitives with new primitives, as pictured in Fig. 3.10:

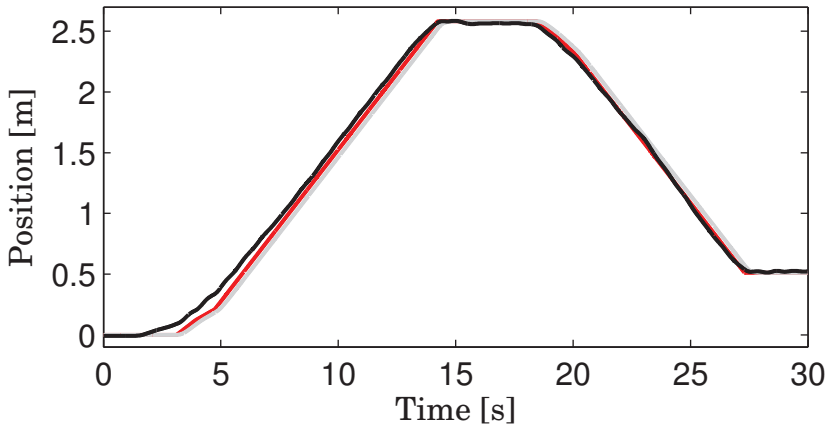

Figure 3.7: Trajectories of the object: the admittance controller output $\mathbf{X}$ *in black, follower desired trajectory* $\mathbf{X}_d$ *in gray, motion primitives* $\mathcal{X}$ *in red (integral of* $\mathcal{V}$*).*

- **Stop:** no motion;
- **Walk:** walk forward or backward;
- **Side:** walk sideways;
- **Turn:** spin around;
- **Walk/Turn:** turn while walking forward or backward.

Table 3.2: Example of Primitive and $\mathcal{V}$ *Sequences.*

Primitive	Frontal	Lateral	Vertical	Angular
Stop	0	0	0	0
Walk	0.5	0	0	0
Walk	0.4	0	0	0
Stop	0	0	0	0
Side	0	0.4	0	0
Walk	0.5	0	0	0
Walk/Turn	0.5	0	0	0.5
Stop	0	0	0	0

Sequencing these primitives allows to generate various motions, as in Fig. 3.11, while preventing some unnatural motions like walking in diagonal, i.e. **Walk/Side**. Moreover, we do not allow every sequence. For instance, **Side** cannot follow **Walk**: the robot must stop walking before moving sideways. Each primitive is associated with a three dimension velocity vector $\mathcal{V}$ in a local frame (frontal, lateral and angular velocities) which is updated at each

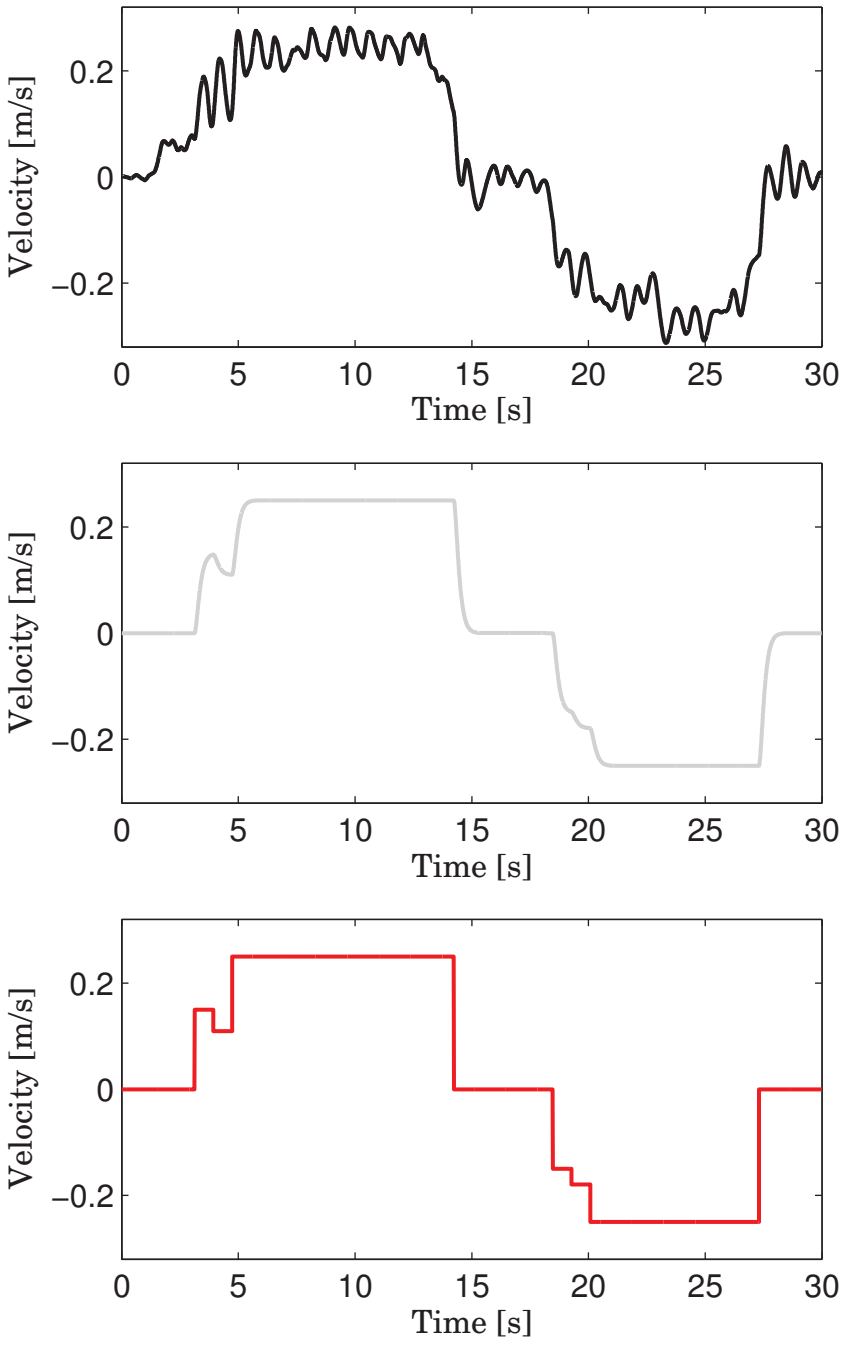

Figure 3.8: Velocities of the object: the admittance controller output $\dot{\mathbf{X}}$ in black (top), follower desired velocity $\dot{\mathbf{X}}_d$ in gray (middle), motion primitives $\mathcal{V}$ in red (bottom).

transition. Since we use a four-dimension description, we may add the vertical translation component to remain consistent for addition and matrix multiplication, but it is always zero.

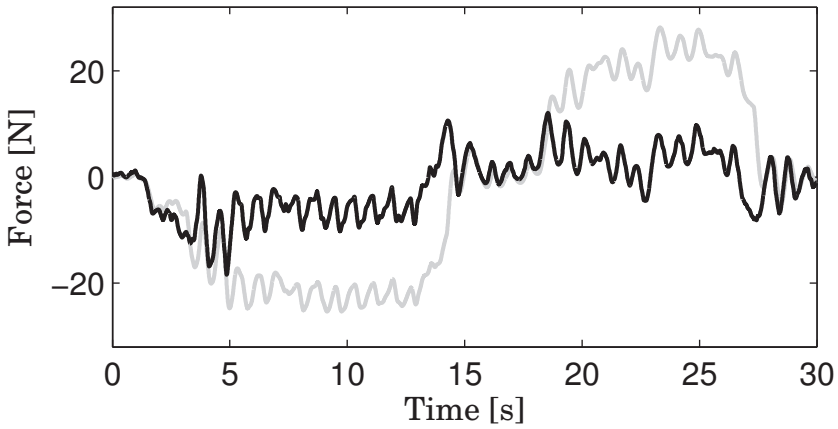

Figure 3.9: Force applied by the robot on the object (black). The gray curve represents the damping part of the interaction force $\mathbf{F} = -B\dot{\mathbf{X}}$: it is the force that would be applied by the robot with a passive behavior to obtain the same velocity.

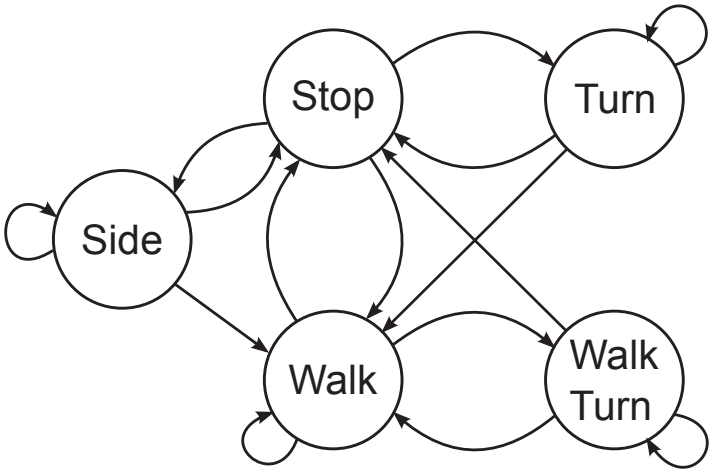

Figure 3.10: Finite State Machine describing the possible primitives sequencing. It can generate sequences for both leader and follower modes. The transitions are triggered differently depending on the chosen mode.

3.4.2 Robot local frame

Firstly, we need to define the frames used in the control. The impedance constraint (3.7) is expressed in the Cartesian global frame. However, for the robot, the forward direction is not fixed in the world frame. Thus we need a local frame in which we can naturally describe the *direction* of the velocity plan. Its amplitude, however, is expressed in reference to a fixed point in the global frame. Therefore, we are only interested in the orientation of the local frame.

The first solution is to use the robot's waist orientation to determine the forward direction. However, we choose to decouple the gait – that directly impacts the waist orientation – from the motion of the grippers in the world frame. Therefore, the relative orientation of the

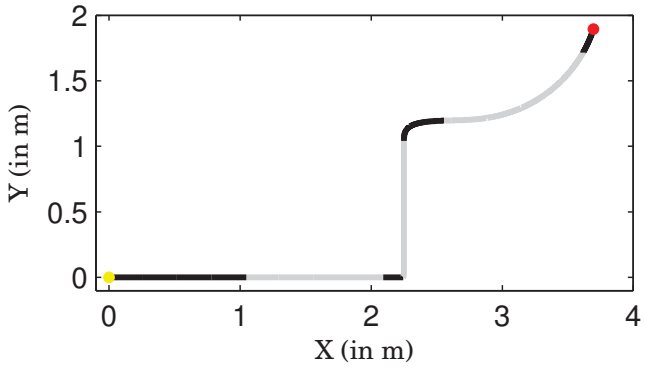

Figure 3.11: Example of desired trajectory from yellow dot to red dot. The sequence of primitives is **Stop**, **Walk**, **Walk***(with a different* $\mathcal{V}$*)*, **Stop**, **Side**, **Walk**, **Walk/Turn**, **Stop**. *The alternation of black and gray pictures the alternation of primitives. The sequence of* $\mathcal{V}$ *used is given by Table 3.2.*

robot's grippers and waist might be important, and consequently not the direction the human intended.

The second solution is to use the frame attached to the object, or equivalently attached to the robot's grippers since it is holding the object firmly, as shown in Fig. 3.12. The problem with this choice comes from the oscillations of the grippers. As we can see in Fig. 3.9, the gait introduces oscillations in the force signal, causing the orientation of the grippers to oscillate as well through the impedance constraint.

Therefore, the desired orientation of the robot's grippers is a good candidate, since the FSM produces smooth trajectories as shown in Fig. 3.8. However, we need to ensure that the intended orientation generated by the FSM and the object's are close from one another, which is fulfilled by processing equation (3.32). Besides, computing this robot local orientation is easy with our choice of coordinates. Indeed, the transformation matrix $\mathbf{R}_d$ that represents the local frame in the world coordinates is computed with

$$\mathbf{R}_d = f(\mathbf{X}_d) = \begin{bmatrix} \cos(\theta_d) & -\sin(\theta_d) & 0 & 0 \\ \sin(\theta_d) & \cos(\theta_d) & 0 & 0 \\ 0 & 0 & 1 & 0 \\ 0 & 0 & 0 & 1 \end{bmatrix} \tag{3.49}$$

The velocity plan is rotated and smoothed using a low-pass second order filter of cut-off pulsation ω_0 to obtain the robot intended velocity $\dot{\mathbf{X}}_d$ in the global frame

$$\frac{\dot{\mathbf{X}}_d}{\mathcal{V}} = \frac{\omega_0^2}{(s+\omega_0)^2}\mathbf{R}_d \tag{3.50}$$

For example, when transiting from **Stop** to **Walk**, the value of the first component of $\mathcal{V}$ instantly switches from 0 to 0.5 m/s. This velocity step needs to be smoothed into a more human-like motion with filter (3.50).

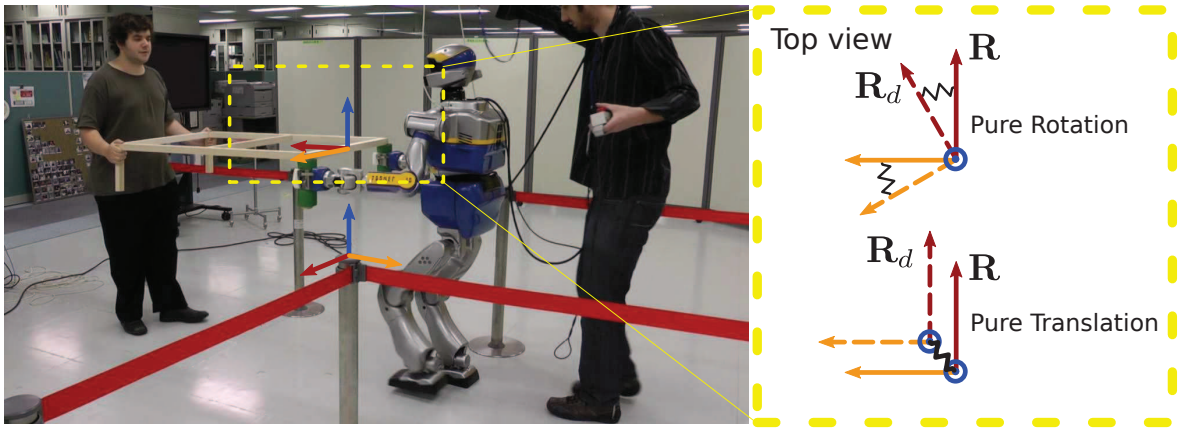

Figure 3.12: Important frames used in our 3D control scheme (x in red, y in orange, z in blue). The first one is the fixed global word frame that is visible in the foreground of the picture. The two other ones are attached to the object and are pictured within the yellow rectangle. The frame $\mathbf{R}$ is rigidly linked to the object while the frame $\mathbf{R}_d$ is linked to the object by the impedance. The latter one is the impedance nodic reference.

3.4.3 Reactive Generation of Primitives Sequences

Every motion primitive is characterized by the components of the velocity plan that are non-zero. They are represented in Table 3.3

Table 3.3: Zero and Non-zero components of the velocity plan for each primitive.

Primitive	Frontal	Lateral	Vertical	Angular
Stop	0	0	0	0
Walk	+	0	0	0
Side	0	+	0	0
Turn	0	0	0	+
Walk/Turn	+	0	0	+

The same switching criteria from Section 3.3 are used, on the component of interest. The only particular cases are the switches from **Turn** or **Side** to **Walk**. We consider that walking forward/backward is the privileged way of moving during a transportation task, so we allow these two quick transitions.

3.4.4 Turning

As stated in Section 3.2, the point $\mathbf{X}$ may be chosen anywhere as long as it is rigidly linked to the object. This choice was of little importance in the 1D case. Indeed, every two points rigidly linked to the object are separated by a vector that is constant in the world frame. It is important in the 3D case. The impedance nodic reference $\mathbf{X}_d$ can be conceived as an

intended position for the point $\mathbf{X}$. And given our choice of rotation motion primitives, $\mathbf{X}_d$ will be the rotation center of the object. In other words, the rotation center of the object will be close to $\mathbf{X}$.

Ideally, the center of rotation of the object should be parametrizable depending on the motion to perform. For instance, when only rotating the table (primitive **Turn**), the center of the object is the most reasonable choice if we wish to minimize the distance both partners have to travel. However, putting the center of rotation too far away from the robot's body also forces the robot to perform lateral steps, which puts a lot of strain on it. We therefore choose either the middle of the robot's grippers or its CoM as the $\mathbf{X}$ point and leave the dynamic determination of a center of rotation to future work. The drawback is that it forces the human partner to travel much more distance than the robot when rotating the object on the spot.

3.5 Switch to Leader Mode with a Joystick

As stated in Section 3.2, our pHRI control law is independent of how the desired trajectory $\mathbf{X}_d$ is generated and thus allows easy role switching between follower and leader behaviors. To demonstrate the capability of our control scheme to handle appropriately this issue, we generate an intended trajectory $\mathbf{X}_d$ for the robot directly from a joystick to give a leader behavior to the robot. Hence a second human can pilot the robot during the task of transporting the table with the first human partner.

We use a joystick with a digital directional touchpad to control the robot in leader mode. We use the same FSM as in the follower mode (Fig. 3.10), where the transitions are triggered by the touchpad state instead of haptic clues, thus determining the motion direction. The velocity amplitude is set constant and not controlled by the joystick. The output plan $\mathcal{V}$ from the FSM is then used the same way it is in Section 3.4 to compute the desired trajectory $\mathbf{X}_d$ for the impedance control. The joystick operator can assume or give up the leadership of the task by pressing a specific key on the joystick. The minimal input we use from the joystick and the unnecessary force feedback assess the robustness of our control scheme.

3.6 3D Experimentation with the HRP-2 Humanoid Robot

3.6.1 Scenario

To validate our proposed control scheme, we realize the scenario described in Fig. 3.1. We use the same low-level control scheme as in Section 3.3.3.

3.6.2 Results

As pictured in Fig. 3.13, the robot successfully performs the proposed scenario with a human partner. Trajectories $\mathbf{X}$ and $\mathbf{X}_d$ are shown in Fig. 3.14. Their corresponding velocities on the frontal axis – the direction of the motion – are shown in Fig. 3.15. Forces applied by the

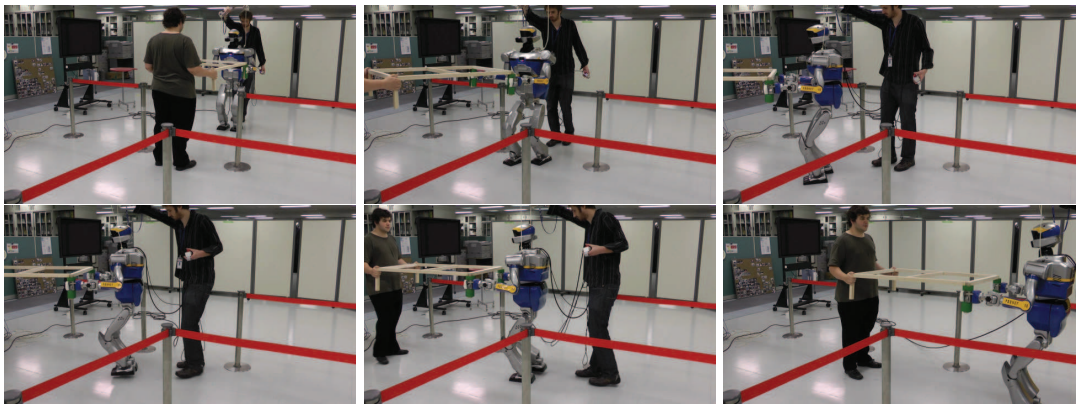

Figure 3.13: HRP-2 realizing the 3D transportation task with a human partner, as a proactive follower (first line) and then as a leader (last line)

robot on the object on the frontal axis are shown in Fig. 3.16. We can observe that although the robot's plan $\mathbf{X}_d$ roughly approximates the object's effective trajectory, the force applied on the object by the robot is greatly reduced compared to a fully passive behavior during the follower mode (until $t = 20$s). Note that during the follower mode, the robot applies negative mechanical power on the object. Around $t = 12$s the robot wrongly detects an intention to stop from the leader, but is able to quickly recover and start again. It results in a high peak in the force profile. Such a misunderstanding might also happen with a human/human dyad.

At around $t = 20$s, the joystick operator takes over the control on the robot and completes the scenario. The human partner is then able to follow the robot. The interesting point is that during the second part of the scenario, the force applied by the robot on the object and the velocity of the object have the same sign. The robot applies positive mechanical power on the object, and therefore the human partner applies negative power at constant velocity. Moreover, the leader phase's force intensity is similar to the follower phases, which shows that our implementation of the robot's follower behavior yields similar results to the human partner's performance as a follower, force-wise at least.

3.7 Discussion and Concluding Remarks

We propose a complete control scheme that allows the HRP-2 robot to perform a 1D, then a 3D beam transportation task with locomotion, jointly with a human partner.

The first main contribution is a control law for physical interaction that unifies leader and follower collaborative modes for trajectory-based tasks. Although we presented it for a simple impedance controller, it can be generalized to more complex impedances –e.g. non-linear.

The second important contribution is the decomposition of a trajectory in a few motion primitives that allows succinctly describing a large diversity of motions. The example we described and implemented is but a simple one. It can be made more complex with additional primitives to widen the possible motions and tasks. We are thinking about primitives that

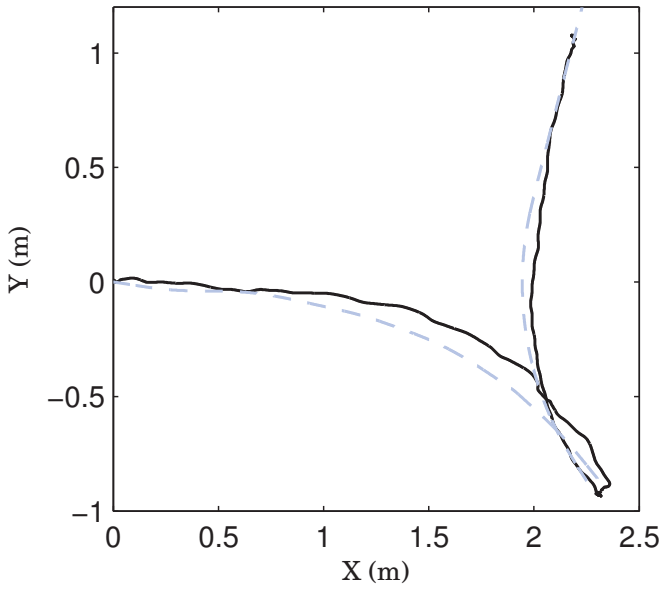

Figure 3.14: Trajectories of the object in the XY plan: the admittance controller output $\mathbf{X}$ *in black, follower desired trajectory* $\mathbf{X}_d$ *in dotted light blue. The transportation starts at* $(0, 0)$ *and ends around* $(2, 1)$*. The role switching occurs when the object is around* $(2.3, -1)$*.*

allow precise positioning of the manipulated object, which we are not considering in our beam transportation task. Nevertheless, adding more primitives also made more complex the design of a reactive generator of primitives' sequences. It can also be generalized to completely different tasks if one can find a good decomposition of the task in elementary subtasks and a method to determine the switch timings between these subtasks.

Besides, our control scheme produces a proactive follower behavior. Thanks to a decomposition of the task in sub-motions, the robot is able to guess the human partner's intended trajectory that leads to a substantial reduction of the workless interaction force. Its amplitude is similar to the one observed when the human partner acts as a follower. Our results are similar to the ones obtained in [10] with a similar approach, but allows performing a wider variety of motions.

The third important contribution is the possibility to switch between the follower and leader behaviors in the course of the task. The future investigation step is to find a method to reactively generate a leader plan for the robot and how and when to automatically switch between the two modes.

Several other improvements could be brought to our design. For instance, a Hidden Markov Model (HMM) can possibly be used instead of our current FSM. The interpolation method from the primitive parameters to the full motion phase could also be improved. A polynomial interpolation may yield better results: the minimum jerk trajectory would be a very reasonable choice as in [10]. We found in [50] that phase decomposition coupled to minimum jerk interpolation on each phase tended to better describe the motion than a minimum jerk interpolation on the overall motion.

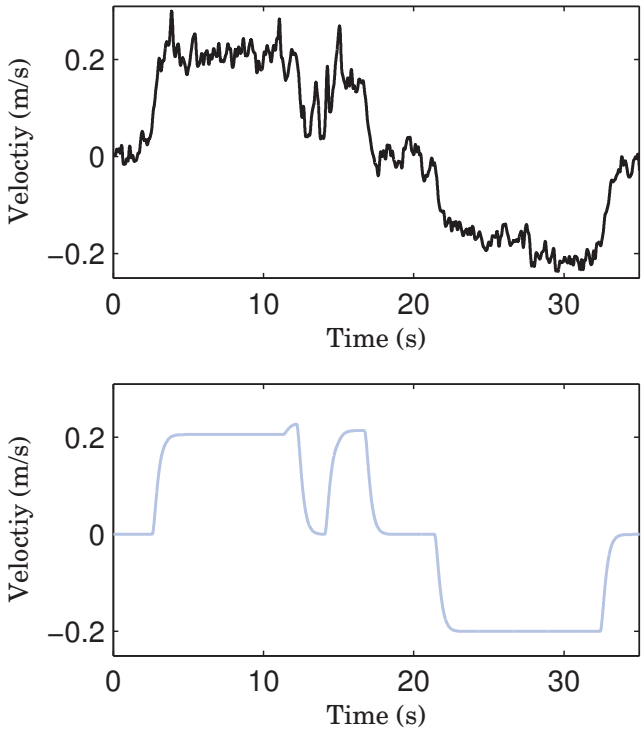

Figure 3.15: Velocities of the object on the robot's frontal axis: the admittance controller output $\dot{\mathbf{X}}$ *in black (top), robot desired velocity* $\dot{\mathbf{X}}_d$ *in light blue (bottom). The role switching occurs at around* $t = 20s$.

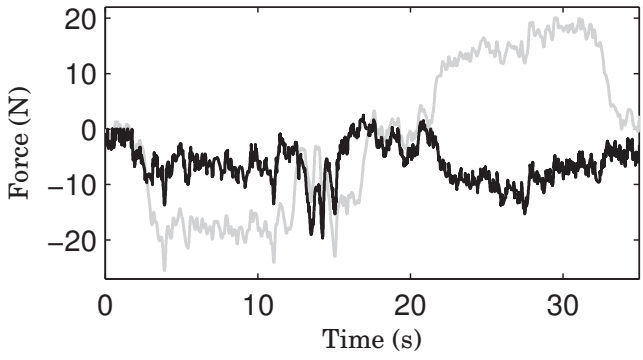

Figure 3.16: Force applied by the robot on the object (black) on the robot's frontal axis. The gray curve represents the damping part of the interaction force $\mathbf{F} = -B\dot{\mathbf{X}}$*: it is the force that would be applied by the robot with a passive behavior. The role switching occurs at around* $t = 20s$.

We also use constant impedance parameters. Coupling our approach with a variable impedance one as in [13] may improve the proactive behaviors as well as the quality of the haptic feeling for the human partner.

Improvements can be added to the feed-forward of the object dynamics in the impedance constraint. Indeed the object we use in our experiments is not heavy –two kilograms– thus the

object's inertia barely impede the task execution. However, handling a heavier and bulkier object may be more problematic with our implementation. Besides, the estimation of the object's inertia is not realized online so that the robot is not able to adapt to changes of inertia during the task, if a heavy object is put on the carried object during the transportation for instance or if a ball is rolling on it.

In the next chapter, we focus on the robot's balance and on how the robot can take advantage of the physical interaction with the human partner to maintain and/or restore its balance. This example will highlight the advantages of our unified impedance control law and of the sequencing of primitives.

4

User Studies

Contents

In the previous chapter, we devised a control scheme, which allows a humanoid robot to transport a table jointly with a human. The robot is programmed to act proactively. That is, it predicts the motion and integrates predicted effects of own and human motion into its own controller.

As far as a human user is involved, although our proposed control scheme exhibits good "quantitative" results, one still needs to assess the added value of proactivity in the general practice. In human centric systems, stability and performance in terms of automatic control engineering and practices are not a proof of efficient usability. In this chapter, we conduct two experiments where non-expert users use the humanoid robot as a partner in the transportation task. First, we compare our proactive approach with the *passive approach* proposed by Evrard *et al.* [19]. Then, we perform a second study to evaluate the change in the performance when participants perform the same task repeatedly. Finally, we confront the results to those where human dyads perform a similar task.

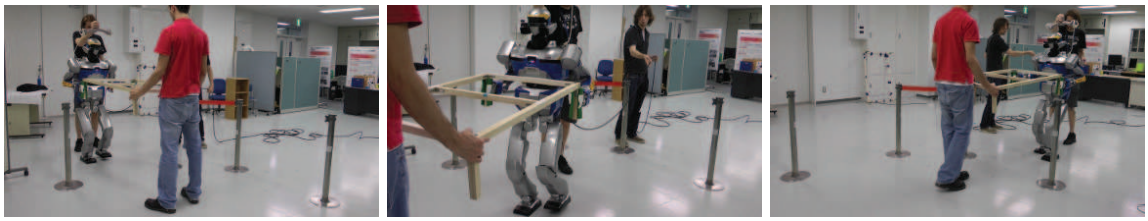

Figure 4.1: The task to perform: The human-robot dyad carries the beam through two doorways that form a 90° angle. The dimensions of the beam do not allow performing the task with a single bend, so that the human has to pass backward through the first door and forward through the second one (and vice versa for the humanoid robot). The first picture (left) shows the starting position, whereas the last one (right) shows the stop condition when half the beam crosses the second doorway.

4.1 Passive dynamic behavior of the hands and decoupled gait

The purpose of this user study is to quantify and qualify the added value of a proactive behavior of the robot, see our Chapter 3, relatively to a pure passive follower controller as proposed in [19]. However, for the reasons we explain shortly, we do not use Evrard's own implementation. We instead re-implemented his approach in our control architecture framework in order to benefit and take advantage of the improvements made on the HRP-2's hardware and software as follows.

4.1.1 Improvements on HRP-2

Evrard's results published in [19] are based on a hardware and software that evolved substantially since many improvements have been made on HRP-2 humanoid robot. On the hardware side, the robot's wrists are improved by an extra degree of freedom –now we have a total of seven dof instead of six– on each arm. Previously, HRP-2 had only two dof per wrists, which impaired its ability to perform gripper's orientation without using upper joints that are the elbow, the shoulder or the torso. Typically, small changes in the orientation of the gripper resulted in large motions of the elbow. The elbow could easily get aligned with the shoulder, resulting in a kinematic singularity, or could also easily collide with the trunk of the robot. With 7dof wrists, this problem is substantially reduced and we needed to account this additional dof in the geometric, kinematic and dynamic models of the robot and integrate this changes to the stack-of-task controller.

In the other side, the HRP-2's embedded computer processor was changed to a more powerful one in order to improve computational performance, which allows the use of more complex algorithms for walking, such as Herdt's Walking Pattern Generator [30]. Moreover, the software architecture also evolved to a newer version that includes new developments together with a more stable OpenHRP simulator and controller.

For all the previous reasons, it is clear that it wasn't fair to confront a passive controller to our proactive one without rewriting honestly the controller proposed in [19], what we fairly did.

4.1.2 Implementation of the passive controller

Evrard's approach can be summarized as follows:

- passive dynamic behavior of the robot's hands in the world frame (explained in the state-of-the-art chapter), and
- decoupling of gait and hands motion.

The decoupling of the gait and hands motion is shared with our approach, as well as the choice to control the dynamic behavior of the hands in the world frame.

4.1.2.1 Passive Dynamic Behavior

Evrard's approach consists in imposing a passive dynamic behavior in the transportation task (i.e. horizontal) plane (x, y and θ), that is

$$\mathbf{F} = M\ddot{\mathbf{X}} + B\dot{\mathbf{X}} \tag{4.1}$$

where we re-use the same notations as in Chapter 3.

The robot has obviously to support, at least partially, the weight of the object on the vertical axis. Evrard's solution was to implement a stiff dynamic behavior on the vertical

axis with a fixed height reference. The general impedance constraint is therefore

$$\mathbf{F} = M\ddot{\mathbf{X}} + B\dot{\mathbf{X}} + K(\mathbf{X} - \mathbf{X}_d) \tag{4.2}$$

where $K = \begin{bmatrix} 0 & 0 & 0 & 0 \\ 0 & 0 & 0 & 0 \\ 0 & 0 & K_z & 0 \\ 0 & 0 & 0 & 0 \end{bmatrix}$ and $\mathbf{X}_d = \begin{bmatrix} 0 \\ 0 \\ z_d \\ 0 \end{bmatrix}$, K_z begin a constant, strictly positive coefficient, z_d being a constant height.

For the comparative user study, we use identical impedance parameters for the proactive and passive implementations when they are not zeros. They are listed in Table 4.1.

Table 4.1: Impedance parameters used in the comparative user study.

Proactive	Passive
$K_{xy} = 60$N/m	$K_{xy} = 0$N/m
$K_z = 250$N/m	$K_z = 250$N/m
$K_\theta = 30$N/rad	$K_\theta = 0$N/rad
$B_{xy} = 90$N.s/m	$B_{xy} = 90$N.s/m
$B_z = 100$N.s/m	$B_z = 100$N.s/m
$B_\theta = 70$N.s/rad	$B_\theta = 70$N.s/rad
$M_{xy} = 8$kg	$M_{xy} = 8$kg
$M_z = 8$kg	$M_z = 8$kg
$M_\theta = 8$kg.m^2	$M_\theta = 8$kg.m^2
$z_d = 1$m	$z_d = 1$m

4.1.2.2 Gait Decoupling

In contrast to the proactive behavior, the robot does not generate a reference trajectory $\mathbf{X}_d$ to determine a gait velocity. Therefore, we use the velocity of the robot's grippers. As can be seen in Chapter 3 (Fig. 3.8 and 3.15) with the proactive behavior, the grippers velocity is disturbed by oscillations that comes from the robot's stepping. To reduce the influence of the oscillations, we use a Kalman filter.

The state of the Kalman filter is a 9-dimension vector composed of the robot's Center of Mass (CoM) desired 3D position (x, y, θ) in the world frame, as well as the desired velocity and acceleration of the same components. The model we choose is a constant acceleration model, so that the state-transition model matrix F_k is

$$F_k = \begin{bmatrix} I_3 & I_3\delta t & I_3\frac{\delta t^2}{2} \\ 0 & I_3 & I_3\delta t \\ 0 & 0 & I_3 \end{bmatrix} \tag{4.3}$$

where I_3 is the 3×3 identity matrix and δt is the time step (5ms in our case).

The observation vector of the Kalman filter is a 3-dimension vector composed of the robot's (CoM) desired 3D position (x, y, θ) in the world frame, so that the observation model matrix H_k is

$$H_k = \begin{bmatrix} I_3 & 0 & 0 \end{bmatrix} \tag{4.4}$$

The desired 3D position $\mathbf{C}_d$ of the robot's CoM, e.g. the observation, is computed from the output position of the admittance controller $\mathbf{X}$ by specifying a constant relative position $\mathbf{L}$ between the grippers and the CoM

$$\mathbf{C}_d = \mathbf{X} + R_z(\theta)\mathbf{L} \tag{4.5}$$

where $R_z(\theta)$ is the rotation matrix around z-axis of angle θ, θ being the angular component of $\mathbf{X}$.

We tune the matrices of covariance of the process and observation noise offline, using data recorded with the proactive behavior. We find a compromise that minimizes the oscillations without adding too much lag.

4.2 Proactive versus Passive Comparative Study

4.2.1 Setting

This comparative user study is based on the scenario described in Fig. 4.1 where participants have to transport a beam with the HRP-2 robot through two doorways, with two different behaviors of the robot: proactive and passive. The purpose of this study is to compare how easy it is for the participants to perform the task with the robot with each behavior. Eight participants take part to the study (3 females, 5 males) of age ranging from 22 to 37 (average 28.3, std 6.0) and height ranging from 155cm to 184cm (average 170cm, std 8.6cm). Every participant is right-handed. They are from various countries: France (3 participants), Japan (2), Mexico (2) and Taiwan (1). Five of them are knowledgeable to robotics, but none had previously interacted physically with a robot. The user study took place at the CNRS-AIST Joint Robotics Laboratory (JRL) in Tsukuba, Japan, from the 26th of June to the 1st of July 2013.

As described previously, the task consists in carrying a beam (See Fig. 4.2) with the HRP-2 humanoid robot through two doorways from a fixed start position. Measurements are stopped once the blue marker on the object has reached the second doorway. Then the experimenter signals the participants to stop the robot. We intentionally did not select the final stop to be the end of the recorded data because it is a singular state, which will require maneuvers and a considerable cognitive load on the user. As a result, the data will be biased. Each doorway consists in two pillars that are 120cm apart from each other (center-to-center). Each pillar is a 84cm-high, 8cm-diameter-wide cylinder, so that a doorway is 112cm wide at body level. Each pillar has a 8mm-high, 30cm-diameter-wide cylindrical base which the robot must not step on, at the risk of losing its balance. Thus, at ground level, the doorway is only 90cm-wide. The complete set-up is pictured in Fig. 4.3.

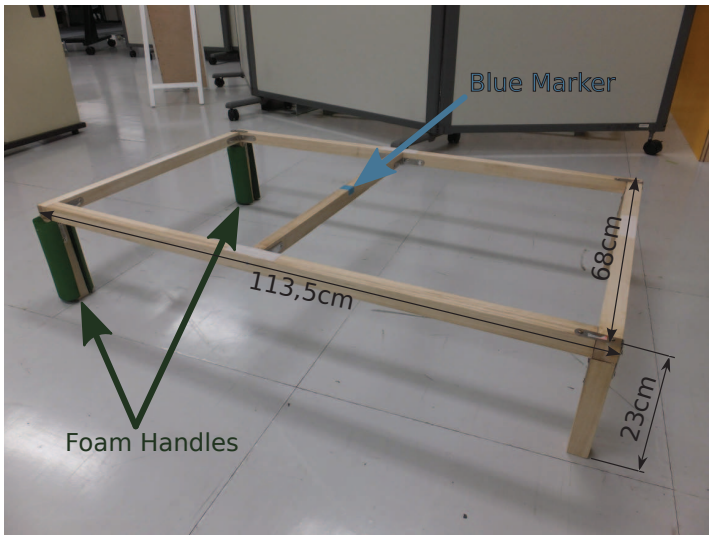

Figure 4.2: Object to transport jointly and its dimensions. The beam is made of wood, reinforced with steel brackets at corners. 2cm-thick green foam handles are added on the robot side so that the robot can safely grasp the object. The total weight is 1.6kg. A blue marker is added at the center of the table: the task is over as soon as this marker aligns with (i.e. reaches) the second doorway (See Fig. 4.3).

For security reasons, the robot's shoulders are loosely attached to a crane by two ropes so that the robot does not fall on the floor if a problem occurs. Instead the robot would hang on the two ropes. A first operator is positioned directly behind the robot to move the crane and follow the robot. This operator carefully positions himself identically in each experiment in order not to disturb the participant. A second operator helps the first by keeping the electric cables out of the robot's way.

To limit the interference between the two control strategies, half the participants start with the proactive behavior and follow with the passive one (Group Pro-Pas), while the other half first tests the passive behavior, then the proactive one (Group Pas-Pro). They are not informed which one they are testing first.

Prior to the experiments, the experimental set-up and the task were explained to the subjects. In particular, since the robot is put in a follower mode, the subjects were informed not to expect cognitive capabilities comparable to that of a human. They were also informed that the robot would not take lateral steps by its own and that they should negotiate the turn as if they were manipulating a non-holonomic two-wheeled cart. We also informed them that the robot is blind and cannot see the pillars, so that they have to guide it, and also that they must keep the beam horizontal. The subjects were explained that the trajectory pictured in Fig. 4.3 is the best option to fulfil the task. To support the explanations, the task was performed twice: one time with subject taking the robot's role while the experimenter takes the role the subject would have during the real experiment, a second time with the experimenter taking the role of the robot while the subject leads the joint action. Both trials were timed with the same conditions as with the robot.

After this, the following instructions were then given to proceed to the experiment:

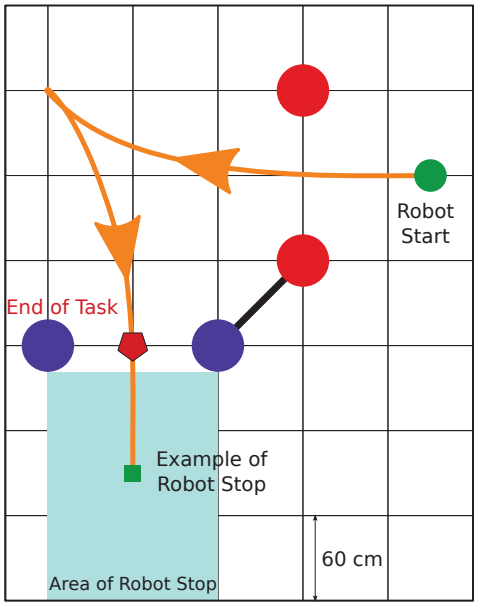

Figure 4.3: Task Set-up: the doorways are delimited by two set of pillars (red and blue circles). An example of robot's trajectory that does not require lateral stepping is pictured in orange. Measurements are stopped once the blue marker on the object (See Fig. 4.2) has reached the second doorway (blue doorway, red pentagon). Then the experimenter signals the participants to stop the object.

1. the robot is blind and cannot see the pillars; you have to guide it,
2. the robot should not be expected to perform lateral steps,
3. the table has to be kept horizontal
4. relax and focus on the task, not on the robot,
5. the task starts as soon as the experimenter tells you it,
6. stop the robot when the experimenter tells you it.

The participants started with a familiarization session, in which they carried out the task with the robot until they succeeded once. No data was recorded during this phase. Then they performed the task again and data was recorded. If they failed to perform the task, data were not saved and the participants started again until they succeeded. The number of failed trials *after* the practice session was recorded. After completion of one successful trial, participants were asked to fill Questionnaire 1 (see Section 4.2.3). Then participants tested the second behavior using the same protocol.

4.2.2 Measurements

The goal of the user studies is to evaluate how easy it is for the participants to perform the task with the robot. To that purpose, we use the variables of the robot control (See Chapter 3,

Fig 3.5). More precisely, we use the force/torque input $\mathbf{F}$ of the admittance controller as well as its velocity output $\dot{\mathbf{X}}$. The force/torque input is computed from data from the robot's wrist force sensors, and the velocity is computed to respect the impedance constraint. Offline, we use this force and velocity data to estimate the mechanical power that is input to the robot, as well as the mechanical work transferred to the robot during the task. We also measure the completion time of the task as well as the number of failures after the practice session. In the following, we detail how each indicator is calculated and what result is expected from the comparative study.

4.2.2.1 Total mechanical work input by the human partner during the trial

In a standalone mode (one person or robot), transporting an object in a horizontal plane, with zero velocities of the object CoM at the beginning and at end of the task, requires theoretically no energy from the transporter. Indeed the work W done by the transporter during the task is equal to the variation of mechanical energy ΔE during the task

$$W = \int_{t_0}^{t_f} \mathbf{F}^T \dot{\mathbf{C}} \mathrm{d}t = \Delta E \tag{4.6}$$

where $\dot{\mathbf{C}}$ is the object's CoM 4D-velocity and $\mathbf{F}$ the 4D-force applied by the transporter on the object's CoM. Both vectors are in the world frame. Since only gravity and the transporter act on the object, the variation of mechanical energy can be decomposed into the variation of kinetic energy ΔE_k and the variation of gravitational potential energy $\Delta E_{p,g}$ between initial time t_0 and final time t_f

$$W = \Delta E_k + \Delta E_{p,g} = \frac{1}{2}\Big[\dot{\mathbf{C}}^T M_O \dot{\mathbf{C}}\Big]_{t_0}^{t_f} + \Big[mgz\Big]_{t_0}^{t_f} \tag{4.7}$$

Thus $\dot{\mathbf{C}}(t_0) = \dot{\mathbf{C}}(t_f) = 0$ (zero initial velocities) and $z(t_0) = z(t_f)$ (horizontal task) imply $W = 0$.

When two robots or persons are collaborating on a common task, the sum of the work they each transfer to the object follows the same rule. However, in general, each work is not zero and the partners exchange energy during the task. Consider the case of a passive behavior of one transporter, as in (4.1). The elementary work input by the passive transporter at point $\mathbf{X}$ on the object is

$$\delta W = (-M\ddot{\mathbf{X}} - B\dot{\mathbf{X}})^T \dot{\mathbf{X}} \delta t = -\ddot{\mathbf{X}}^T M \dot{\mathbf{X}} \delta t - \dot{\mathbf{X}}^T B \dot{\mathbf{X}} \delta t \tag{4.8}$$

The first term integrates straightforwardly over time, but the second does not.

$$W = -\frac{1}{2}\left[\dot{\mathbf{X}}^T M \dot{\mathbf{X}}\right]_{t_0}^{t_f} - \int_{t_0}^{t_f} \dot{\mathbf{X}}^T B \dot{\mathbf{X}} \mathrm{d}t \tag{4.9}$$

In our case, the initial velocity is zero and the final is not, so that the first term is negative because M is definite positive. However, the contribution of this term to the total work is negligible. In the study, the lowest work for the passive behavior we recorded is 67.2J, whereas

the highest velocity and angular velocity norms are 0.33m/s and 0.26rad/s respectively. Since we choose $M = 8I_4$, we have, in the worst case scenario

$$\frac{1}{2}\left[\dot{\mathbf{X}}(t_f)^T M \dot{\mathbf{X}}(t_f)\right] = \frac{8}{2}\dot{\mathbf{X}}(t_f)^T \dot{\mathbf{X}}(t_f) < 4(0.33^2 + 0.26^2) = 0.706 \ll 67.2 \tag{4.10}$$

Thus we can drop the contribution of any variation of kinetic energy in the total work[1] Thus, the important contribution to work $\dot{\mathbf{X}}^T B \dot{\mathbf{X}}$ is always positive, since B is definite positive. Therefore, each elementary work due to the damping part is negative and adds up with the integration over time, unlike the acceleration term. This is considered to be the major drawback of the passive behavior that requires additional energy from the human partner.

The goal with pro-active behaviors is to reduce significantly this extra-energy that is spent by the human partner if s/he has to deal with a pure damping controller, resulting in a passive behavior. This extra energy is transferred to the robot and is the work done on the robot, e.g. the opposite of the work done by the robot on the object. Therefore, we choose mechanical work input into the robot as one of our main indicator of the performance of our control scheme. As stated previously, we do not use a measured velocity, but the output of the admittance controller $\dot{\mathbf{X}}$ instead and suppose the low level position control to be accurate. Thus elementary work δW_r input into the robot is

$$\delta W_r = \mathbf{F}^T \dot{\mathbf{X}} \delta t \tag{4.11}$$

where $\mathbf{F}$ is the total force applied *on* the robot at point $\mathbf{X}$ and the input of the admittance controller. This elementary work δW_r is then discretely integrated with $\delta t = 5$ms to obtain W_r

$$W_r = \sum_{t_0}^{t_f} \mathbf{F}^T \dot{\mathbf{X}} \delta t \tag{4.12}$$

As we claimed, the purpose of pro-activity is to reduce the extra quantity of work the human partner has to input into the object because of the robot. Hence, a significant decrease in the work input into the robot is an important indicator of our control scheme's performance.

4.2.2.2 Completion Time

The time taken to complete the task is also an important indicator of the performance of our control scheme. With the passive behavior of constraint (4.1), a constant velocity of the robot's grippers is linearly linked to the force applied on them. Moreover, a high force, in addition to being uncomfortable for the human partner, is likely to destabilize the robot and topple it. Therefore, the maximal force that can be applied on the robot limits its velocity

[1] The mass of the object is $m = 1.6$kg and thus lower than the inertia parameter in the impedance constraint. Concerning the inertia of the object at point p, we can major it by $mL(p)^2$, where $L(p)$ is the radius of the smallest ball of center p containing the object. Since mechanical work is exchanged through a contact, we are only interested in the points p that are on the object, and thus we can major any $L(p)$ by the major dimension of the object, which is $\sqrt{1.135^2 + 0.23^2 + 0.68^2} = 1.35$m (see Fig. 4.2). Therefore, the object's inertia is also lower than the inertia parameter of the impedance constraint.

in the passive case. In contrast, our proactive behavior allows any combination of force and velocity (yet limited by the capacity of the robot and the human).

As stated previously, we do not measure the actual velocity, but use the output of the admittance controller instead, which is only an approximation – although a good one. That is why we privilege the completion time that is related to the average velocity and is easily measured with a chronometer. We choose this solution to measure the completion time when the participants complete the task with the experimenter. When they perform the task with the robot, an operator clicks in a menu at the start and stop signals from the experimenter. This action launches a command that requests data from the robot's embedded control computer on the current iteration. Because the robot's control computer is real-time, the knowledge of the start and end iterations i_0 and i_f allows computing the completion time τ as simply as

$$\text{Completion Time} = (i_f - i_0 + 1)\delta t \tag{4.13}$$

with $\delta t = 5$ms. It is also used to restrict the other data to the correct time window; for instance, it gives the knowledge of t_0 and t_f for (4.12).

We expect our proactive behavior to allow higher velocities and hence a faster completion time compared to the passive one.

4.2.2.3 Number of Failures

It is important for the task to be repeatable at will in similar experimental conditions. It is somehow a proof of robustness. This is why the number of failures is the last main indicator of our control scheme performance. If the participants easily provoke an error in the robot, such as lost of balance, auto-collision, velocity/acceleration limits violation, it endangers the robot as well as the human partner, which is why the scenario is considered to be failed in such events. A high rate of failure would make our control scheme non-viable. In this case, it is difficult to judge which results to expect. Theoretically, our control scheme could allow the robot to impose, to a certain extent, its limits to the human partner. However, because our implementation of the FSM is simplistic, it would be at the cost of less pro-activity. For this user study, we make the choice to tune the parameters of our control scheme to favor pro-activity over conservativeness. In comparison, the passive behavior seems more conservative. Therefore, a good result would be a similar number of failures between the proactive and passive behaviors.

In the following, we present additional indicators to compare the performances of both controllers' behaviors, but are, to some extent, redundant with the three previous ones.

4.2.2.4 Maximal and average velocity and angular velocity norm over the trial

As we expect relatively lower completion times, we assume velocities (average or maximum) to be higher with the proactive behavior when compared to the passive one. Similarly, we also do not measure velocities directly but use the output $\dot{\mathbf{X}} = \begin{bmatrix} v_x & v_y & v_z & v_\theta \end{bmatrix}^T$ of the admittance controller instead. The velocities' indicators we use are given by the following

formulas

$$\text{Average Velocity Norm} = \frac{1}{i_f - i_0 + 1} \sum_{i=i_0}^{i_f} \sqrt{v_x(i)^2 + v_y(i)^2 + v_z(i)^2} \tag{4.14}$$

$$\text{Maximal Velocity Norm} = \max_{i \in [i_0, i_f]} \left(\sqrt{v_x(i)^2 + v_y(i)^2 + v_z(i)^2} \right) \tag{4.15}$$

$$\text{Average Angular Velocity Norm} = \frac{1}{i_f - i_0 + 1} \sum_{i=i_0}^{i_f} |v_\theta(i)| \tag{4.16}$$

$$\text{Maximal Angular Velocity Norm} = \max_{i \in [i_0, i_f]} |v_\theta(i)| \tag{4.17}$$

4.2.2.5 Maximal and average horizontal force and torque norm over the trial

The force applied on the object by the human not directly necessary to the movement is also an important indicator. The work is more significant since it only counts the forces that are co-linear to the object velocity and also counts them positive if they are in the same direction and negative otherwise. Nonetheless, in the formula of the mechanical work, the amplitude of the forces are mixed with the amplitude of the velocities. Therefore, a decrease in the work can be explained by a decrease of the velocities or of the forces or of both. That is why looking at velocities and forces can be informative. However, we are not interested in the forces that counter the object's weight, thus we do not take the vertical component of the force in this indicator.

We then use the sum of the 4D-forces $\mathbf{F} = \begin{bmatrix} f_x & f_y & f_z & f_\theta \end{bmatrix}^T$ applied on the robot's grippers at point $\mathbf{X}$ in the world frame to compute the forces indicators:

$$\text{Average Horizontal Force Norm} = \frac{1}{i_f - i_0 + 1} \sum_{i=i_0}^{i_f} \sqrt{f_x(i)^2 + f_y(i)^2} \tag{4.18}$$

$$\text{Maximal Horizontal Force Norm} = \max_{i \in [i_0, i_f]} \left(\sqrt{f_x(i)^2 + f_y(i)^2} \right) \tag{4.19}$$

$$\text{Average Torque Norm} = \frac{1}{i_f - i_0 + 1} \sum_{i=i_0}^{i_f} |f_\theta(i)| \tag{4.20}$$

$$\text{Maximal Torque Norm} = \max_{i \in [i_0, i_f]} |f_\theta(i)| \tag{4.21}$$

We expect higher velocities and lower work for the proactive behavior. One solution to obtain this is to have lower average horizontal forces and torque levels. Yet, we expect the proactive behavior to require punctual high forces and torques (peeks), during accelerations and decelerations for instance. It is therefore possible that no difference is observed for the maximal force/torque levels.

4.2.2.6 Maximal and average power norm over the trial

Finally, we compare maximal and average norms of the power input into the robot over the trial. We first exhibit the formulas before making any comment

$$\text{Average Power Norm} = \frac{1}{i_f - i_0 + 1} \sum_{i=i_0}^{i_f} \left| \mathbf{F}^T(i) \dot{\mathbf{X}}(i) \right| \tag{4.22}$$

$$\text{Maximal Power Norm} = \max_{i \in [i_0, i_f]} \left| \mathbf{F}^T(i) \dot{\mathbf{X}}(i) \right| \tag{4.23}$$

Note that equation (4.22) is similar to the work in (4.12) but with absolute values. In the force indicator section, we claimed that the combination of lower work and higher velocities could be obtained with lower forces. Another option is to have elementary works that compensate each other in the sum (4.12). Note that for the passive behavior in (4.8), this compensation mechanism never works for the damping term which is the dominant part. The elementary works for the damping part are always negative and thus add up. This compensation mechanism would not appear with the mean of the absolute values. We define a power ratio ρ with

$$\rho = \frac{\sum_{i_0}^{i_f} \mathbf{F}^T(i) \dot{\mathbf{X}}(i)}{\sum_{i_0}^{i_f} \left| \mathbf{F}^T(i) \dot{\mathbf{X}}(i) \right|} \leq 1 \tag{4.24}$$

It can be easily verified, using (4.12)(4.13) and (4.22) that

$$\rho = \frac{\text{Work}}{\text{Average Power Norm} \times \text{Completion Time}} \tag{4.25}$$

Since the kinetic energy variations are negligible, we expect $\rho = 1$ in the passive case. The power ratio indicates what part of a decrease in mechanical work levels must be attributed to the compensation with elementary work of opposite signs.

To summarize, a decrease in mechanical work can be caused by

- a decrease in velocity;
- a decrease in force;
- a shorter completion time;
- a compensation due to the robot inputting work into the human.

Theoretically, another cause would be to have uncorrelated forces and velocities such that $\mathbf{F}^T \dot{\mathbf{X}}$ is close to zero[2]. However, we cannot figure-out how this could happen in practice because of physical causality.

Since we expect higher velocities, the decrease in mechanical work should be explained by a decrease in force, a shorter completion time, and the robot inputting work into the human. We hypothesize a decrease of force to be the major cause.

[2]For instance, sinusoidal forces and velocities that have a phase offset of $\pi/2$.

4.2.3 Questionnaires

In addition to data, we submit a questionnaire to the participants after each condition. Questionnaire 1 is given to the participant after the first condition and consists in six statements regrouped in three factors, that are described in Table 4.2. The participants have to evaluate each statement on a seven-point Likert scale, which range from "Strongly Disagree" to "Strongly Agree". Questionnaire 1 also contains a free remarks section. The choice of the factors and statements is based on similar experiments found in the literature, e.g. [71] [54].

Table 4.2: Questionnaire 1 factors and statements.

Factor	**Statement**
Ease of Task	It was easy to perform the task with the robot.
Ease of Task	I perceived that the robot understood what I wanted it to do.
Co-Experience	The physical contact with the robot felt natural.
Co-Experience	I liked to interact with the robot.
Feeling of Security	I feared to use the robot, as an error might harm me.
Feeling of Security	I feared to use the robot, as an error might harm the robot.

Table 4.3: Questionnaire 2 factors and statements.

Factor	**Statement**
Ease of Task	It was easier to perform the task with the robot than with previous condition.
Ease of Task	I perceived that the robot better understood what I wanted it to do more than with previous condition.
Co-Experience	The physical contact with the robot felt more natural than with previous condition.
Co-Experience	I liked to interact with the robot more than with previous condition.
Feeling of Security	I feared to use the robot more than with previous condition, as an error might harm me.
Feeling of Security	I feared to use the robot more than with previous condition, as an error might harm the robot.

Questionnaire 2 is submitted after the second condition. It reuses the same statements as Questionnaire 1, but as a comparison with the first condition, and uses the same seven-point Likert scale as Questionnaire 1, as well as a free remarks section. Factors and statements are presented in Table 4.3.

4.2.4 Results

For each indicator, we plot a bar chart that presents the value of this indicator in both passive (red) and proactive (blue) cases for each participant (Fig. 4.4 to 4.10). The participants are separated in two groups: the "Pro-Pas Group" (Subject 1 to 4) that started the experiment with a proactive behavior of the humanoid robot, then did the passive one, and the "Pas-Pro Group" (Subject 5 to 8) that started the experiment with the passive behavior, then the proactive one.

For each indicator, we perform two t-tests using the `ttest2` function from MATLAB®. The first test assumes equal variances, whereas the second does not. Both tests yield very similar results though. The results of these tests are presented in Tables 4.4 and 4.5.

4.2.4.1 Important Indicators

The most notable result of this comparative study is the much lower work input into the robot in the proactive case as seen in Fig. 4.4, top. The p-value is extremely low (the lowest of the study at 5.5×10^{-9}, see Table 4.4). This result validates the performance of our proactive control scheme, energy-wise. Looking at the mean work among the participants, our proactive control scheme allows a reduction of 71% of the work input into the robot. This is the result we expected, but not with such important discrepancy.

Table 4.4: Important Indicators t-tests results, assuming equal ($=$) and unequal ($\neq$) variances, with 5% significance level. Blue cells indicate that a significant statistical difference is observed (p-value $< 5\%$).

Indicator	Proactive Mean	Passive Mean	p-value $=$	p-value $\neq$
Work [J]	22.6	78.2	5.5×10^{-9}	9.2×10^{-8}
Completion Time [s]	36.3	52.2	2.3×10^{-2}	2.4×10^{-2}
Nb of Failures	1.0	0.2	9.0×10^{-2}	1.0×10^{-1}

Although the number of failures seems slightly higher in the proactive case than in the passive one (Fig. 4.4, bottom), no significant statistical difference is observed (p-value of 9.0×10^{-2}, see Table 4.4). Although this result shows that our approach is not too poor in terms of repeatability, it also shows that more testing, i.e. more participants, is necessary to really evaluate the performance of our proactive control scheme in this regard. Besides, it is worth noting that some subjects had difficulties to complete the training phase with the proactive behavior. Particularly, two subjects that are knowledgeable to robotics failed many times to achieve the task during the proactive training phase.

Finally, Figure 4.5 compares the task completion times. The completion times achieved when the participants performed the task in a human dyad with the experimenter are shown as another indication. The proactive case shows a shorter completion time, which is confirmed by the t-tests results (p-value of 2.3×10^{-2}, see Table 4.4). Comparing the means

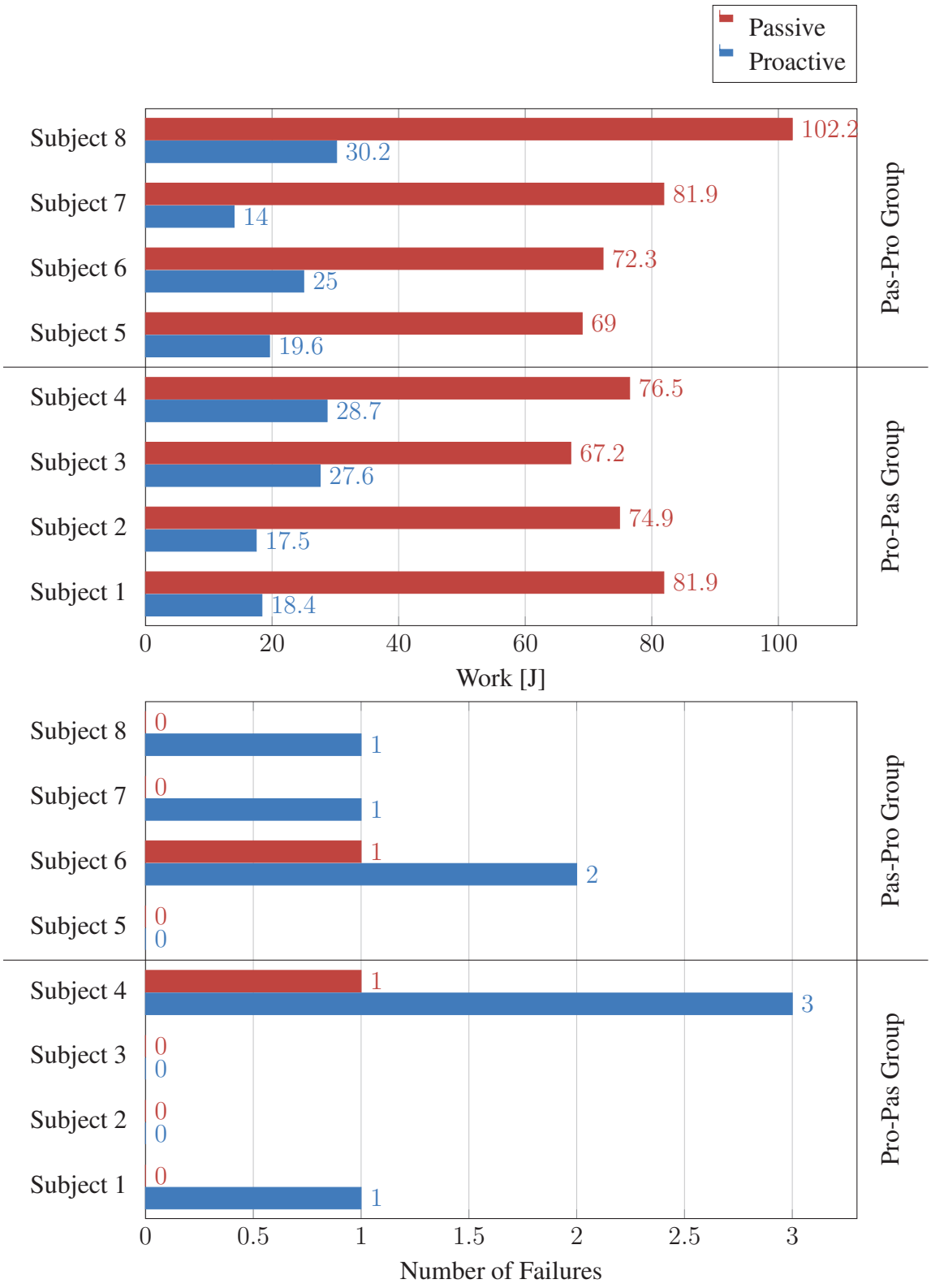

Figure 4.4: Work and Number of failures in the comparative user study.

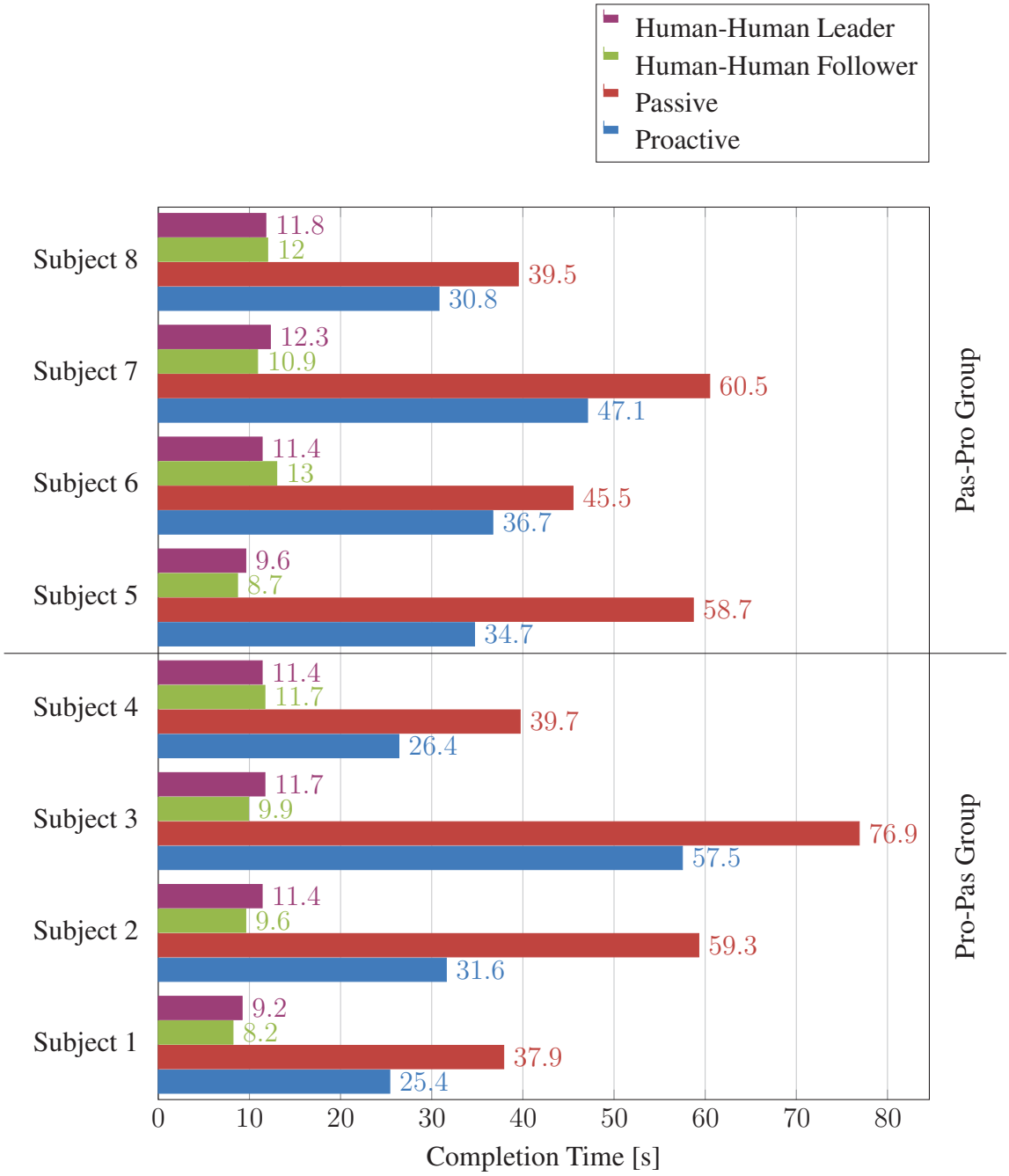

Figure 4.5: Completion times in the comparative user study. Here the completion times achieved when the participants performed the task with the experimenter are shown. First, the participants followed the lead of the experimenter (green), then they lead the task (purple).

gives an improvement of 30% of the completion time between proactive and passive. The improvement of the completion time is limited by the walking capabilities of the robot. Indeed, we believe that the velocity of the robot is limited by the interaction in the passive case. The proof is that the robot performs the task faster with the proactive behavior. Contrariwise, we limit the velocity plan $\mathcal{V}$ of the robot (See Chapter 3) to prevent the robot's grippers to move faster than the robot can walk. For instance, on the frontal axis, the maximal walking velocity of the robot is 0.3m/s. Therefore we limit the velocity plan of the robot's gripper to 0.25m/s. Because of the impedance, the actual velocity of the grippers might be greater than 0.25m/s, or even than 0.3m/s, but at the cost of an increased force from the human partner. We believe that improving the walking capabilities of the robot will contribute to improve the completion time even further in both schemes, and for the proactive behavior in particular. Improving the robot's walking capabilities will certainly improve task repeatability.

To summarize, the results concerning the decrease of mechanical work exceed by far our expectations. By comparison, the improvements of the completion time are satisfactory, but could be improved further with better walking capabilities of the humanoid robot. Further investigations are necessary to validate or invalidate the repeatability of our proactive control scheme. In the following we analyze the other indicators in order to deepen the comparison.

4.2.4.2 Other Indicators

The t-test results are presented in Table 4.5.

Velocity indicators. The results (see Fig. 4.6) indicate an improvement of 41% in average velocity norm (p-value of 7.7×10^{-3}) and 36% in maximal velocity norm (p-value of 2.3×10^{-3}) and are coherent with the improvement of completion time. However, Fig. 4.7 shows no such significant improvement in angular velocity norm, whether average or maximal (p-values of 8.9×10^{-2} and 5.6×10^{-2} respectively). The major cause for this is, again, the walking capabilities of the robot, that are even more limited in rotation than in the frontal direction. We limit the velocity plan in rotation to $0,18$rad/s for a limit in rotation gait of 0.2rad/s, which is punctually exceeded by every participant but Subject 7.

Force/Torque indicators. The results (see Fig. 4.8) indicate a 50% decrease in the average horizontal force norm with an excellent p-value of 2.9×10^{-6}, which is the second distinguishing result of the study. As expected, the force levels strongly contribute to the 71% decrease in mechanical work. The t-test also indicate a 28% decrease in the maximal horizontal force norm (p-value of 2.3×10^{-2}). It is a good point because the human partner has to input less force, but also regarding the robot stability. The robot toppling likeliness is lower because of an excessive force with our proactive control scheme. It is worth noting though that the ratio of the maximal horizontal force norm over the average horizontal force norm is greater in the proactive case (around 3) than in the passive case (around 2). This highlights the differences in passive and proactive behaviors. The force pikes are likely to correspond to velocity pikes in the passive case, whereas they are more likely to occur during changes of plan –changes of motion primitive for instance– in the proactive case. Note also the results

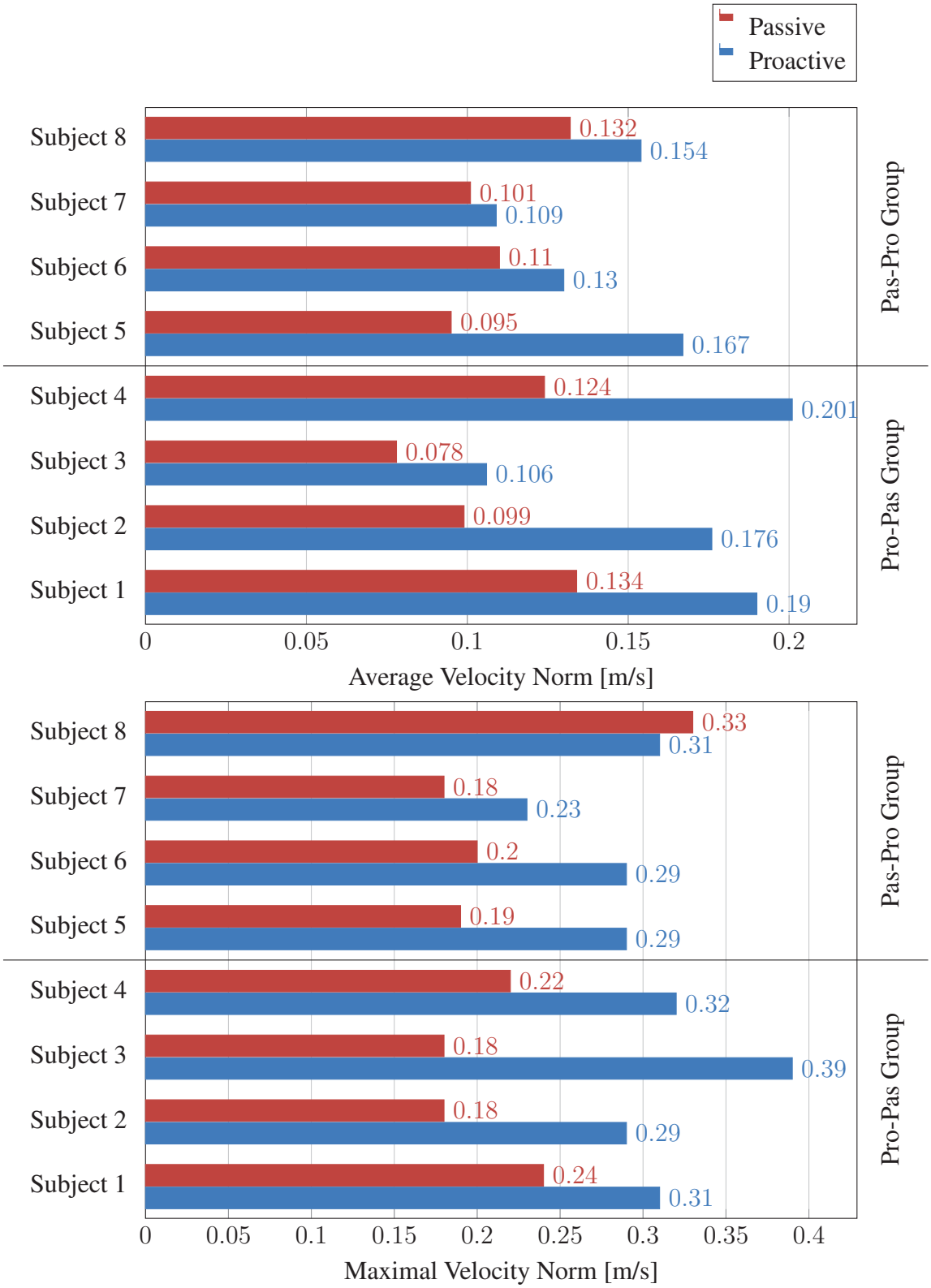

Figure 4.6: Average and maximum velocity norms in the comparative user study.

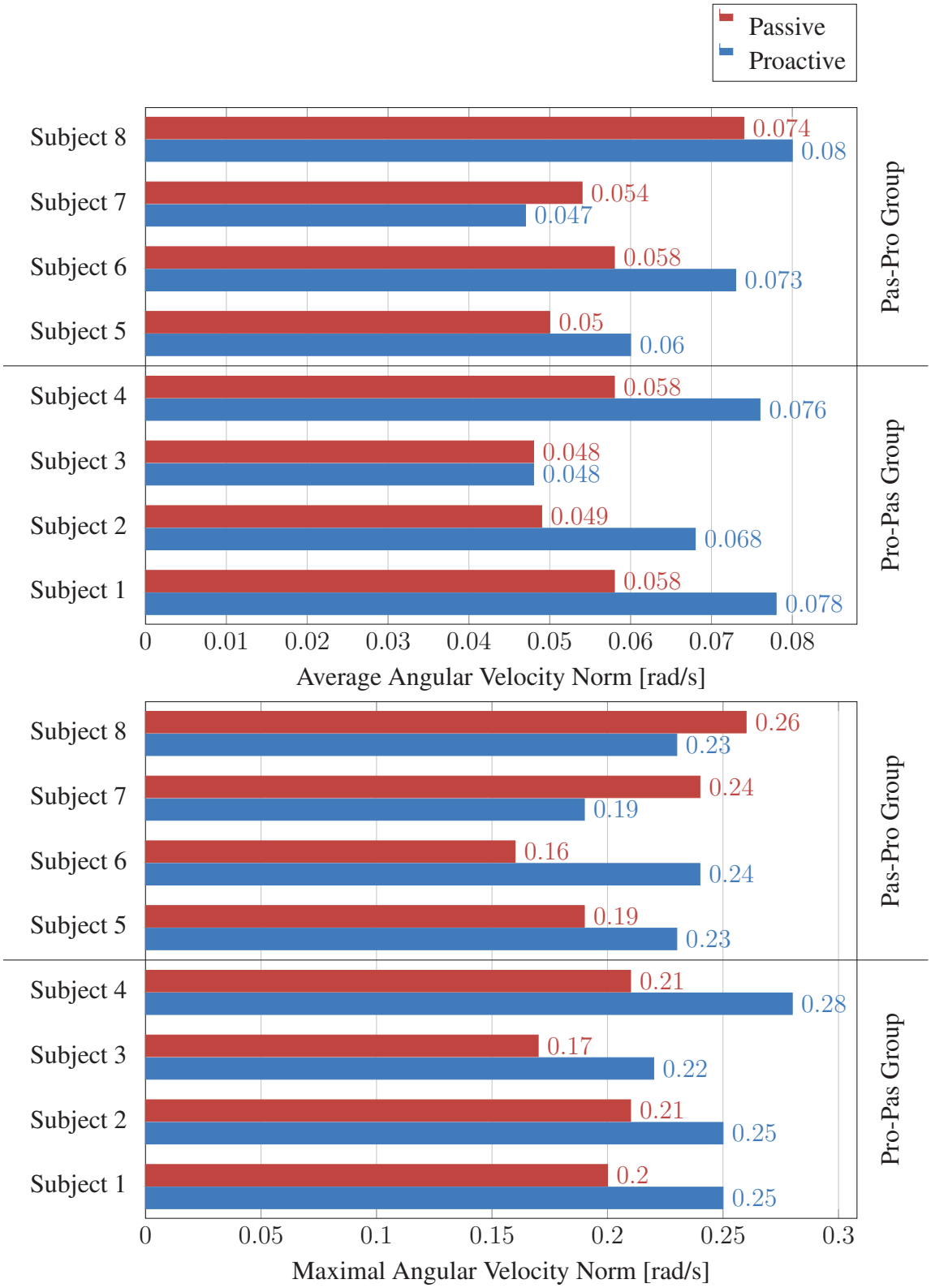

Figure 4.7: Average and maximum angular velocity norms in the comparative user study.

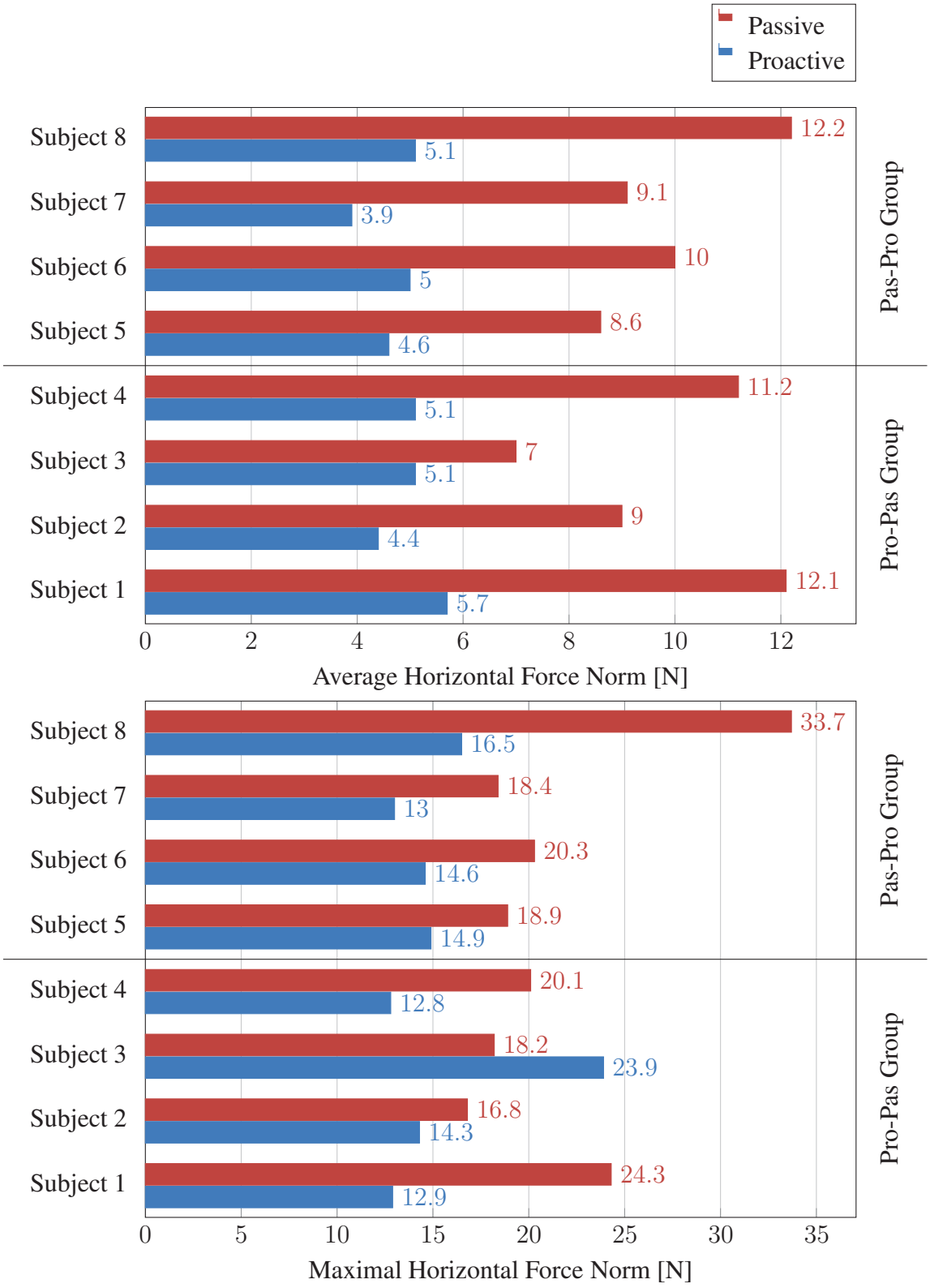

Figure 4.8: Average and maximum horizontal force norms in the comparative user study.

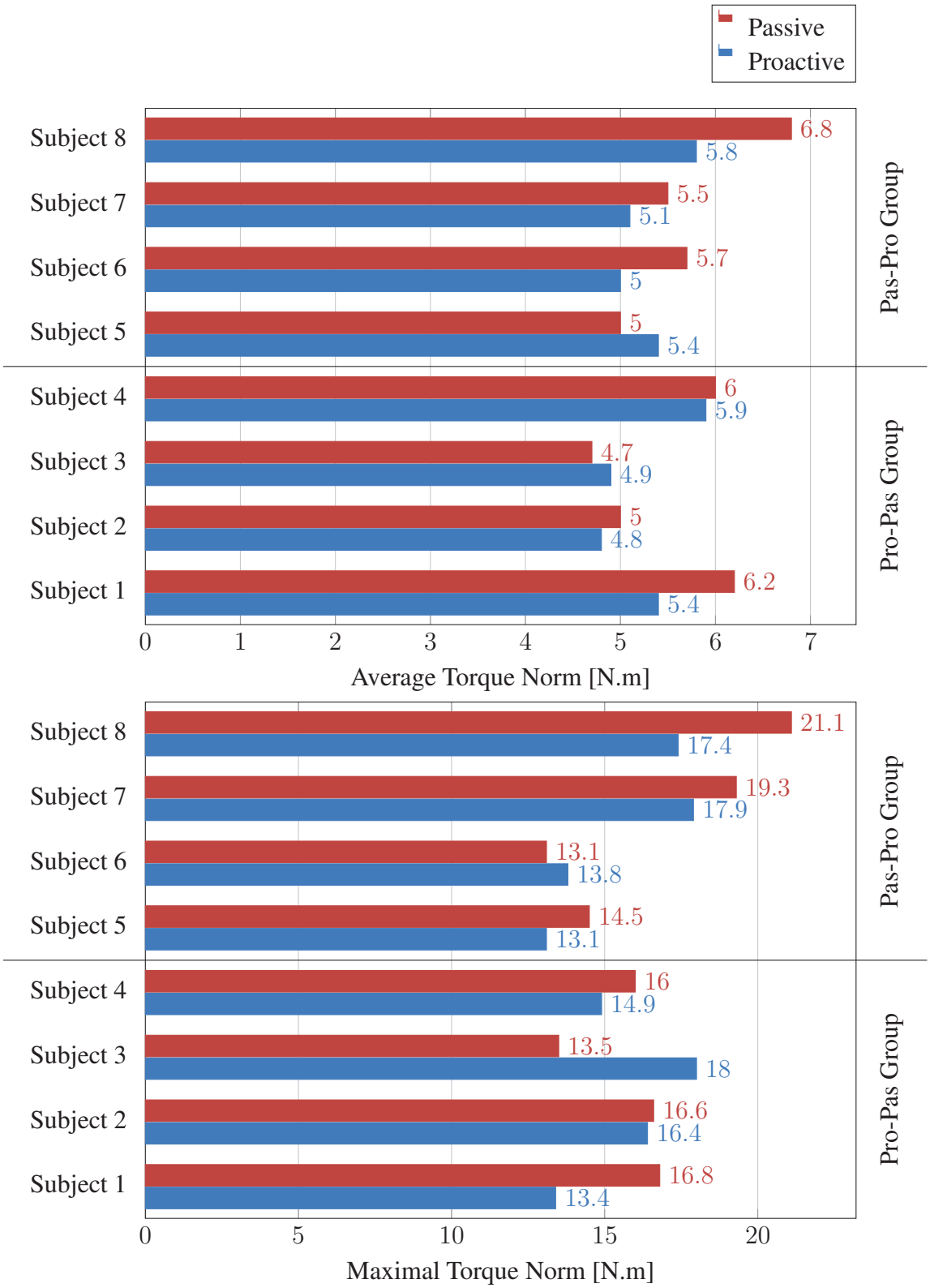

Figure 4.9: Average and maximum torque norms in the comparative user study.

of Subject 3; the maximal horizontal force norm is higher in the proactive case than in the passive one. In this case, Subject 3 applied a high force at the beginning of the task. This event also shows in the maximal power norm chart. The event is punctual and does not affect much the average horizontal force norm.

Both average and maximal torque norm show no significant statistical difference. Globally, the results in rotation are less convincing, e.g. lower p-values, than the translational ones. The limitation in velocity may explain that difference. It might also simply point at lower performances of our control scheme in rotation. Further investigations are necessary in this regard.

Power indicators. The results (see Fig. 4.10) show a 49% decrease in the average power norm (p-value of 2.9×10^{-3}), which is in the same line as the average force/torque decrease. No significant difference is observed in the maximal power norm. Note the high maximal power norm in the proactive case for Subject 3. As explained in the force paragraph, this event does not particularly affect the average power norm. This validates the fact that the proactive behavior can lead to *punctual* power pikes, but it allows to globally decrease the power input into the robot.

Fig. 4.11 shows the power ratio defined by (4.24). As expected, the power ratio is equal to 1 in the passive case. In the proactive case, all participants have a power ratio ranging from 0.75 to 0.9, except for Subject 7 who has a very low power ratio of around 0.55. Thus, the compensation of elementary works of opposite signal plays an important role in the decrease of the global work, although not comparable to the decrease of the horizontal force norm.

To summarize, our proactive control scheme shows substantial quantitative performances comparatively to the passive approach. It shows:

- a 71% decrease of mechanical work input into the robot;
- a 30% decrease in completion time;
- a 41% increase of average velocity norm and a 36% increase of maximal velocity norm;
- a 50% decrease of average horizontal force norm, as well as a 28% decrease of maximal horizontal force norm;
- a 49% decrease of average power norm.

The most convincing results are the highly significant decrease of work and average horizontal force ($p < 10^{-5}$), the latter being the major cause of the former. The decrease of mechanical work is also caused by the compensation of elementary works of opposite signs. The results of completion time and velocity are also good, although limited by the walking capabilities of the robot. Further investigations are also necessary regarding the rotation part of the control scheme.

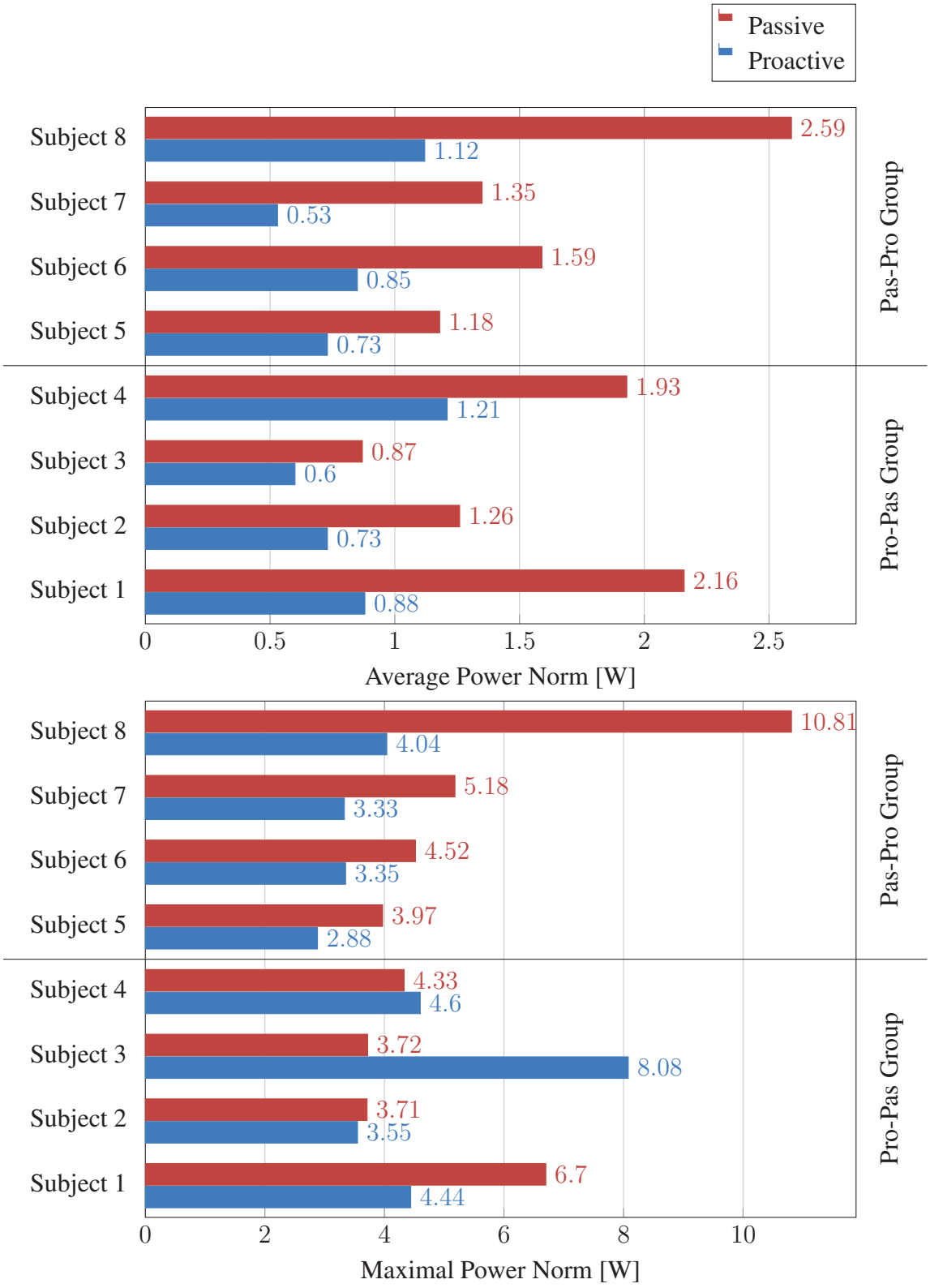

Figure 4.10: Average and maximum powers in the comparative user study.

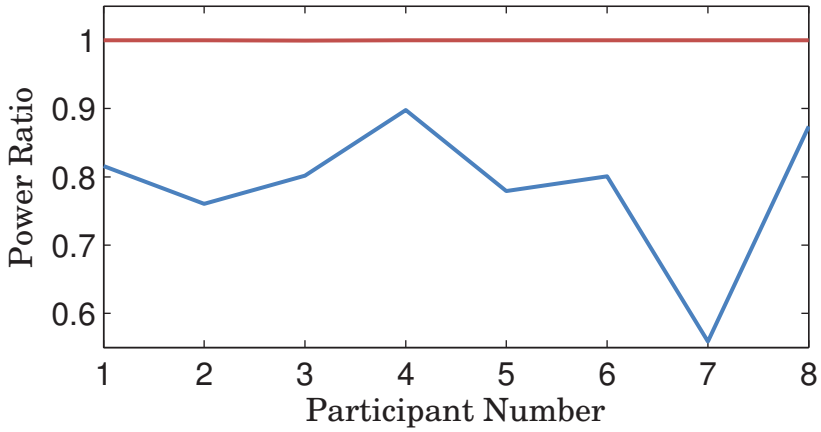

Figure 4.11: Power Ratio for in the passive (red) and proactive (blue) cases.

Table 4.5: Other Indicators t-tests results, assuming equal ($=$) and unequal ($\neq$) variances, with 5% significance level. A blue cell indicates that a significant statistical difference is observed (p-value $< 5\%$).

Indicator	**Proactive Mean**	**Passive Mean**	p-**value** $=$	p-**value** $\neq$
Average Velocity Norm [m/s]	0.154	0.109	7.7×10^{-3}	1.0×10^{-2}
Maximal Velocity Norm [m/s]	0.30	0.22	2.3×10^{-3}	2.4×10^{-3}
Average Angular Velocity Norm [rad/s]	0.066	0.056	8.9×10^{-2}	9.3×10^{-2}
Maximal Angular Velocity Norm [rad/s]	0.24	0.21	5.6×10^{-2}	5.8×10^{-2}
Average Horizontal Force Norm [N]	4.9	9.9	2.9×10^{-6}	6.0×10^{-5}
Maximal Horizontal Force Norm [N]	15.4	21.3	2.3×10^{-2}	2.5×10^{-2}
Average Torque Norm [N.m]	5.3	5.6	2.5×10^{-1}	2.5×10^{-1}
Maximal Torque Norm [N.m]	15.6	16.4	5.4×10^{-1}	5.5×10^{-1}
Average Power Norm [W]	0.83	1.62	2.9×10^{-3}	5.5×10^{-3}
Maximal Power Norm [W]	4.28	5.37	3.1×10^{-1}	3.1×10^{-1}

4.2.4.3 Questionnaire Results

To compare the questionnaire results, we only use the comparative questionnaire, i.e. questionnaire 2 that contains the statements of Table 4.3. For each statement, a score ranging from -3, for "Strongly disagree", to 3, for "Strongly Agree", is attributed. Therefore a score of zero means that the participants evaluated both proactive and passive to be equivalent regarding the statement. Because questionnaire 2 asks the participants to evaluate the second condition relatively to the first one, to obtain the score of the proactive behavior, questionnaire 2 counts positively for Pas-Pro Group and negatively for Pro-Pas Group. For example, if a participant of Pas-Pro Group rates a statement with "Agree", we count a score of 2 for the proactive behavior and a score of -2 for the passive one. Conversely, if a participant of the Pro-Pas also rates a statement with "Agree", we count a score of 2 for the passive behavior and a score of -2 for the proactive one. As the score of the proactive behavior is the opposite of the score of the passive behavior, they have necessarily the same variance. Therefore, we only perform a t-test assuming equal variances. The results of the t-tests are presented in Table 4.6. The individual results are presented in charts 4.12 to 4.14. The free remarks made by the participants are presented in Table 4.7.

The results of the questionnaires are as surprisingly bad for the proactive behavior as the results based on the measurement are good. Concerning the Ease of Task, most participants prefer the passive behavior. They generally find that the passive behavior is easier to guide with the passive behavior. And interestingly, the participants give their preference to the passive behavior for statement "I perceived that the robot understood what I wanted it to do", as if they were attributing more cognitive capacities to the passive behavior than to the proactive one[3]. Some participants note than the passive behavior requires more force from them, but most of them still highlight the capacity to guide the robot correctly as more primordial. An explanation might be that the passive behavior of the robot is more predictable than the proactive one. A course of action would be to train/teach the participants so that they can better predict the reactions of the proactive behavior, which is studied in Section 4.3. It is also clear that these difficulties to predict the robot behavior comes from the difficulties for the participants to assess the physical capacities of the robot – how fast it can move and walk for instance. Subject 5 affirms that "it can be hard to know what the robot can handle". Improving our control scheme to make it more human-like is thus necessary. For this, it will be needed to improve the walking capabilities of the robot. In Section 4.4, we compare our approach with the data gathered for Chapter 2 to get an idea about which indicators must be improved.

Another important factor is the fear to harm the robot. This fear is significantly higher with the proactive behavior as shown in Fig 4.14 and in Table 4.6 (p-value of 1.9×10^{-3}). This is to be put in parallel with the number of failures in Fig. 4.4. It is worth noting that

[3] In questionnaire 1 that absolutely rates the first behavior, the proactive behavior was rated 2, 2, -1 and 1 by the participants of the Pro-Pas Group, whereas the passive behavior was rated with 2 by all four participants of the Pas-Pro Group. Although the score of the proactive behavior is lower, these scores show no significant statistical difference, with the assumptions of equal and unequal variances (p-values of 2.1×10^{-1} and 2.5×10^{-1} respectively).

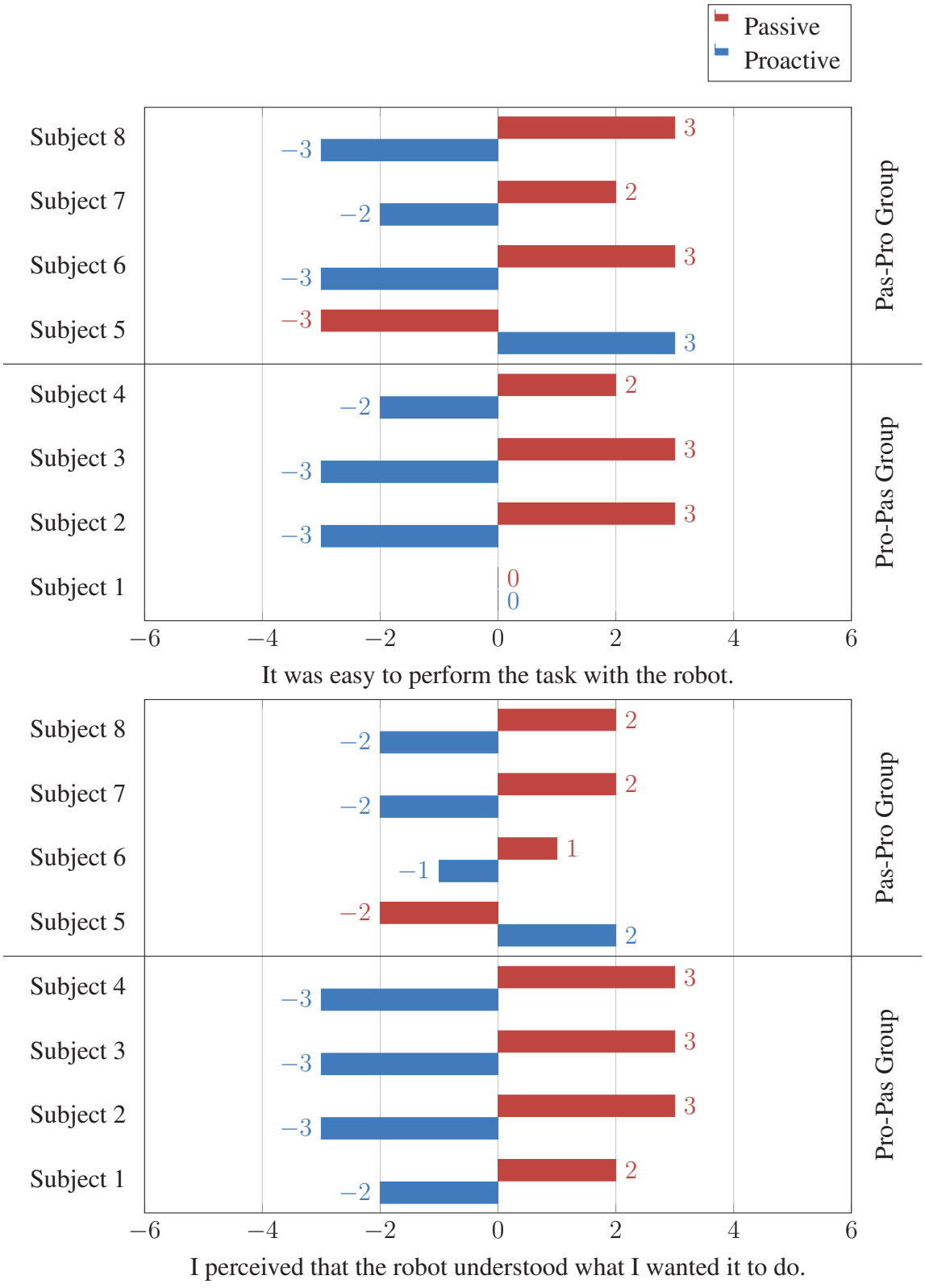

Figure 4.12: Score to 'Ease of Task' items in the comparative user study.

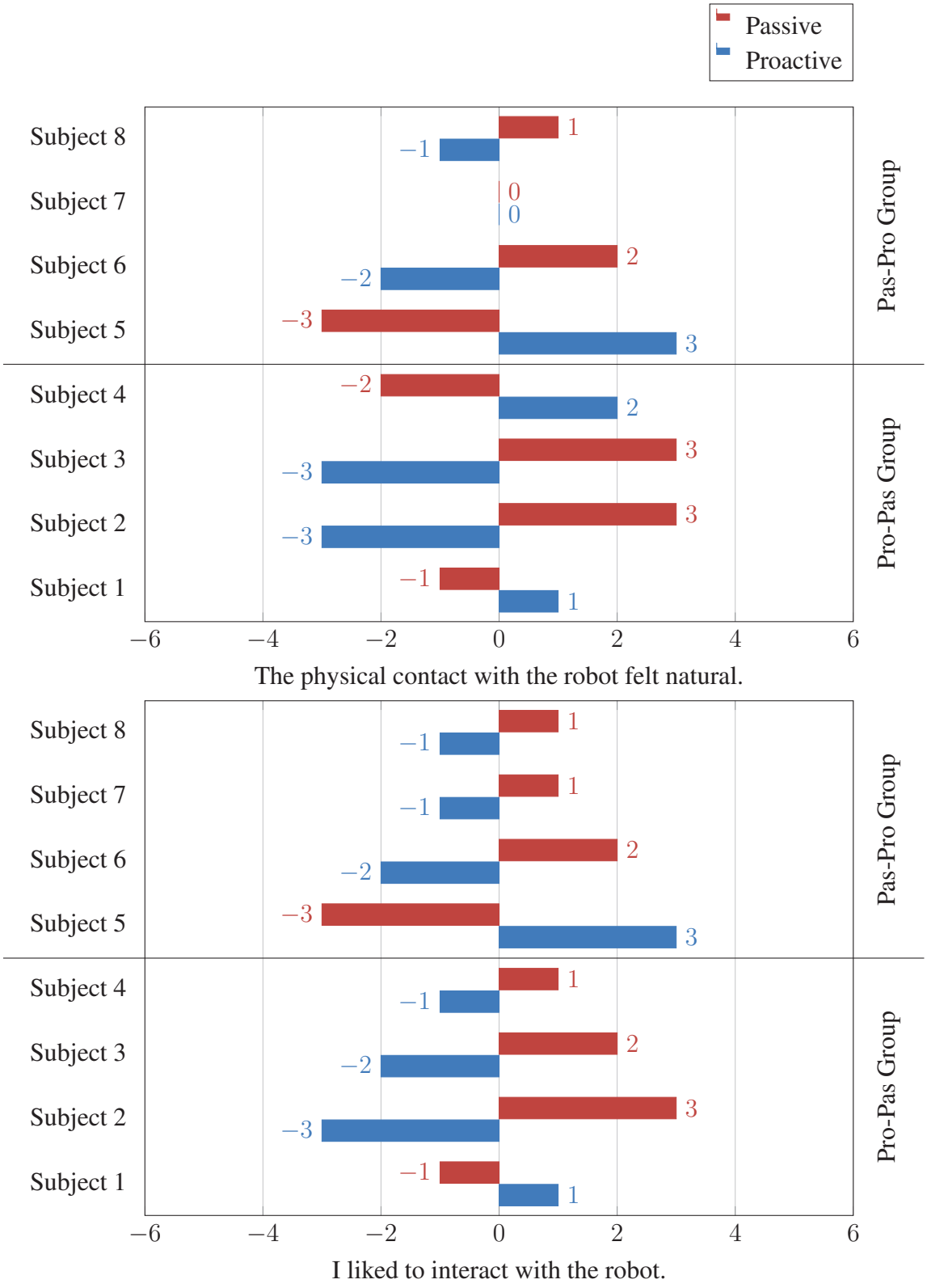

Figure 4.13: Score to 'Co-Experience' items in the comparative user study.

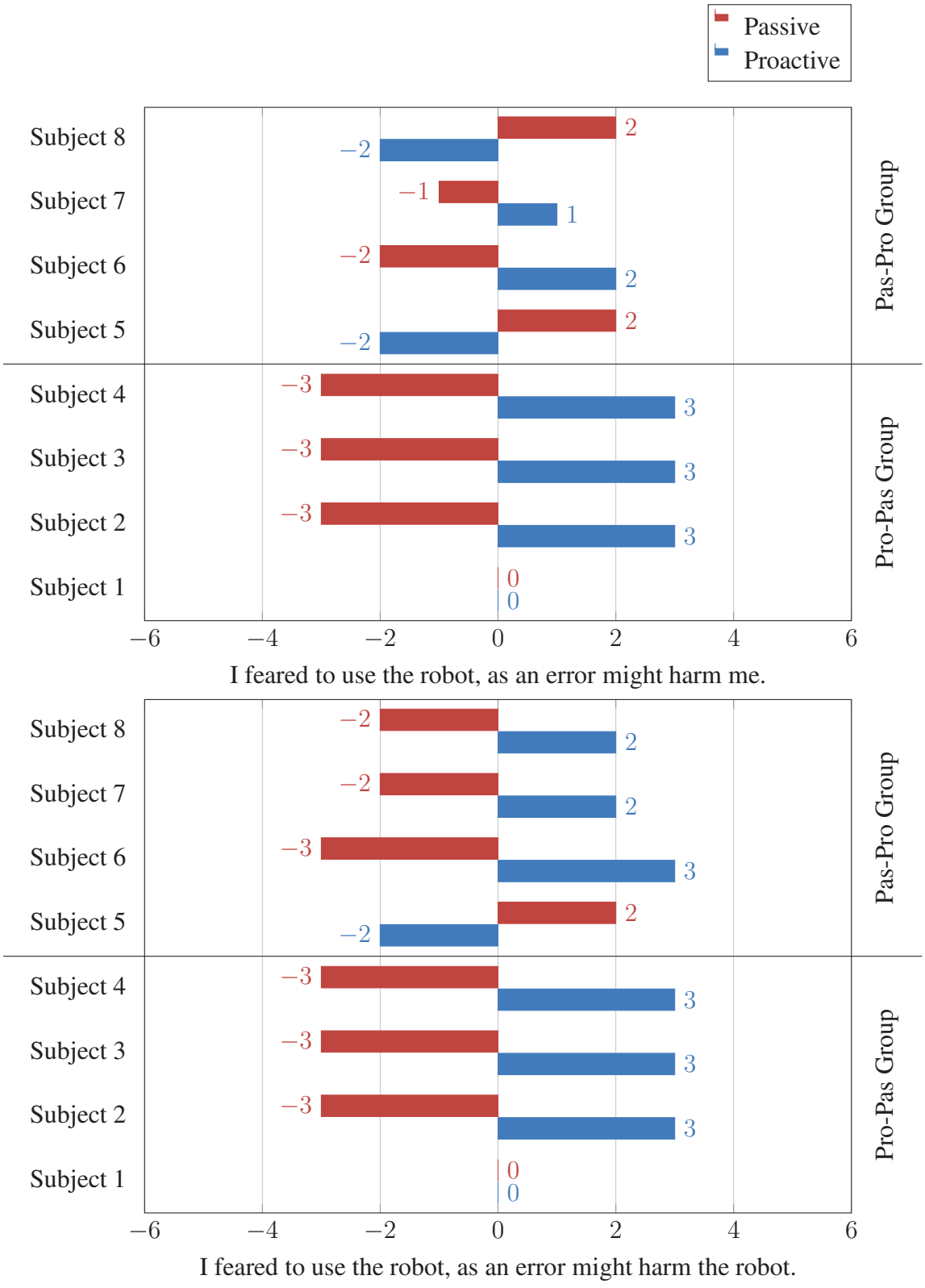

Figure 4.14: Score to 'Feeling of Security' items in the comparative user study.

Table 4.6: Questionnaires t-tests results, assuming equal ($=$) and unequal ($\neq$) variances, with 5% significance level. A blue cell indicates that a significant statistical difference is observed (p-value $< 5\%$).

Item	Proactive Mean	Passive Mean	p-value $=$	p-value $\neq$
It was easy to perform the task with the robot.	-1.6	1.6	8.7×10^{-3}	
I perceived that the robot understood what I wanted it to do.	-1.8	1.8	9.0×10^{-4}	
The physical contact with the robot felt natural.	-0.4	0.4	5.2×10^{-1}	
I liked to interact with the robot.	-0.8	0.8	1.4×10^{-1}	
I feared to use the robot, as an error might harm me.	1.0	-1.0	8.2×10^{-2}	
I feared to use the robot, as an error might harm the robot.	1.8	-1.8	1.9×10^{-3}	

many subjects failed during the proactive behavior experiment. During a failed trial, the experiment cut the power of the robot, which thus falls. Although robot is attached to a crane via ropes, this can be impressive and further increase the anxiety of the participants to harm the robot. This might also explain the preference of the participants for the passive behavior. The passive behavior is more conservative and does not push the robot to its velocity walking limits, unlike the proactive behavior. It is therefore easier to exceed the robot's walking limits with the proactive behavior, thus more likely leading to a failure of the task. We observed that after a failure, participant tend to be much more conservative –too conservative– with the proactive behavior. We hypothesize that they found the starting velocity of the proactive behavior too high –perhaps too risky– and thus tried to slow down the motion. The robot interprets this slowing down as an intention to brake and thus stop while the participants keep pulling to continue the task. Such a sequence is likely to destabilize the robot and cause a failure of the task, which further increases the fear of the participants to harm the robot. Besides, it increases their incomprehension of the robot behavior, as they do not understand what they did wrong to cause such a failure.

In order to decrease this apprehension, we perform an other study where the participants are sound-deprived while performing the task with the proactively behaving robot. The sound deprivation aims at limiting the noise from the robot's actuators. This study is presented in Chapter 5.

Table 4.7: Comments made by the participants in the free remarks section of each questionnaire.

Subject	Questionnaire 1: Proactive	Questionnaire 2: Passive
1		The contact felt more reactive, hence the robot was easier to control but I had to use more force to guide him which felt less like human interaction.
2	The robot seems to have a bit limitation on rotation, range of motion, angular velocity, reaction time.	It seems easier to guide the robot if I rotate with small degrees and slowly.
3	I feel the robot reacts later that I expected. I know that its cognitive capabilities are not the same as with human, however, it is difficult to guide it.	I feel the robot reacted in a smoother way than in the previous experiments.
4	It was a bit more difficult than I expected to cooperate with the robot.	
Subject	**Questionnaire 1: Passive**	**Questionnaire 2: Proactive**
5	Not as easy as it would have been with a human (not as smooth), but still rather straightforward. I perceived that the robot understood what I wanted it to do for the incoming time frame, but not for the long-term plan. I liked to interact with the robot, but still with some fear of doing something wrong. It can be hard to know what the robot can handle. One needs to be extra careful if not used to the robot's actual capabilities.	During both experiments, the robot seemed to "translate" the table to its left towards the end of the experiment. Also, the second experiment decreased the sensation of unease arising from the lack of knowledge on the robot's capabilities. It seemed to catch up more easily with its human partner.
6		It seems that the robot gets an idea of what I want to do during the first seconds of the movements and then sticks to that idea, then it is hard to make him "change his mind".
7	I enjoyed working with the robot. But I was a little bit worried if I broke down the robot. Because the robot is quite expensive!	It felt more difficult to move the robot than previous experiment. When I pulled/pushed the robot, I felt the robot move too much than I expected.
8	I felt that pulling or push the object was a little bit harder than doing that with a human, like if the robot were opposing resistance.	Somehow I felt that it was much more difficult to drive the robot, very unnatural as I perceived it. I think that the first experiment was so much better.

4.2.5 Conclusion of the Comparative Study

Our proactive control scheme allows a 71% decrease in the mechanical input of the human partner, as well as a 50% decrease in the average horizontal forces, while allowing higher velocities and thus a quicker completion of the task. However, these results are contradictory with the participants' feeling that prefer the passive behavior because it is easier to guide and causes less apprehension to harm the robot. Furthermore, many participants perceive

that the passively behaving robot better understands their intentions. We hypothesize that they prefer the passive behavior partly because it is more predictable and more conservative, and thus more reassuring. More thorough investigations are necessary to understand the discrepancy between the good results of the measurements and the bad results from the questionnaires. Improvements on the walking capacities of the robot may also help to decrease the apprehension to harm the robot, as well as bringing the robot's capacities closer to the human's in terms of speed and reactivity. This might make the robot's proactive behavior more predictable.

4.3 Impact of Training on Performance with Proactive

4.3.1 Setting

This user study is based on the same scenario as the previous one. The task is described in Fig. 4.1 where participants have to transport a beam with the HRP-2 robot through two doorways. This time, however, the participants repeat the task five times successfully with our proactive controller solely. The purpose of this study is to evaluate the impact of user repeated training on the performances of our proactive control scheme. Four participants, different from the comparative study, take part to the study (3 females, 1 male) of age ranging from 15 to 30 (average 22.3, std 7.8) and height ranging from 162cm to 180cm (average 169cm, std 8.5cm). Three participants are right-handed the remaining one is left-handed. They are from various countries: France (2 participants), Korea (1) and USA (1). None of them worked in the field of robotics, nor had previously interacted physically with a robot. The user study took place at the CNRS-AIST Joint Robotics Laboratory (JRL) in Tsukuba, Japan, from the 9th to the 11th of July 2013.

The task consists in carrying a beam (See Fig. 4.2) with the HRP-2 through two doorways from a fixed start position. Measurements are stopped once the blue marker on the object has reached the second doorway. Then the experimenter signals the participants to stop the robot. Each doorway consists in two pillars that are 120cm apart from each other (center-to-center). Pillars and doorway have the same dimension as previous studies. The complete set-up is pictured in Fig. 4.3. Similar instructions for security and the experimental set-up are given to the users in this study.

After this, the participants proceed to the first of the five trials; there is no practice session with the robot. We repeat/provide them the following instructions respecting the same sequencing for all the participants:

1. the robot is blind and cannot see the pillars; the participants have to guide it,
2. the robot should not be expected to perform lateral steps,
3. the table has to be kept horizontal
4. the participants has to be relaxed and to focus on the task, not on the robot,

5. the task starts as soon as the experimenter gives the start signal,

6. the participants stops the robot when the experimenter gives the stop signal.

The participants perform five successful trials. If they fail to perform the task, data are not saved and the participants start the trial again until they are successful. We count the number of failures before each trial. For instance, if a participant fails the task twice before Trial 1, two failures are counted for Trial 1. Then, if the same participant fails the task once between Trial 1 and Trial 2, one failure is counted for Trial 2. After five successful trials, participants are asked to fill the same Questionnaire 1 as in the previous study (see Section 4.2.3).

4.3.2 Results

We chose the same indicators as in Section 4.2.2. They are computed in the exact same way. The results are presented for each participant and each trial in Figures 4.15 through 4.24. For each indicator, we compute the mean and standard deviation (STD) over the four participants for each trial; they are presented in Figures 4.17 to 4.25. Again, we perform t-tests using the `ttest2` from MATLAB® assuming both equal and unequal variances. Each trial is compared to every other one. The results of the t-tests are presented in Table 4.8 through 4.19.

4.3.2.1 Important Indicators

The first remark that can be done is that participants performed the task very well compared to the previous study. As shown in Fig. 4.15, only one trial failed over the 21 trials that were performed, thus giving a success rate of 95%. Comparatively, the success rate for the proactive behavior in the comparative study is only 50%, without considering the practice session. This also reflected in the values of the induced work; the minimal work value of the previous study is 14J. In this study, only five trials are over this value and only one is the first trial of a participant. Subject 3 performed the task extremely well energy-wise.

No effect of training on the work or the number of failures can be observed though. The results of the t-tests presented in Table 4.8 confirm that no significant statistical difference between any trial is observed. Therefore this training study is non conclusive as the t-tests yield the same results for every other indicator we chose. We hypothesize that the results show different strategies of training. However, as the study has only four participants, the data are not sufficient to draw conclusions and further investigation is necessary.

We first focus on Subject 1. The work evolution from Fig. 4.15 shows an improvement with training until the third trial. Since this improvement also shows in the average power in Fig. 4.24, we call this strategy “Power decrease”. Except for the first trial, Subject 2 shows a similar evolution of work and average power. It is as if Subject 2 luckily makes a good performance on the first trial and then fails to reproduce a similar performance. Only after a few trials is Subject 2 able to make a similar performance energy-wise. Therefore, we classify Subject 2 in the “Power decrease / Lucky first”. Fig. 4.17 (top) is interesting in this regard. Indeed, it shows a slight decrease in the work in average. But is also shows a decrease of the standard deviation: *there is more variation in the first trials than in the*

Table 4.8: Work t-tests results between each trials, assuming equal (top) and unequal (bottom) variances, with 5% significance level. Each cell shows the p-value of the test. A highlighted cell means that a significant statistical difference is observed (p-value $< 5\%$).

Work				
$=$	Trial 2	Trial 3	Trial 4	Trial 5
Trial 1	9.7×10^{-1}	7.3×10^{-1}	5.0×10^{-1}	3.6×10^{-1}
Trial 2		5.7×10^{-1}	2.8×10^{-1}	1.5×10^{-1}
Trial 3			5.5×10^{-1}	2.7×10^{-1}
Trial 4				5.1×10^{-1}
$\neq$	Trial 2	Trial 3	Trial 4	Trial 5
Trial 1	9.7×10^{-1}	7.4×10^{-1}	5.2×10^{-1}	3.8×10^{-1}
Trial 2		5.8×10^{-1}	3.0×10^{-1}	1.7×10^{-1}
Trial 3			5.5×10^{-1}	2.8×10^{-1}
Trial 4				5.1×10^{-1}

subsequent ones. That is probably the high variance in the first and second trials that makes the t-tests fail.

The work input by Subject 3 over the five trials is very low and its variations are too small to be imputed to training. But if we look the Fig. 4.16, we observe that the completion time of the first trial is much higher than the subsequent ones. This is also remarkable in the evolution of average velocity (see Fig. 4.18). Therefore we classify Subject 3's strategy as "Speed increase". Note that only the first trial is much different from the other. Whereas the first two trials are different in Subject 1 and "Power decrease" strategy cases. However, few data do not allow us to affirm whether this quick learning is specific to the strategy or the subject.

Subject 4 is a bit harder to classify because of the third trial. During this trial, the subject wrongly estimated how to perform the bend to go through the second doorway. Therefore, she had to stop and readjust a few times. However, the task was successfully completed, so it was considered valid. This might explain the high completion time although the average velocity is similar to Trial 2 and 4. The evolution of completion time and average velocity, Trial 3 excepted, leads us to classify Subject 4's strategy as "Speed increase". Unlike with Subject 3, the training seems to take several trials.

To summarize, the training has no significant impact on the means of the indicators we chose. We explain this result by the presence of different training strategies, as "Power decrease" and "Speed increase". The study of the evolution of means and standard deviations of the work input and completion time suggests that *variability decreases with training*. Nevertheless, the limited amount of data we gathered is not sufficient to draw conclusions and further investigation is necessary.

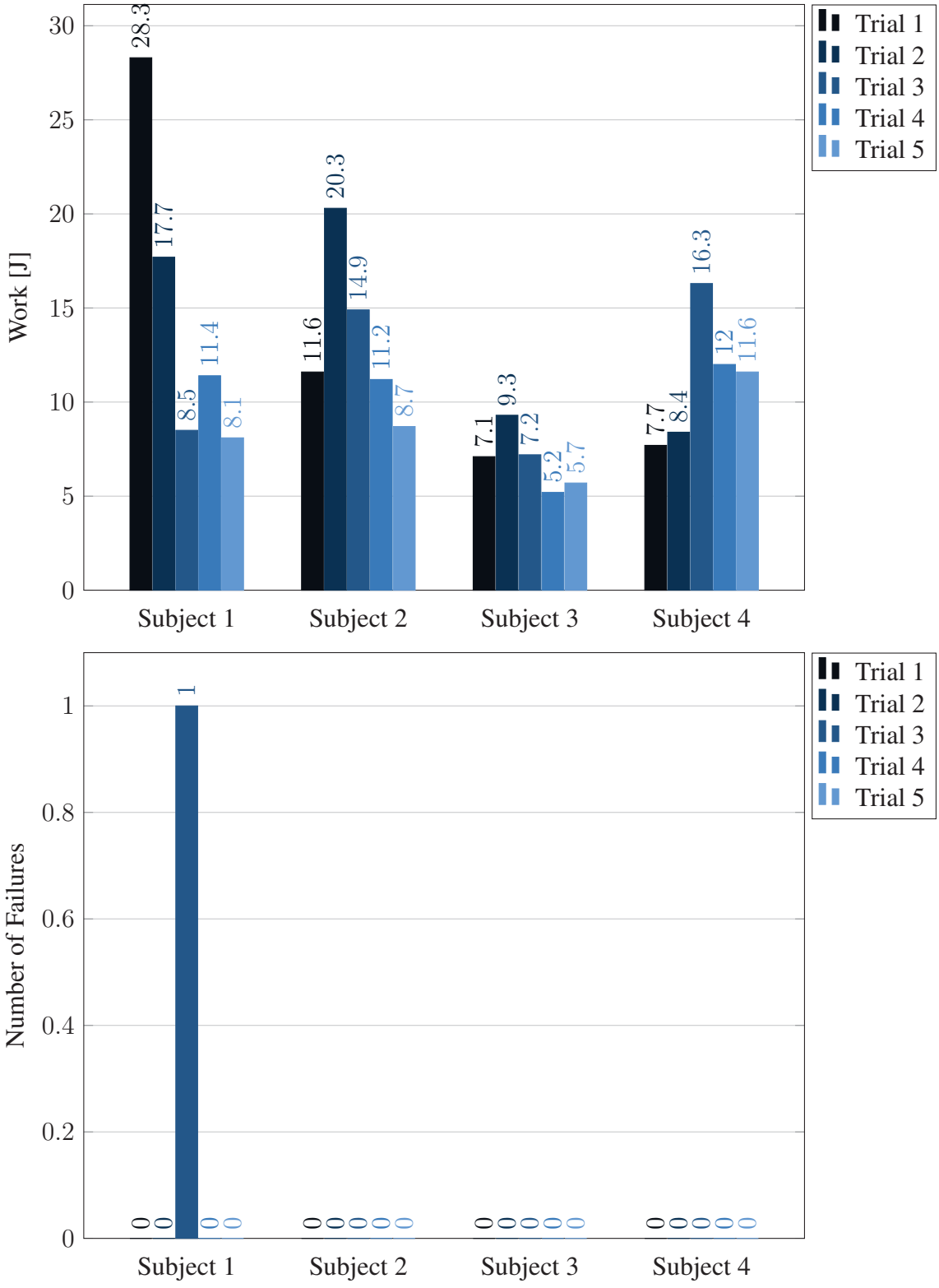

Figure 4.15: Work and Number of failures in the training user study.

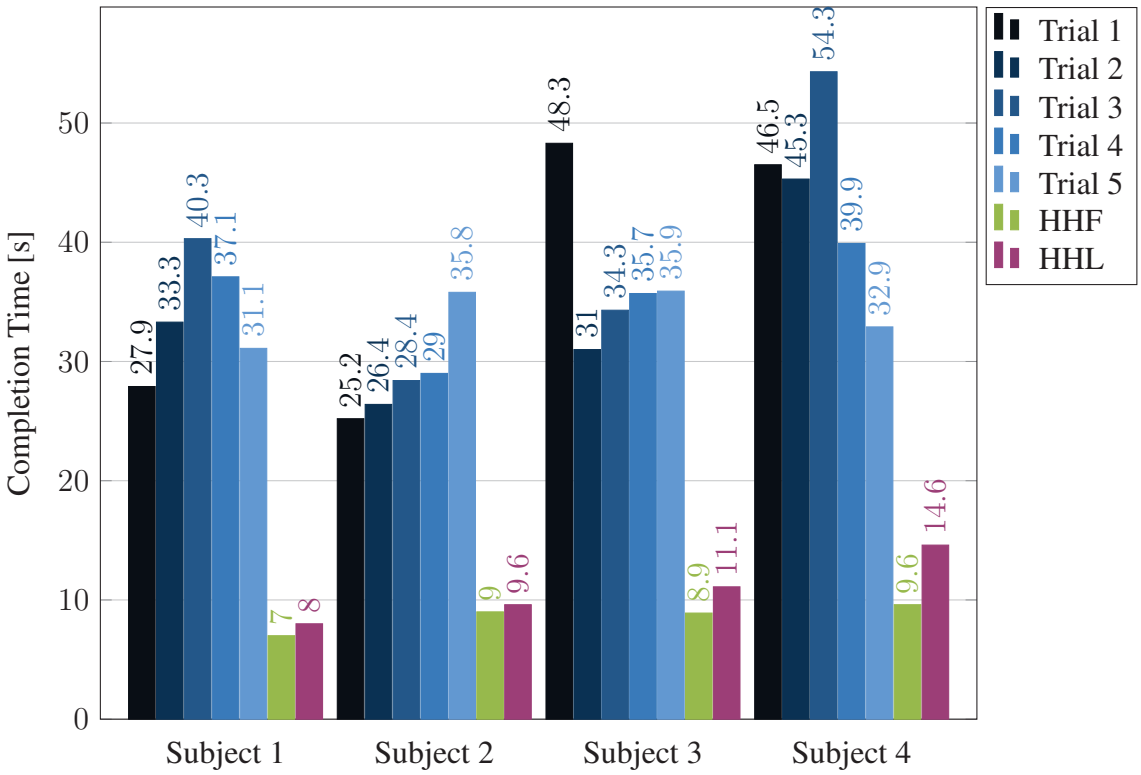

Figure 4.16: Completion times in the comparative user study. Here the completion times achieved when the participants performed the task with the experimenter are shown. First, the participants followed the lead of the experimenter (HHF, green), then they lead the task (HHL, purple).

Table 4.9: Completion time t-tests results between each trials, assuming equal (top) and unequal (bottom) variances, with 5% significance level. Each cell shows the p-value of the test. A highlighted cell means that a significant statistical difference is observed (p-value $< 5\%$).

Completion Time				
$=$	Trial 2	Trial 3	Trial 4	Trial 5
Trial 1	7.0×10^{-1}	7.8×10^{-1}	8.2×10^{-1}	6.4×10^{-1}
Trial 2		4.7×10^{-1}	7.7×10^{-1}	9.8×10^{-1}
Trial 3			5.4×10^{-1}	3.8×10^{-1}
Trial 4				5.8×10^{-1}
$\neq$	Trial 2	Trial 3	Trial 4	Trial 5
Trial 1	7.0×10^{-1}	7.8×10^{-1}	8.2×10^{-1}	6.5×10^{-1}
Trial 2		4.7×10^{-1}	7.7×10^{-1}	9.8×10^{-1}
Trial 3			5.5×10^{-1}	4.1×10^{-1}
Trial 4				5.9×10^{-1}

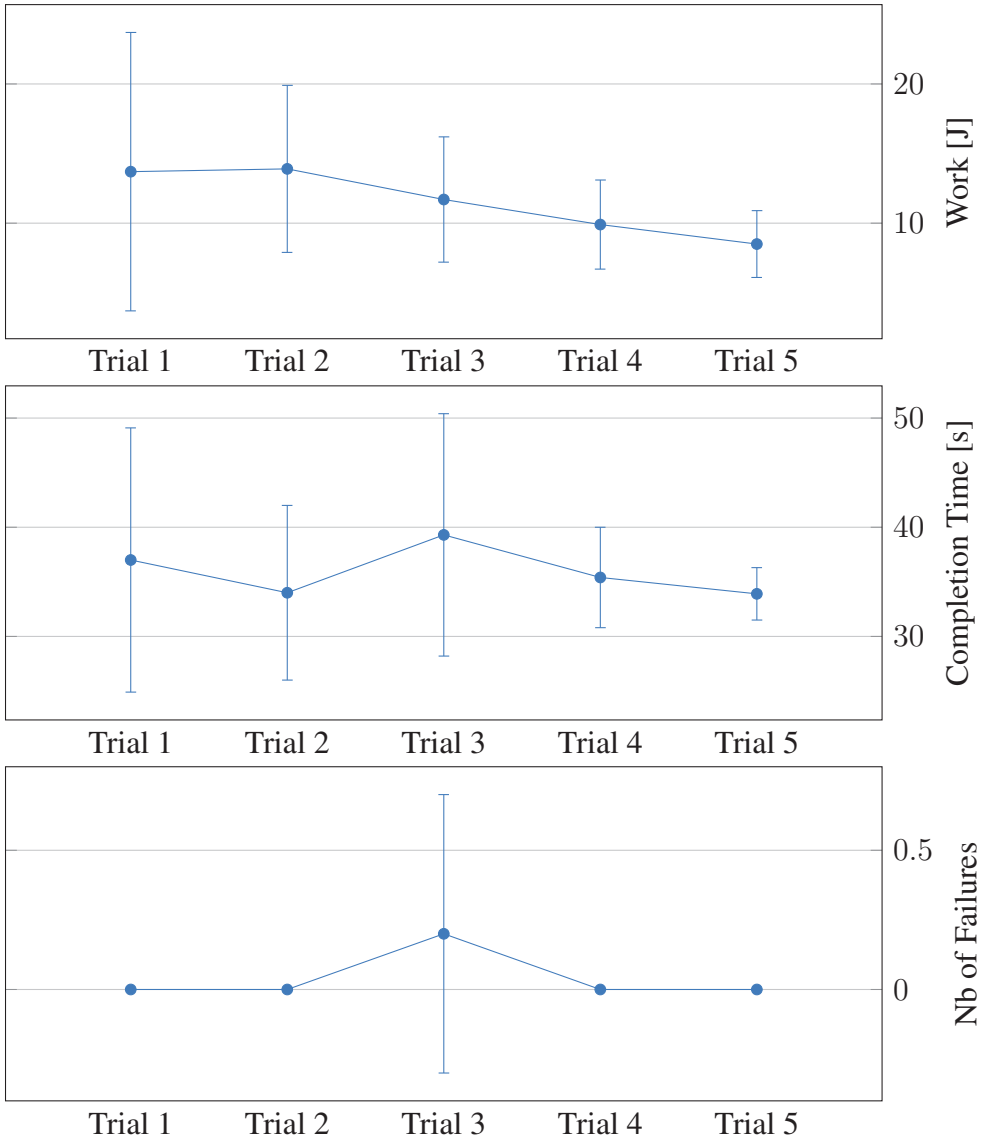

Figure 4.17: Mean and Standard Deviation over all four participants of Work, Completion Time and Number of failures in the training user study.

Table 4.10: Average Velocity Norm t-tests results between each trials, assuming equal (top) and unequal (bottom) variances, with 5% significance level. Each cell shows the p-value of the test. A highlighted cell means that a significant statistical difference is observed (p-value $< 5\%$).

Average Velocity Norm				
$=$	Trial 2	Trial 3	Trial 4	Trial 5
Trial 1	7.6×10^{-1}	8.7×10^{-1}	8.3×10^{-1}	6.2×10^{-1}
Trial 2		8.5×10^{-1}	8.8×10^{-1}	7.8×10^{-1}
Trial 3			9.4×10^{-1}	6.1×10^{-1}
Trial 4				5.5×10^{-1}
$\neq$	Trial 2	Trial 3	Trial 4	Trial 5
Trial 1	7.7×10^{-1}	8.7×10^{-1}	8.3×10^{-1}	6.4×10^{-1}
Trial 2		8.5×10^{-1}	8.8×10^{-1}	7.9×10^{-1}
Trial 3			9.4×10^{-1}	6.3×10^{-1}
Trial 4				5.7×10^{-1}

4.3.2.2 Other Indicators

In the following, we quickly review the other indicators and see if they support our hypothesis of several training strategies and the decrease of variability.

Velocity indicators. There is no significant statistical difference between trials for velocity indicators (Tables 4.10 to 4.13). Concerning the velocity norm, an improvement can be observed for Subjects 3 and 4 unlike Subjects 1 and 2 in Fig. 4.18, which is coherent with the strategies we hypothesize. No such observation can be made for angular velocity norm (Fig. 4.19), except maybe the first trial of Subject 3. The maximal velocity and angular velocity norm are rather constant over the subjects and trials.

Except for the maximal angular velocity norm, we can observe from Fig. 4.20 that variability among the participants tends to decrease with training.

Force/Torque indicators. The average horizontal force norm seems to decrease for the first two subjects, whereas it remains constant for Subject 3 and even increases for Subject 4 (see Fig. 4.21), which is consistent with the strategy repartition. It also explains the lack of significant statistical difference for the force indicators (Tables 4.14 to 4.17). Only the maximal torque norm shows a significant statistical difference between Trial 2 and 3 which we cannot explain. However, the p-value is barely under the 5% significance level. Therefore we consider it as a false positive. Unlike with velocity, the variability of forces levels does not notably decrease with training (Fig. 4.23).

Power indicators. Except for the first trial of Subject 2, which we call "Lucky First", the average and maximal power norms of Subjects 1 and 2 decrease with training while they do

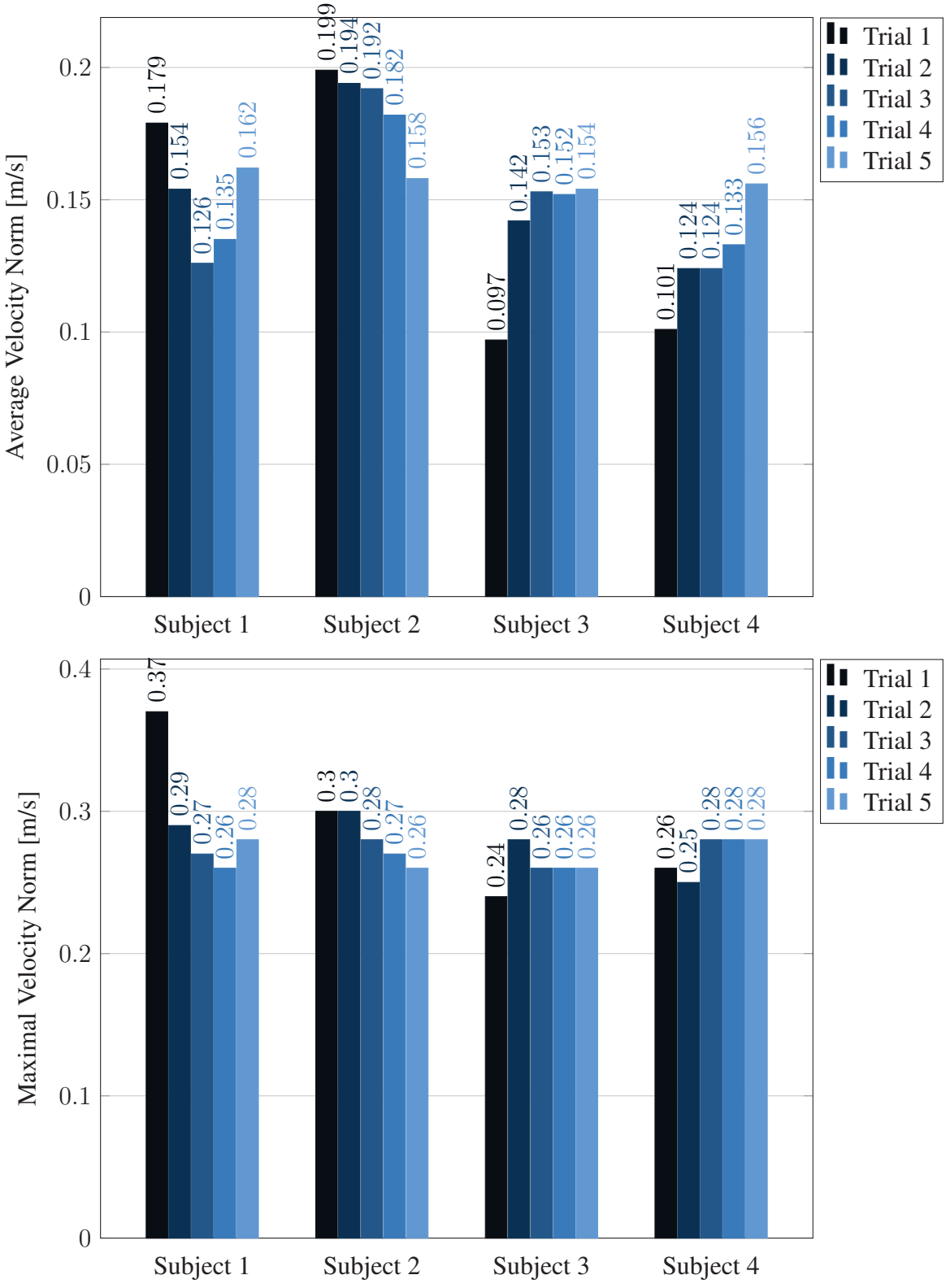

Figure 4.18: Average and maximum velocity norms in the training user study.

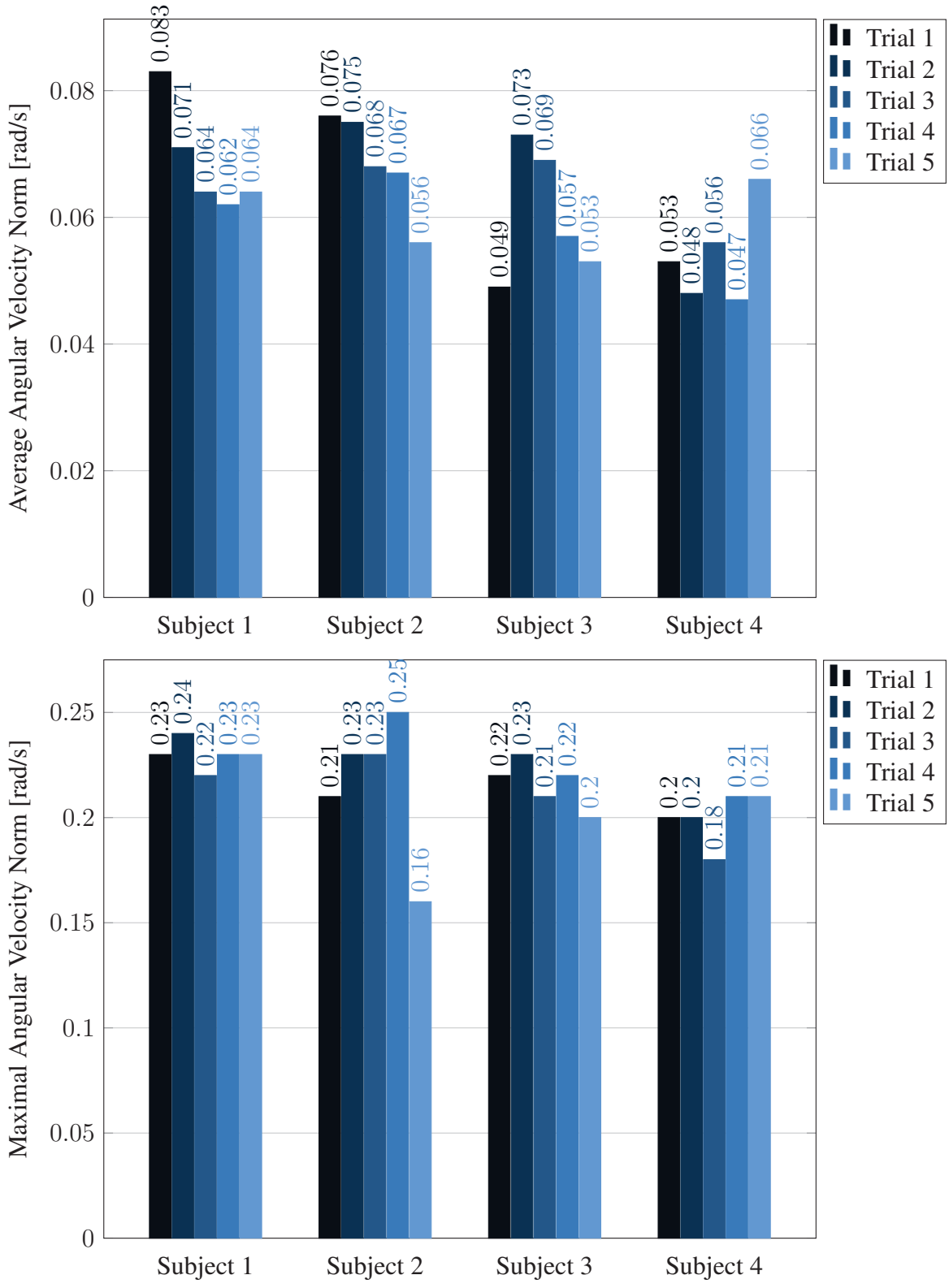

Figure 4.19: Average and maximum angular velocity norms in the training user study.

Table 4.11: Maximal Velocity Norm t-tests results between each trials, assuming equal (top) and unequal (bottom) variances, with 5% significance level. Each cell shows the p-value of the test. A highlighted cell means that a significant statistical difference is observed (p-value $< 5\%$).

Maximal Velocity Norm				
$=$	Trial 2	Trial 3	Trial 4	Trial 5
Trial 1	6.9×10^{-1}	5.0×10^{-1}	4.5×10^{-1}	4.2×10^{-1}
Trial 2		5.7×10^{-1}	4.3×10^{-1}	3.9×10^{-1}
Trial 3			6.0×10^{-1}	5.2×10^{-1}
Trial 4				8.3×10^{-1}
$\neq$	Trial 2	Trial 3	Trial 4	Trial 5
Trial 1	7.0×10^{-1}	5.3×10^{-1}	4.7×10^{-1}	4.5×10^{-1}
Trial 2		5.9×10^{-1}	4.5×10^{-1}	4.1×10^{-1}
Trial 3			6.0×10^{-1}	5.3×10^{-1}
Trial 4				8.3×10^{-1}

Table 4.12: Average Angular Velocity Norm t-tests results between each trials, assuming equal (top) and unequal (bottom) variances, with 5% significance level. Each cell shows the p-value of the test. A highlighted cell means that a significant statistical difference is observed (p-value $< 5\%$).

Average Angular Velocity Norm				
$=$	Trial 2	Trial 3	Trial 4	Trial 5
Trial 1	8.9×10^{-1}	8.9×10^{-1}	4.7×10^{-1}	5.2×10^{-1}
Trial 2		7.0×10^{-1}	2.9×10^{-1}	3.2×10^{-1}
Trial 3			2.8×10^{-1}	2.9×10^{-1}
Trial 4				8.4×10^{-1}
$\neq$	Trial 2	Trial 3	Trial 4	Trial 5
Trial 1	8.9×10^{-1}	8.9×10^{-1}	4.8×10^{-1}	5.4×10^{-1}
Trial 2		7.0×10^{-1}	3.0×10^{-1}	3.3×10^{-1}
Trial 3			2.9×10^{-1}	2.9×10^{-1}
Trial 4				8.4×10^{-1}

Table 4.13: Maximal Angular Velocity Norm t-tests results between each trials, assuming equal (top) and unequal (bottom) variances, with 5% significance level. Each cell shows the p-value of the test. A highlighted cell means that a significant statistical difference is observed (p-value $< 5\%$).

Maximal Angular Velocity Norm				
$=$	Trial 2	Trial 3	Trial 4	Trial 5
Trial 1	4.7×10^{-1}	6.3×10^{-1}	3.1×10^{-1}	2.6×10^{-1}
Trial 2		3.6×10^{-1}	9.2×10^{-1}	1.7×10^{-1}
Trial 3			2.8×10^{-1}	5.4×10^{-1}
Trial 4				1.2×10^{-1}
$\neq$	Trial 2	Trial 3	Trial 4	Trial 5
Trial 1	4.8×10^{-1}	6.3×10^{-1}	3.2×10^{-1}	2.9×10^{-1}
Trial 2		3.6×10^{-1}	9.2×10^{-1}	1.7×10^{-1}
Trial 3			2.8×10^{-1}	5.4×10^{-1}
Trial 4				1.4×10^{-1}

Table 4.14: Average Horizontal Force Norm t-tests results between each trials, assuming equal (top) and unequal (bottom) variances, with 5% significance level. Each cell shows the p-value of the test. A highlighted cell means that a significant statistical difference is observed (p-value $< 5\%$).

Average Horizontal Force Norm				
$=$	Trial 2	Trial 3	Trial 4	Trial 5
Trial 1	7.5×10^{-1}	7.9×10^{-1}	6.7×10^{-1}	9.2×10^{-1}
Trial 2		4.9×10^{-1}	3.3×10^{-1}	5.9×10^{-1}
Trial 3			8.7×10^{-1}	8.4×10^{-1}
Trial 4				6.9×10^{-1}
$\neq$	Trial 2	Trial 3	Trial 4	Trial 5
Trial 1	7.6×10^{-1}	7.9×10^{-1}	6.7×10^{-1}	9.2×10^{-1}
Trial 2		5.0×10^{-1}	3.4×10^{-1}	6.0×10^{-1}
Trial 3			8.7×10^{-1}	8.4×10^{-1}
Trial 4				6.9×10^{-1}

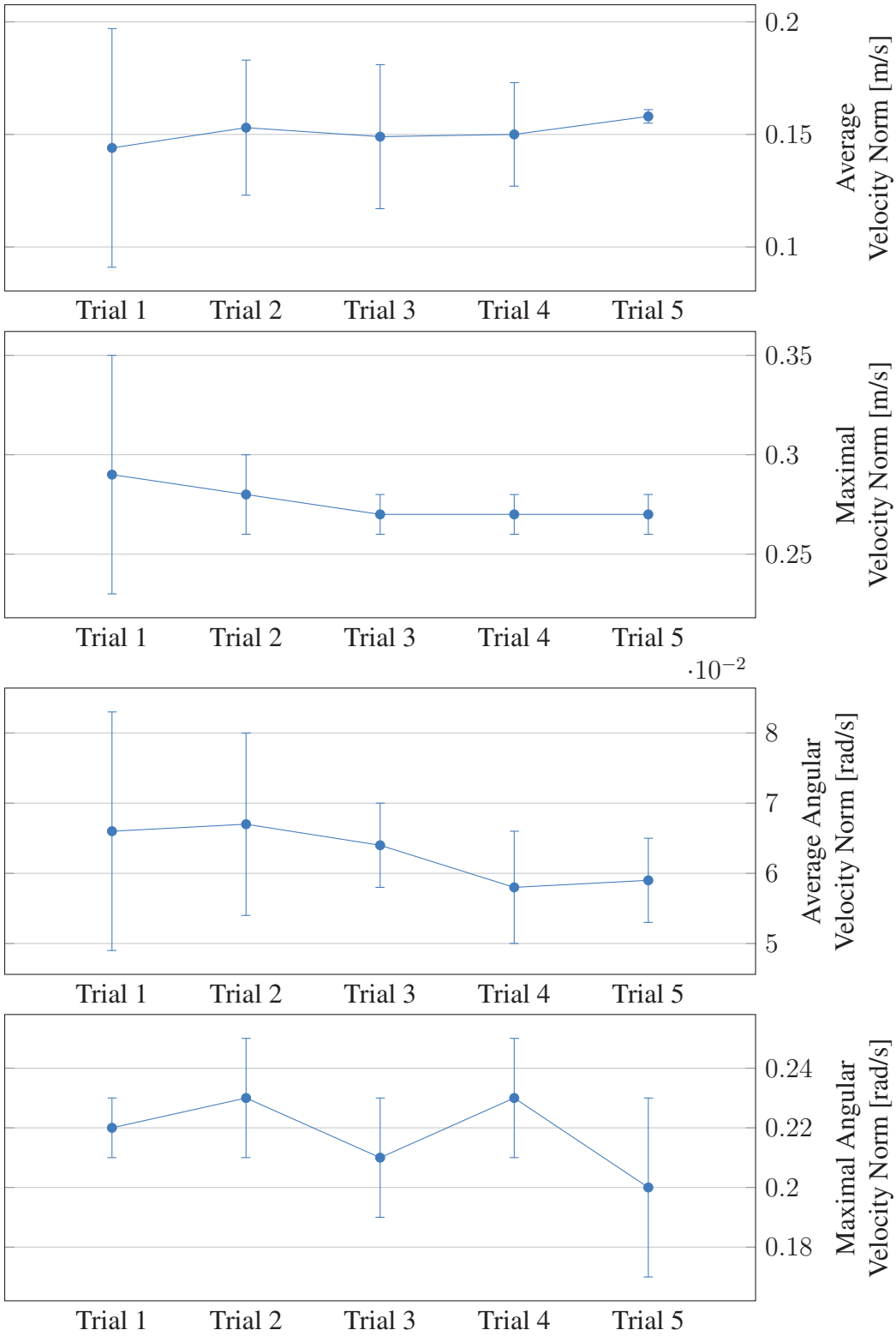

Figure 4.20: Mean and Standard Deviation over all four participants of velocity indicators in the training user study.

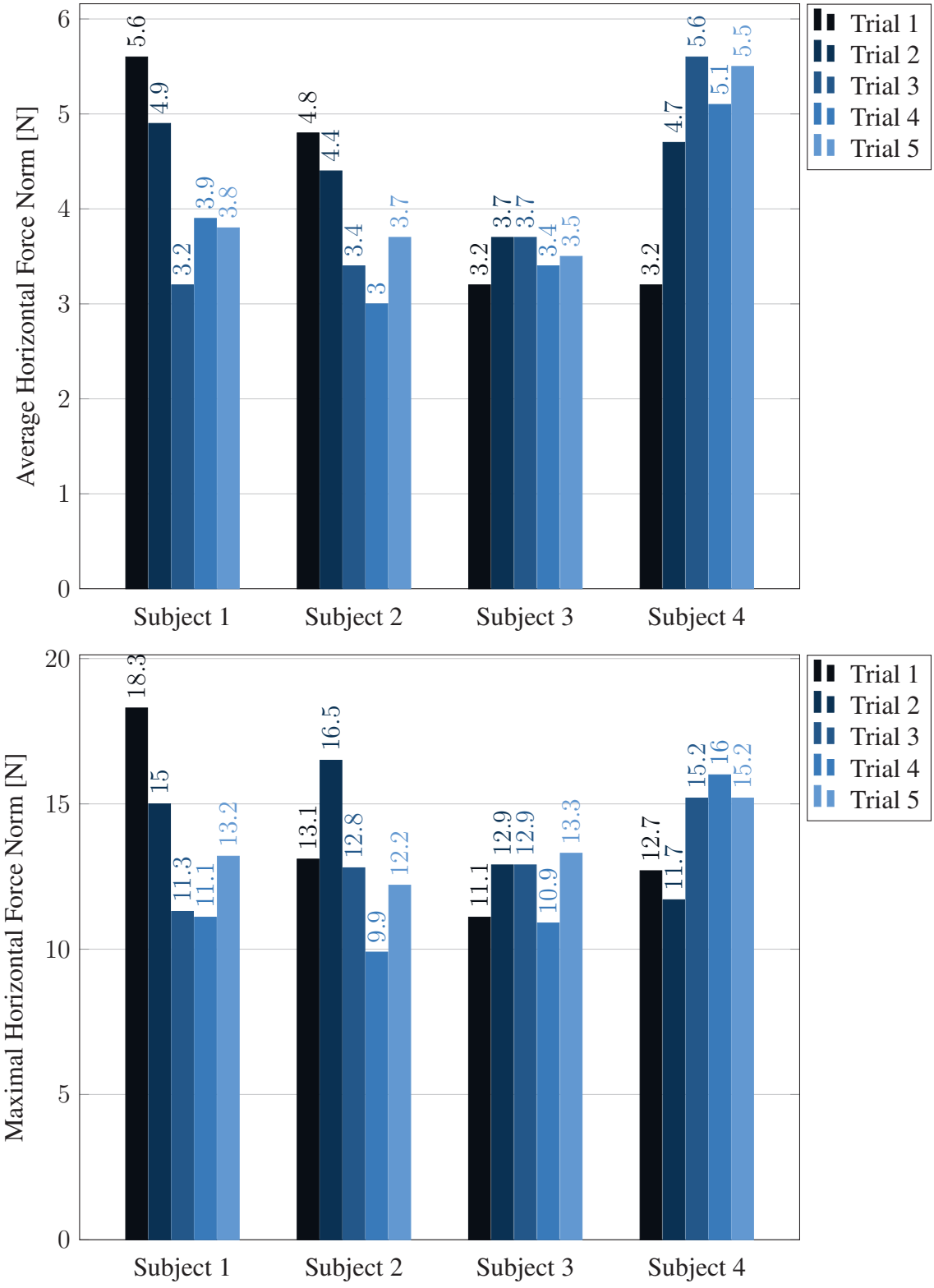

Figure 4.21: Average and maximum horizontal force norms in the training user study.

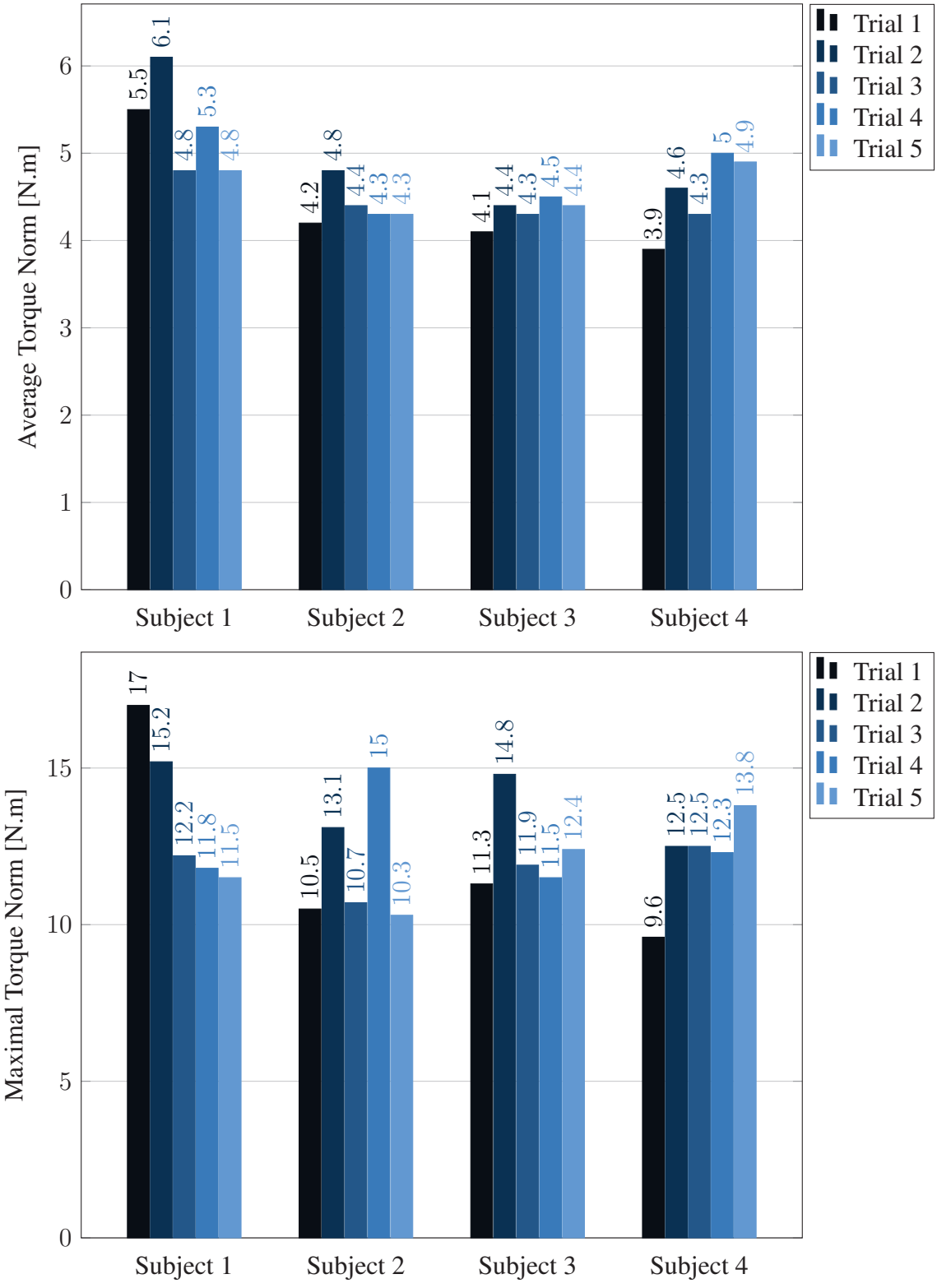

Figure 4.22: Average and maximum torque norms in the training user study.

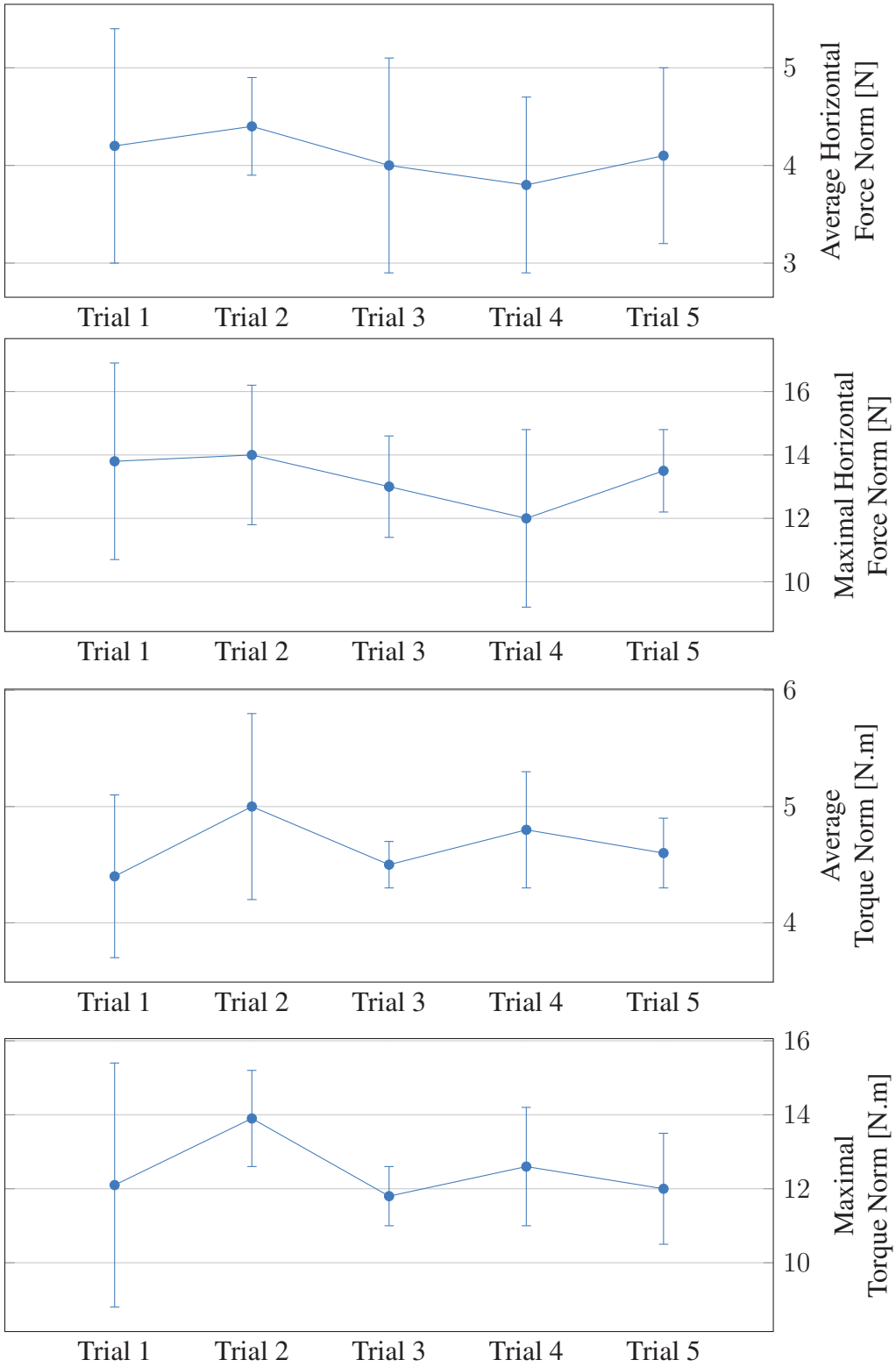

Figure 4.23: Mean and Standard Deviation over all four participants of force/torque indicators in the training user study.

Table 4.15: Maximal Horizontal Force Norm t-tests results between each trials, assuming equal (top) and unequal (bottom) variances, with 5% significance level. Each cell shows the p-value of the test. A highlighted cell means that a significant statistical difference is observed (p-value $< 5\%$).

Maximal Horizontal Force Norm				
$=$	Trial 2	Trial 3	Trial 4	Trial 5
Trial 1	9.2×10^{-1}	6.8×10^{-1}	4.1×10^{-1}	8.4×10^{-1}
Trial 2		5.0×10^{-1}	2.9×10^{-1}	6.7×10^{-1}
Trial 3			5.3×10^{-1}	7.1×10^{-1}
Trial 4				3.7×10^{-1}
$\neq$	Trial 2	Trial 3	Trial 4	Trial 5
Trial 1	9.2×10^{-1}	6.9×10^{-1}	4.1×10^{-1}	8.4×10^{-1}
Trial 2		5.1×10^{-1}	2.9×10^{-1}	6.8×10^{-1}
Trial 3			5.3×10^{-1}	7.1×10^{-1}
Trial 4				3.8×10^{-1}

Table 4.16: Average Torque Norm t-tests results between each trials, assuming equal (top) and unequal (bottom) variances, with 5% significance level. Each cell shows the p-value of the test. A highlighted cell means that a significant statistical difference is observed (p-value $< 5\%$).

Average Torque Norm				
$=$	Trial 2	Trial 3	Trial 4	Trial 5
Trial 1	3.3×10^{-1}	9.1×10^{-1}	4.2×10^{-1}	6.5×10^{-1}
Trial 2		2.4×10^{-1}	7.2×10^{-1}	4.1×10^{-1}
Trial 3			2.4×10^{-1}	4.5×10^{-1}
Trial 4				5.3×10^{-1}
$\neq$	Trial 2	Trial 3	Trial 4	Trial 5
Trial 1	3.3×10^{-1}	9.1×10^{-1}	4.2×10^{-1}	6.5×10^{-1}
Trial 2		2.8×10^{-1}	7.2×10^{-1}	4.3×10^{-1}
Trial 3			2.6×10^{-1}	4.5×10^{-1}
Trial 4				5.3×10^{-1}

Table 4.17: Maximal Torque Norm t-tests results between each trials, assuming equal (top) and unequal (bottom) variances, with 5% significance level. Each cell shows the p-value of the test. A highlighted cell means that a significant statistical difference is observed (p-value $< 5\%$).

Maximal Torque Norm				
$=$	Trial 2	Trial 3	Trial 4	Trial 5
Trial 1	3.5×10^{-1}	8.9×10^{-1}	7.7×10^{-1}	9.7×10^{-1}
Trial 2		3.6×10^{-2}	2.8×10^{-1}	1.1×10^{-1}
Trial 3			4.0×10^{-1}	8.3×10^{-1}
Trial 4				5.9×10^{-1}
$\neq$	Trial 2	Trial 3	Trial 4	Trial 5
Trial 1	3.7×10^{-1}	8.9×10^{-1}	7.8×10^{-1}	9.7×10^{-1}
Trial 2		4.4×10^{-2}	2.8×10^{-1}	1.1×10^{-1}
Trial 3			4.1×10^{-1}	8.3×10^{-1}
Trial 4				5.9×10^{-1}

not with Subjects 3 and 4 (Fig. 4.24). This is what led us to consider the "Power decrease" strategy. Again, the discrepancy of strategies leads to a non-significant statistical difference in the power data (Tables 4.18 and 4.19).

The decrease of variability with training appears in both average and maximal power norm data (Fig. 4.25).

4.3.2.3 Questionnaire Results

Although we reuse Questionnaire 1, we believe that a specific questionnaire must be used if further work is envisaged. However, we present the free remarks made by the participants in Table 4.20.

4.3.3 Conclusion

This training user study does not allow us to draw straight conclusions about the impact of training on the performances of our proactive control scheme. However, we are able to formulate hypotheses about the study's failure. Firstly, there seems to be at least two strategies –"Power decrease" and "Speed increase"– to learn how to better perform the transportation task with the proactive robot. Secondly, this discrepancy of strategies leads to a high variability in the first trials, in work, completion time, velocity and power, that decreases with the training. The phenomenon of a "Lucky first" trial is symptomatic of this high variability, where a participant can brilliantly succeed the first trial, and only manages to reproduce such a trial after a training phase of a few trial.

As interesting as these hypotheses might be, we think that our study cannot assess them strongly given the limited number of subjects. Further investigation is necessary to prove these hypothesis of *different strategies* and *variability decrease with training*.

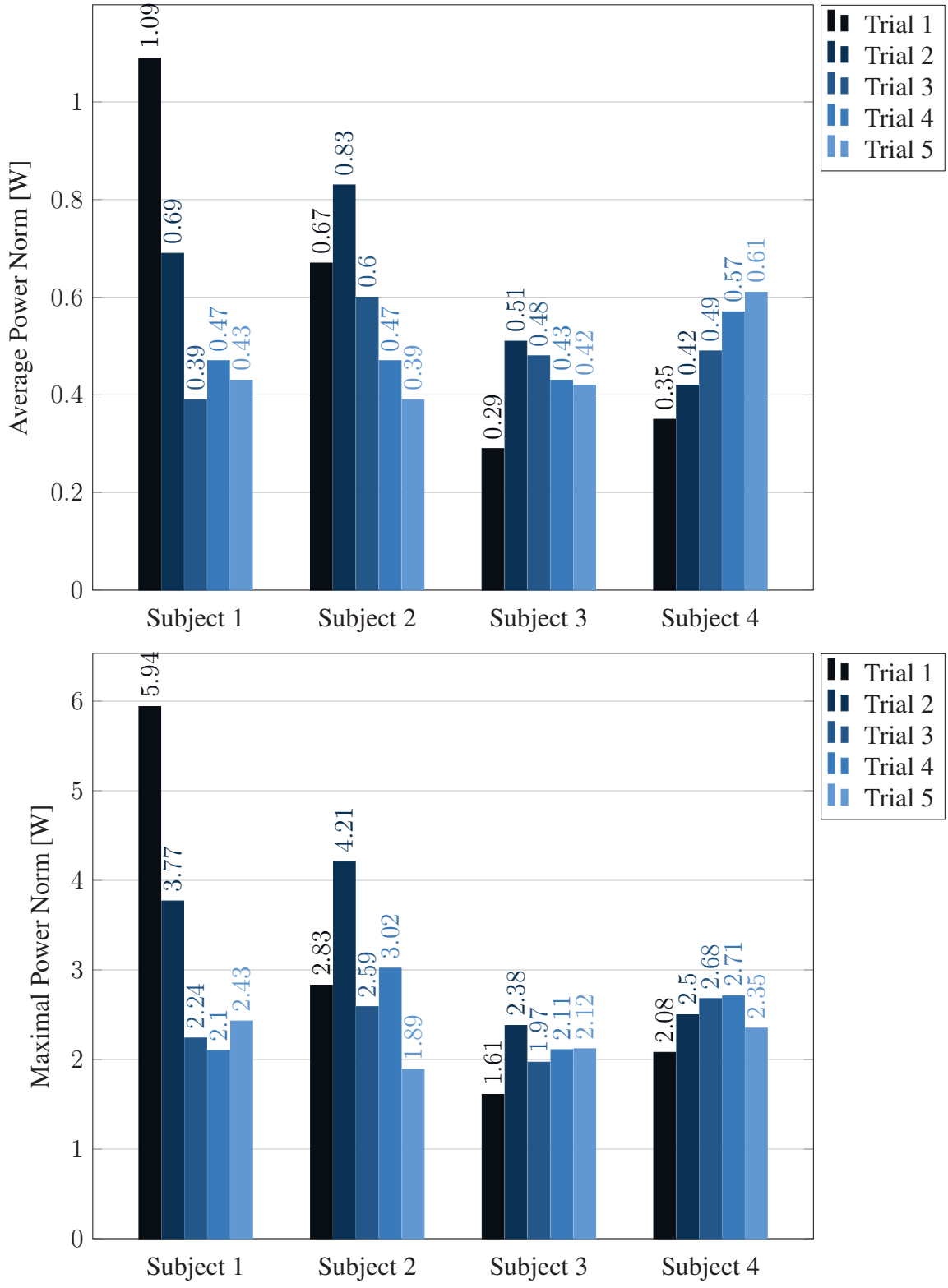

Figure 4.24: Average and maximum powers in the training user study.

Table 4.18: Average Power Norm t-tests results between each trials, assuming equal (top) and unequal (bottom) variances, with 5% significance level. Each cell shows the p-value of the test. A highlighted cell means that a significant statistical difference is observed (p-value $< 5\%$).

Average Power Norm				
$=$	Trial 2	Trial 3	Trial 4	Trial 5
Trial 1	9.6×10^{-1}	5.7×10^{-1}	5.6×10^{-1}	4.9×10^{-1}
Trial 2		2.7×10^{-1}	2.4×10^{-1}	2.0×10^{-1}
Trial 3			9.6×10^{-1}	6.8×10^{-1}
Trial 4				6.7×10^{-1}
$\neq$	Trial 2	Trial 3	Trial 4	Trial 5
Trial 1	9.6×10^{-1}	5.9×10^{-1}	5.8×10^{-1}	5.1×10^{-1}
Trial 2		2.9×10^{-1}	2.7×10^{-1}	2.1×10^{-1}
Trial 3			9.6×10^{-1}	6.8×10^{-1}
Trial 4				6.7×10^{-1}

Table 4.19: Maximal Power Norm t-tests results between each trials, assuming equal (top) and unequal (bottom) variances, with 5% significance level. Each cell shows the p-value of the test. A highlighted cell means that a significant statistical difference is observed (p-value $< 5\%$).

Maximal Power Norm				
$=$	Trial 2	Trial 3	Trial 4	Trial 5
Trial 1	9.3×10^{-1}	4.8×10^{-1}	5.5×10^{-1}	3.9×10^{-1}
Trial 2		1.3×10^{-1}	2.0×10^{-1}	7.5×10^{-2}
Trial 3			7.0×10^{-1}	4.2×10^{-1}
Trial 4				3.1×10^{-1}
$\neq$	Trial 2	Trial 3	Trial 4	Trial 5
Trial 1	9.3×10^{-1}	5.0×10^{-1}	5.7×10^{-1}	4.2×10^{-1}
Trial 2		1.6×10^{-1}	2.2×10^{-1}	1.1×10^{-1}
Trial 3			7.0×10^{-1}	4.3×10^{-1}
Trial 4				3.2×10^{-1}

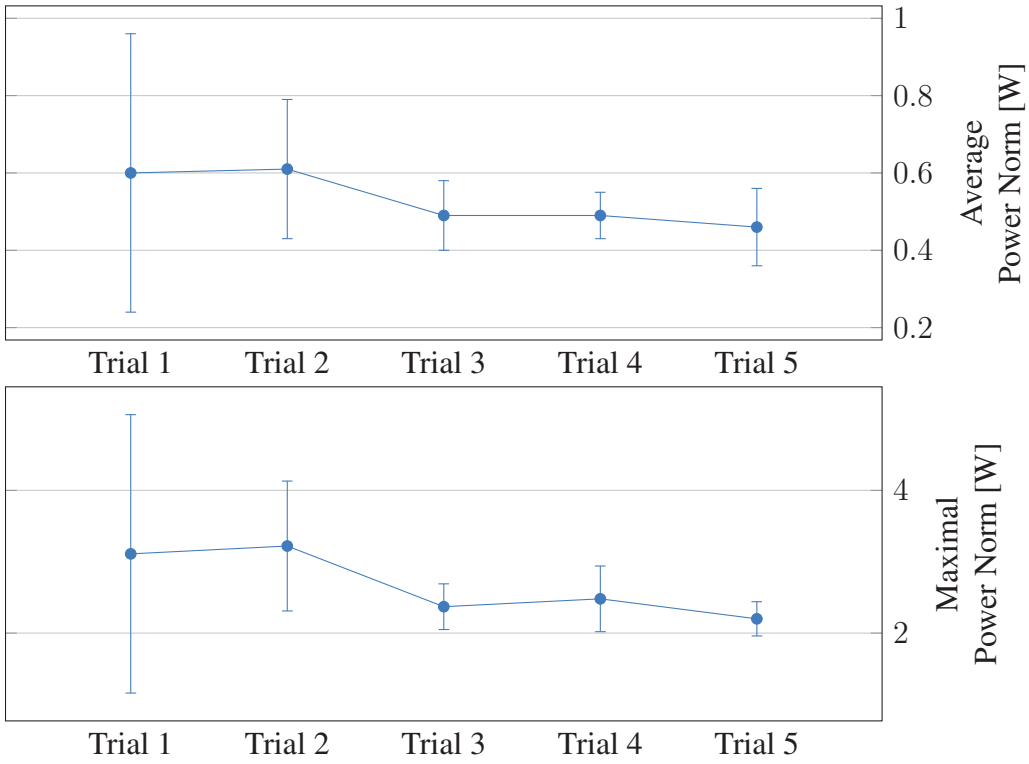

Figure 4.25: Mean and Standard Deviation over all four participants of power indicators in the training user study.

Table 4.20: Comments made by the participants in the free remarks section of Questionnaire 1 in the training study.

Subject	**Questionnaire 1**
1	It definitely felt very different from doing the same task with a human. It seems like it takes practice to figure out how the robot moves and what its limitations are. While I'd prefer to do the task with another human, I can see where a robot could be very helpful if other people were not around.
2	It was unclear how to make the robot go backward.
3	I could do that all day long!
4	Impacts were producing tremors.

4.4 Comparison with Human-Human Collaboration Data

To conclude this chapter, we compare the data we gathered in both user studies with the data we gathered with human dyads for Chapter 2. The results we present in this part are to be considered with high caution. They are not strictly rigorous since the data we compare come from various experiments that differ from more than one factor. However, they can allow us to explain some results found in the comparative study in Section 4.2.

4.4.1 Data Sets

In this section, we compare four sets of data:

1. human-human data with no role assignment, denoted HH for Human-Human
2. human-human data with a leader and a follower, denoted HHF for Human-Human Follower since we use the data from the follower point-of-view
3. human-robot data with robot's proactive behavior, denoted HRPro for Human-Robot Proactive
4. human-robot data with robot's passive behavior, denoted HRPas for Human-Robot Passive

Both data sets HH and HHF are extracted from the data gathered during the human-human experiment of Chapter 2. This experiment consists of two human carrying a table-like object backward and forward along one degree of freedom. Compared to the human-robot experiments:

- there is no turning,
- the distance is not exactly the same, although of the same order,
- the object is heavier,
- the task is repeated multiple times,
- the subjects are grouped in dyads to perform the task, whereas every participant does the task with the robot in the human-robot experiment,
- the instructions are not identical.

Each dyad is asked to perform the task five times without being assigned any roles. The experimenter then assigns the role of leader to the first subject of the dyad and the role of follower to the second. The dyad performs the task five times. Finally, roles are switched and the dyad performs the task five more times. To limit the effect of training we use the fifth trial in each case. The fifth trial of the task performed with no role assignment composes the HH data set, whereas both fifth trials of the task performed with role assignments compose

the HHF data set. Because eight dyads participate to the human-human experiment, the HH data set is composed of 8 trials and the HHF is composed of 16 trials.

Similarly, the HRPro data set is composed of the fifth trial of the training study, which represents 4 trials. The HRPas data set is composed of the passive trial of the comparative study, which represents 8 trials.

4.4.2 Indicators

We use the same translational indicators that are described in Section 4.2.2. In other words, we exclude the angular velocity and torque indicators. However, the contributions of rotation to both work and power are conserved in the human-robot data. The contributions of rotation are neglected in the human-human data.

We need to compute a velocity and a force for the human-human experiments. For the velocity, as the task is on one degree of freedom, all the points of the object have the same velocity, we thus use the object's CoM velocity. In the human-robot experiment, we use the force applied on the robot's grippers. Since the robot acts as a follower, we need the force applied on the follower's hands in the human-human experiment too. Although it is easy to determine the follower in the role assignment case, there might not even be a follower in the non-role assignment case. If we neglect the object's inertia, which is a crude approximation, both forces are thus roughly opposite, which has no impact on the force and power indicators. However, choosing a sign for the forces implies of a choice of sign for the work input into a partner. In the human-robot experiment, the work input into the robot's gripper is always positive. Therefore, for the HH data set, we arbitrarily choose the forces felt by the first subject of the dyad and compute the work input into his hands. If it is negative, then we take its absolute value, which is the work input into the other subject's hands if we neglect the variation of the kinetic energy. Note however, that this is an arbitrary choice since we observed negative work to be input into the follower's hands in some trials with role assignments.

To determine the completion time in the HH and HHF data sets, we use the trapezoidal fit performed in Chapter 2. This trapezoidal fit allows us to roughly determine the starting and ending time of the task. Because the velocity is modelled as an affine function of time during the acceleration phases this estimated starting time is late compared to the effective one. Therefore we subtract half a second to this estimation of the starting time. For similar reasons, we add half a second to the estimation of the ending time.

We also present the power ratios computed with (4.25).

4.4.3 Results

For each data set, we plot the mean and standard deviation (STD) for each indicator in Fig. 4.26 to 4.28. We also compare each data set to the HHF data set using two t-tests using the `ttest2` function from MATLAB®. The first test assumes equal variances, whereas the second does not. The results of these tests are presented in Tables 4.21 to 4.29.

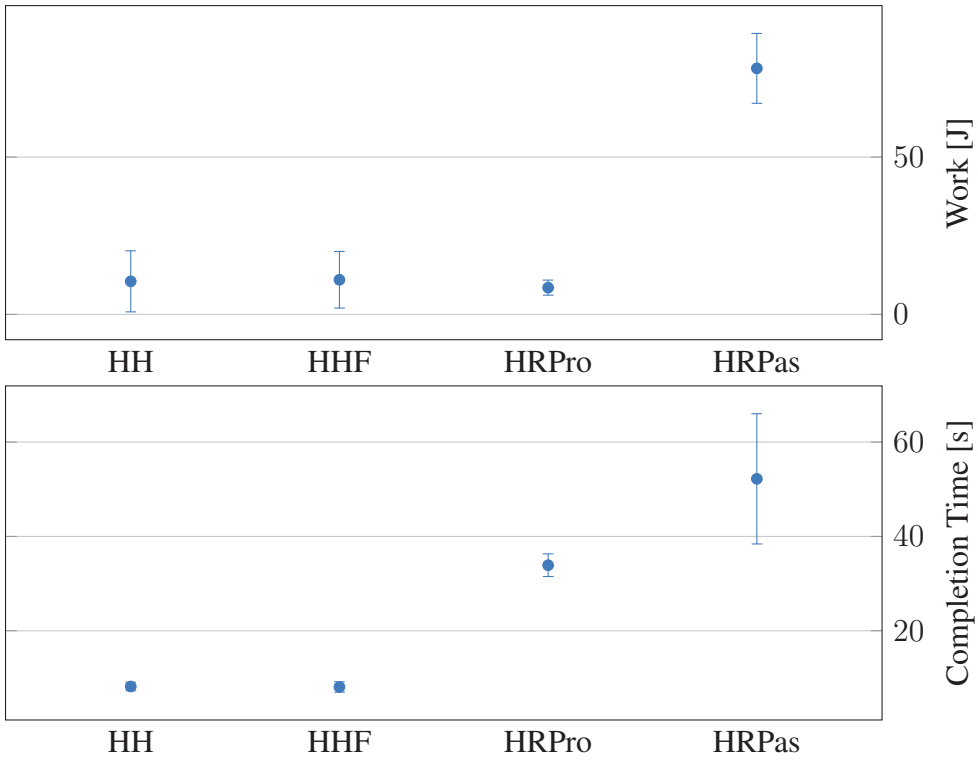

Figure 4.26: Mean and Standard Deviation for Work and Completion Time for each data set.

The first result is that there is no significant statistical difference between the HH and HHF data sets. None of the indicators we choose allows classifying the trials where roles are assigned from the ones with no role assignment. In the following, we thus only compare the HRPro and HRPas data sets with the HHF data set.

4.4.3.1 Important Indicators

The work input in the follower partner is similar between HHF and HRPPro data sets, whereas it is much higher in the HRPas data set (see Fig. 4.26 and Table 4.21). This is a good point for our proactive control scheme, since we achieve similar work levels between humans and a robot as within human dyads. However, as we said previously, the causes of such a low work in both data sets might be different and therefore must be identified using the other indicators.

As expected, the completion time of the task is much higher when the task is performed with the robot than by a human dyad (see Fig. 4.26 and Table 4.22). This comes from the limited walking capabilities of the robot and also reflects in the velocity indicators (see Fig. 4.27 and Tables 4.23 and 4.24). This shorter completion time might have an impact on a low work in the HHF data set.

Table 4.21: Work t-tests results between each data set, assuming equal ($=$) and unequal ($\neq$) variances, with 5% significance level. A highlighted cell means that a significant statistical difference is observed (p-value $< 5\%$).

Work [J]			
Data Set	**Mean**	p-**value** $=$	p-**value** $\neq$
HH	10.5	9.0×10^{-1}	9.0×10^{-1}
HHF	11.0	–	–
HRPro	8.5	6.0×10^{-1}	3.5×10^{-1}
HRPas	78.2	1.3×10^{-13}	5.2×10^{-9}

Table 4.22: Completion Time t-tests results between each data set, assuming equal ($=$) and unequal ($\neq$) variances, with 5% significance level. A highlighted cell means that a significant statistical difference is observed (p-value $< 5\%$).

Completion Time [s]			
Data Set	**Mean**	p-**value** $=$	p-**value** $\neq$
HH	8.2	7.0×10^{-1}	6.8×10^{-1}
HHF	8.1	–	–
HRPro	33.9	1.3×10^{-17}	1.1×10^{-4}
HRPas	52.2	8.8×10^{-12}	4.1×10^{-5}

Table 4.23: Average Velocity Norm t-tests results between each data set, assuming equal ($=$) and unequal ($\neq$) variances, with 5% significance level. A highlighted cell means that a significant statistical difference is observed (p-value $< 5\%$).

Average Velocity Norm [m/s]			
Data Set	**Mean**	p-**value** $=$	p-**value** $\neq$
HH	0.437	7.1×10^{-1}	6.8×10^{-1}
HHF	0.447	–	–
HRPro	0.158	1.7×10^{-7}	3.1×10^{-11}
HRPas	0.109	4.3×10^{-12}	1.5×10^{-13}

Table 4.24: Maximal Velocity Norm t-tests results between each data set, assuming equal ($=$) and unequal ($\neq$) variances, with 5% significance level. A highlighted cell means that a significant statistical difference is observed (p-value $< 5\%$).

Maximal Velocity Norm [m/s]			
Data Set	**Mean**	p-**value** $=$	p-**value** $\neq$
HH	0.80	8.2×10^{-1}	8.0×10^{-1}
HHF	0.81	–	–
HRPro	0.27	3.6×10^{-7}	5.3×10^{-11}
HRPas	0.22	5.5×10^{-11}	6.7×10^{-13}

4.4.3.2 Other Indicators

Velocity and Force indicators. As stated previously, HRPro and HRPas data sets have significantly lower velocity indicators than the HHF data set, as shown in Fig. 4.27 and Tables 4.23 and 4.24, which is expected because of the limited walking capabilities of the robot.

The force indicators are much more interesting. First notice that the STD of force indicators of the HRPro data set are different from the STD of the HHF data set (see Fig. 4.27). We should therefore consider the results of the t-tests that assume unequal variances in this case, because both t-tests indicate different results (Tables 4.25 and 4.26). What we notice then, is that the force levels are much lower in the HRPro data set than in the HHF data set, whereas HHF and HRPas data sets show similar force indicators. This may be a cause of the discrepancy we observe between the measurement results and the questionnaire results in the comparative study of Section 4.2. The force levels with the passive behavior are higher than the proactive behavior, but they are still within limits than humans experience when performing the task with another human. Higher force levels in this case might not be considered as prejudicial as not being able to make the robot do what we want.

Besides, such high force levels cannot be the cause of the low work value in the HHF data set.

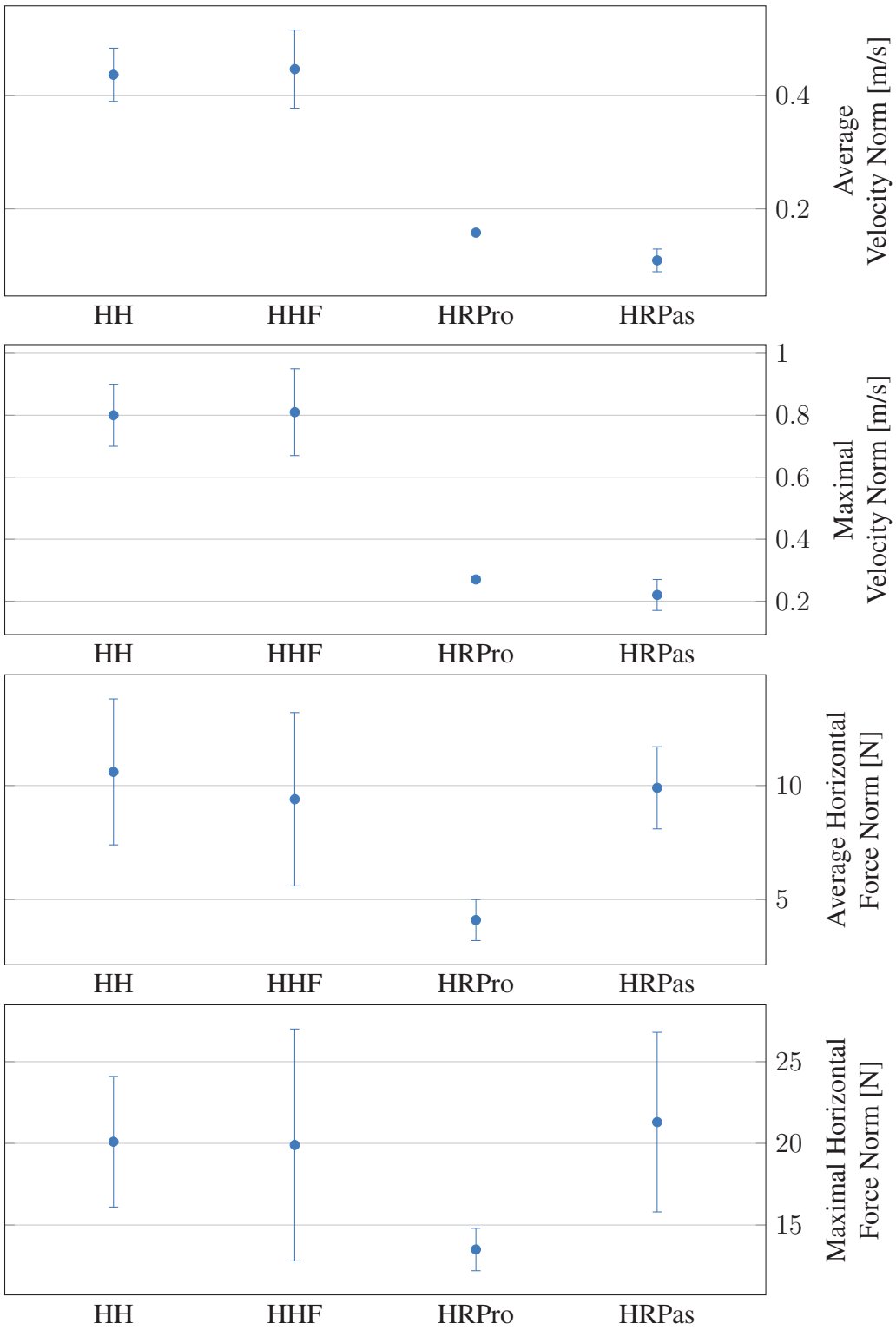

Figure 4.27: Mean and Standard Deviation for Velocity and Force Indicators for each data set.

Table 4.25: Average Horizontal Force Norm t-tests results between each data set, assuming equal ($=$) and unequal ($\neq$) variances, with 5% significance level. A highlighted cell means that a significant statistical difference is observed (p-value $< 5\%$).

Average Horizontal Force Norm [N]			
Data Set	**Mean**	p**-value** $=$	p**-value** $\neq$
HH	10.6	4.8×10^{-1}	4.6×10^{-1}
HHF	9.4	–	–
HRPro	4.1	1.3×10^{-2}	7.6×10^{-5}
HRPas	9.9	7.5×10^{-1}	6.9×10^{-1}

Table 4.26: Maximal Horizontal Force Norm t-tests results between each data set, assuming equal ($=$) and unequal ($\neq$) variances, with 5% significance level. A highlighted cell means that a significant statistical difference is observed (p-value $< 5\%$).

Maximal Horizontal Force Norm [N]			
Data Set	**Mean**	p**-value** $=$	p**-value** $\neq$
HH	20.1	9.5×10^{-1}	9.4×10^{-1}
HHF	19.9	–	–
HRPro	13.5	9.1×10^{-2}	3.0×10^{-3}
HRPas	21.3	6.3×10^{-1}	6.0×10^{-1}

Table 4.27: Average Power Norm t-tests results between each data set, assuming equal ($=$) and unequal ($\neq$) variances, with 5% significance level. A highlighted cell means that a significant statistical difference is observed (p-value $< 5\%$).

Average Power Norm [W]			
Data Set	**Mean**	p-**value** $=$	p-**value** $\neq$
HH	3.42	6.9×10^{-1}	6.8×10^{-1}
HHF	3.68	–	–
HRPro	0.46	4.3×10^{-4}	2.3×10^{-7}
HRPas	1.62	9.8×10^{-4}	6.9×10^{-5}

Table 4.28: Maximal Power Norm t-tests results between each data set, assuming equal ($=$) and unequal ($\neq$) variances, with 5% significance level. A highlighted cell means that a significant statistical difference is observed (p-value $< 5\%$).

Maximal Power Norm [W]			
Data Set	**Mean**	p-**value** $=$	p-**value** $\neq$
HH	13.19	7.0×10^{-1}	7.0×10^{-1}
HHF	12.53	–	–
HRPro	2.20	6.7×10^{-5}	2.1×10^{-8}
HRPas	5.37	1.1×10^{-4}	1.9×10^{-5}

Power indicators. The power indicators are much high in the HHF data set than in the HRPro and HRPas data sets, as shown in Fig. 4.28 and Tables 4.27 and 4.28. This is consistent with the high force and velocity levels observed. This leads to a lower power ratio, though the difference between the HHF and HRPro is not significant (see Table 4.29). We believe that a significant statistical difference may be observed with more participants.

These results show that human dyads spend a significant amount of energy in the task when compared to the HRPro and HRPas data sets. The low power ratio suggests that power is exchanged in both senses –from or to a partner– a lot.

4.4.4 Conclusion

The comparison between the human-human and human-robot data sets teaches us valuable lessons in order to improve our control scheme. The first teaching is that our results are good when considering the work input into the follower partner. The power ratio is also good. They express a *bilateral*[4] exchange of power between the robot and the human that is also found in the human-human data. In comparison, the power exchange with the passive behavior is *unilateral* because the power is always input positively into the robot.

[4]The power flow input into each partner switches between positive and negative during the task.

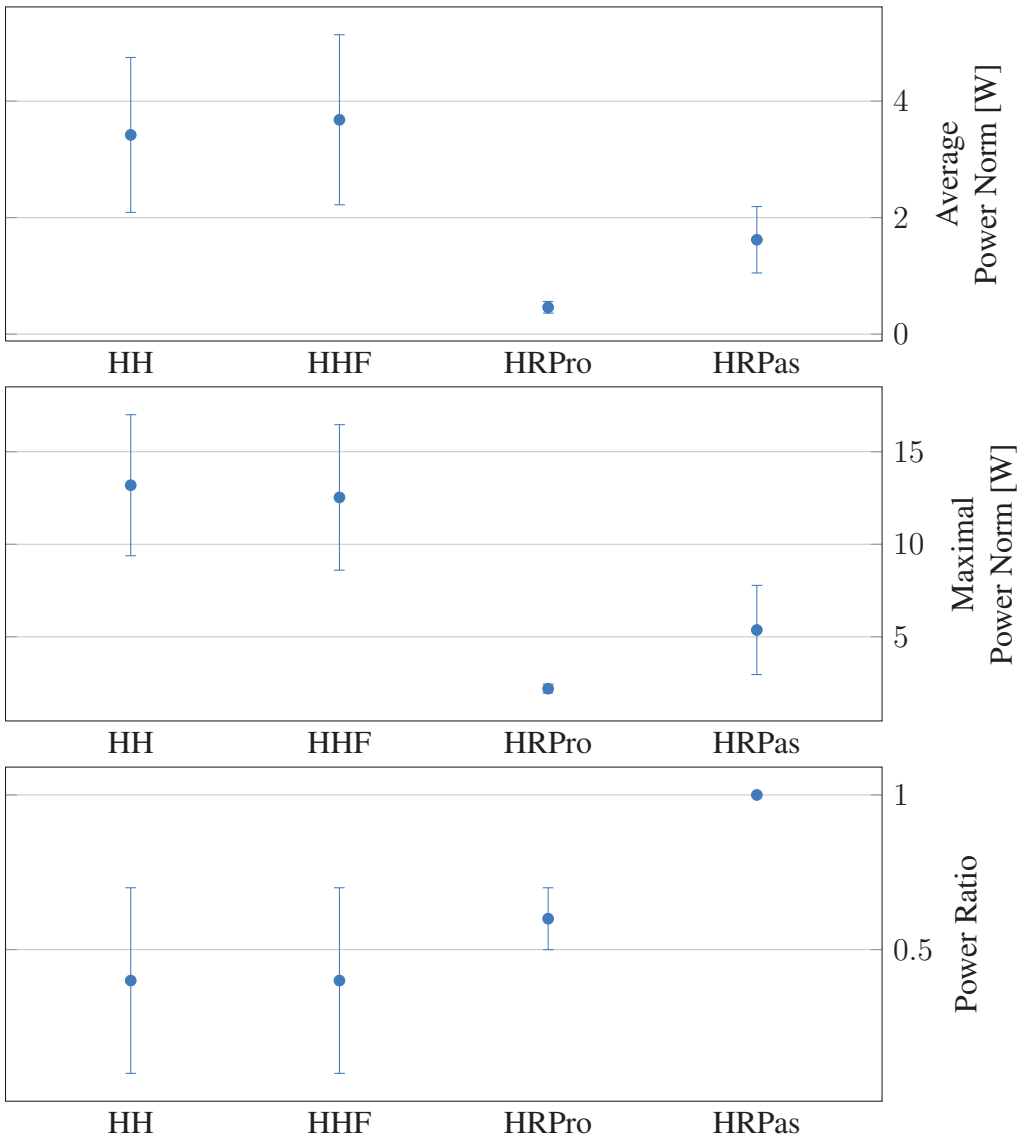

Figure 4.28: Mean and Standard Deviation for Power Indicators for each data set.

Table 4.29: Power Ratio t-tests results between each data set, assuming equal ($=$) and unequal ($\neq$) variances, with 5% significance level. A highlighted cell means that a significant statistical difference is observed (p-value $< 5\%$).

Power Ratio			
Data Set	**Mean**	p-**value** $=$	p-**value** $\neq$
HH	0.4	9.9×10^{-1}	9.9×10^{-1}
HHF	0.4	–	–
HRPro	0.6	3.5×10^{-1}	1.2×10^{-1}
HRPas	1.0	3.8×10^{-5}	2.4×10^{-6}

Nonetheless, the power exchanges in the human-human case are more important, that is more power and forces are exchanged and the task is performed at higher velocities –and probably higher accelerations. The robot, in its current state (software and maybe hardware) cannot withstand such power exchanges. The force and power levels input with the robot's passive behavior are within the limits of what is input in the human-human experiments. This is likely a cause of the preference of the participants for the passive behavior: the force and power levels are not hindering enough comparatively to the difficulty to guide the robot. However, further investigations are necessary to understand exactly what the participants did not like in the proactive behavior and how to solve them.

4.5 Conclusion

In this chapter, we first compare a passive behavior of the robot based on Evrard's approach [19] to our proactive control scheme. The quantitative results yielded by the measurements are very good. The robot's proactive behavior allows a 71% decrease in the work input of the human partner, as well as a 50% decrease in the average horizontal forces, while allowing higher velocities and thus a quicker completion of the task. However, in the qualitative comparative questionnaire, the participants to the study give their preference to the passive behavior because they feel that the robot better understands what they want it to do.

In a second investigation, we study the impact of training on the performances of the proactive behavior. The results show no significant improvement and rather point at different strategies of learning the task with the robot. The non-continuous improvement of the quantitative or the qualitative measures is normal, since an optimal value is reached after several trials. The obtained results may suggest that in fact the learning process can be fast.

Finally, we compare the data of both robot's behaviors with the data gathered from human dyads of Chapter 2. Our proactive control scheme shows good results in terms of work input into the follower partner, and even too good in terms of force and power input. The force and power levels of the passive behavior are within limits of those from human dyads, which may explain why these levels are less discriminating than the robot's manipulability when the participants have to compare the proactive and passive behaviors.

The main way to improve our proactive control scheme would be to improve the walking capabilities of the robot, both in velocity and stability. Concerning stability, physical interaction offers the incredible opportunity to use the contact with the human partner to increase the robot's equilibrium options. The next chapter presents a tentative study on the stabilization through physical interaction. It also introduces preliminary works on the possible future developments of our proactive control scheme, including its extension to direct physical interaction, as well as the addition of vision-based control.

5 Further Potential Extensions

Contents

In the previous chapter, we studied the performances of our proactive control scheme. We found that although it showed good quantitative performances when compared to the passive approach, qualitative assessment investigation through subjective questionnaire shows that users preferred a passive-behavior humanoid robot. A small number of users experienced the proactive behavior in order to see if performance can be improved through repeated practice and learning, but this was not the case. We hypothesize that the only way to improve the qualitative (and even quantitative) performance and usability is to seek for improvement of the technology to change the view of the user on the robot and its capability.

First, we thought that the sound from the robot's actuators might have disturbed the participants and increase their fear to harm the robot. In Section 5.1, we investigate the effect of robot's sound on the performances of our proactive control scheme.

We also highlighted that the walking capacities of the robot needed to be improved. Indeed, the stabilizer of the walking pattern generator is designed to work for a humanoid walking in standalone, a physical contact is seen as an external perturbation and it is certainly not designed to work in a sustained physical contact interaction with a human. In Section 5.2, we discuss how to improve the robot's balance during walking, which would eventually lead to improved walking capacities.

In Section 5.3, we present possible extensions of our motion primitive approach to two other tasks that require direct interaction: guiding the robot by the hand and handshaking.

Finally, we present on-going research for an extension of our work that includes vision in Section 5.4 and constitutes a first step toward multi-modal interaction.

5.1 Sound Deprivation User Study

This section presents a user study which aims at determining the impact of robotic sound (inherent from actuation) deprivation on the performances and impressions of human subjects that perform a transportation task with the proactive HRP-2. Indeed, in Chapter 4, one important factor is that participants fear to harm the robot more with the proactive behavior than with the passive behavior. The sounds from the robot actuators might be a source of this anxiety. Therefore we hypothesize that diminishing this noise may improve the performance and feelings of the participants when performing the transportation task.

5.1.1 Conditions and setting

The setting, scenarios, the measurements and the questionnaires are identical to the ones used for the comparative user study of Section 4.2. Only the conditions that are compared are different. Whereas Section 4.2 compares the passive and proactive behaviors of the robot, we compare the task performed with and without sound deprivation, both with the robot's proactive behavior.

Figure 5.1: Headset used to deprive the participants of audition.

To deprive the participants of audition, we use the headset of Fig. 5.1. To limit the impact of learning, the participants are separated in two groups. The "Sound-NoSound Group" starts by the task without sound deprivation and continues with the task with sound deprivation. The "NoSound-Sound Group" does the reverse. Hand signals are used in addition to voice to give the start and stop signals when the participants wear the helmet. The same eight participants that take part to the user study of Section 4.2 participate to this one. The groups are changed. Whereas the groups consists in Subject 1 to 4 and 5 to 8 in the previous study, we keep the same numeration of subjects and put the odd-numbered subjects in the NoSound-Sound Group and the even-numbered subjects in the Sound-NoSound Group. The user study took place at the CNRS-AIST Joint Robotics Laboratory (JRL) in Tsukuba, Japan, from the 27th of June to the 1st of July 2013.

5.1.2 Results

For each indicator, we plot a bar chart that presents the value of this indicator in both passive (red) and proactive (blue) cases for each participant (Fig. 5.2 to 5.8).

For each indicator, we perform two t-tests using the `ttest2` function from MATLAB®. The first test assumes equal variances, whereas the second does not. Both tests yield very similar results though. The results of these tests are presented in Tables 5.1 and 5.2.

The t-tests show that no significant statistic difference can be observed in any indicators.

5.1.2.1 Questionnaire Results

The questionnaire results show no significant statistic difference in general either. The only exception is the item "I perceived that the robot understood what I wanted it to do". Besides only three subjects rate it differently than zero, and one of them, Subject 8, admits that it might come from habit rather than from the sound deprivation. Given the other results, we would rather consider it as a false positive.

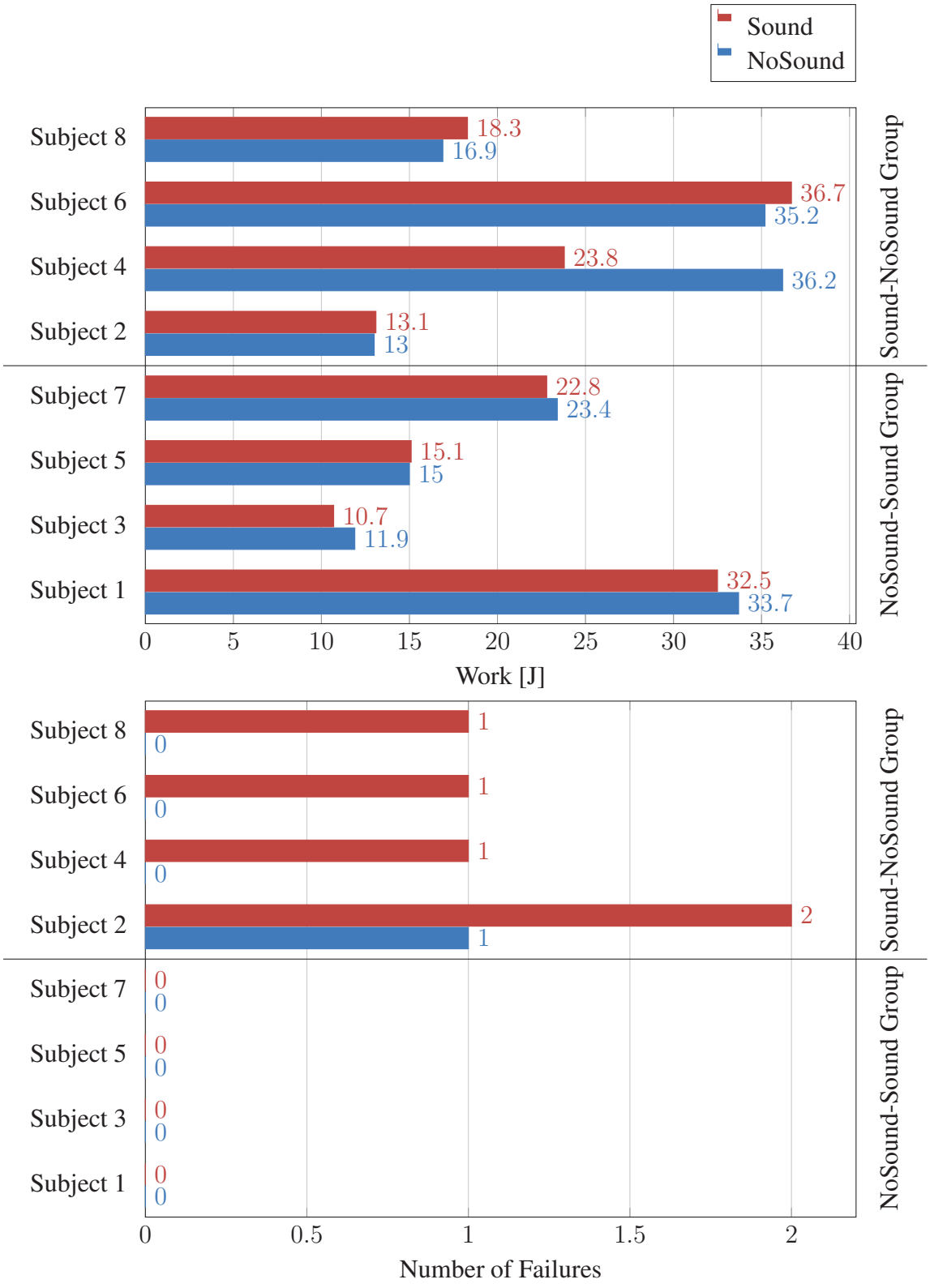

Figure 5.2: Work and Number of failures in the comparative user study.

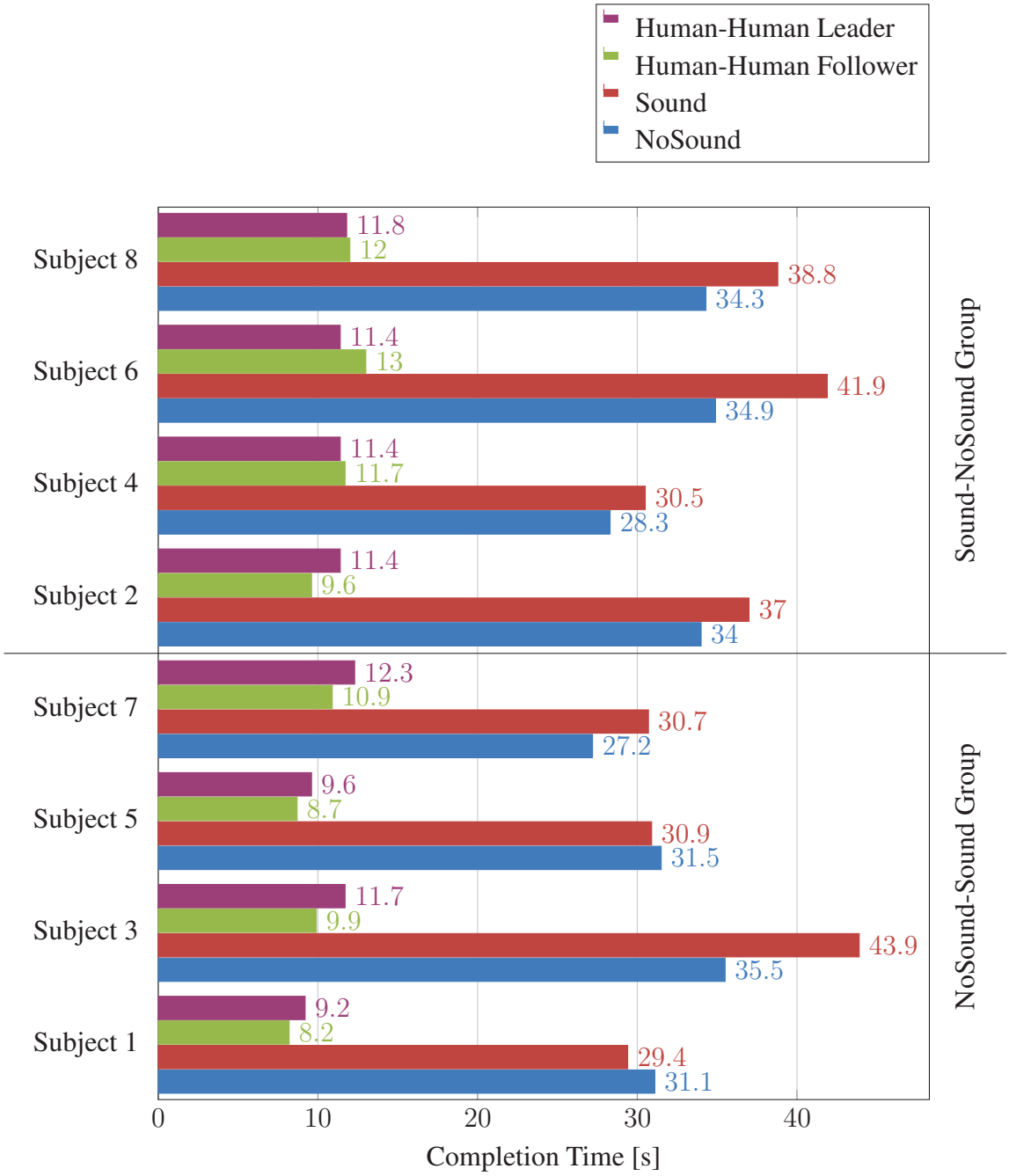

Figure 5.3: Completion times in the comparative user study. Here the completion times achieved when the participants performed the task with the experimenter are shown. First, the participants followed the lead of the experimenter (green), and then they lead the task (purple).

Table 5.1: Important Indicators t-tests results, assuming equal ($=$) and unequal ($\neq$) variances, with 5% significance level. A blue cell indicates that a significant statistic difference is observed (p-value $< 5\%$).

Indicator	**NoSound Mean**	**Sound Mean**	p-**value** $=$	p-**value** $\neq$
Work [J]	23.2	21.6	7.6×10^{-1}	7.6×10^{-1}
Completion Time [s]	32.1	35.4	1.8×10^{-1}	1.8×10^{-1}
Nb of Failures	0.1	0.6	1.1×10^{-1}	1.2×10^{-1}

Table 5.2: Other Indicators t-tests results, assuming equal ($=$) and unequal ($\neq$) variances, with 5% significance level. A blue cell indicates that a significant statistic difference is observed (p-value $< 5\%$).

Indicator	**NoSound Mean**	**Sound Mean**	p-**value** $=$	p-**value** $\neq$
Average Velocity Norm [m/s]	0.166	0.159	6.5×10^{-1}	6.5×10^{-1}
Maximal Velocity Norm [m/s]	0.31	0.30	5.0×10^{-1}	5.0×10^{-1}
Average Angular Velocity Norm [rad/s]	0.065	0.061	2.3×10^{-1}	2.3×10^{-1}
Maximal Angular Velocity Norm [rad/s]	0.23	0.21	4.2×10^{-1}	4.3×10^{-1}
Average Horizontal Force Norm [N]	5.5	5.4	9.0×10^{-1}	9.0×10^{-1}
Maximal Horizontal Force Norm [N]	16.8	16.5	9.1×10^{-1}	9.1×10^{-1}
Average Torque Norm [N.m]	5.6	5.5	9.4×10^{-1}	9.4×10^{-1}
Maximal Torque Norm [N.m]	14.6	14.5	9.4×10^{-1}	9.4×10^{-1}
Average Power Norm [W]	0.89	0.82	6.4×10^{-1}	6.4×10^{-1}
Maximal Power Norm [W]	5.05	4.20	3.8×10^{-1}	3.8×10^{-1}

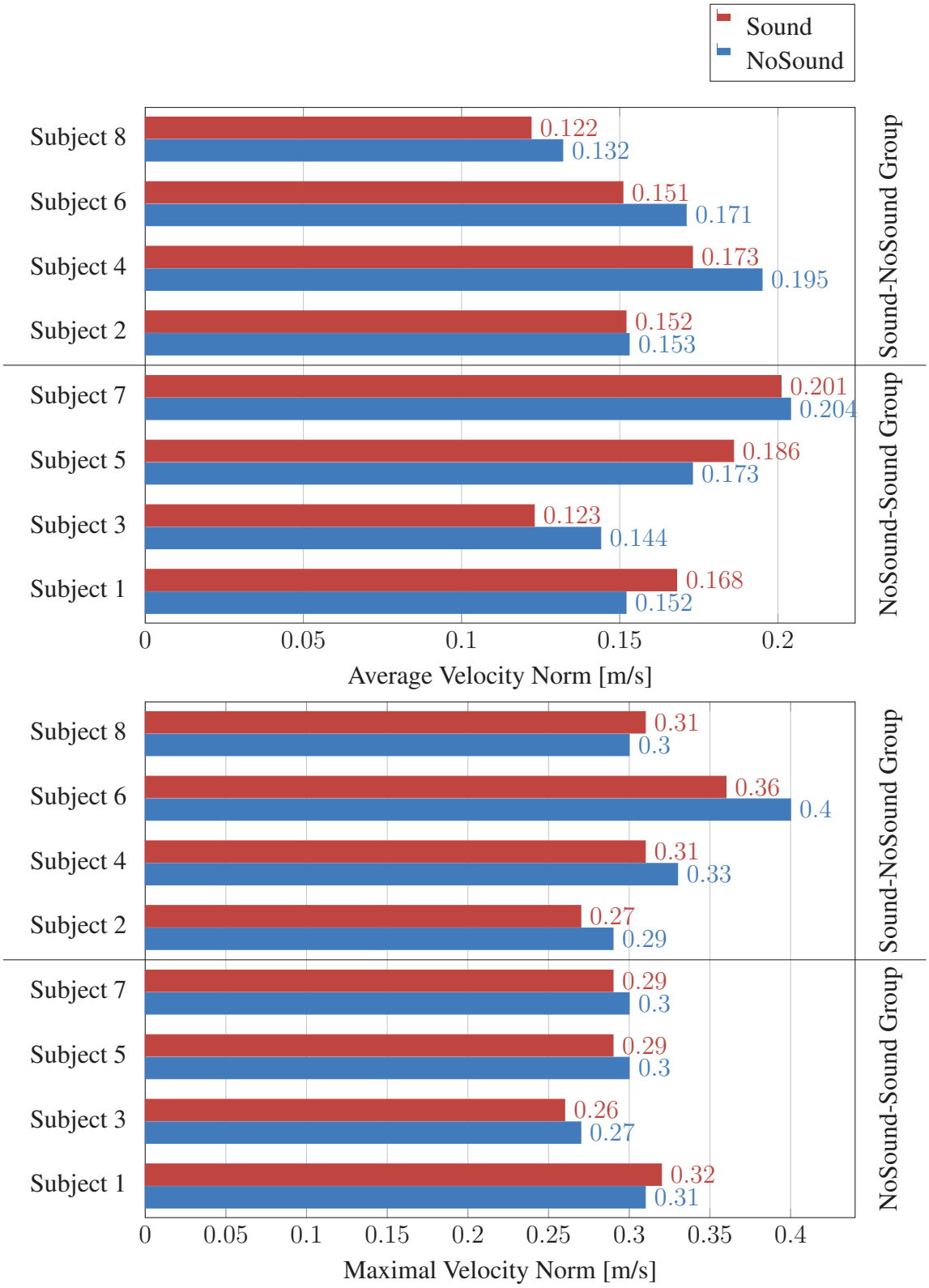

Figure 5.4: Average and maximum velocity norms in the comparative user study.

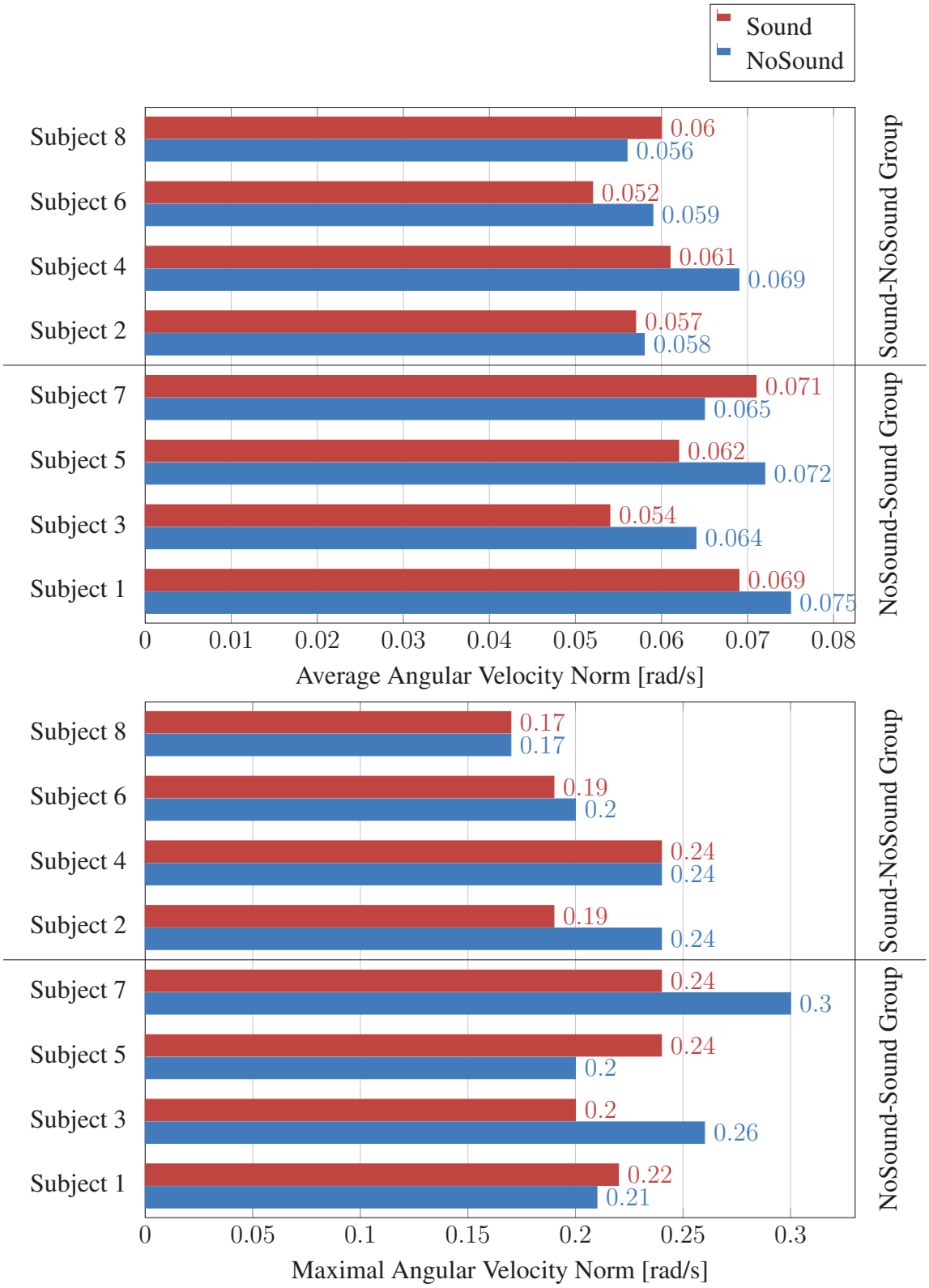

Figure 5.5: Average and maximum angular velocity norms in the comparative user study.

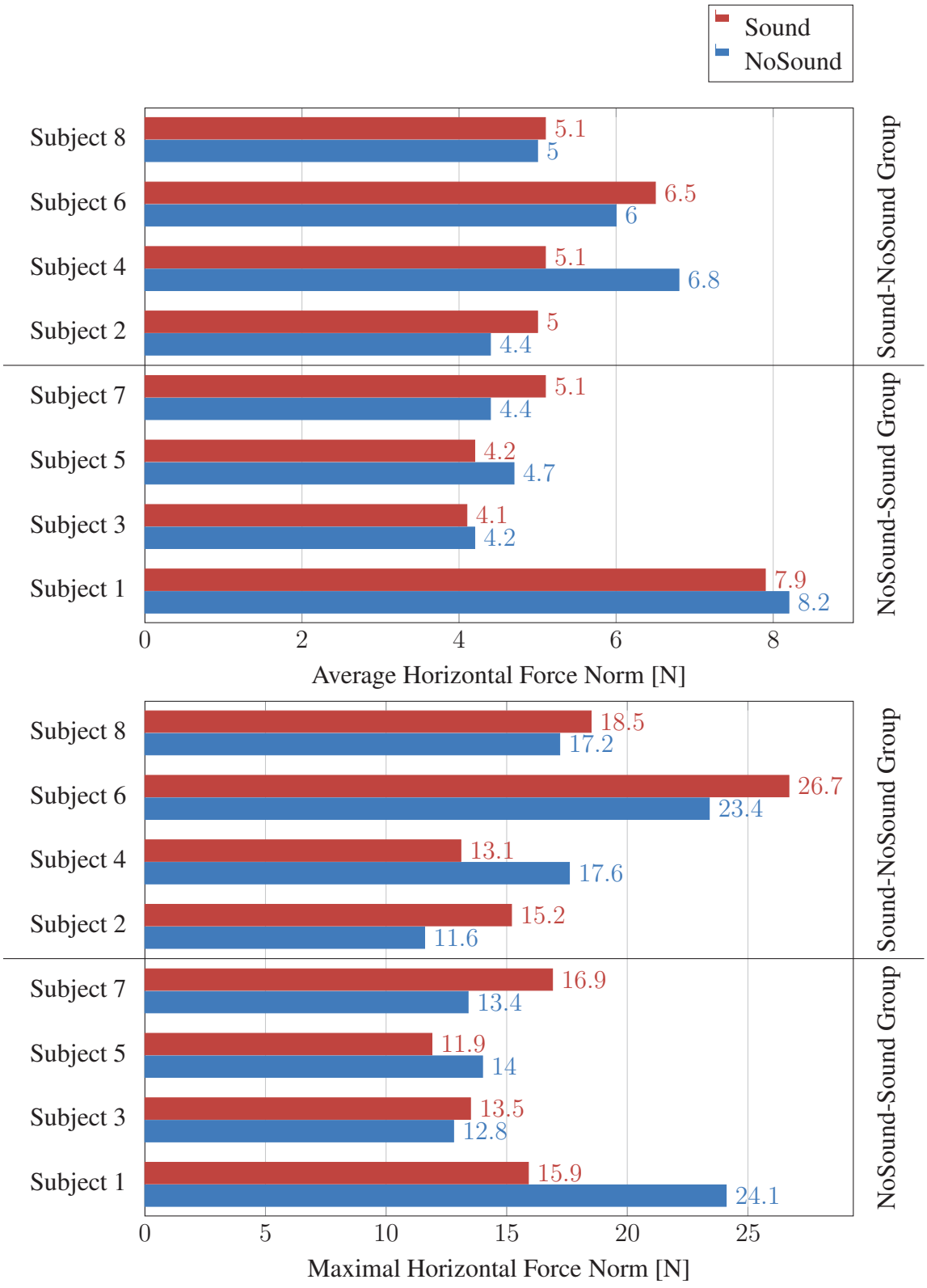

Figure 5.6: Average and maximum horizontal force norms in the comparative user study.

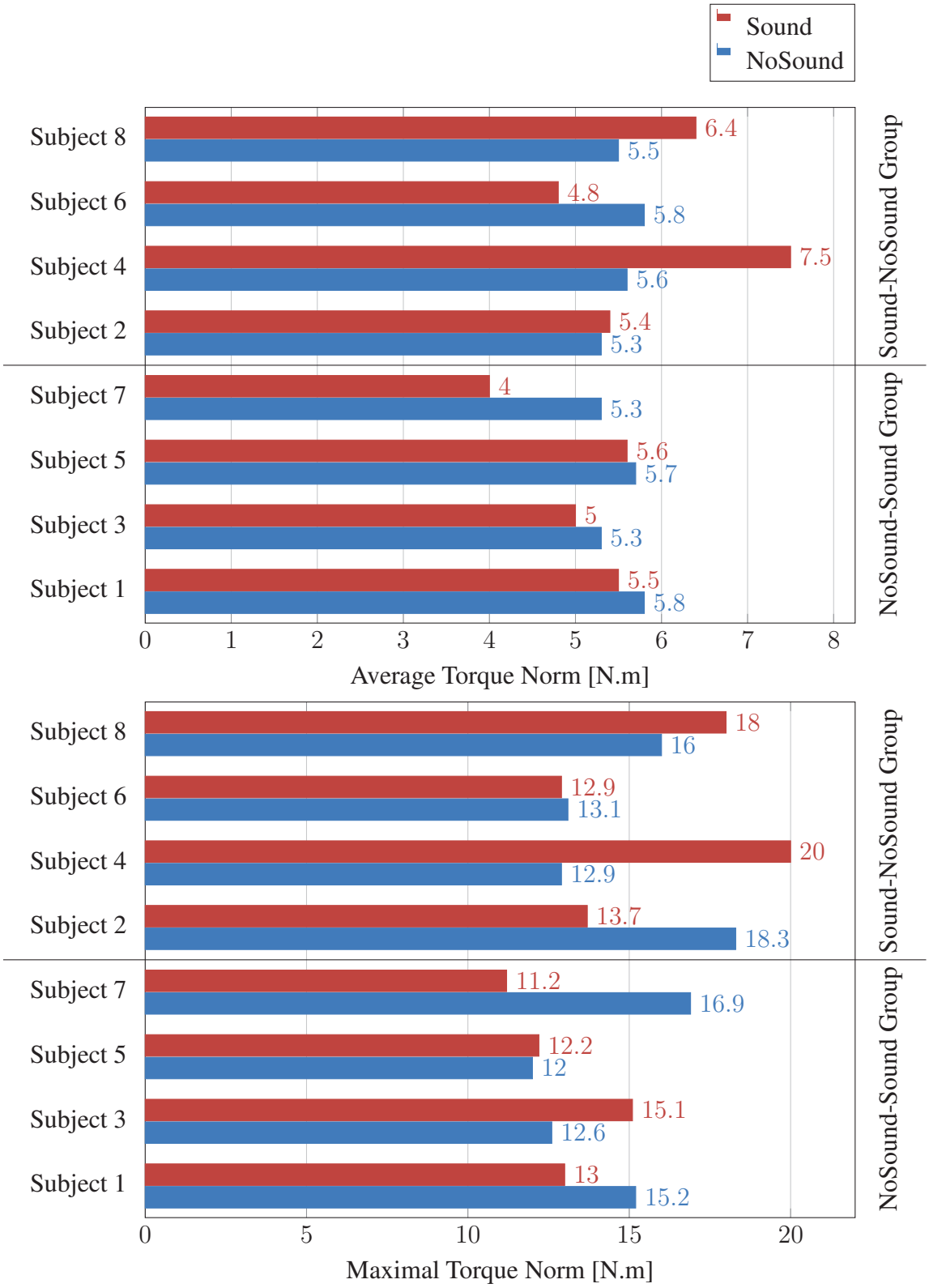

Figure 5.7: Average and maximum torque norms in the comparative user study.

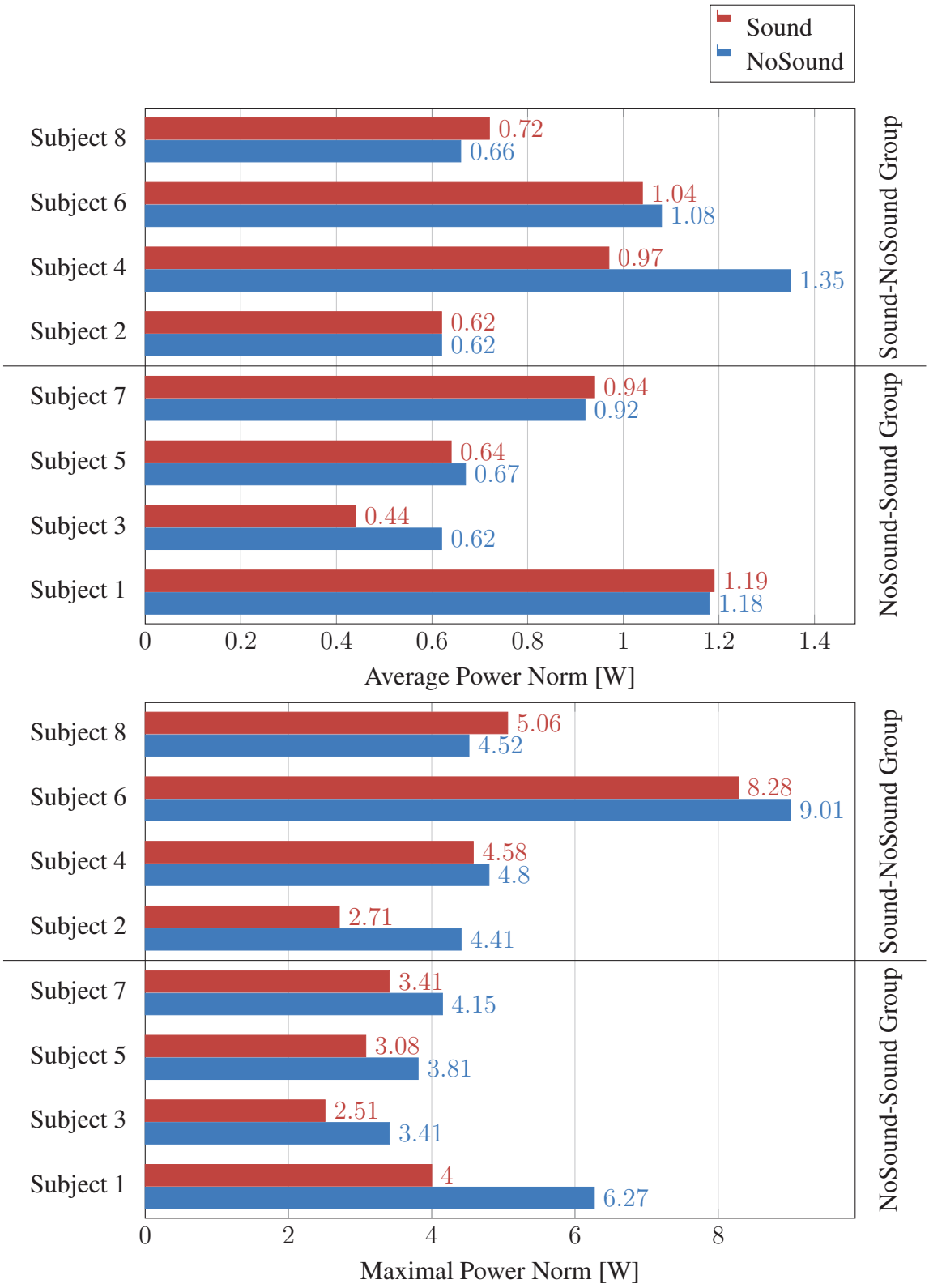

Figure 5.8: Average and maximum powers in the comparative user study.

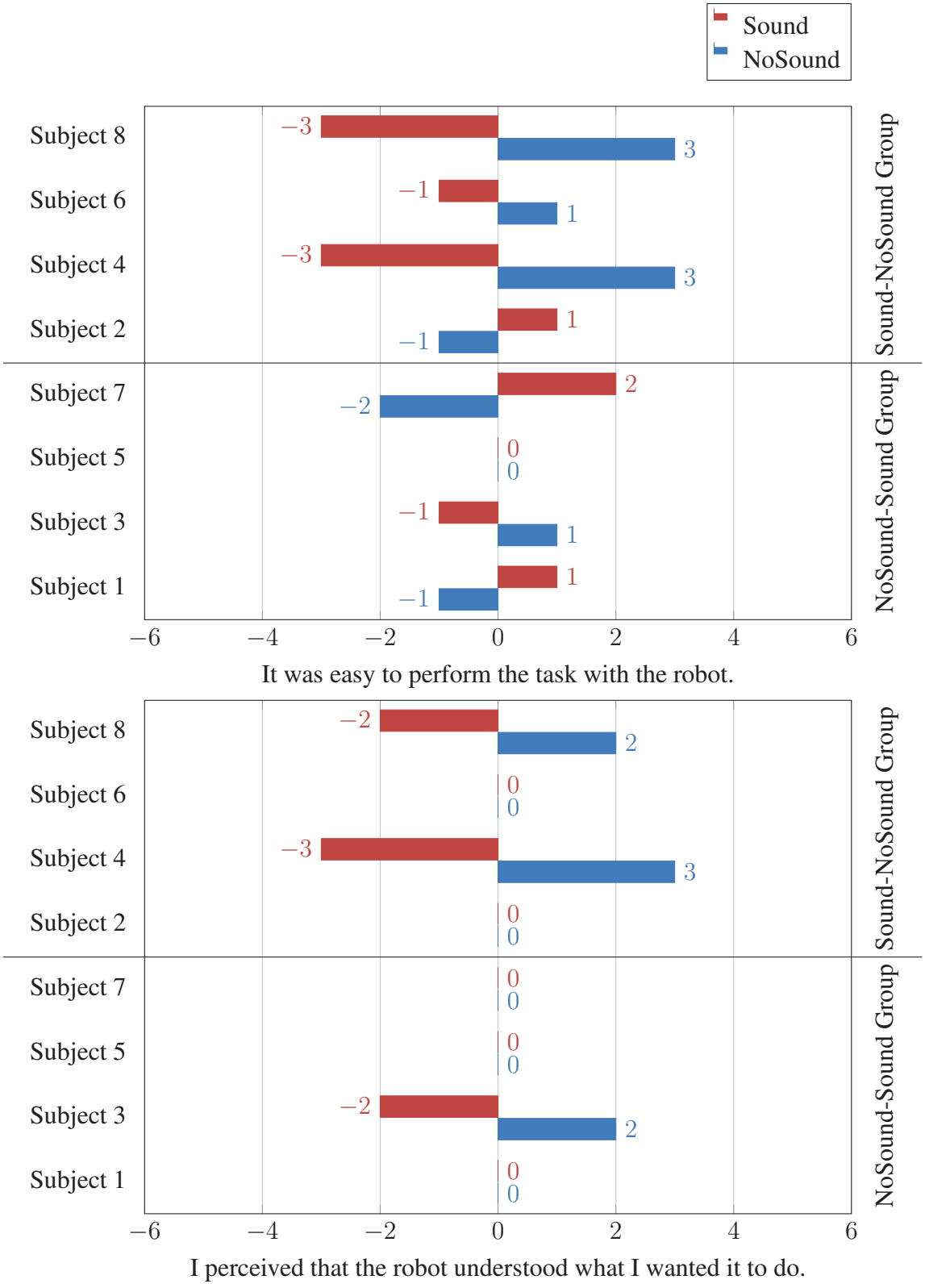

Figure 5.9: Score to 'Ease of Task' items in the comparative user study.

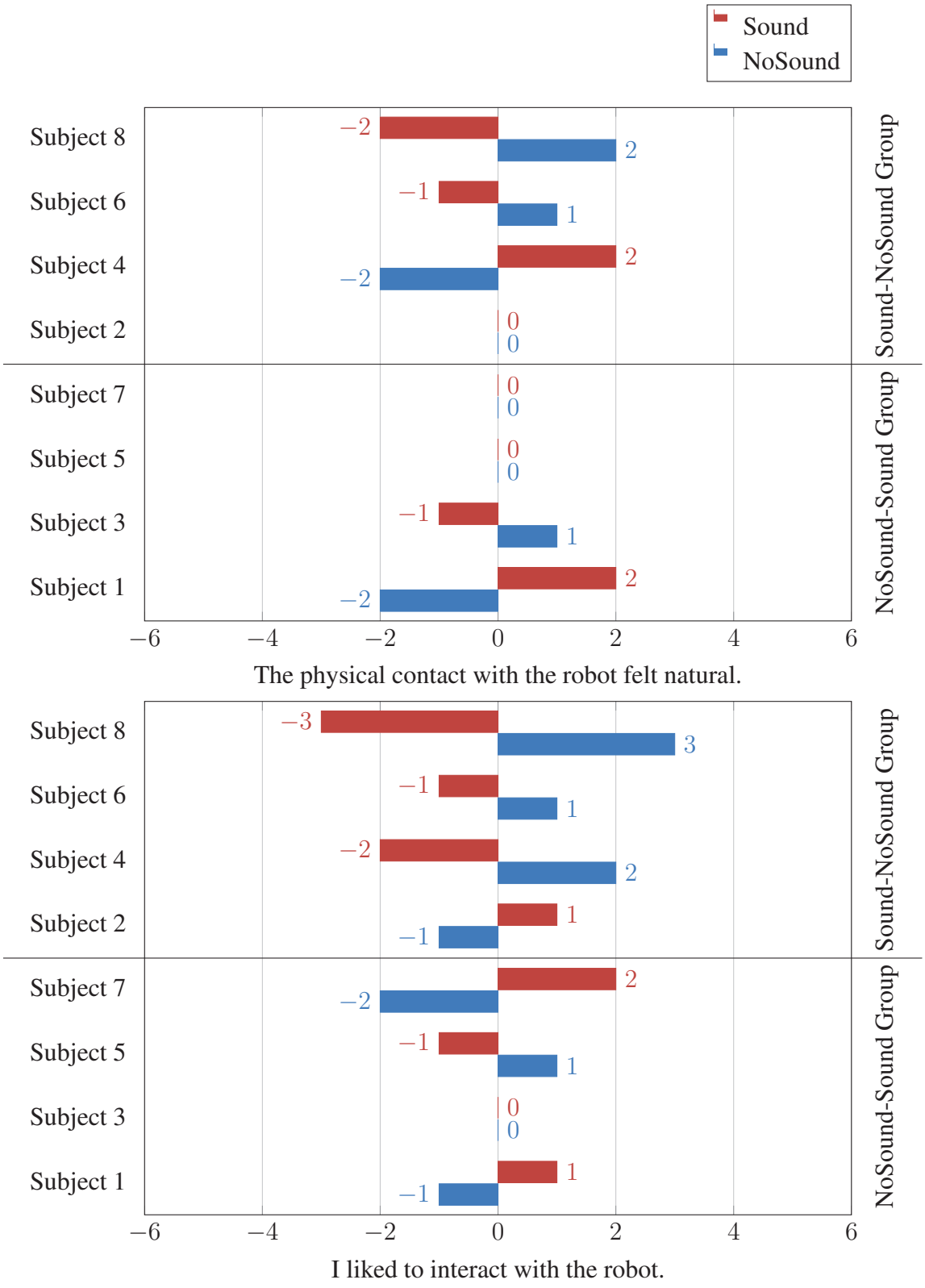

Figure 5.10: Score to 'Co-Experience' items in the comparative user study.

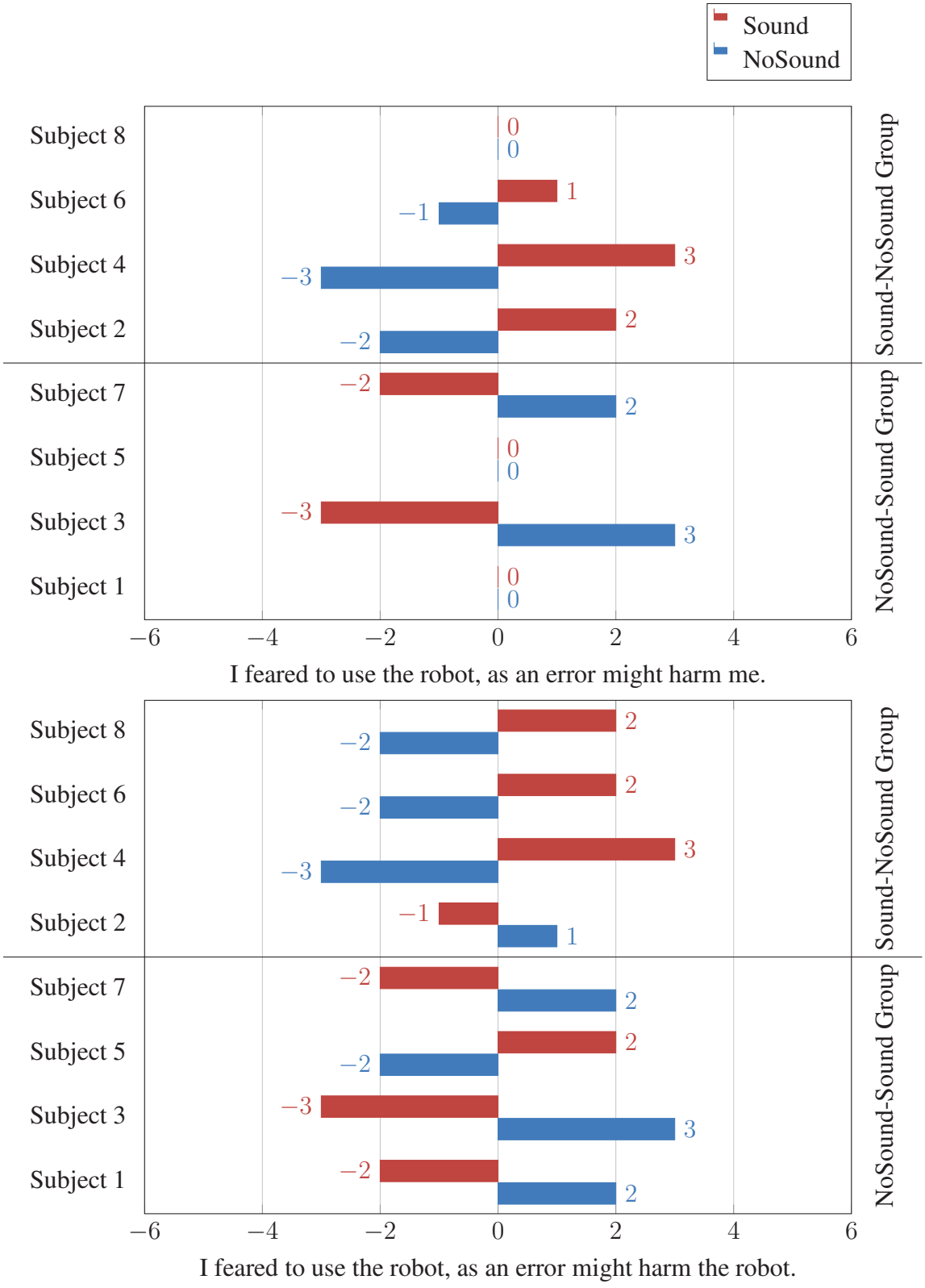

Figure 5.11: Score to 'Feeling of Security' items in the comparative user study.

Table 5.3: Questionnaires t-tests results, assuming equal ($=$) and unequal ($\neq$) variances, with 5% significance level. A blue cell indicates that a significant statistic difference is observed (p-value $< 5\%$).

Indicator	NoSound Mean	Sound Mean	p-value $=$	p-value $\neq$
It was easy to perform the task with the robot.	0.5	-0.5	3.0×10^{-1}	3.0×10^{-1}
I perceived that the robot understood what I wanted it to do.	0.9	-0.9	1.4×10^{-2}	1.4×10^{-2}
The physical contact with the robot felt natural.	0.0	0.0	1.0×10^{0}	1.0×10^{0}
I liked to interact with the robot.	0.4	-0.4	3.9×10^{-1}	3.9×10^{-1}
I feared to use the robot, as an error might harm me.	-0.1	0.1	8.0×10^{-1}	8.0×10^{-1}
I feared to use the robot, as an error might harm the robot.	-0.1	0.1	8.4×10^{-1}	8.4×10^{-1}

The measurements and questionnaire results are rather disappointing since no clear difference shows up. However, the free remarks section, whose results are presented in Table 5.4, contains some interesting quotes about the usefulness of sound deprivation. Only Subject 5 noted that it lessens the anxiety from the sound of the robot's actuators. Contrariwise, Subjects 1 and 2 prefers to hear the sound from the robot because they associate it with the velocity of the limits of the robot. Finally, Subjects 7 and 8 seems skeptical about the impact of the headset.

5.1.3 Conclusion

To summarize this study, sound deprivation has no visible effect on the performances or on the feeling of the participants. As with the user study in training, we hypothesize that the participants can be classified in at least three groups:

1. those who prefer to hear the robot's sounds because it gives information about the robot's state,
2. those who prefer not to hear the robot's sounds because it increases anxiety,
3. those who do not mind either.

This highlights that participants are not only interacting physically with the robot but also through sound; and most likely visually too. Although the present work focuses on physical interaction, the visual and audio stimuli the robot sends to the human should not be

Table 5.4: Comments made by the participants in the free remarks section of each questionnaire.

Subject	Questionnaire 1: NoSound	Questionnaire 2: Sound
1	Because it failed at the very end, it was a little strange. Otherwise, it felt very natural even though I had to make him turn in two phases.	It felt lighter to control the robot (less force) and having the sound gives more info on the state of the robot. It was still very enjoyable!
3	I feel the robot takes a little time to respond when I pull or push it, then when I want to begin (or change) the motion I have to wait for the response of the robot before keeping pushing or pulling.	I feel the motion was more natural in the experiment before than in this one, but I think it was due to my own behavior. I mean, I wanted to reproduce exactly the nice behavior achieved the last time, and maybe that stressed me a little.
5		The noise-cancelling device probably made it easier since it dampened the mechanical sounds of the actuators and the steps, which can be source of worry when not used to it.
7	I felt that the robot reacted a little bit late when I pushed it or stopped.	Compared to the previous condition, I was more relaxed to move the robot. But I don't think it is easier to perform the task even if I do it without the headset.
Subject	**Questionnaire 1: Sound**	**Questionnaire 2: NoSound**
2	Not easy to guide the robot when rotating.	I felt easier to guide the robot without the headset. (The sound of the seep helps me to know its velocity.) Finally, I understand how to guide it better by maintaining the same velocity.
4		
6		
8	It was not so difficult to guide the robot at the beginning but at the moment of turning I felt it kind of unnatural. I couldn't avoid trying to adapt the robot.	I found easier to make the robot turn in its place, rather than walking and turning at the same time. I found it easier but I don't know if it is because I already got accustomed to the robot or because I was using the ear covers.

neglected. The robot making a weird motion or emitting a strange noise has a non-negligible impact on the human partner. Therefore, vision and audition should be considered even though one does not consider multi-modal interaction.

Even the noise of the actuators has some importance; we consider it to be similar to the noise electrical cars are designed to make. As a car, a robot is a powerful machine that can hurt and kill a human. In both cases, sound is linked to the power produced by the machine and therefore is a strong indicator of the potential danger of this machine –for the human or itself. Therefore, completely eliminating the sound emitted by a robot's actuators might not be a good idea.

As the deprivation of humanoid's sound has no visible effect on the performances of our control scheme, we focus, in the next section, in improving the robot's capabilities. In particular we investigate how to use the physical interaction to improve the robot's balance, and thus its walking capacities. The next section presents preliminary results.

5.2 Self-Stabilization through pHRI

5.2.1 Evaluation of Stability

Before finding strategies for the robot to maintain its balance, we need criteria to *evaluate* the robot's stability. It means being able to detect whether it is losing its balance or not –a binary criterion– but also being able to evaluate how close the robot is from losing its balance –a "distance" criterion.

The main indicators we choose are based on the Zero-Moment Point or ZMP [58], since the robot is walking on a horizontal even floor. During gait without interaction, the robot loses its balance when the ZMP is on the edge of the support polygon. This criterion is not valid in our case however, since a human partner applies forces on the robot's grippers that might stabilize the robot even if the ZMP lies on the edge of the support polygon. In other words, the human partner can hold the robot back and prevent it from falling through the physical interaction. Still, this is not a sustainable situation because the robot is heavy –around 50kg for the HRP-2 case– and we do not want the robot to rely too much on the human to stabilize itself (the latter can obviously destabilize the humanoid by a wrong maneuver). Therefore, although the ZMP being on the edge of the support polygon does not necessarily mean a loss of balance, an action must be undertaken for the robot to gain a more "stable" and safe state.

To summarize, the ZMP indicators we develop thereafter cannot determine if the robot is losing its balance strictly speaking. However, they can help us to assess how close the robot is from a dangerous situation where the human partner would have to exert a lot of force on the robot to prevent its fall. This necessitates computing the ZMP position.

5.2.1.1 Computation of ZMP from force sensors

Since the ZMP coincides with the Center of Pressure (CoP) [58], we compute the ZMP using measurements from the robot's feet force sensors. The ZMP computation algorithm is taken

from [35]. First, we compute the position of the ZMP for a single support phase, i.e. when only one foot is on the floor, in the given foot local frame. We develop the formulas for the right foot, but the computation is the same for the left foot. The foot local frame is pictured in Fig. 5.12. The six-axis force sensor is positioned so that its center of measure is located on the z-axis of the foot local frame. Moreover, the frame of measure is aligned with the foot local frame, so that the homogeneous matrix ${}^{R}\mathbf{H}_{S_r}$ that transform the measure frame into the foot local frame is

$$ {}^{R}\mathbf{H}_{S_r} = \begin{bmatrix} 1 & 0 & 0 & 0 \\ 0 & 1 & 0 & 0 \\ 0 & 0 & 1 & d \\ 0 & 0 & 0 & 1 \end{bmatrix} \tag{5.1} $$

In the case of HRP-2, $d = -0.0195$m.

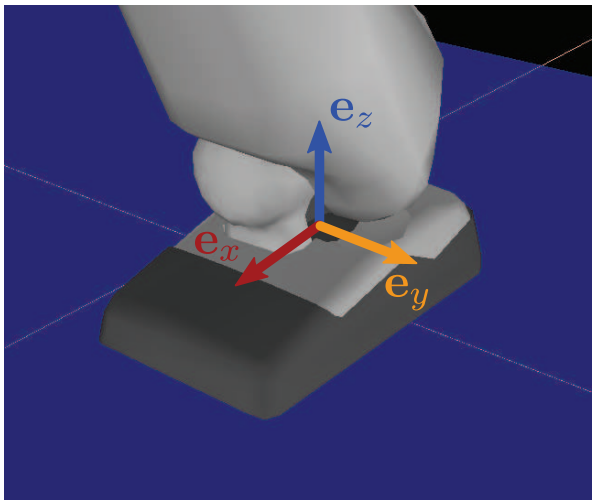

Figure 5.12: Foot local frame. It is chosen so that the z-axis is confounded with the gravity axis when walking on a horizontal floor. Besides the x-axis is the forward direction, thus making the y-axis the lateral direction.

Besides, the origin of the foot frame is located at a height $h = 0.105$m from the sole. The right force sensor measures the force $\mathbf{F}_R = \begin{bmatrix} f_{Rx} & f_{Ry} & f_{Rz} & \tau_{Rx} & \tau_{Ry} & \tau_{Rz} \end{bmatrix}^T$. The position $\mathbf{p}_R$ of the ZMP in the right foot frame is given by[1]

$$ {}^{R}\mathbf{p}_R = \begin{bmatrix} \dfrac{-\tau_{Ry} - f_{Rx}(h+d)}{f_{Rz}} \\ \dfrac{\tau_{Rx} - f_{Ry}(h+d)}{f_{Rz}} \\ -h \\ 1 \end{bmatrix} \tag{5.2} $$

[1]This is equations (3.26) and (3.27) from [35] on page 71. However, in [35], d is the distance of the sensor from the floor, hence the difference.

in homogeneous coordinates. As the SoT is providing the homogeneous matrix of the feet frames ${}^{W}\mathbf{H}_R$ and ${}^{W}\mathbf{H}_L$ in the world frames, we can compute the position of the ZMP of each foot ${}^{W}\mathbf{p}_R$ and ${}^{W}\mathbf{p}_L$ in the world frame

$$\begin{cases} {}^{W}\mathbf{p}_R = {}^{W}\mathbf{H}_R {}^{R}\mathbf{p}_R \\ {}^{W}\mathbf{p}_L = {}^{W}\mathbf{H}_L {}^{L}\mathbf{p}_L \end{cases} \tag{5.3}$$

When the robot is in double support, the global ZMP ${}^{W}\mathbf{p}$ is computed as

$${}^{W}\mathbf{p} = \frac{f_{Rz} {}^{W}\mathbf{p}_R + f_{Lz} {}^{W}\mathbf{p}_L}{f_{Rz} + f_{Lz}} \tag{5.4}$$

The advantage with equation (5.4) is that it can be adapted to encompass both single and double support by setting $f_{Rz} = 0$ or $f_{Lz} = 0$[2] during single support phases. Single support phases are determined when f_{Rz} or f_{Lz} is below a given force threshold. In such a case, the corresponding ZMP local position ${}^{R}\mathbf{p}_R$ or ${}^{L}\mathbf{p}_L$ is set to $\begin{bmatrix} 0 & 0 & -h & 1 \end{bmatrix}^T$.

The inconvenient with this method is that it depends on the position/orientation of the feet in the world frame ${}^{W}\mathbf{H}_R$ and ${}^{W}\mathbf{H}_L$, which are computed by the Stack-of-Tasks (SoT) and therefore are not accurate since they do not account for the modifications made by the stabilizer.

5.2.1.2 Distance to Support Polygon

The first indicator is the distance of the ZMP to the support polygon formed by the robot's feet. Because we also need information on which direction the robot is losing balance, we need to compute the vector that realizes that distance. By modelling the robot's sole as a rectangle, computing the robot's support polygon is computing the convex hull of a cloud of four or eight points in 2D, which is done using Andrew's monotone chain algorithm [2]. We then compute a signed distance of the ZMP to the support polygon and the vector that realizes this distance; the distance is counted negative if the ZMP is outside the support polygon[3].

Figure 5.13 shows the results of the algorithm for one time step of data from a real experiment with the robot. The signed distance to the support polygon is pictured in Figure 5.14 as well as the vector that realizes it. The main observation is that these data are discontinuous. Such discontinuities in the distance come from the alternation of single and double support phases during the robot gait. Besides, the vector that realizes the distance can become very discontinuous when the ZMP is in the middle of the support polygon. This is not a problem to detect when the robot is losing its balance, but it might be if we plan to use these values to compute a command.

Moreover, the computation of the support polygon highly relies on the relative position/orientation of the feet given by the SoT during double support phases, which is modified by the stabilizer. However, this does not explain the negative signed distance observed in the

[2] In practice, force thresholds are used to determine null forces.

[3] Note that the ZMP is *always* inside the support polygon. The ZMP being outside is the result of measurements errors.

data (the minimum is 7.5mm; it means that the ZMP is outside the support and thus the robot should have fallen but it did not) since all the negative distance but one ($t = 50.3$s) occurred during single support phases for which the algorithm does not depend on the feet relative position.

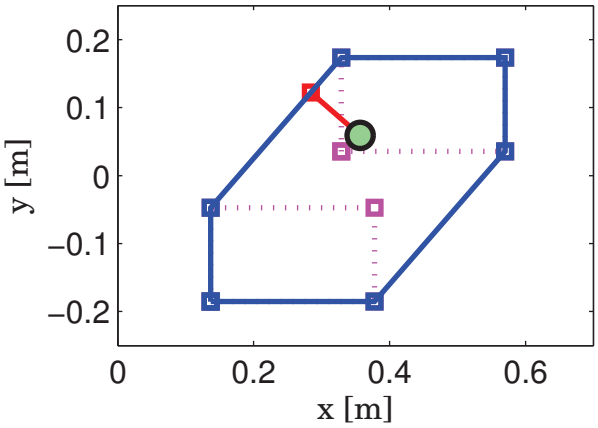

Figure 5.13: Support polygon and ZMP while the robot is in double support. The support polygon is in blue, while the parts of the feet that do not belong to the support polygon are in magenta. The green dot is the ZMP. The red dot is the projection of the ZMP on the support polygon, e.g. the point of the polygon that minimizes the distance, and the red line is the vector that realizes this distance.

5.2.1.3 Distance to Feet Geometric Middle

The second indicator is the distance to a safe value. In this case, a safe point: the geometric middle of the feet that are in contact with the ground. It consists in defining a safe point for each foot in that foot local frame, respectively noted ${}^{R}\mathbf{q}_R$ and ${}^{L}\mathbf{q}_L$. In this study, they are chosen so that they are the middle of the rectangle that is used to model the plant of the robot's feet. However, choosing their x and y components as zero may have been a better choice. Then the geometric middle ${}^{W}\mathbf{q}$ can be computed as follows

$$ {}^{W}\mathbf{q} = \begin{cases} {}^{W}\mathbf{H}_R \, {}^{R}\mathbf{q}_R + {}^{W}\mathbf{H}_L \, {}^{L}\mathbf{q}_L \text{ in double support} \\ {}^{W}\mathbf{H}_R \, {}^{R}\mathbf{q}_R \text{ or } {}^{W}\mathbf{H}_L \, {}^{L}\mathbf{q}_L \text{ in single support} \end{cases} \tag{5.5} $$

In double support phase, we thus have

$$ {}^{W}\mathbf{p} - {}^{W}\mathbf{q} = {}^{W}\mathbf{H}_R \left[\frac{f_{Rz}}{f_{Rz} + f_{Lz}} {}^{R}\mathbf{p}_R - {}^{R}\mathbf{q}_R \right] + {}^{W}\mathbf{H}_L \left[\frac{f_{Lz}}{f_{Rz} + f_{Lz}} {}^{L}\mathbf{p}_L - {}^{L}\mathbf{q}_L \right] \tag{5.6} $$

Because of the force ratios factors, the fourth components of

$$ \frac{f_{Rz}}{f_{Rz} + f_{Lz}} {}^{R}\mathbf{p}_R - {}^{R}\mathbf{q}_R \quad \text{and} \quad \frac{f_{Lz}}{f_{Rz} + f_{Lz}} {}^{L}\mathbf{p}_L - {}^{L}\mathbf{q}_L $$

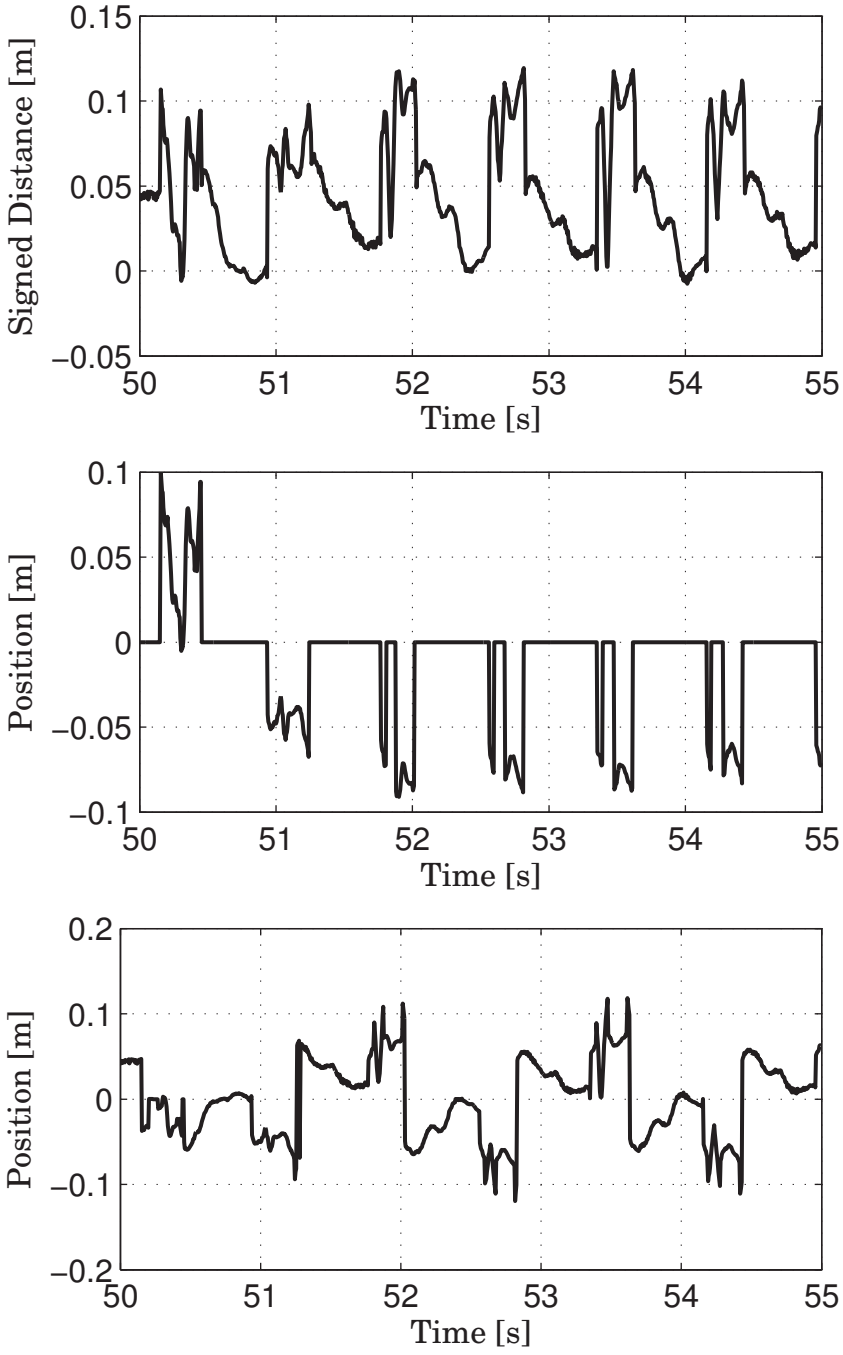

Figure 5.14: Signed distance to the support polygon (top) and vector that realizes this distance (x and y components: middle and bottom respectively), between $t = 50$s and $t = 55$s. The total experiment goes from $t = 45$s to $t = 80$s. The main observation is that these values are highly discontinuous.

are non-zero (but they cancel out so that the fourth component of ${}^W\mathbf{p} - {}^W\mathbf{q}$ is zero). Therefore, ${}^W\mathbf{p} - {}^W\mathbf{q}$ will depend on the translation part of ${}^W\mathbf{H}_R$ and ${}^W\mathbf{H}_L$, e.g. of the feet relative position. The results are presented in Figures 5.15 and 5.16.

The main advantage of this indicator over the distance to the support polygon is that zero is now a safe value rather than a value to avoid. The zero is decreed the *safest* position, whereas a safest position is harder to define with the support polygon. It is also easier to compute. However, the distance is still discontinuous because of the alternation of single and double support during the gait.

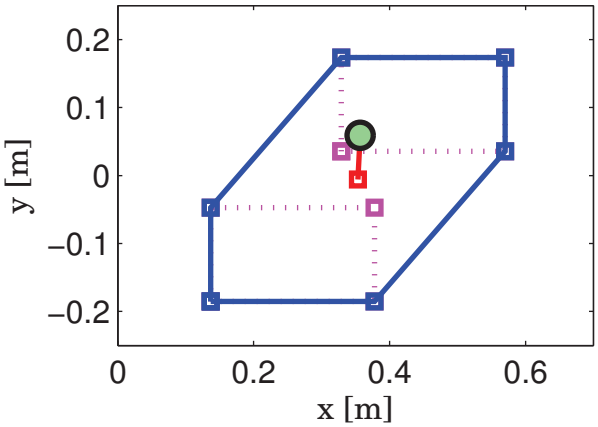

Figure 5.15: Feet geometric middle and ZMP while the robot is in double support. The support polygon is in blue, while the parts of the feet that do not belong to the support polygon are in magenta. The green dot is the ZMP. The red dot is the geometric middle of the feet and the red line is the vector between this middle and the ZMP.

5.2.1.4 Distance to Feet Weighted Middle

To eliminate the problem of discontinuities, we compute a weighted middle point of the feet inspired from (5.4). First we choose a safe point for each foot ${}^{R}\mathbf{r}_R$ and ${}^{L}\mathbf{r}_L$. In this study, we choose the x and y components as zero, which explains why the computed distance comes closer to zero in Fig. 5.18 in comparison to Fig. 5.16. Then we compute the weighted middle point in the world frame as follows

$$ {}^{W}\mathbf{r} = \frac{f_{Rz}\,{}^{W}\mathbf{H}_R\,{}^{R}\mathbf{r}_R + f_{Lz}\,{}^{W}\mathbf{H}_L\,{}^{L}\mathbf{r}_L}{f_{Rz} + f_{Lz}} \tag{5.7} $$

which is valid for both single and double support if using a force threshold for f_{Rz} and f_{Lz}. Thus, the vector from the ZMP to this weighted middle point is

$$ {}^{W}\mathbf{p} - {}^{W}\mathbf{r} = \frac{f_{Rz}}{f_{Rz} + f_{Lz}}\,{}^{W}\mathbf{H}_R\left[{}^{R}\mathbf{p}_R - {}^{R}\mathbf{r}_R\right] + \frac{f_{Lz}}{f_{Rz} + f_{Lz}}\,{}^{W}\mathbf{H}_L\left[{}^{L}\mathbf{p}_L - {}^{L}\mathbf{r}_L\right] \tag{5.8} $$

Since ${}^{R}\mathbf{p}_R - {}^{R}\mathbf{r}_R$ and ${}^{L}\mathbf{p}_L - {}^{L}\mathbf{r}_L$ fourth component is zero, ${}^{W}\mathbf{p} - {}^{W}\mathbf{r}$ does not depend on the feet relative position, but only on their relative orientation. Therefore, this algorithm is less dependent on the modifications made by the stabilizer. Moreover, the computed data in Figure 5.18 seems less discontinuous. Indeed, the *safest point* moves continuously as the

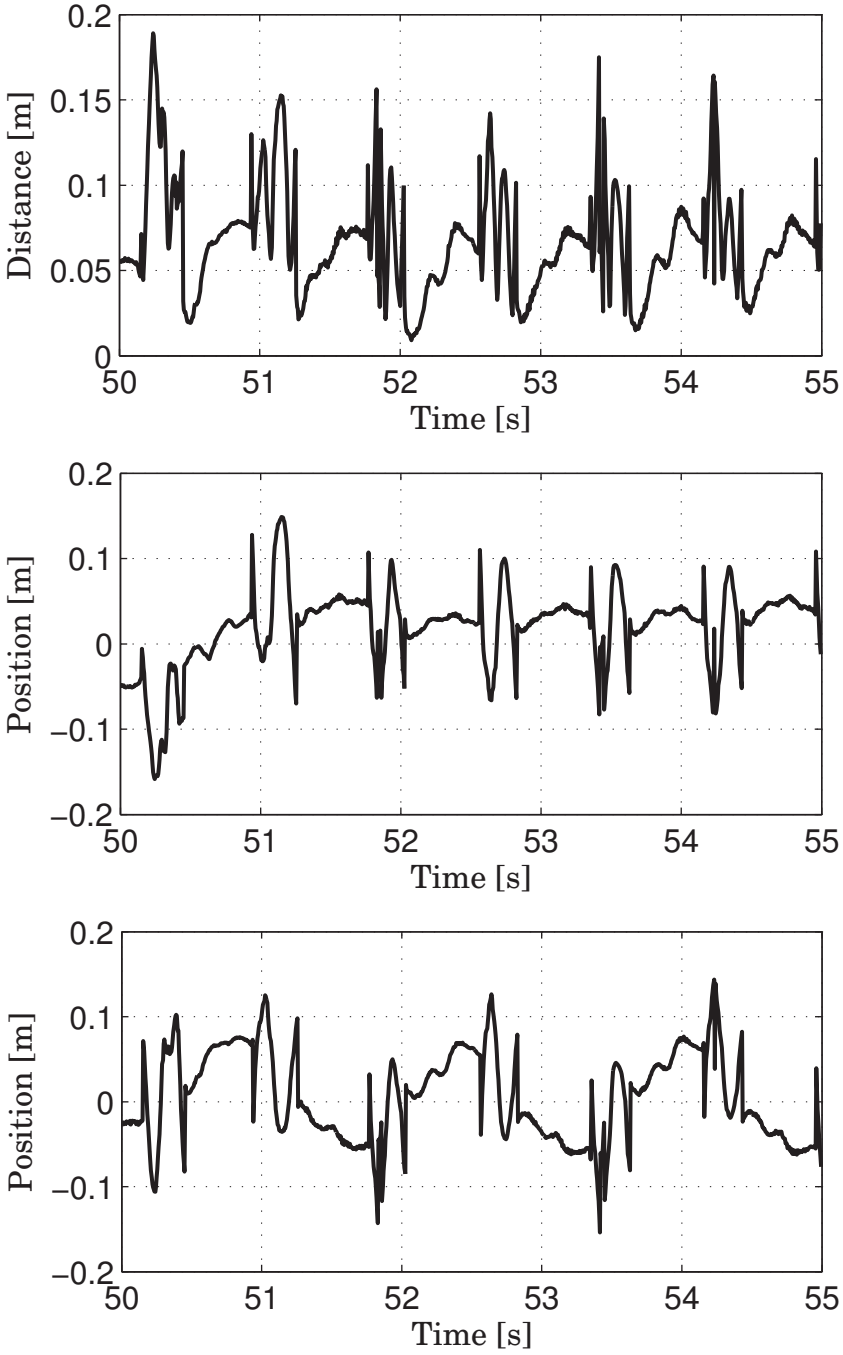

Figure 5.16: Distance to geometric middle point (top) and vector ZMP-geometric middle point (x and y components: middle and bottom respectively), between $t = 50s$ and $t = 55$s. The total experiment goes from $t = 45$s to $t = 80$s. These values are highly discontinuous, too.

robot lays a foot on the floor and switches between single and double support. This might be a more suited input for command. Besides, the distance varies less and the time $t = 50.3$s stands out as more unbalanced than the rest. This timing corresponds to the robot's first step,

where the Walking Pattern Generator is asked to produce a high acceleration, making the generated gait less balanced. An example is shown in Fig. 5.17.

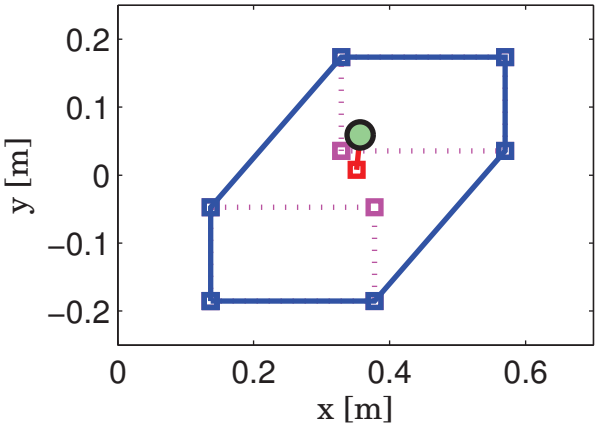

Figure 5.17: Feet weighted middle and ZMP while the robot is in double support. The support polygon is in blue, while the parts of the feet that do not belong to the support polygon are in magenta. The green dot is the ZMP. The red dot is the weighted middle of the feet and the red line is the vector between this middle and the ZMP.

To summarize, the distance to the support polygon may be the best indicator to evaluate the stability of the robot offline. For command however, using the vector to the weighted feet middle may be preferable because it is less discontinuous and not sensible to the measurement error of the feet relative position.

5.2.1.5 Horizontal Force and Torque Norm

Besides the ZMP approaches, it is also useful to look at the forces applied by the human partner through the beam on the robot's grippers, especially if the human is asked to maintain the robot's balance. Therefore, the horizontal force norm can yield useful information. For $\mathbf{F} = \begin{bmatrix} f_x & f_y & f_z & \tau_x & \tau_y & \tau_z \end{bmatrix}^T$, it is computed as follows

$$\text{Horizontal Force Norm} = \sqrt{f_x^2 + f_y^2} \tag{5.9}$$

Similarly, we compute the torque norm:

$$\text{Torque Norm} = \sqrt{\tau_x^2 + \tau_y^2 + \tau_z^2} \tag{5.10}$$

The advantage of this indicator is that it is easy to measure and also works for uneven floors. Besides it yields more information when the robot is off-balance. When the ZMP is on an edge of the support polygon, the robot start rotating around that edge. Whatever this angle of rotation is, the ZMP will always remain on the edge. Contrariwise, depending on the angular acceleration of the robot around that edge, the human partner has to apply more or less force to keep the robot's balance. The horizontal force norm applied by the human thus yield complementary information to the ZMP indicators.

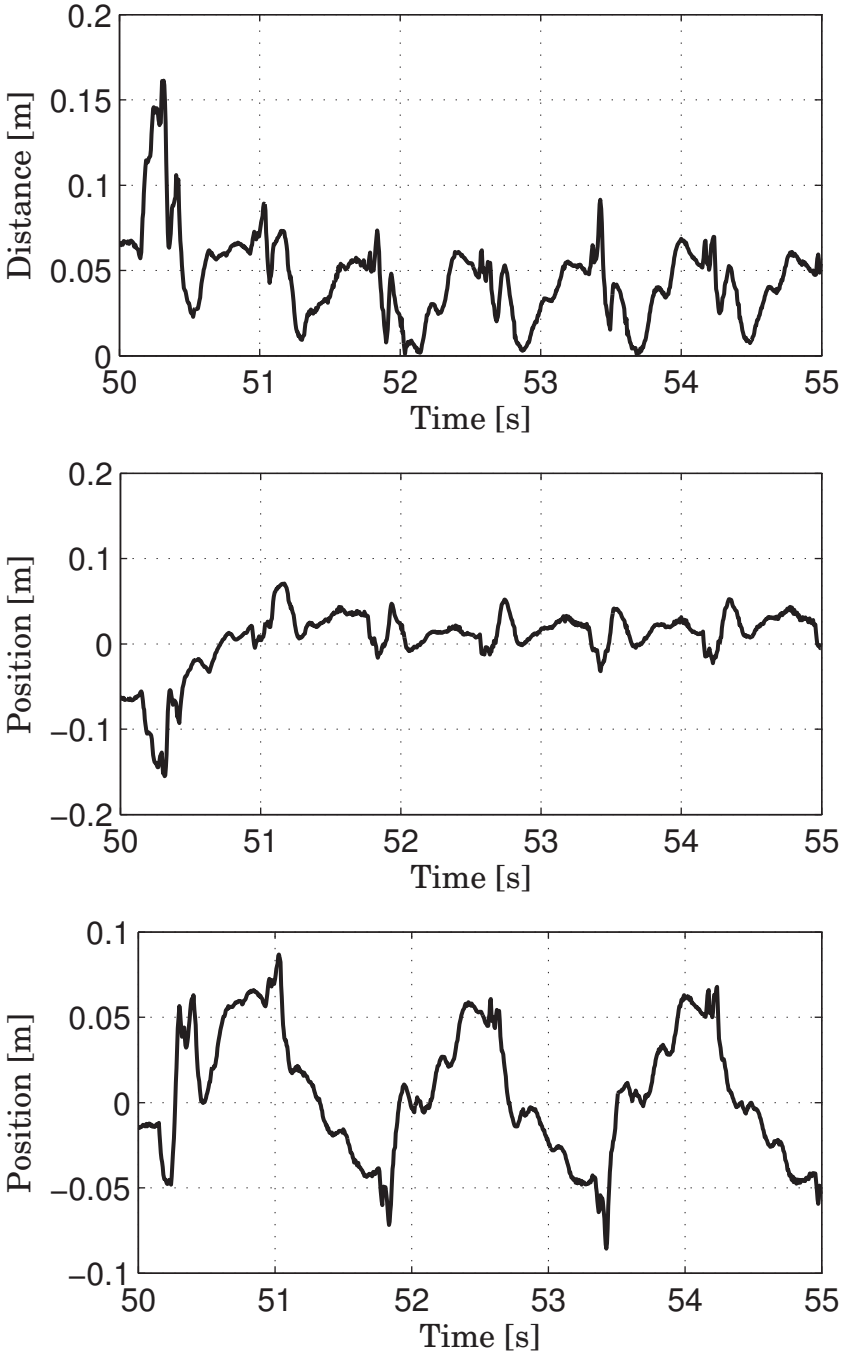

Figure 5.18: Distance to weighted middle point (top) and vector ZMP-weighted middle point (x and y components: middle and bottom respectively), between $t = 50$s and $t = 55s$. The total experiment goes from $t = 45$s to $t = 80$s. These values are less discontinuous than the two previous sets of data.

The important drawback of the force indicator is that it is difficult to separate the interaction force from the force applied for the robot's stabilization. Moreover, the human partner is

likely to apply more force than necessary to stabilize the robot. Therefore, the force indicator is useful when performing a benchmark test of stabilization through interaction, e.g. in very specific situations where the human partner is asked to only focus on the stabilization of the robot through interaction, and to limit interaction forces when possible.

5.2.2 Benchmark test Scenario

To evaluate stabilization through interaction, we design a one-degree-of-freedom scenario. The robot and the human partner have to transport a table-like object over a few meters. No turning is required. The robot is walking forwards and the human partner is walking backwards.

The robot is controlled using the control scheme from Chapter 3, except that the robot assumes a leader role. As in Chapter 3, the leader behavior is controlled by a human that generates the velocity plan $\mathcal{V}$. Then the control scheme is identical. The human that controls sends a constant velocity plan of 0.1m/s to the robot and the human that is interacting with the robot tries to keep the robot from falling by exerted forces on the object. The scenario is illustrated in Fig. 5.19.

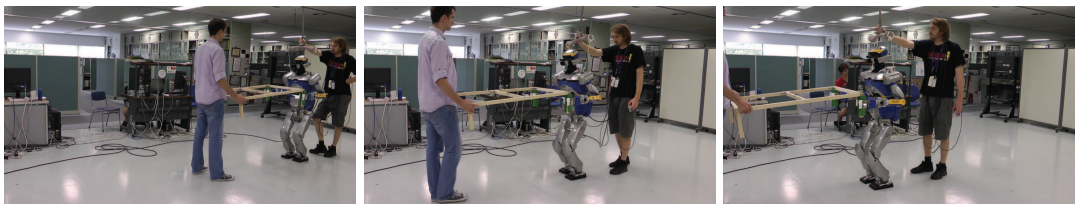

Figure 5.19: Benchmark test scenario for stabilization through interaction. The robot walks over a short distance (a few meters) at a limited speed of 0.1m/s. The human tries to prevent the robot from falling by applying force on the object when necessary.

We increase significantly the robot's grippers' stiffness and damping so the human partner can apply higher forces on the grippers. The impedance values are presented in Table 5.5.

Table 5.5: Stiffness, Damping and Inertia coefficients for the stabilization experiments.

Stiffness	Damping	Inertia
$K_{xy} = 250$N/m	$B_{xy} = 200$N.s/m	$M_{xy} = 8$kg
$K_z = 250$N/m	$B_z = 100$N.s/m	$M_z = 8$kg
$K_\theta = 250$N/rad	$B_\theta = 200$N.s/rad	$M_\theta = 8$kg.m^2

5.2.3 Benchmark test with and without Stabilizer

Without the stabilizer, the robot can only make a few steps before losing its balance. The Walking Pattern Generator (WPG) [30] generates a ZMP desired trajectory, but the errors ac-

cumulate and the robot fall after a few steps. The WPG generates the ZMP desired trajectory according to constraints on its distance $d(ZMP, SP)$ to the support polygon. The constraint of the robot's stability is

$$d(ZMP, SP) > 0 \tag{5.11}$$

In practice a security margin m is enforced

$$d(ZMP, SP) > m > 0 \tag{5.12}$$

In simulation, we notice that modifying m impacts on the number of steps the robot could do before falling. We determine by dichotomy the optimal value for m, at a precision of 1mm, to maximize the number of steps done by the robot before falling. We find $m = 0.063$m, when the robot's feet are 0.138m-wide.

With this value for m, we first perform the test scenario with the stabilizer on. The measured distance of the ZMP to the SP remains higher than 0.03m as pictured in Fig. 5.20. The horizontal force applied on the grippers globally remains lower than 4N with two pikes at 6.6 and 5N (see Fig. 5.21), while the torque norm remains lower than 7.7N.m (Fig. 5.22). The human partner does not need to stabilize the robot through the interaction.

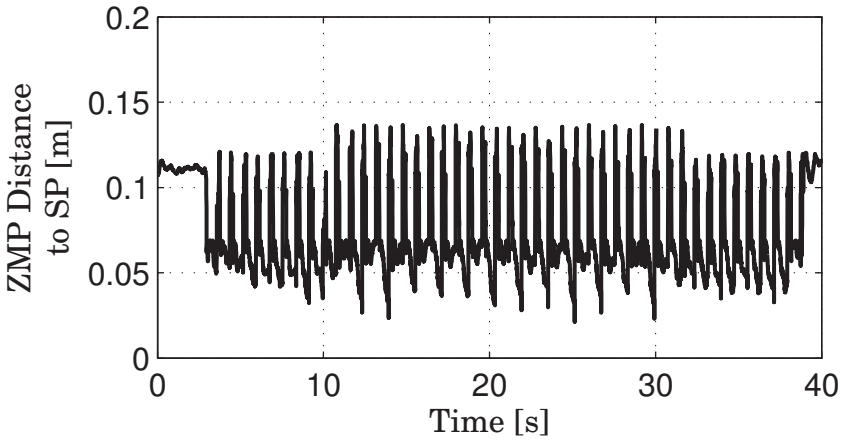

Figure 5.20: Signed distance of ZMP to the Support Polygon (SP) with the stabilizer active. A negative distance means that the ZMP is measured outside the SP.

We then perform the same test with the stabilizer off. Results are presented in Fig. 5.23 to 5.25. The results show that the ZMP is often measured outside the SP (20 times) and that a horizontal force and torque up to 27.6N and 20N.m respectively are necessary to stabilize the robot. These values are high, but not higher than the maximal values applied by the participants in the comparative user study (see Fig. 4.8 and 4.9). Still, the operator that ensures the security has to help stabilizing the robot as shown in Fig. 5.26 (right).

5.2.4 Legs Impedance Control

We notice that the shocks of the robot's feet on the ground seem to destabilize the robot. We therefore implement impedance control for the robot's feet to partially absorb these shocks.

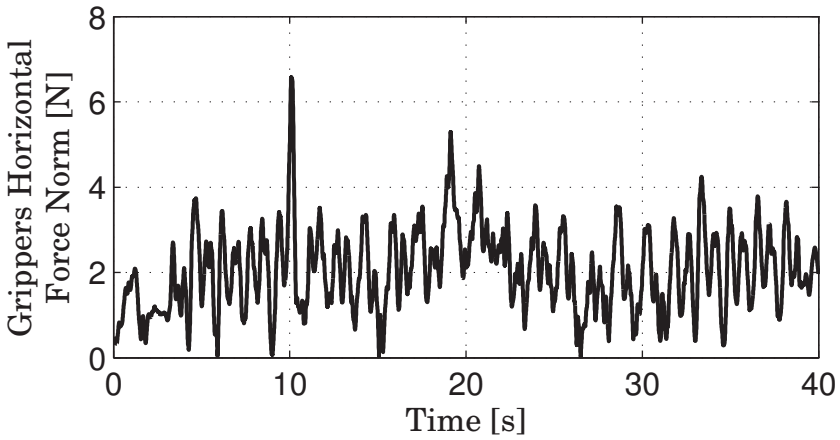

Figure 5.21: Horizontal force norm exerted on the robot's grippers with the stabilizer active.

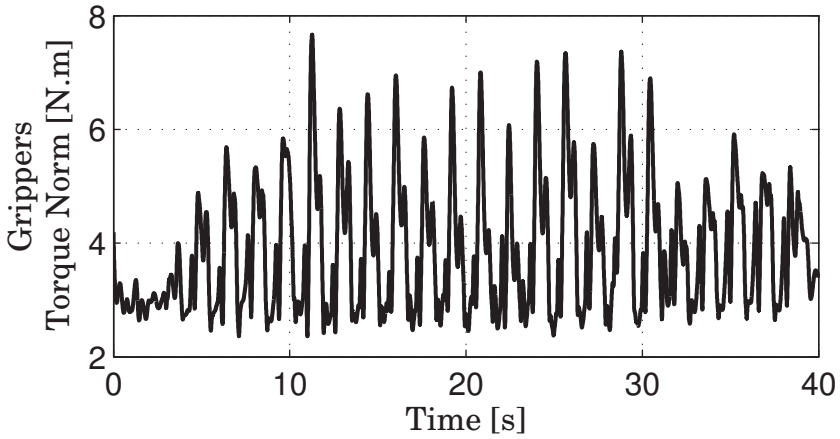

Figure 5.22: Torque norm exerted on the robot's grippers with the stabilizer active.

5.2.4.1 Implementation

The WPG generates a 6D trajectory for each foot in the world frame. However, we focus only on the desired height z_d that we use as the nodic reference of the impedance controller. Therefore, we also use only the vertical force f_z applied on a foot. We implement the following damping-stiffness impedance constraint

$$b(\dot{z} - \dot{z}_d) + k(z - z_d) = f_z \tag{5.13}$$

where b and k are the damping and stiffness coefficients respectively. We use z as the height input for the command of the foot through the SoT instead of the WPG height output z_d.

Concerning b and k, we need two sets of values: one "soft" set to absorb the impact of the foot on the floor, one "hard" set so the robot does not sag under its weight while in single support. The ideal case for the hard set is to choose b and k infinite, which is not practical to

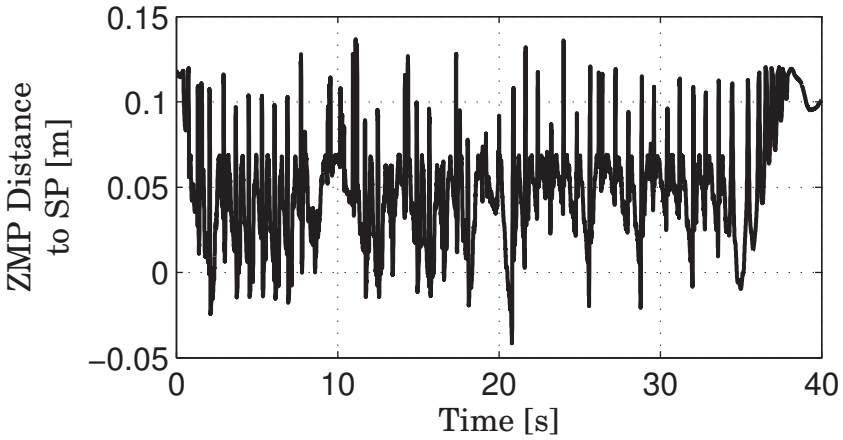

Figure 5.23: Signed distance of ZMP to the Support Polygon (SP) with the stabilizer turned off. A negative distance means that the ZMP is measured outside the SP.

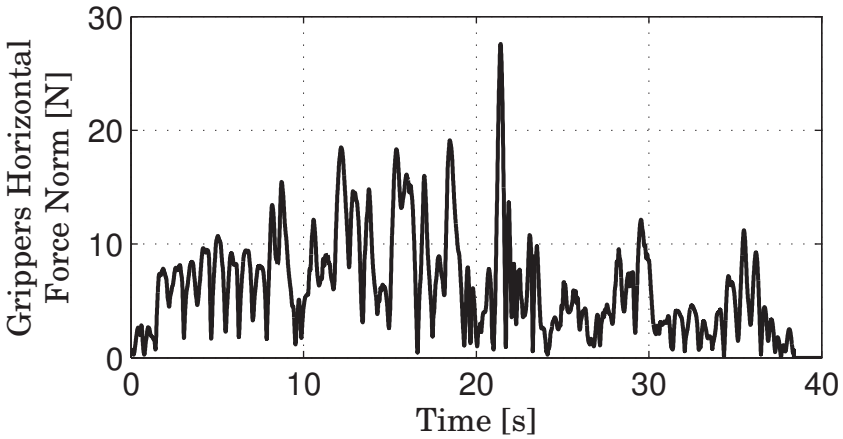

Figure 5.24: Horizontal force norm exerted on the robot's grippers with the stabilizer turned off.

realize. Therefore, we perform the following variable substitution

$$\begin{cases} g = \dfrac{1}{k} \\ \omega_0 = \dfrac{k}{b} \end{cases} \tag{5.14}$$

which yields the impedance constraint when replaced in (5.13)

$$(\dot{z} - \dot{z}_d) + \omega_0(z - z_d) = g\omega_0 f_z \tag{5.15}$$

or in the Laplace s-domain

$$\frac{z - z_d}{f_z} = \frac{g}{1 + \frac{s}{\omega_0}} \tag{5.16}$$

Therefore g is a static gain and ω_0 a cutoff frequency. To implement an infinite impedance, we set $g = 0$ which is the same as de-activating the force input. Setting g to zero from any

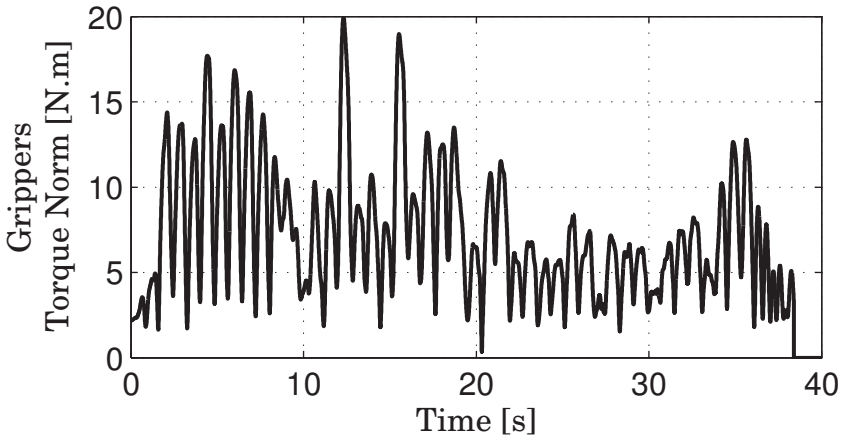

Figure 5.25: Torque norm exerted on the robot's grippers with the stabilizer turned off.

Figure 5.26: Test scenario with the stabilizer on (left) and off (right). The robot remains straight with the stabilizer on while it is leaning dangerously without it. The operator behind the robot has to assist in stabilizing the robot by stretching the ropes that are holding the robot in case it is falling.

positive value causes an step response of the impedance. The height z converges towards z_d in a given among of time. The convergence at 99% is reached after a time of $5\tau = \frac{5}{\omega_0}$.

The advantage with this choice of variables is that we can switch from the "soft" set to the hard set by setting g to zero. There is no need to interpolate g to zero since we can tune ω_0 so that the robot pushes on the floor at the velocity we desire. We choose $g = 0.00006$m/N and $\omega_0 = 10\text{s}^{-1}$, which gives a convergence at 99% in 0.5s.

To determine when to switch from one set to another, we use information from the WPG. The WPG plans a periodic succession of single and double support phases that always last the same amount of time: 0.1s for double support and 0.7s for single support. The WPG also determines a support foot. We set g to zero for a foot when this foot is considered the support foot by the WPG and for 0.4s after the WPG stops considering it as the support foot. Therefore, the impedance is activated during the single support phase before the foot landing and de-activated during the double support phase just after, as can be seen in Fig. 5.27.

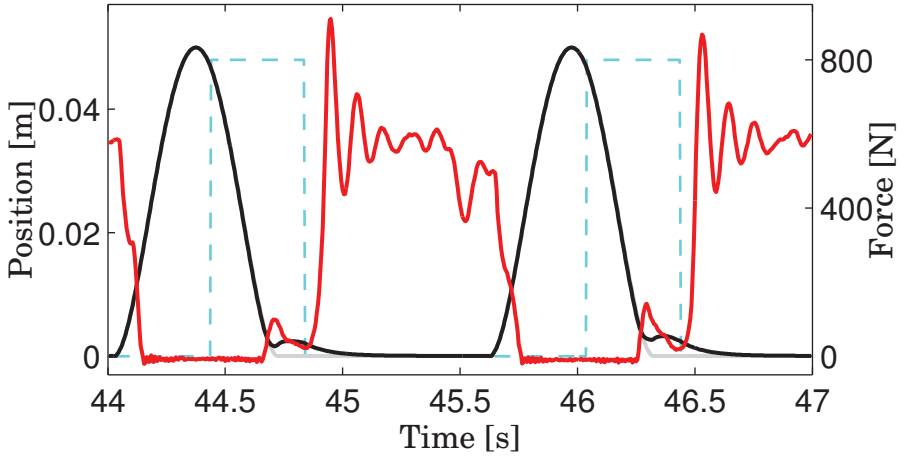

Figure 5.27: Example of inputs and outputs of the right foot impedance control. The vertical force f_z applied on the foot is in red (right scale), the desired trajectory z_d generated by WPG is in grey (left scale). The output trajectory z of the impedance controller is in black (left scale). The dotted light blue line is a multiple of the gain g. When it is positive, impedance control is active, when it is zero, impedance control is inactive and z converges towards z_d.

5.2.4.2 Results of the test scenario

We perform the test scenario with the stabilizer off and with the impedance-controlled legs. The results are presented in Fig. 5.28 to 5.30. The ZMP is measured outside the SP only 6 times. More importantly, the force pikes are not higher than 9.5N[4], and the torque ones no higher than 8.7N.m. This is less than half than the force and torque levels in the test with no stabilizer. Besides the human partner is able to stabilize the robot by himself using only the interaction through the object.

These results demonstrate that it is possible for a human to stabilize a humanoid robot through physical interaction with:

1. a Walking Pattern Generator that plans a stable gait,
2. an impedance controller that reduces the shock of the feet on the ground.

5.2.5 Stabilization through Interaction

With the knowledge that it is possible to stabilize a humanoid robot through physical interaction with limited forces, our goal is now to endow the robot with the capacity to stabilize itself through the interaction.

5.2.5.1 Implementation

The idea is that the robot adapts its velocity plan $\mathcal{V}$ to stabilize itself. For instance, when the robot is leaning backwards, it should pull on the object to stabilize itself, and push on the

[4]The impedance of the legs is de-activated in the last five seconds when the robot stops stepping, which explains the last high force pike

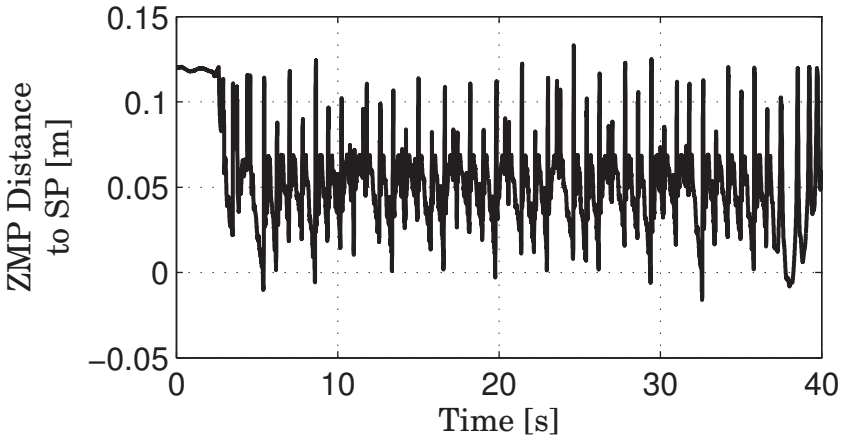

Figure 5.28: Signed distance of ZMP to the Support Polygon (SP) with the stabilizer turned off and impedance-controlled legs. The legs impedance is de-activated during the last five seconds at robot stop. A negative distance means that the ZMP is measured outside the SP.

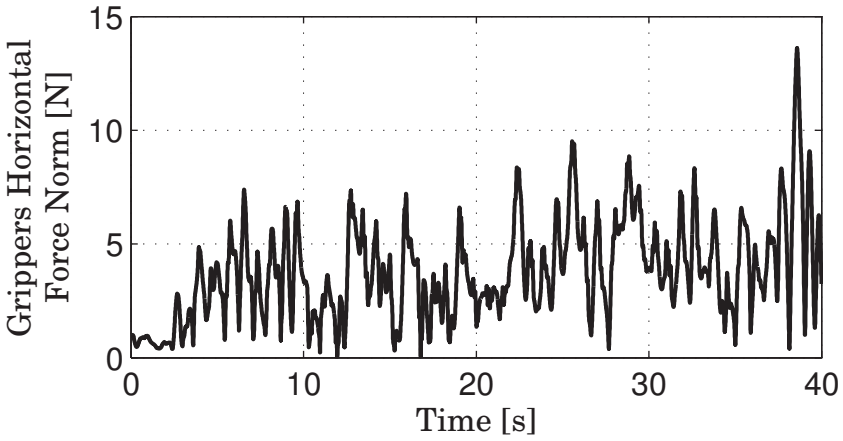

Figure 5.29: Horizontal force norm exerted on the robot's grippers with the stabilizer turned off and impedance-controlled legs. The legs impedance is de-activated during the last five seconds at robot stop, which explains the pike of force.

object when leaning forwards.

Since the task we consider only consists in a translational motion of the robot, the world frame is always parallel to the foot frame pictured in Fig. 5.12. When the robot is leaning backwards, the ZMP is moving towards the negative x; the x-component of the vector of the feet geometric middle to the ZMP from (5.6) becomes negative. Since pulling on the object means giving it a negative velocity, our stabilization control law could be

$$\mathcal{V}_{stab} = K_p({}^W\mathbf{p} - {}^W\mathbf{q}) \tag{5.17}$$

where ${}^W\mathbf{p}$ is the position of the ZMP and ${}^W\mathbf{q}$ the position of the feet geometric middle, both in the world frame. Their difference is given by (5.6). K_p is a positive proportional gain.

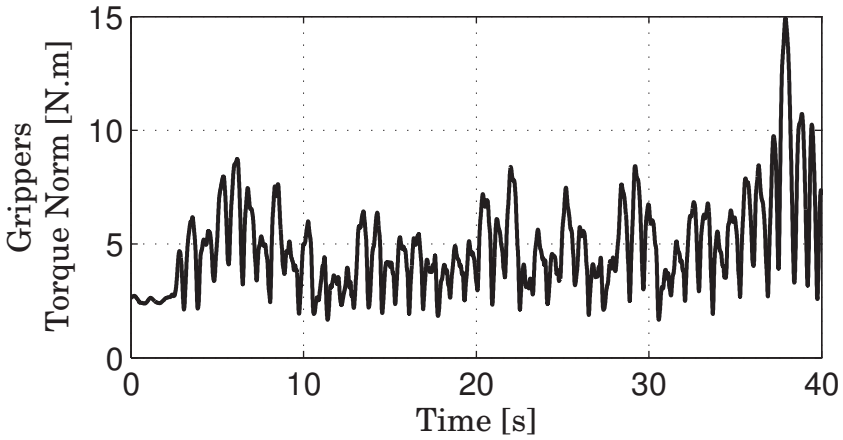

Figure 5.30: Torque norm exerted on the robot's grippers with the stabilizer turned off and impedance-controlled legs. The legs impedance is de-activated during the last five seconds at robot stop, which explains the pike of torque.

$\mathcal{V}_{stab}$ is the velocity plan for self stabilization through interaction, or stabilization velocity plan for short. The stabilization velocity plan is used in our control scheme of Chapter 3.

However, as stated in Section 5.2.1.3, ${}^{W}\mathbf{p} - {}^{W}\mathbf{q}$ is discontinuous when the robot switches between single and double support. Although the velocity plan $\mathcal{V}_{stab}$ is filtered by the low-pass filter from (3.50), we prefer to use the weighted middle of the feet. Therefore, our stabilization control law is, using notations from (5.8)

$$\mathcal{V}_{stab} = K_p({}^{W}\mathbf{p} - {}^{W}\mathbf{r}) \tag{5.18}$$

where ${}^{W}\mathbf{r}$ is the position of the weighted middle of the feet in the world frame.

We finally combine the stabilization velocity plan $\mathcal{V}_{stab}$ with the velocity plan for the transportation of the object $\mathcal{V}_{tr}$ to get the total velocity plan $\mathcal{V}_{total}$

$$\mathcal{V}_{total} = \mathcal{V}_{tr} + \mathcal{V}_{stab} \tag{5.19}$$

Because the transportation velocity plan is set by a human, $\mathcal{V}_{stab}$ has no influence on $\mathcal{V}_{tr}$. However, it may not be so if we had chosen a follower behavior for the robot, where $\mathcal{V}_{tr}$ is determined by a Finite State Machine (FSM) based on haptic cues. Indeed, the haptic cues are impacted by the stabilization process through $\mathcal{V}_{stab}$. The FSM, in its implementation of Chapter 3, does not take this impact into account and is likely to misinterpret the stabilization process as an intention of the human partner. This is the main reason we choose a leader behavior for the robot over a follower one.

5.2.5.2 Results of the test scenario

We perform the test scenario with the self-stabilization process. The legs are still impedance-controlled. This time, however, the human partner is asked to not stabilize the robot, but only to keep the interaction forces low. The results are shown in Fig. 5.31 to 5.33. The ZMP is

measured 18 times outside the SP. As with the previous test, the last five seconds correspond to the stop of the robot when the impedance control is de-activated. Therefore, we do not take the last force pike into account. The horizontal force is not higher than 12N while the torque is not higher than 9.6N. Fig. 5.34 shows the nodic trajectory of the impedance constraint: the robot moves its grippers laterally to stabilize itself.

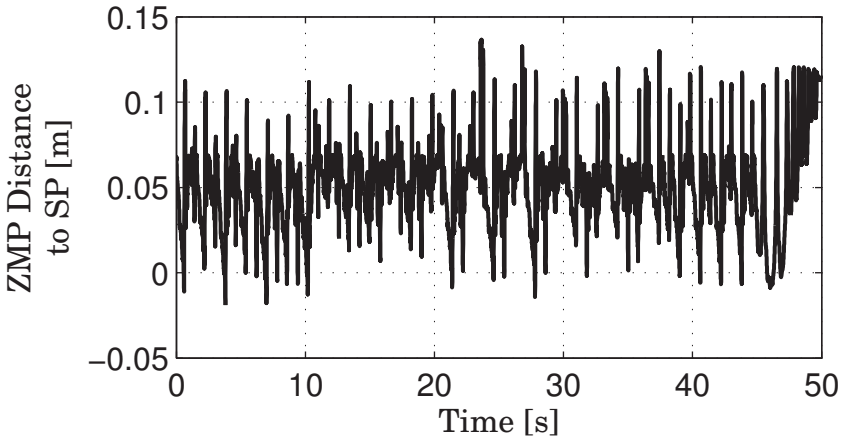

Figure 5.31: Signed distance of ZMP to the Support Polygon (SP) with the stabilizer turned off, impedance-controlled legs and stabilization through interaction. A negative distance means that the ZMP is measured outside the SP. The legs impedance is de-activated during the last five seconds at robot stop.

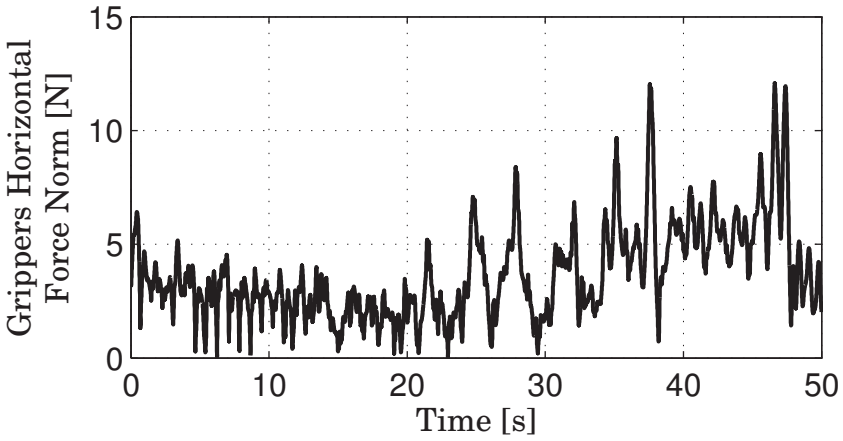

Figure 5.32: Horizontal force norm exerted on the robot's grippers with the stabilizer turned off, impedance-controlled legs and stabilization through interaction. The legs impedance is de-activated during the last five seconds at robot stop, which explains the pike of force.

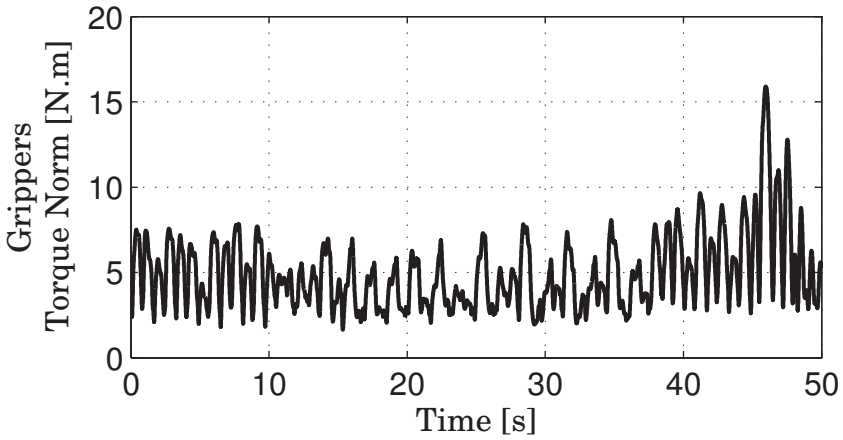

Figure 5.33: Torque norm exerted on the robot's grippers with the stabilizer turned off, impedance-controlled legs and stabilization through interaction. The legs impedance is de-activated during the last five seconds at robot stop, which explains the pike of torque.

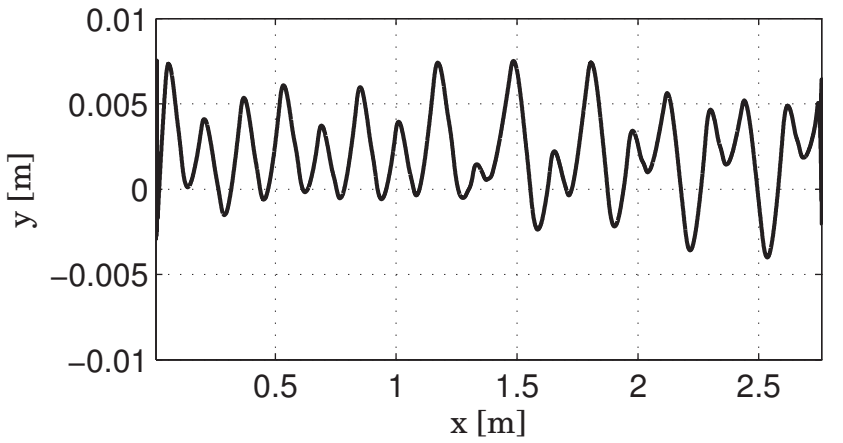

Figure 5.34: Impedance nodic trajectory $\mathbf{X}_d$ for the robot's grippers in the world frame. The robot moves from $(0, 0)$ towards the positive x. The axis are not normalized.

5.2.6 Discussion

The results of all four test scenarios are presented in Table 5.6, as well as the average torque and horizontal force norms.

These results show that the impedance control of the legs is very efficient in increasing the robot's stability. The addition of self-stabilization shows no improvements. However, the human partner does not try to stabilize the robot in this case whereas s/he does not with only the impedance-controlled legs.

In any case, the work presented in this section shows the feasibility of self-stabilization through physical interaction. It is made possible by the nodicity of our impedance constraint. The nodic trajectory $\mathbf{X}_d$ can be used for pro-activity or for self-stabilization. A challenge is to mix both in a follower behavior where the robot can also stabilize itself. This would

Table 5.6: Results of Test Scenario.

	ZMP measured outside the SP	Average Horizontal Force Norm [N]	Maximal Horizontal Force Norm [N]	Average Torque Norm [N.m]	Average Torque Norm [N.m]
Stabilizer On	0	2.0	6.6	3.8	7.7
Stabilizer Off	20	6.7	27.6	7.3	20.0
Impedance-Controlled Legs	5	3.5	9.5	4.4	8.7
Self-Stabilization through Interaction	18	3.4	12.0	4.7	9.6

require a long investigation and a complete rewriting of the stabilizer with the PG and is left for a future work beyond this thesis.

In the remaining of this chapter, we present further applications of our control scheme.

5.3 Direct Physical Interaction

5.3.1 Guiding the robot by the hand

Guiding the robot by the hand shares many similarities with the object transportation task. The robot guesses the human's intentions from the haptic cues on the hand that is held and moves accordingly.

From this observation, we adapted our control scheme developed in Chapter 3 to guide the HRP-2 robot by the hand. We change only a few things. Firstly, the robot is guided through its left gripper. The right arm is no longer impedance controlled; we fix its posture to lie along its body. Secondly we change the point that is impedance controlled. For the transportation task, it is the middle of the robot's grippers to get symmetry between the left and right grippers. In the present case, we only control the left gripper. As shown in Fig. 5.35, if we do not change the control point, a frontal force applied on the gripper results in a torque at the middle of the gripper, which we wants to avoid. Therefore we position the control point 20cm behind the left gripper on the frontal axis (the yellow point in Fig. 5.35). Note that when the human apply a lateral force on the gripper, it results in a torque at the new control point, which eases the turning of the robot. Finally, we slightly re-tune the Finite State Machine.

A human is thus able to guide the robot by the hand with the same control scheme as shown in Fig. 5.36 (left). We obtain similar results in term of trajectory (Fig. 5.37), velocity (Fig. 5.38) and force (Fig. 5.39). This highlights that the motion primitives we describe in

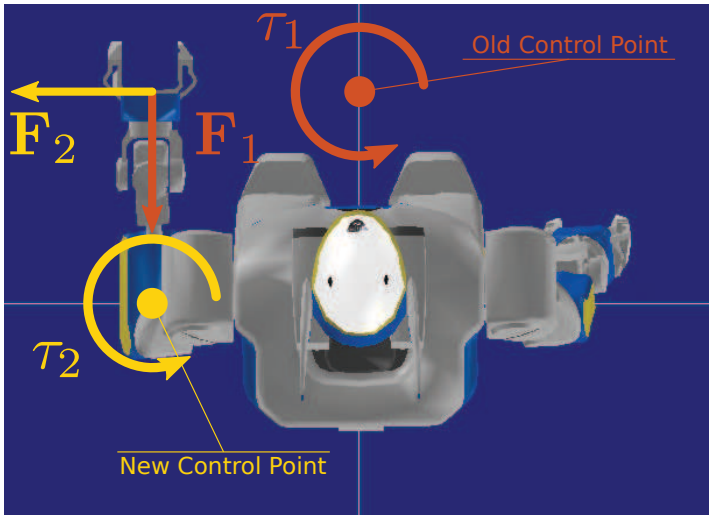

Figure 5.35: Old and new control points. With the old control point, a frontal force $\mathbf{F}_1$ applied on the left gripper results in a torque τ_1 at the control point. With the new control point, a lateral force $\mathbf{F}_2$ applied on the left gripper results in a torque τ_2 at the control point

Chapter 3 are not specific to the transportation task but can be used for different tasks and motions.

Figure 5.36: HRP-2 being guided by the hand in a lab environment (left) and at the French Embassy in Japan on July 14th 2012 (right).

5.3.2 Handshaking

Given that our choice of motion primitives can be re-used to guide the robot by the hand, we try to use them for handshaking.

5.3.2.1 Implementation

We simply model handshaking as an up and down motion in the world Cartesian frame. Therefore we use the 1DoF Finite State Machine of Chapter 3 to generate a reference trajectory on the vertical axis. This simple FSM has only two motion primitives:

- **Stop:** no motion;

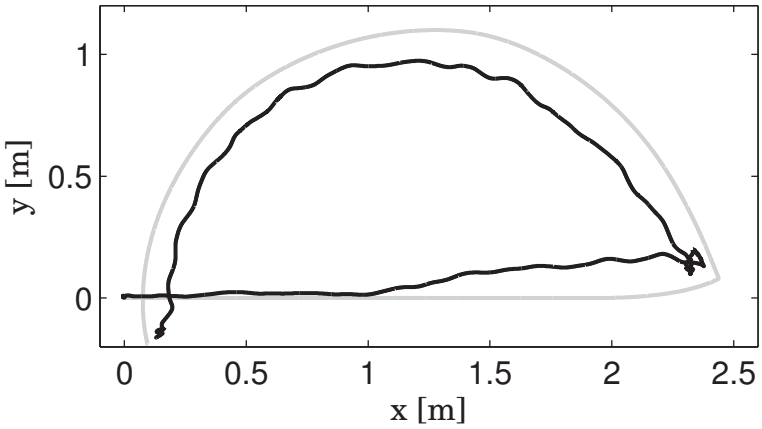

Figure 5.37: Trajectories of the robot's gripper in the XY plan: the admittance controller output $\mathbf{X}$ in black, follower desired trajectory $\mathbf{X}_d$ in grey. The motion starts at $(0, 0)$ towards the positive x. In a second time, the human guides the robot in a half-circular trajectory back to $(0, 0)$.

- **Move:** move the gripper up or down.

Unlike the 1DoF transportation task, the FSM only detects the intentions of the human through force thresholds.

We only add a security limit to prevent the hand from going too high or too low. This security consists in two mechanisms. If the robot is performing the **Move** primitive upwards and the desired gripper's height reaches the upper position limit, the FSM transitions to the **Stop** primitive. Once the desired height is higher than the upper position limit, the FSM cannot transition to the **Move** primitive for upwards motions, but only downwards. The rule for the lower position limit is identical.

The FSM is also tuned differently and we use different impedance parameters presented in Table 5.7.

Table 5.7: Stiffness, Damping and Inertia coefficients for the handshaking experiments.

Stiffness	Damping	Inertia
$K_{xy} = 250$N/m	$B_{xy} = 200$N.s/m	$M_{xy} = 8$kg
$K_z = 100$N/m	$B_z = 60$N.s/m	$M_z = 8$kg
$K_\theta = 160$N/rad	$B_\theta = 160$N.s/rad	$M_\theta = 10$kg.m^2

5.3.2.2 Results

When handshaking with the robot, it does not feel proactive at all. However, when looking at the trajectory generated by the FSM (Fig. 5.41 in grey), it follows the actual trajectory, if slowly. We also find that the force applied on the robot is almost perfectly in phase with the

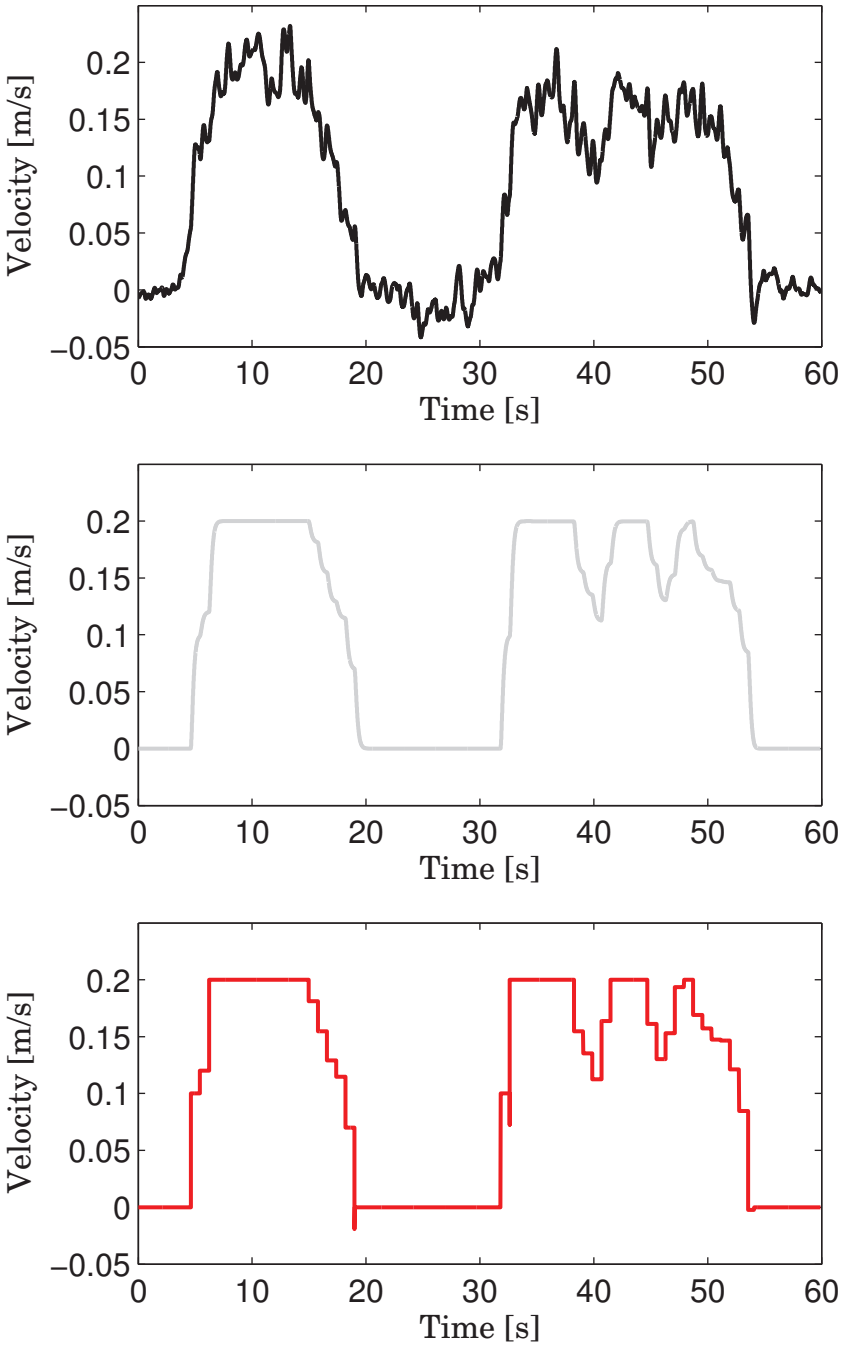

Figure 5.38: Velocities of the gripper on the robot's frontal axis: the admittance controller output $\dot{\mathbf{X}}$ in black (top), robot desired velocity $\dot{\mathbf{X}}_d$ in grey (middle) an velocity plan $\mathcal{V}$ (bottom).

gripper's velocity, as shown in Fig. 5.42. This reflects in the power measurement of Fig. 5.43 where the power input into the robot's gripper is almost the same as the power dissipated by the damping part of the impedance constraint. These results show that our control scheme

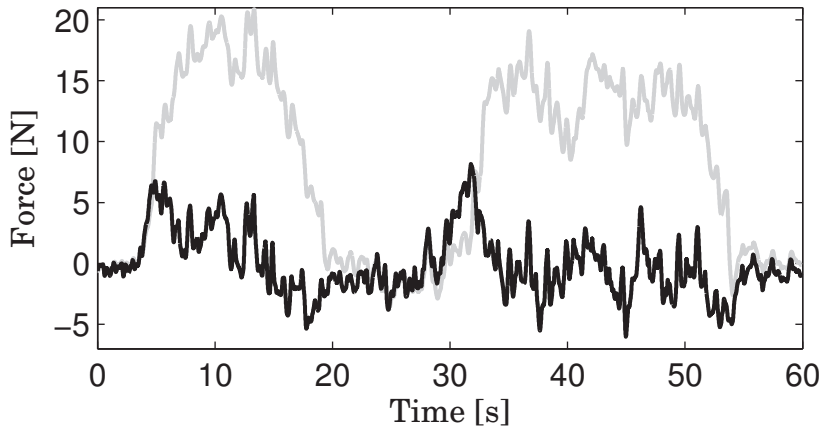

Figure 5.39: Force applied on the robot's gripper by the human (black) on the robot's frontal axis. The gray curve represents the damping part of the interaction force $\mathbf{F} = B\dot{\mathbf{X}}$: it is the force the human would need to apply on the robot with a passive behavior.

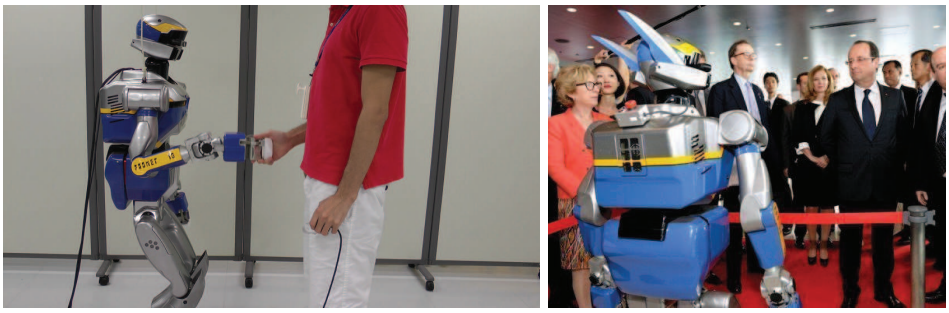

Figure 5.40: HRP-2 shaking hands with a human (left). HRP-2 also shook the hand of the French President François Hollande on June 7th 2013 in Japan (right).

fails at being proactive in the handshaking scenario.

To verify the uselessness of the intended trajectory generated by the FSM, we impose a zero intended trajectory on the impedance constraint and perform handshaking with the robot again (Fig. 5.44). We obtain similar results in force, velocity and power, as shown in Fig. 5.45 and 5.46.

Such poor performances are easily explained. Our choice of motion primitives is based on Constant Velocity Phases (CVP). This makes sense for a transportation task, for which we observed in Chapter 2 that they represent the most important part of the task. We designed our FSM to roughly estimate the human's intentions during the acceleration phases and to catch up during the CVPs.

Handshaking, however, is only composed of successive accelerations and decelerations. Therefore, the FSM estimation is always rough, as can be seen in Fig. 5.41. To obtain a good proactive behavior, an option is to generate appropriate acceleration and deceleration motion primitives. Another option is to change radically our point of view and to define motion primitives that are specific to handshaking. Our intuition is to define a periodic handshaking

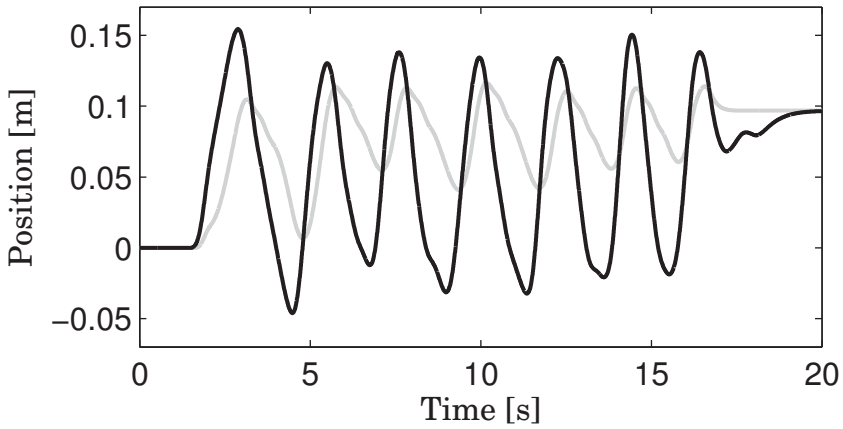

Figure 5.41: Gripper's vertical intended (grey) and effective (black) trajectories with the proactive control scheme.

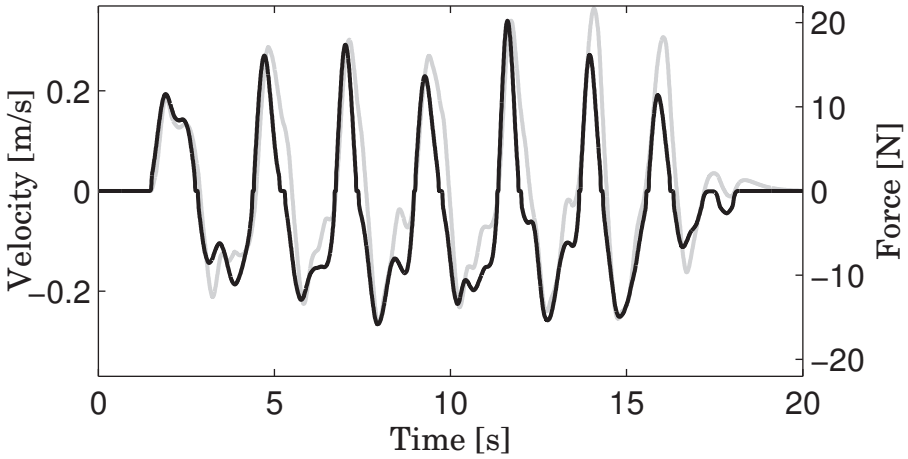

Figure 5.42: Gripper's vertical velocity (grey) and force (black) with the proactive control scheme. They are almost perfectly in phase.

motion primitive that would be parameterized by its frequency and amplitude.

5.3.3 Discussion

These two examples of direct physical interaction –guiding by the hand and handshaking– perfectly show the possibility and the limits of our control scheme using motion primitives. The key is to define the right set of motion primitives for a given task. Then the difficulty resides in *when* and *how* to switch between two primitives. Our control scheme uses a FSM but other methods, such as Markov Models, can be considered.

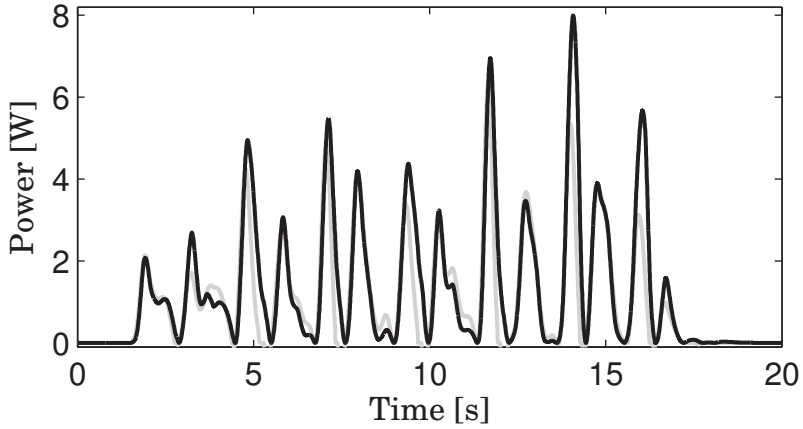

Figure 5.43: Power input into the gripper on the vertical axis (black) with the proactive control scheme. In grey is the power dissipated by the damping part, i.e. bv_z^2. The proactive control does not reduce the power input at all.

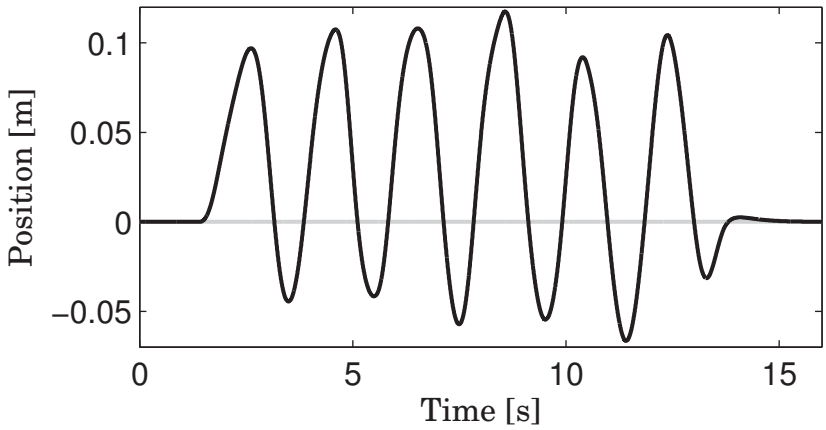

Figure 5.44: Gripper's vertical intended (grey) and effective (black) trajectories with no intended trajectory.

5.4 Extension with vision-based control

This work is achieved jointly with a new PhD student which thesis will deal more thoroughly in combining haptics with vision in pHRI. Another extension of our work is to include multi-modal information. For instance adding visual information to haptic cues to realize a task with a human. As a preliminary work, we realize the following scenario with the HRP-2 robot: the task still consists in transporting a beam over a few meters on one-degree of freedom, as in Chapter 3 but the robot has the extra task to keep the table horizontal. The robot uses haptic cues to guess the human's intentions and transport the table horizontally, but also uses visual information to keep the beam horizontal during the transportation.

The transportation task is performed using our proactive control scheme. To keep the

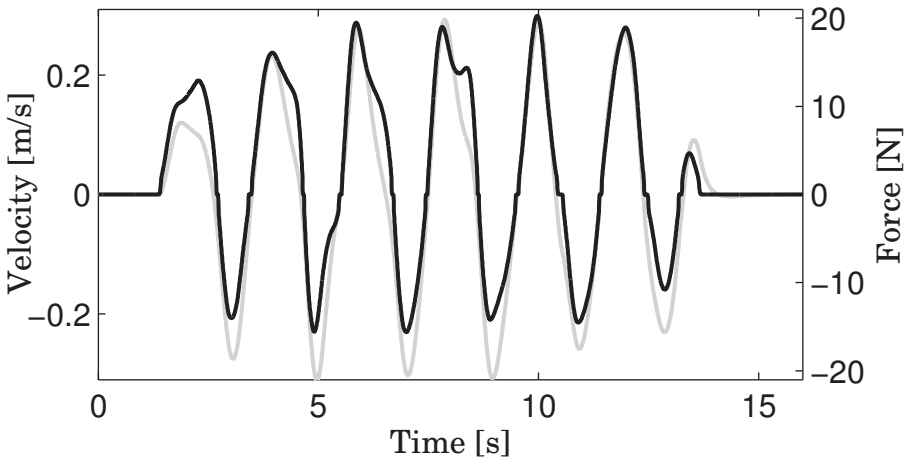

Figure 5.45: Gripper's vertical velocity (grey) and force (black) with no intended trajectory. They are almost perfectly in phase.

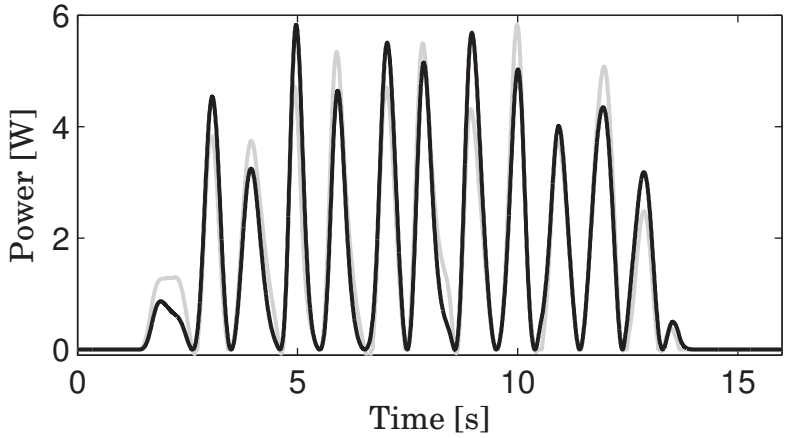

Figure 5.46: Power input into the gripper on the vertical axis (black) with no intended trajectory. In grey is the power dissipated by the damping part, i.e. bv_z^2. The stiffness part does not reduce the power input at all.

beam horizontal, the robot detects a green cube on the beam and moves its grippers vertically to keep it horizontal. Keeping the beam horizontal also involves the rotation around the robot's frontal axis, but this is left for future work. Thus, the robot only controls the angle θ around the sagittal axis as shown in the block diagram of the control scheme which is presented in Fig. 5.47.

5.4.1 Cube detection

The orientation of the cube is determined with visual tracking. The edges of the cube are tracked throughout the images. Then a robust optimization process is used to obtain the orientation of the cube in the camera frame by fitting the tracked edges onto the model of the cube. Typical results of the visual tracking are presented in Fig. 5.48. We can then compute

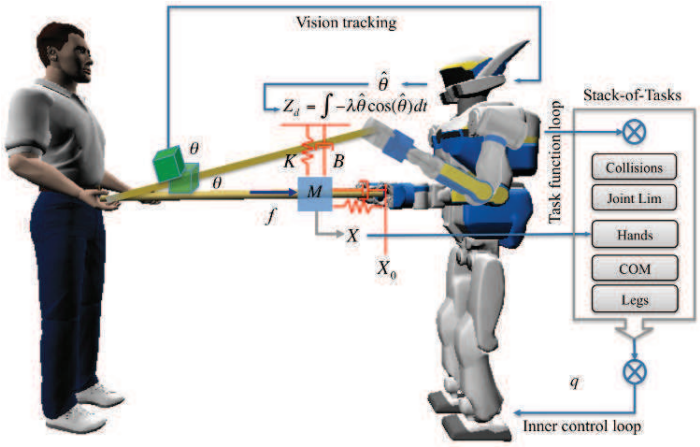

Figure 5.47: A simplified block diagram of the control framework. A green cube is used to determine the orientation of the beam using vision.

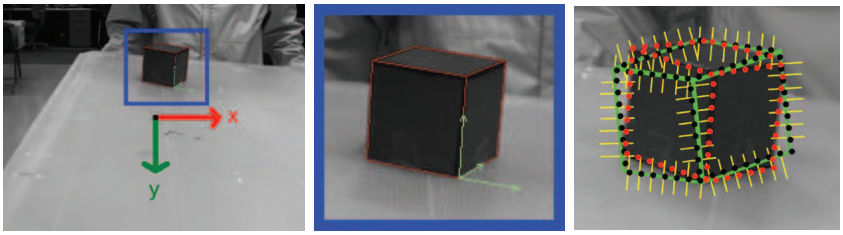

Figure 5.48: Typical result of the visual tracker. The full image is at the left. The middle image is a zoomed-in portion bordered by blue with the projection of the cube's model in red, and the object frame in green. The right image shows how edges are tracked.

the estimation of the angle $\hat{\theta}$ using the robot's direct geometric model.

5.4.2 Visual Servoing

Given the estimation of the angle $\hat{\theta}$, we compute a desired vertical velocity $\dot{z}_d$ for the robot's grippers

$$\dot{z}_d = -\lambda\hat{\theta}\cos\hat{\theta} \tag{5.20}$$

where λ is the control gain. $\dot{z}_d$ is then numerically integrated into z_d, i.e. at the k-th control step

$$z_d(k) = z_d(k-1) + \dot{z}_d(k)\delta t \tag{5.21}$$

z_d is then used as the vertical component of the nodic reference $\mathbf{X}_d$ of the impedance control. The other components are determined by the FSM.

5.4.3 Results

This visual servoing allows HRP-2 to perform the transportation task while keeping the table horizontal as shown in Fig. 5.49.

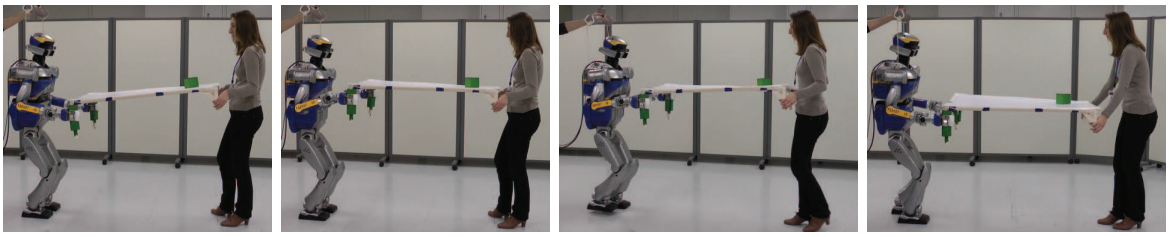

(a) (b) (c) (d)

Figure 5.49: Image results: (a) before vision control is activated, (b) result after the vision controller is activated, (c)(d) results while walking with the robot and changing table height

This experiment demonstrates the possibility to couple visual and haptic information to control a humanoid robot. However, the coupling is limited in this scenario since the visual servoing only affects the vertical axis while the haptic cues are used to determine the robot's intended trajectory on the other components. Nonetheless, this is a first step towards a control scheme where both visual and haptic cues are used to take a decision and determine the human's intention. Considering the transportation task, the robot could use the image of the human going to the side in addition to haptic cues in order to detect turning. The redundancy of information would make the detection of intention more robust.

5.5 Conclusion

In this chapter, we presented and investigated some pathways that can be considered in the future in order to improve our proactive control scheme.

First, the user study revealed that diminishing the noise made by the robot's actuators does not cause any substantial improvement on the quantitative and qualitative performance. In the contrary, some users tend to rely on sound as a substitute cue in speed state perception of the robot. At this stage, depriving the user from sound does not improve the interaction, which means that more serious issues are to be considered.

Then, we presented preliminary results of self-stabilization through interaction. Although the results are limited, they show the feasibility of such an approach to improve the robot's walking capacities. It is clear that the current stabilizer that is designed for standalone walking might not be suitable for walking in sustained physical interaction with a human. However, it might be enough to consider the joint action interaction force compensation in the walking pattern generator while keeping the current stabilizer. We think that this issue deserves another thesis to be fully addressed.

Another possible extension is to diversify the task the robot can perform with the motion primitives approach. Guiding the robot by the hand can be achieved using the same set of motion primitives. However, for other tasks, such as handshaking, additional primitives are necessary.

Finally, we presented a preliminary approach of a multi-modal task, which demonstrates an example of coupling vision and physical interaction. However, the interaction in itself is

not yet multi-modal.

The three last improvements integrate straightforwardly in our control scheme that uses a nodic reference trajectory in the impedance constraint. For instance, the stabilization through interaction and the extension using vision could not be achieved with a simple passive impedance constraint.

Conclusion

THIS thesis introduced and investigated a novel proactive control scheme to endow the HRP-2 robot with the capability to perform haptic actions jointly with a human partner. Although our analysis and development concerned particularly human-humanoid table transportation task, we believe that our methodology in dealing with this challenging case study extends to the more general cases of human-humanoid haptic joint actions.

Main Contributions

My thesis did continue our group's research in human-humanoid joint action initiated with the thesis of Paul Evrard. Paul Evrard used an engineering approach in programming the humanoid to achieve the task and introduced the idea of human-humanoid equal responsibility sharing using leader/follower homotopy switching. The limitations encountered in his experiments and the difficulty to identify the homotopy function suggested to use another approach to the problem. Therefore, we started by studying how human dyads perform a one-degree-of-freedom (1DoF) transportation task together using motion capture and force/torque sensors, and modelling. To the best of our knowledge this is the first investigation of this task. We observed that the human partners use *constant velocity phases* in the object's motion in the world frame, thus that forwards and backwards motion can be decomposed into the sequence **Zero Velocity** - **Positive Velocity** - **Zero Velocity** - **Negative Velocity** - **Zero Velocity**, with intermediary acceleration phases. We determined that jointly carried object motion can subsequently be decomposed in elementary bricks of motion or *motion primitives*, so that any motion is a sequence of appropriate primitives. Therefore, predicting a human's intended motion reduces to guessing the next motion primitive. Using known motion primitives allows a local estimation of future motion that can be used by the robot to anticipate the human partner's behaviour. Using this model, we devised a proactive

controller scheme based on impedance, and implemented it on the HRP-2 humanoid robot to perform the same 1DoF transportation task as the human dyads. A Finite State Machine (FSM) was used to determine the sequence of motion primitives that fitted the human's intentions. Compliance tuning allowed smooth transition between motion primitives. We then successfully extended our approach to a 3DoF transportation task.

In thorough user performance studies, we compared our approach to a passive dynamic behavior of the robot. Quantitative comparative measurement revealed drastic decreases in the energy and forces the human partner had to provide because of the robot, as well as increased velocity. However, qualitative investigations (questionnaire and analysis of subjective assessments) revealed that the participants had a better acceptance of the passive behavior. They found that the robot better understood their intentions with the passive behavior. To try and explain this unexpected result, we performed an additional user study to evaluate the training on the performances and feeling of the participants, and compared these data to the data obtained with the human dyads. This showed that humans could withstand high levels of force during the task, so that the decrease in force levels in the proactive case was not as significant as the perceived difficulty to be understood by the robot. Finally, we started to investigate potential improvements and extensions to our work. A third user study showed that eliminating the noise from the robot's actuator to decrease the fear of the human to harm the robot did not bring any improvement. Some participants liked to hear it, as it informed them on the robot's state, whether they could go faster or not for instance. We also demonstrated the possibility for the robot to stabilize itself through physical interaction. In other words, the robot was able to push or pull on the human through the transported object to keep from falling. This preliminary result could lead to improvements in the robot's walking, and thus allow the robot to perform the transportation task at higher velocity. We then presented the generalization to our motion primitives' model to two tasks: guiding the robot by the hand, and handshaking. We used the same set of motion primitives as for the transportation task. We could easily guide the robot by the hand, but handshaking showed poor results. It indicated that completing our set of motion primitives is necessary. Finally, we introduced an extension of our work that coupled a haptic joint action with visual control, which is a first step towards multi-modal human-robot interaction.

Perspectives

An important future perspective of our work is to develop the motion primitives model. In the medium term, their detection and parameterization method could be improved. But more importantly, in the long term, a generalization is necessary. The idea is to automatically perform what we did manually in the second and third chapter: identify motion primitives in human dyads motions and generate a program able to identify online which primitive a human partner wishes to do based on haptic cues. The first step would be to implement a classifier able to automatically detect and decompose human motion into primitives, even offline. Such classifiers already exist; the works of Kulic and Nakamura [44,45] propose very promising solutions. The second step would be to be able to automatically generate the rules

to switch between primitives. Machine learning techniques are likely one of the solutions to this problem [9]. Besides, we only mention motion primitives, but the primitive model can naturally be extended to force primitives, or even combined force-motion primitives. The space the primitives are defined in –the Cartesian motion space in our case– can be enriched. And finding the right space for the primitives is not a trivial issue at all, especially for an automated classifier. For instance, a classifier that focuses only on joint trajectories may have missed the constant velocity phases in the world frame we identified in this thesis. Such tools would endow a robot with the ability to proactively collaborate with a human in a large variety of tasks by only studying how human dyads perform the same tasks.

Another promising field is Robot Learning from Demonstration (RLfD). In this case, the robot would not learn from human dyads but directly by performing the task. For instance, a human could teach the robot by performing the task with it while it has a passive behavior. Then, each time the robot performs the task; it will become more efficiently proactive by identifying the right model to assist the human.

Improving the walking capacities of the robot and its stabilization strategy in close interaction with a human partner is clearly an important pathway to improve our work. Although this problem is general in the field of biped humanoid robotics, it is possible, in the medium term, to use the specificity of pHRI to improve the stability of the robot, as we demonstrated in the fifth chapter. Finally, the more global perspective to our work is Multi-Modal Human-Robot Interaction. pHRI is not meant to be separated from visual or auditory communication, simply because humans use all their senses when they perform collaborative tasks. In the short or medium term, it is possible to realize specific tasks using two or three senses. However, everything we developed in the beginning of this section about learning primitives can be applied to Multi-Modal Interaction. But adding the visual cue to haptic joint action (visuo-haptic pHRI in human-humanoid) drastically increases the complexity of the problem. Thus, automated and fully merged multi-modal interaction is a very long-term perspective that started by a new thesis in our group.

A

Two partners Impedance

Contents

In this appendix, we study the dynamic behavior of an object attached to two nodic impedance at two different points. We first establish the dynamic equations in a simplified form, before studying the equilibrium points and their stability.

A.1 Dynamic Equation

Consider two partners, indicated by numbers 1 and 2 respectively, that are interacting with an object at two different points $\mathbf{X}_1$ and $\mathbf{X}_2$, so that the object has the following dynamics

$$\begin{cases} \mathbf{F}_{1,\mathbf{X}_1} = M_1(\ddot{\mathbf{X}}_{d,1} - \ddot{\mathbf{X}}_1) + B_1(\dot{\mathbf{X}}_{d,1} - \dot{\mathbf{X}}_1) + K_1(\mathbf{X}_{d,1} - \mathbf{X}_1) \\ \mathbf{F}_{2,\mathbf{X}_2} = M_2(\ddot{\mathbf{X}}_{d,2} - \ddot{\mathbf{X}}_2) + B_2(\dot{\mathbf{X}}_{d,2} - \dot{\mathbf{X}}_2) + K_2(\mathbf{X}_{d,2} - \mathbf{X}_2) \\ M_C\ddot{\mathbf{C}} = \mathbf{F}_{1,\mathbf{C}} + \mathbf{F}_{2,\mathbf{C}} \end{cases} \tag{A.1}$$

where $\mathbf{C}$ is the object's CoM generalized 4D position. Note that all three points $\mathbf{C}$, $\mathbf{X}_1$ and $\mathbf{X}_2$ have the same angular parameter θ, and consequently represent the same orientation matrix $\mathbf{R}$ of the object. The problem with equation (A.1) is that it is expressed at three

different points of the object. The goal of this appendix is to write this system at a given point $\mathbf{Y}$ of the object. We will use notations similar to Featherstone's in [20]. To that purpose, we define the positions of $\mathbf{C}$, $\mathbf{X}_1$ and $\mathbf{X}_2$ relatively to $\mathbf{Y}$ in the object frame

$$\begin{cases} \mathbf{X}_1 = \mathbf{Y} + \mathbf{R}\mathbf{L}_1 \\ \mathbf{X}_2 = \mathbf{Y} + \mathbf{R}\mathbf{L}_2 \\ \mathbf{C} = \mathbf{Y} + \mathbf{R}\mathbf{L}_C \end{cases} \tag{A.2}$$

Note that the angular component θ of $\mathbf{L}_C$, $\mathbf{L}_1$ and $\mathbf{L}_2$ are zero. As we said, $\mathbf{R} = \mathbf{R}(\theta)$

$$\mathbf{R} = \begin{bmatrix} \cos\theta & -\sin\theta & 0 & 0 \\ \sin\theta & \cos\theta & 0 & 0 \\ 0 & 0 & 1 & 0 \\ 0 & 0 & 0 & 1 \end{bmatrix} \tag{A.3}$$

so that the matrix $\frac{1}{\theta}(\mathbf{R} - I_4)$ can be defined by continuity for $\theta = 0$ as 0. Equation (A.2) becomes

$$\begin{cases} \mathbf{X}_1 = \mathbf{Y} + \dfrac{1}{\theta}(\mathbf{R} - I_4)\mathbf{L}_1\theta + \mathbf{L}_1 \\ \mathbf{X}_2 = \mathbf{Y} + \dfrac{1}{\theta}(\mathbf{R} - I_4)\mathbf{L}_2\theta + \mathbf{L}_2 \\ \mathbf{C} = \mathbf{Y} + \dfrac{1}{\theta}(\mathbf{R} - I_4)\mathbf{L}_C\theta + \mathbf{L}_C \end{cases} \tag{A.4}$$

$$\frac{1}{\theta}(\mathbf{R} - I_4)\mathbf{L}_1\theta = \begin{bmatrix} l_{1,x}\frac{\cos\theta - 1}{\theta} - l_{1,y}\frac{\sin\theta}{\theta} \\ l_{1,x}\frac{\sin\theta}{\theta} + l_{1,y}\frac{\cos\theta - 1}{\theta} \\ 0 \\ 0 \end{bmatrix} \theta = \Big[Q_1(\theta) - I_4\Big]\mathbf{Y} \tag{A.5}$$

where

$$Q_1(\theta) = \begin{bmatrix} 1 & 0 & 0 & l_{1,x}\frac{\cos\theta - 1}{\theta} - l_{1,y}\frac{\sin\theta}{\theta} \\ 0 & 1 & 0 & l_{1,x}\frac{\sin\theta}{\theta} + l_{1,y}\frac{\cos\theta - 1}{\theta} \\ 0 & 0 & 1 & 0 \\ 0 & 0 & 0 & 1 \end{bmatrix} \tag{A.6}$$

Finally, we have

$$\begin{cases} \mathbf{X}_1 = Q_1(\theta)\mathbf{Y} + \mathbf{L}_1 \\ \mathbf{X}_2 = Q_2(\theta)\mathbf{Y} + \mathbf{L}_2 \\ \mathbf{C} = Q_C(\theta)\mathbf{Y} + \mathbf{L}_C \end{cases} \tag{A.7}$$

The matrices Q_i have the form of translation matrices in Plücker coordinates, as in [20]. For time derivatives, we have

$$\dot{\mathbf{X}}_1 = \dot{\mathbf{Y}} + \dot{\mathbf{R}}(\theta)\mathbf{L}_1 = \dot{\mathbf{Y}} + \mathbf{R}'(\theta)\mathbf{L}_1\dot{\theta} = \dot{\mathbf{Y}} + \Big[P_1(\theta) - I_4\Big]\dot{\mathbf{Y}} \tag{A.8}$$

where

$$P_1(\theta) = \begin{bmatrix} 1 & 0 & 0 & -l_{1,x}\sin\theta - l_{1,y}\cos\theta \\ 0 & 1 & 0 & l_{1,x}\cos\theta - l_{1,y}\sin\theta \\ 0 & 0 & 1 & 0 \\ 0 & 0 & 0 & 1 \end{bmatrix} \tag{A.9}$$

which yields

$$\begin{cases} \dot{\mathbf{X}}_1 = P_1(\theta)\dot{\mathbf{Y}} \\ \dot{\mathbf{X}}_2 = P_2(\theta)\dot{\mathbf{Y}} \\ \dot{\mathbf{C}} = P_C(\theta)\dot{\mathbf{Y}} \end{cases} \tag{A.10}$$

Note the P_i are the translation matrices defined by Featherstone[1]. And, by differentiating relatively to time, we obtain the accelerations

$$\begin{cases} \ddot{\mathbf{X}}_1 = P_1(\theta)\ddot{\mathbf{Y}} + U_1(\theta,\dot{\theta})\dot{\mathbf{Y}} \\ \ddot{\mathbf{X}}_2 = P_2(\theta)\ddot{\mathbf{Y}} + U_2(\theta,\dot{\theta})\dot{\mathbf{Y}} \\ \ddot{\mathbf{C}} = P_C(\theta)\ddot{\mathbf{Y}} + U_C(\theta,\dot{\theta})\dot{\mathbf{Y}} \end{cases} \tag{A.11}$$

where $U_i(\theta,\dot{\theta}) = \dot{\theta}P_i'(\theta)$

We repeat the same process for the desired trajectories $\mathbf{X}_{d,1}$ and $\mathbf{X}_{d,2}$

$$\begin{cases} \mathbf{X}_{d,1} = \mathbf{Y}_{d,1} + \mathbf{R}_{d,1}\mathbf{L}_1 \\ \mathbf{X}_{d,2} = \mathbf{Y}_{d,2} + \mathbf{R}_{d,2}\mathbf{L}_2 \end{cases} \tag{A.12}$$

and we get

$$\begin{cases} \mathbf{X}_{d,1} = Q_1(\theta_{d,1})\mathbf{Y}_{d,1} + \mathbf{L}_1 \\ \mathbf{X}_{d,2} = Q_2(\theta_{d,2})\mathbf{Y}_{d,2} + \mathbf{L}_2 \end{cases} \tag{A.13}$$

$$\begin{cases} \dot{\mathbf{X}}_{d,1} = P_1(\theta_{d,1})\dot{\mathbf{Y}}_{d,1} \\ \dot{\mathbf{X}}_{d,2} = P_2(\theta_{d,2})\dot{\mathbf{Y}}_{d,2} \end{cases} \tag{A.14}$$

and

$$\begin{cases} \ddot{\mathbf{X}}_{d,1} = P_1(\theta_{d,1})\ddot{\mathbf{Y}}_{d,1} + U_1(\theta_{d,1},\dot{\theta}_{d,1})\dot{\mathbf{Y}}_{d,1} \\ \ddot{\mathbf{X}}_{d,2} = P_2(\theta_{d,2})\ddot{\mathbf{Y}}_{d,2} + U_2(\theta_{d,2},\dot{\theta}_{d,2})\dot{\mathbf{Y}}_{d,2} \end{cases} \tag{A.15}$$

Equation (A.1) becomes

$$\begin{cases} \mathbf{F}_{1,\mathbf{X}_1} = M_1\Big[P_1(\theta_{d,1})\ddot{\mathbf{Y}}_{d,1} - P_1(\theta)\ddot{\mathbf{Y}}\Big] \\ \qquad + M_1\Big[U_1(\theta_{d,1},\dot{\theta}_{d,1})\dot{\mathbf{Y}}_{d,1} - U_1(\theta,\dot{\theta})\dot{\mathbf{Y}}\Big] \\ \qquad + B_1\Big[P_1(\theta_{d,1})\dot{\mathbf{Y}}_{d,1} - P_1(\theta)\dot{\mathbf{Y}}\Big] \\ \qquad + K_1\Big[Q_1(\theta_{d,1})\mathbf{Y}_{d,1} - Q_1(\theta)\mathbf{Y}\Big] \\ \mathbf{F}_{2,\mathbf{X}_2} = M_2\Big[P_2(\theta_{d,2})\ddot{\mathbf{Y}}_{d,2} - P_2(\theta)\ddot{\mathbf{Y}}\Big] \\ \qquad + M_2\Big[U_2(\theta_{d,2},\dot{\theta}_{d,2})\dot{\mathbf{Y}}_{d,2} - U_2(\theta,\dot{\theta})\dot{\mathbf{Y}}\Big] \\ \qquad + B_2\Big[P_2(\theta_{d,2})\dot{\mathbf{Y}}_{d,2} - P_2(\theta)\dot{\mathbf{Y}}\Big] \\ \qquad + K_2\Big[Q_2(\theta_{d,2})\mathbf{Y}_{d,2} - Q_2(\theta)\mathbf{Y}\Big] \\ M_C P_C(\theta)\ddot{\mathbf{Y}} + M_C U_C(\theta,\dot{\theta})\dot{\mathbf{Y}} = \mathbf{F}_{1,\mathbf{C}} + \mathbf{F}_{2,\mathbf{C}} \end{cases} \tag{A.16}$$

[1] Actually, it is their transpose because we use a translation-rotation 4D notation, whereas Featherstone uses a rotation-translation notation.

We define Varignon's formula for our 4D Cartesian description between points $\mathbf{A}$ and $\mathbf{B}$

$$\mathbf{F_A} = \mathbf{F_B} + (\mathbf{B} - \mathbf{A})_\times \mathbf{F_B} \tag{A.17}$$

where

$$\mathbf{X}_\times = \begin{bmatrix} x \\ y \\ z \\ \theta \end{bmatrix}_\times = \begin{bmatrix} 0 & 0 & 0 & 0 \\ 0 & 0 & 0 & 0 \\ 0 & 0 & 0 & 0 \\ -y & x & 0 & 0 \end{bmatrix} \tag{A.18}$$

Thus we have

$$\begin{cases} \mathbf{F}_{1,\mathbf{Y}} = \mathbf{F}_{1,\mathbf{C}} + (\mathbf{RL}_C)_\times \mathbf{F}_{1,\mathbf{C}} = \mathbf{F}_{1,\mathbf{X}_1} + (\mathbf{RL}_1)_\times \mathbf{F}_{1,\mathbf{X}_1} \\ \mathbf{F}_{2,\mathbf{Y}} = \mathbf{F}_{2,\mathbf{C}} + (\mathbf{RL}_C)_\times \mathbf{F}_{2,\mathbf{C}} = \mathbf{F}_{2,\mathbf{X}_2} + (\mathbf{RL}_2)_\times \mathbf{F}_{2,\mathbf{X}_2} \end{cases} \tag{A.19}$$

Noticing that $I_4 + (\mathbf{RL}_i)_\times = P_i^T(\theta)$ as in Featherstone [20], we get

$$\begin{cases} \mathbf{F}_{1,\mathbf{Y}} = P_C^T(\theta)\mathbf{F}_{1,\mathbf{C}} = P_1^T(\theta)\mathbf{F}_{1,\mathbf{X}_1} \\ \mathbf{F}_{2,\mathbf{Y}} = P_C^T(\theta)\mathbf{F}_{2,\mathbf{C}} = P_2^T(\theta)\mathbf{F}_{2,\mathbf{X}_2} \end{cases} \tag{A.20}$$

Since P_i matrices are invertible, we multiply third equation of (A.1) by $P_C^T(\theta)$ to obtain

$$P_C^T(\theta)M_C P_C(\theta)\ddot{\mathbf{Y}} + P_C^T(\theta)M_C U_C(\theta,\dot{\theta})\dot{\mathbf{Y}} = \mathbf{F}_{1,\mathbf{Y}} + \mathbf{F}_{2,\mathbf{Y}} \tag{A.21}$$

In order to shorten equations' writing, we write, for $i \in \{1, 2, C\}$

$$\begin{cases} \tilde{M}_i = \tilde{M}_i(\theta) = P_i^T(\theta)M_i P_i(\theta) \\ \tilde{G}_i = \tilde{G}_i(\theta,\dot{\theta}) = P_i^T(\theta)M_i U_i(\theta,\dot{\theta}) \\ \tilde{B}_i = \tilde{B}_i(\theta) = P_i^T(\theta)B_i P_i(\theta) \\ \tilde{K}_i = \tilde{K}_i(\theta) = P_i^T(\theta)K_i Q_i(\theta) \end{cases} \tag{A.22}$$

with $B_C = 0$ for the object. Similarly for desired trajectories

$$\begin{cases} \tilde{M}_{d,i} = \tilde{M}_{d,i}(\theta,\theta_{d,i}) = P_i^T(\theta)M_i P_i(\theta_{d,i}) \\ \tilde{G}_{d,i} = \tilde{G}_{d,i}(\theta,\theta_{d,i},\dot{\theta}_{d,i}) = P_i^T(\theta)M_i U_i(\theta_{d,i},\dot{\theta}_{d,i}) \\ \tilde{B}_{d,i} = \tilde{B}_{d,i}(\theta,\theta_{d,i}) = P_i^T(\theta)B_i P_i(\theta_{d,i}) \\ \tilde{K}_{d,i} = \tilde{K}_{d,i}(\theta,\theta_{d,i}) = P_i^T(\theta)K_i Q_i(\theta_{d,i}) \end{cases} \tag{A.23}$$

Finally, combining with (A.16) and (A.20), and using notations from (A.22) and (A.23), system (A.21) becomes

$$\begin{aligned} (\tilde{M}_C + \tilde{M}_1 + \tilde{M}_2)\ddot{\mathbf{Y}} + (\tilde{G}_C + \tilde{G}_1 + \tilde{G}_2)\dot{\mathbf{Y}} + (\tilde{B}_1 + \tilde{B}_2)\dot{\mathbf{Y}} + (\tilde{K}_1 + \tilde{K}_2)\mathbf{Y} \\ = \sum_{i=1}^{2} \tilde{M}_{d,i}\ddot{\mathbf{Y}}_{d,i} + (\tilde{G}_{d,i} + \tilde{B}_{d,i})\dot{\mathbf{Y}}_{d,i} + \tilde{K}_{d,i}\mathbf{Y}_{d,i} \end{aligned} \tag{A.24}$$

A.2 Equilibrium positions

In this section, we show that the number of equilibrium may vary with the parameters. We study the case where

$$\mathbf{L}_1 = -\mathbf{L}_2 = \begin{bmatrix} l \\ 0 \\ 0 \\ 0 \end{bmatrix} \tag{A.25}$$

We choose the impedance nodic references similarly

$$\forall t, \mathbf{X}_{d,1}(t) = -\mathbf{X}_{d,2}(t) = \begin{bmatrix} l \\ 0 \\ 0 \\ 0 \end{bmatrix} \tag{A.26}$$

Therefore, equation (A.13) simply becomes $\mathbf{Y}_{d,1} = \mathbf{Y}_{d,2} = 0$. Besides, as we seek to identify equilibrium positions, we have $\dot{\mathbf{Y}} = \ddot{\mathbf{Y}} = 0$, and equation A.24 becomes

$$(\tilde{K}_1 + \tilde{K}_2)\mathbf{Y} = 0 \tag{A.27}$$

For simplicity, we choose simple stiffness matrices

$$\mathbf{K}_1 = \mathbf{K}_2 = \begin{bmatrix} kI_3 & 0 \\ 0 & k_\theta \end{bmatrix} \tag{A.28}$$

We set

$$p = \begin{bmatrix} -l\sin\theta \\ l\cos\theta \end{bmatrix} \qquad q = \begin{bmatrix} l\frac{\cos\theta - 1}{\theta} \\ l\frac{\sin\theta}{\theta} \end{bmatrix} \tag{A.29}$$

so that

$$\begin{aligned} P_1^T(\theta) &= \begin{bmatrix} I_3 & 0 \\ p^T & 1 \end{bmatrix} \qquad Q_1(\theta) = \begin{bmatrix} I_3 & q \\ 0 & 1 \end{bmatrix} \\ P_2^T(\theta) &= \begin{bmatrix} I_3 & 0 \\ -p^T & 1 \end{bmatrix} \qquad Q_2(\theta) = \begin{bmatrix} I_3 & -q \\ 0 & 1 \end{bmatrix} \end{aligned} \tag{A.30}$$

From (A.22), we obtain

$$\tilde{K}_1(\theta) = \begin{bmatrix} kI_3 & kq \\ kp^T & k_\theta + kp^Tq \end{bmatrix} \qquad \tilde{K}_2(\theta) = \begin{bmatrix} kI_3 & -kq \\ -kp^T & k_\theta + kp^Tq \end{bmatrix} \tag{A.31}$$

Thus, our equilibrium equation (A.27) becomes

$$\begin{bmatrix} kI_3 & 0 \\ 0 & k_\theta + kp^Tq \end{bmatrix} \mathbf{Y} = 0 \tag{A.32}$$

The translation part yields

$$x_{eq} = y_{eq} = z_{eq} = 0 \tag{A.33}$$

while the rotation part yields

$$\theta_{eq}\Big[k_\theta + kp^T(\theta_{eq})q(\theta_{eq})\Big] = 0 \tag{A.34}$$

With

$$p^T(\theta)q(\theta) = \frac{l^2}{\theta}\left[-\sin\theta(\cos\theta - 1) + \cos\theta\sin\theta\right] = \frac{l^2\sin\theta}{\theta} \tag{A.35}$$

we have

$$\theta_{eq}\left[k_\theta + \frac{kl^2\sin\theta_{eq}}{\theta_{eq}}\right] = 0 \tag{A.36}$$

whose solutions are

$$\theta_{eq} = 0 \quad \text{or} \quad \frac{\sin\theta_{eq}}{\theta_{eq}} = -\frac{k_\theta}{kl^2} \tag{A.37}$$

This shows that there may be several equilibrium positions as shown in Fig. A.1, depending on the value of $\frac{k_\theta}{kl^2}$. Besides, we considered both partners had the same stiffness which simplified the calculation. To picture the different stable equilibrium positions, imagine a beam fixed by a pin on the floor on its middle, so that it can only rotate around the vertical axis. The pin acts as a torsion spring so that when the beam is rotated, it seeks to return to the equilibrium position $\theta = 0$. Now fix two translation springs to each end of the beam. If the torsion spring is strong enough, you can rotate the beam as you wish, but it will always return to the equilibrium position $\theta = 0$. Contrariwise, if the torsion spring is weak enough, once you have made one turn of the beam, the torsion spring will try to bring back to beam to the equilibrium angle $\theta = 0$, but will be counteracted by the two translational springs. The lower the ratio $\frac{k_\theta}{k}$ is, the more turns you will be able to do and find other equilibrium positions.

Equation (A.36) gives the elastic force $f_e(\theta)$ on the angular component

$$f_e(\theta) = k_\theta\theta + kl^2\sin\theta \tag{A.38}$$

that we can differentiate to determine the stability of equilibrium positions

$$\frac{1}{kl^2}\frac{\mathrm{d}f_e}{\mathrm{d}\theta} = \cos\theta + \frac{k_\theta}{kl^2} \tag{A.39}$$

For $\theta = 0$, this is strictly positive which assesses the stability of this equilibrium position. For the other positions θ_{eq}, we use (A.37), which gives

$$\frac{1}{kl^2}\frac{\mathrm{d}f_e}{\mathrm{d}\theta}(\theta_{eq}) = \cos\theta_{eq} - \frac{\sin\theta_{eq}}{\theta_{eq}} = \theta_{eq}\frac{\theta_{eq}\cos\theta_{eq} - \sin\theta_{eq}}{\theta_{eq}^2} \tag{A.40}$$

or

$$\frac{1}{kl^2}\frac{\mathrm{d}f_e}{\mathrm{d}\theta}(\theta_{eq}) = \theta_{eq}\frac{\mathrm{d}}{\mathrm{d}\theta}\left[\frac{\sin\theta}{\theta}\right](\theta_{eq}) \tag{A.41}$$

Thus the stability of each equilibrium position other than zero can be assessed from the derivative of the curve of Fig. A.1 at the given position.

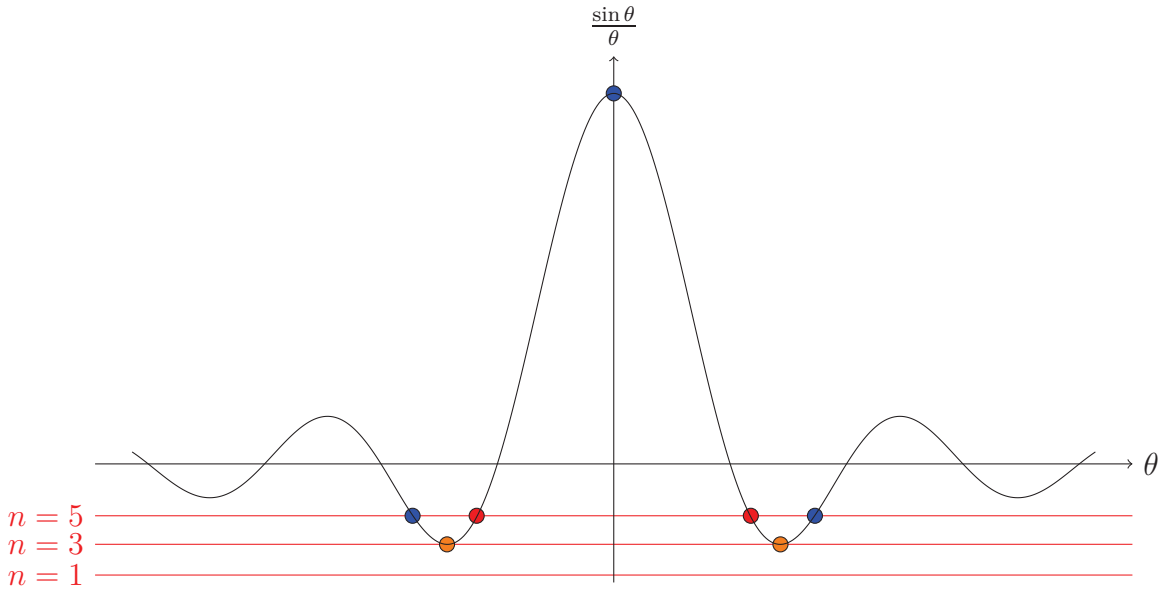

Figure A.1: Number of equilibrium positions n depending on the value of $\frac{k_\theta}{kl^2}$. The equilibrium position $\theta_{eq} = 0$ is counted in n. Stable equilibrium positions are picture by a blue dot, while metastable and unstable equilibrium positions are pictured with orange and red dots respectively.

This results demonstrates that it is not possible to find a Lyapunov Candidate Function in the general case, with general impedance parameters. It might be possible to do so with constraints on these parameters. In the general case, it might be possible to use the Krasovskii-Lasalle principle to demonstrate local asymptotic convergence to zero. And the case we developed in this section only considered fixed impedance nodic references...

A.3 Energy of the system

In this section, we consider

$$\forall t, \begin{cases} \mathbf{X}_{d,1}(t) = \mathbf{L}_1 \\ \mathbf{X}_{d,2}(t) = \mathbf{L}_2 \end{cases} \tag{A.42}$$

so that (A.13) becomes

$$\forall t, \begin{cases} \mathbf{Y}_{d,1}(t) = 0 \\ \mathbf{Y}_{d,2}(t) = 0 \end{cases} \tag{A.43}$$

and also for the successive derivatives. Thus (A.24) becomes

$$(\tilde{M}_C + \tilde{M}_1 + \tilde{M}_2)\ddot{\mathbf{Y}} + (\tilde{G}_C + \tilde{G}_1 + \tilde{G}_2)\dot{\mathbf{Y}} + (\tilde{B}_1 + \tilde{B}_2)\dot{\mathbf{Y}} + (\tilde{K}_1 + \tilde{K}_2)\mathbf{Y} = 0 \tag{A.44}$$

Consider the energy of this system

$$V(\mathbf{Y}, \dot{\mathbf{Y}}) = \frac{1}{2} \sum_{i \in \{1,2,C\}} \left[(\mathbf{X}_i - \mathbf{L}_i)^T K_i (\mathbf{X}_i - \mathbf{L}_i) + \dot{\mathbf{X}}_i^T M_i \dot{\mathbf{X}}_i \right] \tag{A.45}$$

with $K_C = 0$. Differentiating over time yields

$$\dot{V}(\mathbf{Y}, \dot{\mathbf{Y}}) = \frac{1}{2} \sum_{i \in \{1,2,C\}} \left[\dot{\mathbf{X}}_i^T K_i (\mathbf{X}_i - \mathbf{L}_i) + (\mathbf{X}_i - \mathbf{L}_i)^T K_i \dot{\mathbf{X}}_i + \ddot{\mathbf{X}}_i^T M_i \dot{\mathbf{X}}_i + \dot{\mathbf{X}}_i^T M_i \ddot{\mathbf{X}}_i \right] \tag{A.46}$$

Note that

$$\begin{cases} (\mathbf{X}_i - \mathbf{L}_i)^T K_i \dot{\mathbf{X}}_i = \left[(\mathbf{X}_i - \mathbf{L}_i)^T K_i \dot{\mathbf{X}}_i \right]^T = \dot{\mathbf{X}}_i^T K_i (\mathbf{X}_i - \mathbf{L}_i) \\ \ddot{\mathbf{X}}_i^T M_i \dot{\mathbf{X}}_i = \left[\ddot{\mathbf{X}}_i^T M_i \dot{\mathbf{X}}_i \right]^T = \dot{\mathbf{X}}_i^T M_i \ddot{\mathbf{X}}_i \end{cases} \tag{A.47}$$

because they are scalar, so that

$$\dot{V}(\mathbf{Y}, \dot{\mathbf{Y}}) = \sum_{i \in \{1,2,C\}} \dot{\mathbf{X}}_i^T \left[K_i (\mathbf{X}_i - \mathbf{L}_i) + M_i \ddot{\mathbf{X}}_i \right] \tag{A.48}$$

Using the transformation equations (A.7), (A.10) and (A.11), it becomes

$$\dot{V}(\mathbf{Y}, \dot{\mathbf{Y}}) = \sum_{i \in \{1,2,C\}} \dot{\mathbf{Y}}^T P_i^T \left[K_i Q_i \mathbf{Y} + M_i P_i \ddot{\mathbf{Y}} + M_i U_i \dot{\mathbf{Y}} \right] \tag{A.49}$$

which is

$$\dot{V}(\mathbf{Y}, \dot{\mathbf{Y}}) = \sum_{i \in \{1,2,C\}} \dot{\mathbf{Y}}^T \left[\tilde{K}_i \mathbf{Y} + \tilde{M}_i \ddot{\mathbf{Y}} + \tilde{G}_i \dot{\mathbf{Y}} \right] \tag{A.50}$$

From the dynamic equation (A.44), it comes

$$\dot{V}(\mathbf{Y}, \dot{\mathbf{Y}}) = -\dot{\mathbf{Y}}^T (\tilde{B}_1 + \tilde{B}_2) \dot{\mathbf{Y}} \leq 0 \tag{A.51}$$

We can also use the transformation equations to rewrite the energy equation (A.45)

$$V(\mathbf{Y}, \dot{\mathbf{Y}}) = \frac{1}{2} \sum_{i \in \{1,2,C\}} \left[\mathbf{Y}^T Q_i^T K_i Q_i \mathbf{Y} + \dot{\mathbf{Y}}^T \tilde{M}_i \dot{\mathbf{Y}} \right] > 0 \text{ when } \mathbf{Y} \neq 0 \tag{A.52}$$

Conversely, (A.51) can also be written

$$\dot{V}(\mathbf{Y}, \dot{\mathbf{Y}}) = - \sum_{i \in \{1,2\}} \left[\dot{\mathbf{X}}_i^T B_i \dot{\mathbf{X}}_i \right] \tag{A.53}$$

The energy V is thus positive definite and $\dot{V}$ is only negative semidefinite, which confirms that it is required to use the Krasovskii-Lasalle principle to prove the global or local asymptotic stability.

A.4 General Case

We use a state representation

$$\mathbb{X} = \begin{bmatrix} \Delta \mathbf{X}_1 \\ \Delta \mathbf{X}_2 \\ \mathbf{C} \\ \Delta \dot{\mathbf{X}}_1 \\ \Delta \dot{\mathbf{X}}_2 \\ \dot{\mathbf{C}} \end{bmatrix} \tag{A.54}$$

where

$$\begin{cases} \Delta\mathbf{X}_1 = \mathbf{X}_{d,1} - \mathbf{X}_1 \\ \Delta\mathbf{X}_2 = \mathbf{X}_{d,2} - \mathbf{X}_2 \end{cases} \tag{A.55}$$

And we write the energy function

$$V(\mathbb{X}) = \frac{1}{2}\left[\dot{\mathbf{C}}^T M_C \dot{\mathbf{C}} + \sum_{i\in\{1,2\}} \left[\Delta\mathbf{X}_i^T K_i \Delta\mathbf{X}_i + \Delta\dot{\mathbf{X}}_i^T M_i \Delta\dot{\mathbf{X}}_i\right]\right] \tag{A.56}$$

Differentiating over time yields

$$\dot{V}(\mathbb{X}) = \dot{\mathbf{C}}^T M_C \ddot{\mathbf{C}} + \sum_{i\in\{1,2\}} \left[\Delta\dot{\mathbf{X}}_i^T K_i \Delta\mathbf{X}_i + \Delta\dot{\mathbf{X}}_i^T M_i \Delta\ddot{\mathbf{X}}_i\right] \tag{A.57}$$

Using (A.1), we obtain

$$\dot{V}(\mathbb{X}) = \dot{\mathbf{C}}^T \sum_{i\in\{1,2\}} \mathbf{F}_{i,\mathbf{C}} + \sum_{i\in\{1,2\}} \Delta\dot{\mathbf{X}}_i^T \left[\mathbf{F}_{i,\mathbf{X}_i} - B_i \Delta\dot{\mathbf{X}}_i\right] \tag{A.58}$$

With (A.20) we have

$$\dot{V}(\mathbb{X}) = \dot{\mathbf{C}}^T \sum_{i\in\{1,2\}} P_C^{-T} P_i^T \mathbf{F}_{i,\mathbf{X}_i} + \sum_{i\in\{1,2\}} \Delta\dot{\mathbf{X}}_i^T \mathbf{F}_{i,\mathbf{X}_i} - \sum_{i\in\{1,2\}} \Delta\dot{\mathbf{X}}_i^T B_i \Delta\dot{\mathbf{X}}_i \tag{A.59}$$

or

$$\dot{V}(\mathbb{X}) = \sum_{i\in\{1,2\}} \left[P_i P_C^{-1} \dot{\mathbf{C}} + \Delta\dot{\mathbf{X}}_i\right]^T \mathbf{F}_{i,\mathbf{X}_i} - \sum_{i\in\{1,2\}} \Delta\dot{\mathbf{X}}_i^T B_i \Delta\dot{\mathbf{X}}_i \tag{A.60}$$

From (A.10), we have

$$\dot{\mathbf{X}}_i = P_i P_C^{-1} \dot{\mathbf{C}} \tag{A.61}$$

which yields

$$\dot{V}(\mathbb{X}) = \sum_{i\in\{1,2\}} \dot{\mathbf{X}}_{d,i}^T \mathbf{F}_{i,\mathbf{X}_i} - \sum_{i\in\{1,2\}} \Delta\dot{\mathbf{X}}_i^T B_i \Delta\dot{\mathbf{X}}_i \tag{A.62}$$

We prefer the transpose writing in the first sum, e.g.

$$\dot{V}(\mathbb{X}) = \sum_{i\in\{1,2\}} \mathbf{F}_{i,\mathbf{X}_i}^T \dot{\mathbf{X}}_{d,i} - \sum_{i\in\{1,2\}} \Delta\dot{\mathbf{X}}_i^T B_i \Delta\dot{\mathbf{X}}_i \tag{A.63}$$

This result shows that the energy of the system may grow, but will decrease as soon as

$$\forall t > t_f, \dot{\mathbf{X}}_{d,1}(t) = \dot{\mathbf{X}}_{d,2}(t) = 0 \tag{A.64}$$

Thus, if we can guarantee condition (A.64), our system will be asymptotically stable.

Bibliography

[1] Mirko Aach, Renate Meindl, Tomohiro Hayashi, Irene Lange, Jan Geßmann, Andre Sander, Volkmar Nicolas, Peter Schwenkreis, Martin Tegenthoff, Yoshiyuki Sankai, and Thomas A. Schildhauer. Exoskeletal neuro-rehabilitation in chronic paraplegic patients – initial results. In José L. Pons, Diego Torricelli, and Marta Pajaro, editors, *Converging Clinical and Engineering Research on Neurorehabilitation*, volume 1 of *Biosystems & Biorobotics*, pages 233–236. Springer Berlin Heidelberg, 2013.

[2] AM Andrew. Another efficient algorithm for convex hulls in two dimensions. *Information Processing Letters*, 9(5):216–219, 1979.

[3] Hirohiko Arai, Tomohito Takubo, Yasuo Hayashibara, and Kazuo Tanie. Human-robot cooperative manipulation using a virtual nonholonomic constraint. In *IEEE International Conference on Robotics and Automation*, pages 4064–4070, San Francisco, CA, USA, April 2000. IEEE.

[4] Brenna D. Argall and Aude G. Billard. A survey of tactile human–robot interactions. *Robotics and Autonomous Systems*, 58(10):1159–1176, 2010.

[5] Guy Avraham, Ilana Nisky, Hugo L. Fernandes, Daniel E. Acuna, Konrad P. Kording, Gerald E. Loeb, and Amir Karniel. Toward perceiving robots as humans: Three handshake models face the turing-like handshake test. *IEEE Transactions on Haptics*, 5(3):196–207, 2012.

[6] M. Benali-Khoudjal, M. Hafez, J.-M. Alexandre, J. Benachour, and A. Kheddar. Thermal feedback model for virtual reality. In *Micromechatronics and Human Science, 2003. MHS 2003. Proceedings of 2003 International Symposium on*, pages 153–158, oct. 2003.

[7] Karim Bouyarmane and Abderrahmane Kheddar. Humanoid robot locomotion and manipulation step planning. *Advanced Robotics*, 26(10):1099–1126, 2012.

[8] Stephen P. Buerger and Neville Hogan. Complementary stability and loop shaping for improved human–robot interaction. *IEEE Transactions on Robotics*, 23(2):2, April 2007.

[9] Sylvain Calinon, Paul Evrard, Elena Gribovskaya, Aude Billard, and Abderrahmane Kheddar. Learning collaborative manipulation tasks by demonstration using a haptic interface. In *IEEE International Conference on Advanced Robotics*, pages 1–6, Munich, Germany, June 2009.

[10] B. Corteville, E. Aertbelien, Herman Bruyninckx, Joris De Schutter, and Hendrik Van Brussel. Human-inspired robot assistant for fast point-to-point movements. In *IEEE International Conference on Robotics and Automation*, pages 3639–3644, Roma, Italy, April 2007. IEEE.

[11] S. Dalibard, A. El Khoury, F. Lamiraux, A. Nakhaei, M. Taïx, and J.-P. Laumond. Dynamic walking and whole-body motion planning for humanoid robots: an integrated approach. *The International Journal of Robotics Research*, 2013. to appear.

[12] C. Disalvo, F. Gemperle, J. Forlizzi, and E. Montgomery. The hug: an exploration of robotic form for intimate communication. In *Robot and Human Interactive Communication, 2003. Proceedings. ROMAN 2003. The 12th IEEE International Workshop on*, pages 403–408, oct.-2 nov. 2003.

[13] Vincent Duchaine and Clement M. Gosselin. General model of human-robot cooperation using a novel velocity based variable impedance control. In *Joint EuroHaptics Conference and Symposium on Haptic Interfaces for Virtual Environment and Teleoperator Systems*, pages 446–451, Washington, DC, USA, 2007. IEEE.

[14] Vincent Duchaine and Clément M. Gosselin. Investigation of human-robot interaction stability using lyapunov theory. In *IEEE International Conference on Robotics and Automation*, pages 2189–2194, Pasadena, CA, USA, May 2008. IEEE.

[15] J. Dumora, F. Geffard, C. Bidard, T. Brouillet, and P. Fraisse. Experimental study on haptic communication of a human in a shared human-robot collaborative task. In *Intelligent Robots and Systems (IROS), 2012 IEEE/RSJ International Conference on*, pages 5137–5144, oct. 2012.

[16] Ashish Dutta and Goro Obinata. Impedance control of a robotic gripper for cooperation with humans. *Control Engineering Practice*, 10(4):379–389, April 2002.

[17] Paul Evrard and Abderrahmane Kheddar. Homotopy-based controller for human-robot interaction. In *18th IEEE Int. Symposium on Robot and Human Interactive Communication (Ro-Man 2009)*, pages 1–6, Toyama, Japan, September-October 2009.

[18] Paul Evrard and Abderrahmane Kheddar. Homotopy switching model for dyad haptic interaction in physical collaborative tasks. In *Joint EuroHaptics Conference and Symposium on Haptic Interfaces for Virtual Environment and Teleoperator Systems*, pages 45–50, Salt Lake City, UT, USA, March 2009. IEEE.

[19] Paul Evrard and Abderrahmane Kheddar. Human-humanoid co-working in a joint table transportation. In *Proceedings of the 4th international conference on Social Robotics*, ICSR'12, pages 357–366, Berlin, Heidelberg, 2012. Springer-Verlag.

[20] Roy Featherstone. *Rigid Body Dynamics Algorithms*. Springer, 2008.

[21] Daniela Feth, Raphaela Groten, Angelika Peer, Sandra Hirche, and Martin Buss. Performance related energy exchange in haptic human-human interaction in a shared virtual object manipulation task. In *Joint EuroHaptics Conference and Symposium on Haptic Interfaces for Virtual Environment and Teleoperator Systems*, pages 338–343, Salt Lake City, UT, USA, March 2009. IEEE.

[22] T. Finni, P. V. Komi, and J. Lukkariniemi. Achilles tendon loading during walking: application of a novel optic fiber technique. *European Journal of Applied Physiology and Occupational Physiology*, 77:289–291, 1998. 10.1007/s004210050335.

[23] T. Flash. The control of hand equilibrium trajectories in multi-joint arm movements. *Biological Cybernetics*, 57:257–274, 1987.

[24] Tamar Flash and Neville Hogan. The coordination of arm movements: An experimentally confirmed mathematical model. *The Journal of Neuroscience*, 5(7):1688–1703, July 1985.

[25] Mohamed Guiatni, Abderrahmane Kheddar, et al. Modeling identification and control of peltier thermoelectic modules for telepresence. *Journal of Dynamic Systems, Measurement, and Control*, 133(3), 2011.

[26] Priska Gysin, Terry R. Kaminski, and Andrew M. Gordon. Coordination of fingertip forces in object transport during locomotion. *Experimental Brain Research*, 149:371–379, 2003.

[27] Priska Gysin, Terry R. Kaminski, Chris J. Hass, Cécile E. Grobet, and Andrew M. Gordon. Effects of gait variations on grip force coordination during object transport. *Journal of Neurophysiology*, 100:2477–2485, 2008.

[28] Sami Haddadin, Alin Albu-Schaffer, and Gerd Hirzinger. Soft-tissue injury in robotics. In *Robotics and Automation (ICRA), 2010 IEEE International Conference on*, pages 3426–3433. IEEE, 2010.

[29] R. Ham, T.G. Sugar, B. Vanderborght, K.W. Hollander, and D. Lefeber. Compliant actuator designs. *Robotics Automation Magazine, IEEE*, 16(3):81–94, 2009.

[30] Andreï Herdt, Nicolas Perrin, and Pierre-Brice Wieber. Walking without thinking about it. In *IEEE/RSJ International Conference on Intelligent Robots and Systems (IROS)*, pages 190–195, 2010.

[31] Yasuhisa Hirata, Yosuke Ojima, and Kazuhiro Kosuge. Variable motion characteristics control of an object by multiple passive mobile robots in cooperation with a human. In *IEEE International Conference on Robotics and Automation*, pages 1346–1351, Pasadena, CA, USA, May 2008. IEEE.

[32] Neville Hogan. Impedance control: an approach to manipulation. *Journal of Dynamic Systems, Measurement, and Control*, 107:1–24, March 1985.

[33] Nathanaël Jarrassé, Themistoklis Charalambous, and Etienne Burdet. A framework to describe, analyze and generate interactive motor behaviors. *PloS one*, 7(11):e49945, 2012.

[34] Abdelhamid Kadiallah, Gary Liaw, Mitsuo Kawato, David W Franklin, and Etienne Burdet. Impedance control is selectively tuned to multiple directions of movement. *Journal of neurophysiology*, 106(5):2737–2748, 2011.

[35] Shuuji Kajita, Hirohisa Hirukawa, Kensuke Harada, Kazuhito Yokoi, and Sophie Sakka. *Introduction a la commande des robots humanoides : de la modelisation a la generation du mouvement*. Springer, 1 edition, 2005.

[36] F. Kanehiro, K. Kaneko, K. Fujiwara, K. Harada, S. Kajita, K. Yokoi, H. Hirukawa, K. Akachi, and T. Isozumi. The first humanoid robot that has the same size as a human and that can lie down and get up. In *Robotics and Automation, 2003. Proceedings. ICRA '03. IEEE International Conference on*, volume 2, pages 1633–1639 vol.2, 2003.

[37] Jonas T Kaplan and Marco Iacoboni. Getting a grip on other minds: Mirror neurons, intention understanding, and cognitive empathy. *Social neuroscience*, 1(3-4):175–183, 2006.

[38] H. Kazerooni. Human augmentation and exoskeleton systems in berkeley. *International Journal of Humanoid Robotics*, 04(03):575–605, 2007.

[39] François Keith, Paul Evrard, Jean-Rémy Chardonnet, Sylvain Miossec, and Abderrahmane Kheddar. Haptic interaction with virtual avatars. In Manuel Ferre, editor, *EuroHaptics*, volume 5024 of *Lecture Notes in Computer Science*, pages 630–639. Springer, 2008.

[40] Abderrahmane Kheddar. Human-robot haptic joint actions: Is an equal control-sharing approach possible? In *4th International Conference on Human System Interactions (HSI)*, pages 269–273, Yokohama, Japan, 19-21 May 2011.

[41] Scott R. Klemmer, Björn Hartmann, and Leila Takayama. How bodies matter: five themes for interaction design. In *Proceedings of the 6th conference on Designing Interactive systems*, DIS '06, pages 140–149, New York, NY, USA, 2006. ACM.

[42] K. Kosuge, H. Yoshida, and T. Fukuda. Dynamic control for robot-human collaboration. In *Proceedings of the 2nd IEEE International Workshop on Robot and Human Communication*, pages 389–401, Tokyo, Japan, 1993. IEEE.

[43] Kazuhiro Kosuge, Manabu Sato, and Norihide Kazamura. Mobile robot helper. In *IEEE International Conference on Robotics and Automation*, pages 583–588, San Francisco, CA, USA, April 2000. IEEE.

[44] Dana Kulić and Yoshihiko Nakamura. Incremental learning and memory consolidation of whole body human motion primitives. *Adaptive Behavior*, 17(6):484–507, 2009.

[45] Dana Kulić, Wataru Takano, and Yoshihiko Nakamura. Incremental learning, clustering and hierarchy formation of whole body motion patterns using adaptive hidden markov chains. *The International Journal of Robotics Research*, 27(7):761–784, 2008.

[46] M. Lawitzky, J.R. Medina, Dongheui Lee, and S. Hirche. Feedback motion planning and learning from demonstration in physical robotic assistance: differences and synergies. In *Intelligent Robots and Systems (IROS), 2012 IEEE/RSJ International Conference on*, pages 3646–3652, 2012.

[47] Christian Liedtke, Steven A.W. Fokkenrood, Jasper T. Menger, Herman Kooij van der van der, and Peter H. Veltink. Evaluation of instrumented shoes for ambulatory assessment of ground reaction forces. *Gait and Posture*, 26(1):3924–47, 2007.

[48] Yusuke Maeda, Takayuki Hara, and Tamio Arai. Human-robot cooperative manipulation with motion estimation. In *IEEE/RSJ International Conference on Robots and Intelligent Systems*, pages 2240–2245, Maui, Hawaii, USA, October-November 2001. IEEE/RSJ.

[49] Nicolas Mansard, Olivier Stasse, Paul Evrard, and Abderrahmane Kheddar. A versatile generalized inverted kinematics implementation for collaborative humanoid robots: The stack of tasks. In *IEEE International Conference on Advanced Robotics*, pages 1–6, Munich, Germany, June 2009.

[50] Sylvain Miossec and Abderrahmane Kheddar. Human motion in cooperative tasks: Moving object case study. In *IEEE International Conference on Robotics and Biomimetics*, pages 1509–1514, Bangkok, Thailand, February 2008. IEEE.

[51] Chrystopher L Nehaniv and Kerstin Dautenhahn. *Imitation and social learning in robots, humans and animals: behavioural, social and communicative dimensions*. Cambridge University Press, 2007.

[52] Günter Niemeyer and J-JE Slotine. Stable adaptive teleoperation. *Oceanic Engineering, IEEE Journal of*, 16(1):152–162, 1991.

[53] K. Nishiwaki and K. Yano. Variable impedance control of meal assistance robot using potential method. In *Intelligent Robots and Systems, 2008. IROS 2008. IEEE/RSJ International Conference on*, pages 3242–3247, 2008.

[54] Jing Qin, Kup-Sze Choi, Renheng Xu, Wai-Man Pang, and Pheng-Ann Heng. Effect of packet loss on collaborative haptic interactions in networked virtual environments: An experimental study. *Presence: Teleoper. Virtual Environ.*, 22(1):36–53, February 2013.

[55] Md. Mozasser Rahman, Ryojun Ikeura, and Kazuki Mizutani. Investigation of the impedance characteristic of human arm for development of robots to cooperate with humans. *JSME International Journal*, 45(2):510–518, 2002.

[56] M.M. Rahman, R. Ikeura, and K. Mizutani. Control characteristics of two humans in cooperative task. In *IEEE International Conference on Systems, Man, and Cybernetics*, volume 2, pages 1301–1306. IEEE, 2000.

[57] Kyle B. Reed. *Understanding the Haptic Interactions of Working Together*. PhD thesis, Northwestern University, Evanston, Illinois, USA, June 2007.

[58] Philippe Sardain and Guy Bessonnet. Forces acting on a biped robot. center of pressure - zero moment point. *IEEE Transactions on Systems, Man, and Cybernetics*, 34(5):630–637, September 2004.

[59] Andre Schiele. An explicit model to predict and interpret constraint force creation in phri with exoskeletons. In *IEEE International Conference on Robotics and Automation*, pages 1324–1330, Pasadena, CA, USA, May 2008. IEEE.

[60] Natalie Sebanz, Harold Bekkering, and Günther Knoblich. Joint action: bodies and minds moving together. *Trends in cognitive sciences*, 10(2):70–76, 2006.

[61] Greg L Stewart, Susan L Dustin, Murray R Barrick, and Todd C Darnold. Exploring the handshake in employment interviews. *Journal of Applied Psychology*, 93(5):1139, 2008.

[62] J. Stuckler and S. Behnke. Following human guidance to cooperatively carry a large object. In *Humanoid Robots (Humanoids), 2011 11th IEEE-RAS International Conference on*, pages 218–223, oct. 2011.

[63] Y. X. Su, C. H. Zheng, P. C. Mueller, and B. Y. Duan. A simple improved velocity estimation for low-speed regions based on position measurements only. *IEEE Transactions on Control Systems Technology*, 14(5):937–942, September 2006.

[64] Nobuhiro Takahashi, Ryuta Okazaki, Hiroyuki Okabe, Hiromi Yoshikawa, Kanako Aou, Shumpei Yamakawa, Maki Yokoyama, and Hiroyuki Kajimoto. Sense-roid: Emotional haptic communication with yourself. In *Proceedings of Virtual Reality International Conference (VRIC 2011)*, April 2011.

[65] Takahiro Takeda, Yasuhisa Hirata, and Kazuhiro Kosuge. HMM-based error recovery of dance step selection for dance partner robot. In *IEEE International Conference on Robotics and Automation*, pages 1768–1773, Roma, Italy, April 2007. IEEE.

[66] R.H. Taylor and D. Stoianovici. Medical robotics in computer-integrated surgery. *Robotics and Automation, IEEE Transactions on*, 19(5):765–781, oct. 2003.

[67] Anand Thobbi, Ye Gu, and Weihua Sheng. Using human motion estimation for human-robot cooperative manipulation. In *Intelligent Robots and Systems (IROS), 2011 IEEE/RSJ International Conference on*, pages 2873–2878, 2011.

[68] Toru Tsumugiwa, Ryuichi Yokogawa, and Kei Hara. Variable impedance control with regard to working process for man-machine cooperation-work system. In *IEEE/RSJ International Conference on Robots and Intelligent Systems*, pages 1564–1569, Maui, Hawaii, USA, October-November 2001. IEEE/RSJ.

[69] Toru Tsumugiwa, Ryuichi Yokogawa, and Kazunobu Yoshida. Stability analysis for impedance control of robot for human-robot cooperative task system. In *IEEE/RSJ International Conference on Robots and Intelligent Systems*, pages 3883–3888, Sendai, Japan, September-October 2004. IEEE/RSJ.

[70] Zheng Wang, Angelika Peer, and Martin Buss. An HMM approach to realistic haptic human-robot interaction. In *Joint EuroHaptics Conference and Symposium on Haptic Interfaces for Virtual Environment and Teleoperator Systems*, pages 374–379, Salt Lake City, UT, USA, March 2009. IEEE.

[71] Astrid Weiss, Regina Bernhaupt, Manfred Tscheligi, and Eiichi Yoshida. Addressing user experience and societal impact in a user study with a humanoid robot. In *AISB2009: Proceedings of the Symposium on New Frontiers in Human-Robot Interaction (Edinburgh, 8-9 April 2009), SSAISB*, pages 150–157. Citeseer, 2009.

[72] Chenguang Yang and Etienne Burdet. A model of reference trajectory adaptation for interaction with objects of arbitrary shape and impedance. In *Intelligent Robots and Systems (IROS), 2011 IEEE/RSJ International Conference on*, pages 4121–4126. IEEE, 2011.

[73] Chenguang Yang, Gowrishankar Ganesh, Sami Haddadin, Sven Parusel, Alin Albu-Schaeffer, and Etienne Burdet. Human-like adaptation of force and impedance in stable and unstable interactions. *Robotics, IEEE Transactions on*, 27(5):918–930, 2011.

[74] Kazuhiko Yokoyama, Hiroyuki Handa, Takakatsu Isozumi, Yutaro Fukase, Kenji Kaneko, Fumio Kanehiro, Yoshihiro Kawai, Fumiaki Tomita, and Hirohisa Hirukawa. Cooperative works by a human and a humanoid robot. In *IEEE International Conference on Robotics and Automation*, pages 2985–2991, Taipei, Taiwan, September 2003. IEEE.

Contributions

[75] Don Joven Agravante, Andrea Cherubini, Antoine Bussy, and Abderrahmane Kheddar. Human-humanoid joint haptic table carrying task with height stabilization using vision. In *Intelligent Robots and Systems (IROS), 2013 IEEE/RSJ International Conference on*. IEEE, 2013.

[76] Antoine Bussy, Pierre Gergondet, Abderrahmane Kheddar, François Keith, and André Crosnier. Proactive behavior of a humanoid robot in a haptic transportation task with a human partner. In *21th IEEE Int. Symposium on Robot and Human Interactive Communication (Ro-Man 2012)*, 2012.

[77] Antoine Bussy, Abderrahmane Kheddar, André Crosnier, and François Keith. Human-humanoid haptic joint object transportation case study. In *IEEE/RSJ International Conference on Robots and Intelligent Systems*, 2012. Best Paper Award Finalist.

TITRE : Approche cognitive pour la représentation de l'interaction proximale haptique entre un homme et un humanoïde

RÉSUMÉ : Les robots sont tout près d'arriver chez nous. Mais avant cela, ils doivent acquérir la capacité d'interagir physiquement avec les humains, de manière sûre et efficace. De telles capacités sont indispensables pour qu'il puissent vivre parmi nous, et nous assister dans diverses tâches quotidiennes, comme porter une meuble. Dans cette thèse, nous avons pour but de doter le robot humanoïde bipède HRP-2 de la capacité à effectuer des actions haptiques en commun avec l'homme. Dans un premier temps, nous étudions comment des dyades humains collaborent pour transporter un objet encombrant. De cette étude, nous extrayons un modèle global de primitives de mouvement que nous utilisons pour implémenter un comportement proactif sur le robot HRP-2, afin qu'il puisse effectuer la même tâche avec un humain. Puis nous évaluons les performances de ce schéma de contrôle proactif au cours de tests utilisateur. Finalement, nous exposons diverses pistes d'évolution de notre travail: la stabilisation d'un humanoïde à travers l'interaction physique, la généralisation du modèle de primitives de mouvements à d'autres tâches collaboratives et l'inclusion de la vision dans des tâches collaboratives haptiques.

MOTS-CLEFS : Haptique, Interaction Physique, Interaction Homme-Robot, Robot Humanoïde.

TITLE : Cognitive approach for representing the haptic physical human-humanoid interaction

ABSTRACT : Robots are very close to arrive in our homes. But before doing so, they must master safe and efficient physical interaction with humans. Such capacities are essential for them to live among us, and assit us in various everyday tasks, such as carrying heavy and cumbersome objects. In this thesis, we focus on endowing the biped humanoid robot HRP-2 with the capacity to perform haptic joint actions with humans. First, we study how human dyads collaborate to transport a cumbersome object. From this study, we define a global motion primitives' model that we use to implement a proactive behavior on the HRP-2 robot, so that it can perform the same task with a human. Then, we assess the performances of our proactive control scheme by perfoming user studies. Finally, we expose several potential extensions to our work: self-stabilization of a humanoid through physical interaction, generalization of the motion primitives' model to other collaboratives tasks and the addition of visionto haptic joint actions.

KEYWORDS : Haptics, Physical Interaction, Human-Robot Interaction, Humanoid Robot.

DISCIPLINE : Génie Informatique, Automatique et Traitement du Signal

Laboratoire d'Informatique, de Robotique et de Microélectronique de Montpellier
UMR 5506 CNRS/Université de Montpellier 2
161 rue Ada - 34095 Montpellier Cedex 5 - FRANCE